

Superdiffusion in Scale-Free Inhomogeneous Environments

Dissertation

zur Erlangung des Doktorgrades
der Mathematisch-Naturwissenschaftlichen Fakultäten
der Georg-August-Universität zu Göttingen

vorgelegt von

Dirk Brockmann

aus Braunschweig

Göttingen 2003

D7

Referent:

Korerefentin:

Tag der mündlichen Prüfung:

Prof. Dr. Theo Geisel

Prof. Dr. Annette Zippelius

27. Juni 2003

For Kurt



Contents

1. Introduction	9
2. Everything You Always Wanted to Know About Superdiffusion, but Were Afraid to Ask	15
2.1. Random Walks	15
2.1.1. The Central Limit Theorem	16
2.1.2. The Wiener Process	17
2.2. Physics	19
2.2.1. Diffusion Processes and Langevin Dynamics	20
2.2.2. Probabilistic Models	21
2.3. Thermodynamics	22
2.4. A Tale of Tails	23
2.4.1. Lévy Flights	25
2.4.2. Lévy Stable Processes	26
2.5. Fractional Calculus	29
2.5.1. The Mother of Them All	29
2.6. Generalized Langevin Dynamics	31
2.6.1. Mother's Darling	32
2.6.2. Physics, Again	34
2.6.2.1. A Lévy Gas on the Computer	36
2.6.3. Probabilistic Models, Again	37
2.7. Fractal Time Processes	38
2.8. Summary	40
3. Topological Superdiffusion	43
3.1. Preliminary Considerations	43
3.2. Random Motion on a Folding Polymer – A Paradigm	47
3.2.1. Rigid chains	49
3.3. Mean Field Theory for Non-Local Transitions	51
3.3.1. The Coiled Polymer	53
3.4. The FFPE for Topological Superdiffusion	54
3.5. The Fractional Schrödinger Equation	59
3.5.1. Topological Superdiffusion in the Harmonic Potential	60
3.5.2. Perturbation Theory for Weak Potentials	62



3.6. Generalizations of the Approach	63
3.6.1. Higher Dimensions	66
3.7. Discussion	67
4. Comparison of Models	71
4.1. Motivation	71
4.2. Of Apples, Pears and Potatoes	72
4.2.1. Sometimes They Agree, But Mostly They Do Not	73
4.3. Scaling Laws	74
4.3.1. Ordinary Diffusion	75
4.3.2. Free Superdiffusion	76
4.3.3. Topological Superdiffusion	77
4.3.3.1. Potentials with a Length Scale	78
4.3.3.2. x^n -Potentials	79
4.3.4. Generalized Langevin Dynamics	79
4.3.5. Subordinated Superdiffusion	81
4.4. Relaxation in the Harmonic Potential	82
4.4.1. Topological Superdiffusion	82
4.4.2. Subordination	84
4.4.3. Generalized Langevin Dynamics	85
4.4.4. Trajectories, Relaxation and Spectra	87
4.5. Escape Dynamics in a Double Well	90
4.6. Discussion	94
5. Periodic Potentials	95
5.1. Motivation	96
5.2. Bloch Theory for Superdiffusive Processes	98
5.3. Bands	103
5.3.1. Band Gaps Everywhere	103
5.3.2. Dancing Bands	105
5.3.3. The Ups and Downs	107
5.4. Asymptotics	110
5.5. Universal Behavior in Weak Potentials	113
5.5.1. Energy Levels Distant to the Bragg Planes	113
5.5.2. Energy Levels Near the Bragg Planes	114
5.5.3. Asymptotic Behavior in Weak Potentials	114
5.6. Finite Systems	118
5.7. Discussion	120
6. Random Environments	123
6.1. Motivation	124
6.2. Random Potentials	126



6.2.1. Modeling Random Environments with Random Phases	127
6.3. Density of States and Return Probability	130
6.4. Dynamics in Weak Potentials	134
6.4.1. Asymptotics in Weak Potentials	138
6.4.2. Transient Dynamics	138
6.5. Asymptotics	141
6.6. Strange Kinetics on Co-Polymers	141
6.7. Discussion	147
7. The Ecology of Visual Search	149
7.1. Human Eye Movements	149
7.2. Contemporary Theories	152
7.3. A Phenomenological Model	153
7.4. The Lévy Flight Nature of Saccadic Eye Movements	155
7.5. Temporal Optimization	156
7.6. Discussion	158
8. Perspectives	161
A. Fractional Calculus	165
A.1. Fractional Integration	165
A.2. Fractional Differentiation	166
A.2.1. Examples	167
A.3. The Fractional Laplacian $\Delta^{\mu/2}$	167
A.3.1. $\Delta^{\mu/2}$ on the Interval $0 < \mu < 1$	168
A.3.2. $\Delta^{\mu/2}$ on the Interval $1 < \mu < 2$	168
A.3.3. The Boundary Cases $\mu = 1$ and $\mu = 2$	169
A.3.4. Simplicity in k -Space	169
A.3.5. Examples	170
A.3.6. Higher Dimensions	171
B. Langevin Dynamics and the Fokker-Planck Equation	173
C. Homogeneous Detailed Balanced Stochastic Operators	175
C.1. Properties of the Wave Function $ \psi_t\rangle$	177
C.2. Spectral Decomposition	178
C.2.1. Stationary Systems	179
C.2.2. Discrete Spectra	179
C.2.3. Computing Expectation Values	180
C.2.3.1. Examples	181
D. The Fourier Transform	183



E. Generating Random Numbers with Divergent Moments Numerically	187
E.1. Transforming Random Variables	187
E.1.1. Example: Exponentially Distributed Random Variables	188
E.2. Generating Random Numbers with a Power Law Density	188
E.2.1. Finite Intervals	189
E.3. Random Numbers with Lévy Stable Densities	189
Bibliography	191
Acknowledgments	201



1. Introduction

There is a crack in everything,
that's how the light gets in.

(Leonard Cohen)

Diffusion processes are ubiquitous in nature. The first report on diffusion was given by the Scottish botanist Robert Brown in 1828, who observed the erratic movement of pollen suspended in liquid¹. Although Brown himself postulated that erratically changing microscopic forces induce the irregular motion of the particles, nearly a century had to pass before Einstein explained Brownian motion in one of his seminal 1905 papers [37], validating the molecular kinetic theory of heat. It so happened that in the same year the term *random walk* entered the scientific literature. In a letter to Nature [100], K. Pearson asked the community for a solution of the two-dimensional random walk. The approximate solution was provided by Lord Rayleigh in the same issue [78]. Diffusion phenomena and random walks are intimately connected. The study of random walks and Brownian motion has shaped our understanding of fluctuation phenomena far beyond the dispersion of pollen suspended in liquid. The range of applications includes the dynamics of stock prices, thermal noise, and random perturbations in various physical, biological and chemical systems.

A hallmark of Brownian motion and ordinary random walks is a mean square displacement which increases linearly with time. This is frequently expressed in the heuristic “square-root” relation

$$X(t) \sim t^{1/2},$$

in which $X(t)$ estimates the position of the process after a time t . Over the past decades a number of phenomena have been discovered which violate this behavior, yet exhibit a similar heuristic scaling with time,

$$X(t) \sim t^{1/\mu} \quad 0 < \mu \neq 2.$$

¹Like many wealthy scientists of his day, Brown had his results published privately as a pamphlet which he distributed to friends, colleagues and the press. In 2001, a copy of *A Brief Account of Microscopical Observations Made in the Months of June, July and August 1827 on the Particles Contained in the Pollen of Plants; and on the General Existence of Active Molecules in Organic and Inorganic Bodies* was sold for \$ 80, 000 by B & L Rootenberg – Fine Rare Books.



When this occurs we speak of anomalous diffusion. Depending on the value of the exponent μ , these phenomena have been categorized as subdiffusive ($\mu > 2$) and superdiffusive ($\mu < 2$).

Superdiffusive motion, also known as enhanced diffusion, has been observed in a number of physical systems, ranging from the pioneering work of Richardson on turbulent diffusion [108], chaotic dynamical systems [45–47, 139, 143], dynamics of tracer particles in turbulent flows [104], transport in inhomogeneous rocks [111] and micelle diffusion [96], to millennial climate changes [34] and planetary-scale turbulent circulation [125]. The contemporary focus on dynamics on the mesoscopic scale [70, 71] has revealed anomalous diffusion phenomena in living biological cells, such as protein dynamics on DNA strands [135], the motion of molecular motors on actin fibers [4, 77] and enhanced translocation of molecules on networks of microtubuli [29]. Furthermore, enhanced diffusion has been observed in animal locomotion, examples are the movement of bacteria and plankton [72, 93], motion of amoeba [73] and the foraging strategies of albatrosses and spider monkeys [106, 127] and human saccadic eye-movement during visual search [20, 23]. Large fluctuations, often a signature of superdiffusive motion, have also been observed in a variety of economical systems, for example price fluctuations of individual companies [102, 103] and market indices [49].

A variety of theoretical tools have been devised in order to understand these anomalous diffusion phenomena. Generalizing the concept of ordinary random walks, Scher and Montroll introduced continuous time random walks (CTRW) in a study of dispersion in amorphous solids [113]. Since then, CTRW have found wide application, for instance in the description of diffusion of earthquake epicenter aftershocks [53], bacterial chemotaxis [114] and of intermittent chaotic systems [143], to give a few examples, additional ones can be found in [91]. The reason for its popularity is the fact that both sub- and superdiffusive phenomena can be modeled by CTRW in an appealing fashion.

A class of random walks known as Lévy flights has advanced our understanding of enhanced diffusion more than anything else. Unlike ordinary random walks which consist of independent random increments with a typical scale, single steps of a Lévy flight occur on all scales due to divergent moments in step size. Although their mathematical foundation was developed by Lévy and Khintchine [63, 74] at the same time as Richardson reported the first experimental discovery of enhanced diffusion, the great value of Lévy's work to the physicists remained unappreciated until the 1980's, when fractals and chaotic dynamical systems became a hot topic, and a further decade passed before the first concise collection on Lévy flights in physics [117] and popular articles [64, 116] appeared.

When Lévy flights successfully mimic single realizations of stochastic quantities, the equations which govern the time evolution of probability densities are no longer of the Fokker-Planck type. Until very recently Lévy flight models were given in terms of rate models or within the CTRW scheme, which despite differ-



ences in their form possess similar dynamical properties. The recent introduction of fractional calculus [94] to the study of anomalous diffusion not only unified a number of microscopic approaches, but also greatly advanced our understanding of them [55, 121]. In fractional evolution equations, ordinary differential operators are replaced by generalized non-local integro-differential operators, which share some feature with their integer counterparts but cover a much wider range of possibilities. In early phenomenological models for anomalous diffusion, for example diffusion on fractals [95], fractional differential operators were introduced in an ad-hoc fashion. However, unlike the Fokker-Planck equation which represents the canonical evolution equation for ordinary diffusion, a zoo of fractional generalizations exists, each depicting a different physical situation, which is often not readily deduced from the equation itself. Despite their similarity in appearance to ordinary Fokker-Planck equations, fractional Fokker-Planck equations exhibit a vast range of dynamical properties. Therefore, the ad-hoc introduction of fractional operators must be carried out with care, and a phenomenological approach of this kind must be solidly justified. A series of recently published papers were devoted to bridging the gap between microscopic rate equations and the appropriate fractional Fokker-Planck equations. For example, a popular fractional Fokker-Planck equation for subdiffusion can be obtained from an underlying CTRW with scale-free waiting time distributions [10, 11]. Further examples can be found in [86, 89].

Lévy flight models and fractional evolution equations have been particularly successful in two branches of physics, nonlinear dynamics and statistical physics. Although the mathematics is similar, the interpretation and treatment of the equations involved can differ, compare for example the recent analogous reviews by Metzler and Klafter [88] and Zaslavsky [141]. In chaotic systems, Lévy flights and a variant of them known as Lévy walks, introduced by Geisel et. al. [45], model irregular but deterministic trajectories. The associated fractional Fokker-Planck equations can be interpreted within the framework of thermodynamics of chaotic systems [15]. On the other hand, Lévy flights are frequently employed in statistical physics by means of fractional Langevin equations, in which Lévy stable white noise serves as a highly fluctuating perturbation to a deterministic dynamics [79]. Anomalous noise and deterministic evolution represent independent components of the dynamics. The associated evolution equations generally violate ordinary Gibbs-Boltzmann thermodynamics, and Lévy flights in statistical mechanics typically model non-equilibrium phenomena. In fact, fractional Langevin dynamics and the associated fractional Fokker-Planck equations can be related to non-extensive generalizations of Gibbs-Boltzmann thermodynamics known as Tsallis statistics [26, 105, 123]. Fractional Fokker-Planck equations of this type have attracted much attention in the past [60].

A number of superdiffusive processes evolve in inhomogeneous environments which can be described as external position dependent force fields or potentials. Generally, external fields change the dispersion properties of randomly moving



particles [51]. The influence of external forces can be drastic, especially if they represent a quenched random disorder [5, 19, 118]. External forces, potentials or inhomogeneities can be incorporated into *ordinary* diffusion equations in a straightforward manner by appropriate position dependent drift and diffusion coefficients. In *subdiffusive* systems spatial inhomogeneities generally pose no problem, because subdiffusion is intrinsically a temporal anomaly; spatial inhomogeneity and temporal anomaly represent independent components of the equations involved. In contrast to the above, external fields are a subtle issue in *superdiffusive* fractional evolution equations. Due to the spatially non-local nature of fractional integro-differential operators, no generic way of including position dependent external fields exists, and various possible ways correspond to various physical situations, see for example [25].

The impact of external fields on superdiffusive motion has been studied primarily and extensively within the generalized Langevin scenario [40, 41, 56] which to this day seems to be considered the standard framework for superdiffusion in external fields. However, this approach imposes severe restrictions on the range of systems it can describe. Due to the violation of Gibbs-Boltzmann thermodynamics mentioned above, the fractional Langevin scheme is inappropriate for systems which are thermally inconspicuous.

However, a variety of superdiffusive phenomena occur in a thermally equilibrated medium, for example the intracellular translocation mechanisms mentioned above. The observed enhanced diffusion is caused by the complex topology of the structures on which random motion evolves and not by anomalous noise. The same reasoning applies to random motion on complex scale-free networks, which have attracted much attention recently [2]. Examples of such networks are the internet [3], metabolic networks [58] and social networks such as the cooperation network of film-actors and citation of scientific collaborators [9]. Random motion on scale-free networks is generally anomalous as well [59, 61, 65, 97] and has been investigated in the light of epidemics spreading on these structures [18, 99, 129]. Superdiffusion in scale-free networks is caused by a scale-free connectivity, rather than scale-free fluctuations in a random force. The study of dispersion phenomena on complex networks is particularly important, because it can be used as a basis for devising optimal search strategies in modern technological scale-free networks [1, 92]. In a similar vein, early ideas of optimal search strategies of foraging animals [66] have recently been investigated in models incorporating Lévy flights [12, 17, 126, 128].

For some reason, inhomogeneities in scale-free networks and search strategies have evaded scientific attention. This seems surprising not only because intracellular translocation generally occurs on hetero-polymeric media, but also because the inhomogeneous distribution of resources in an animal's habitat is known to impact on the foraging strategy in some cases [52, 72]. A possible explanation might be the fact that these inhomogeneities are bounded in magnitude and typically fluctuate



as a function of position about some mean value, and the popular approach of fractional Langevin dynamics is asymptotically trivial for such external fields.

Moreover, contemporary models for random motion in complex environments are based on microscopic rate equations, and predictions rely largely on numerical simulations. An exception are models which assume a homogenous, isotropic environment. Unlike superdiffusion in chaotic systems and in non-equilibrium statistical mechanics, which are equipped with standard fractional evolution equations, a unifying fractional approach which combines scale-free topological features with external inhomogeneities is still missing, and universal features of these systems have yet to be revealed.

In this thesis the novel concept of topological superdiffusion is introduced. Based on a plausible underlying mechanism which combines scale-free topological structures and the requirements of Gibbs-Boltzmann statistics, we mold a fractional Fokker-Planck equation which is suitable for the description of the majority of superdiffusive phenomena to have been discovered in experiments in the recent past. The approach unifies a number of models which exhibit identical behavior despite their differences in details, and permits a treatment by the powerful tool of fractional calculus [21]. The approach is general enough to be applicable to any of the aforementioned intracellular translocation phenomena, such as motion of regulatory proteins on folded DNA strands or relaxation dynamics on complex scale-free inhomogeneous networks.

The differences between topological superdiffusion and other popular fractional approaches is established in a detailed scaling analysis and for paradigmatic systems such as the harmonic potential and escape dynamics in a double well potential, see also [25]. In addition, we map the fractional Fokker-Planck equation onto a fractional Schrödinger equation, which permits a treatment and interpretation in terms of quantum mechanical concepts.

Within this new approach we predict that topologically superdiffusive processes exhibit a rich palette of behaviors when external inhomogeneities are present, unlike fractional Langevin dynamics which is unaffected by bounded external fields. We investigate in detail topological superdiffusion in periodic potentials [24]. A generalized Bloch theory is devised and band-spectra of superdiffusive process are computed and compared. The band structure of superdiffusion in periodic potentials is not only very appealing, but also reveals a number of important consequences, for example a high sensitivity of transient dynamics to small changes in temperature, a behavior not seen in ordinary diffusion.

Subsequently, we investigate the impact of random potentials in the paradigmatic system of diffusion on rapidly folding linear hetero-polymers [22]. We show that superdiffusive relaxation dynamics in external fields is strongly susceptible to the overall structure of the potential, as opposed to ordinary diffusion which primarily depends on magnitude variations of the inhomogeneity. Comparing the asymptotics of various degrees of superdiffusion, reflected in the Lévy exponent μ ,



we show that on large spatio-temporal scales the response to the external field is universal, with a discontinuous change in behavior in the limiting case of ordinary diffusion.

In both periodic and random potentials, a perturbation analysis reveals that relaxation dynamics is typically fastest for intermediately superdiffusive processes, and slow for nearly diffusive processes and strongly superdiffusive Lévy flights. This is rather counterintuitive and vastly different from the common belief that the response to external fields decreases with the degree of enhanced diffusion. Our results suggest that search strategies in inhomogeneous environments are optimal for Lévy flights with intermediate Lévy exponents. This prediction is confirmed in a number of experimental observations [20, 23, 106, 127].

As an example, we address the issue of optimal random search in a phenomenological model for human saccadic eye movements. We show that saccadic eye movements can be described as Lévy flights in a inhomogeneous landscape of visual salience. The similarity between model trajectories and real saccadic trajectories is striking, despite the fact that neither memory effects nor spatial hierarchies of processing are involved. The model is equivalent to topological superdiffusion on large scales and predicts intermediate values of the Lévy exponent for optimal search, which is confirmed by psychophysical experiments.

This thesis is organized as follows. Chapter 2 comprises the fundamentals of ordinary diffusion, Lévy flights and superdiffusion. In chapter 3, the central ideas leading to topological superdiffusion are provided along with the novel fractional Fokker-Planck equation. The approach is compared to various others in chapter 4. In chapters 5 and 6, topological superdiffusion is investigated in periodic and quenched random potentials, respectively. The main results, consequences, implications and perspectives on forthcoming research are provided in the discussion at the end. Technical and supplementary information is provided in the Appendices.



2. Everything You Always Wanted to Know About Superdiffusion, but Were Afraid to Ask

A journey of a thousand miles
begins with a single step.

(Lao Tzu)

This chapter offers an introduction to contemporary theoretical concepts for the description of superdiffusive phenomena. The theory of ordinary random walks is discussed and basic related concepts such as the central limit theorem, the Wiener process, stochastic differential equations, and the Fokker-Planck equation (FPE) are explained. Subsequently, superdiffusive random walks known as Lévy flights are introduced, characterized and compared to ordinary random walks. We present the mathematical framework of fractional dynamics, which is intimately connected to anomalous diffusion. Particular emphasis is placed on generalized Langevin dynamics, which is the most popular and thoroughly investigated scenario in which Lévy flights play a role. We derive and investigate the associated fractional Fokker-Planck equation (FFPE). The physical implications of this approach are critically investigated, and the subtleties concerning canonical fractional generalizations of ordinary diffusion are revealed. We present a recently developed theory of superdiffusion from temporal subordination which obeys ordinary Gibbs-Boltzmann thermodynamics, as opposed to generalized Langevin dynamics which does not. The contents of this chapter represent the current state of the art research on superdiffusive motion.

2.1. Random Walks

Random walks in physics, mathematics and other fields of research are usually introduced as a sum of independent identically distributed random variables X_n . These random variables can be interpreted as the single steps a random walker takes, and the sum

$$Y_N = \sum_{n=1}^N X_n, \quad (2.1)$$



represents the location of the random walker after N steps. Without loss of generality we restrict ourselves to one-dimensional random walks, i.e. $X_n, Y_N \in \mathbb{R}$. In the following we assume that single displacements possess the same probability density function (pdf)

$$\rho_X(x) = \langle \delta(X_n - x) \rangle. \quad (2.2)$$

Furthermore, we assume that $\rho_X(x)$ is an even function of position, a step of specific length into one direction is just as likely to occur as a step of the same length into the opposite direction,

$$\rho_X(x) = \rho_X(-x). \quad (2.3)$$

If $\rho_X(x)$ decreases with distance sufficiently rapidly, the expectation value of each step X_n vanishes and the second moment is given by the variance σ^2 , i.e.

$$\langle X_n \rangle = 0, \quad \text{and} \quad \langle X_n^2 \rangle = \sigma^2. \quad (2.4)$$

The typical size of a step X can be quantified by the root of the second moment,

$$X \sim \sigma. \quad (2.5)$$

Equation (2.4) implies

$$\langle Y_N \rangle = 0, \quad \text{and} \quad \langle Y_N^2 \rangle = N\sigma^2. \quad (2.6)$$

Heuristically, the typical value of the sum Y_N as a function of the number of steps N is given by

$$Y_N \sim \sigma\sqrt{N}. \quad (2.7)$$

The sum increases with the square root of the number of steps, a fundamental property intrinsic to all processes which are founded on the simple random walk picture. For example, all ordinary diffusion processes exhibit this behavior.

2.1.1. The Central Limit Theorem

The probability density $\rho_{Y_N}(y)$ for finite N depends on the density $\rho_X(x)$ of the single steps and is not defined in the limit $N \rightarrow \infty$, simply because all moments $\langle Y_N^m \rangle \propto N$ are divergent in that limit. However, the probability density of the sum converges to a Gaussian, if the sum is properly rescaled. This is the key statement of the central limit theorem [38]. In other words, the random variable

$$Z_N = \frac{Y_N}{\sigma\sqrt{N}} \quad (2.8)$$

has a well defined limit density, i.e.

$$\lim_{N \rightarrow \infty} \rho_{Z_N}(z) = \lim_{N \rightarrow \infty} \left\langle \delta \left(\frac{Y_N}{\sigma\sqrt{N}} - z \right) \right\rangle = \frac{1}{\sqrt{2\pi}} \exp \left(-\frac{z^2}{2} \right). \quad (2.9)$$

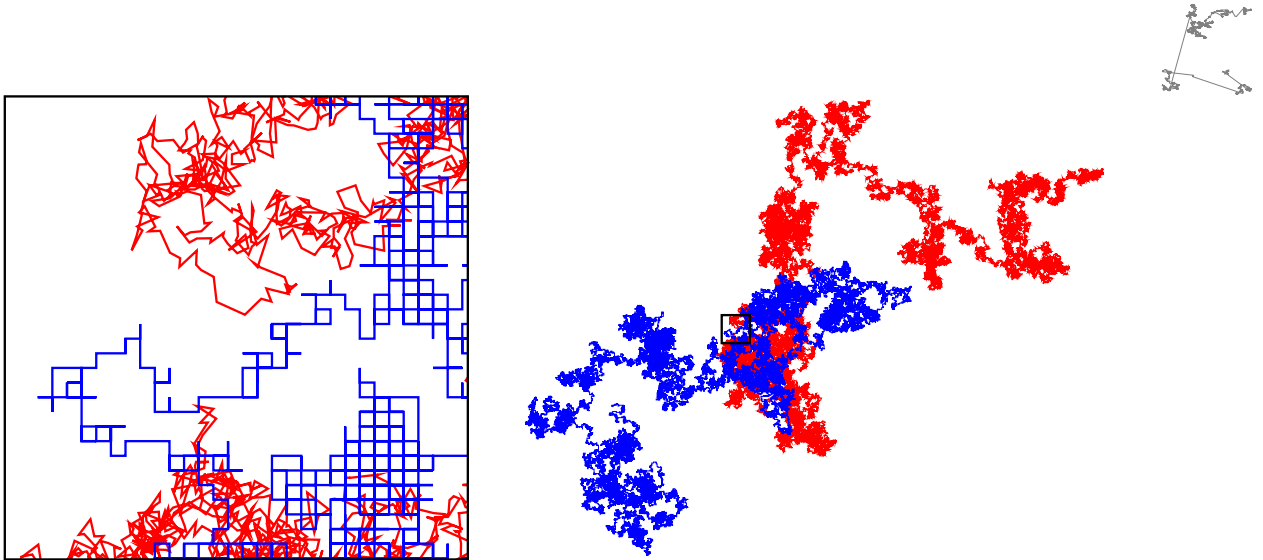


Figure 2.1.: The central limit theorem graphically. The trajectories on the right are realizations $\mathbf{X}_n = (x_1, x_2)_n$ of two different two-dimensional random walks. The red trajectory was generated from a single step density $\rho_{\mathbf{X}}(x_1, y_2) = \pi^{-1} \exp[-(x_1^2 + x_2^2)]$. The blue random walk consists of single steps equally distributed among the four points of the compass with step length $|\mathbf{X}| = 1$. The left panel is a magnification of the region indicated by the little square. On this microscopic scale the difference in single step probabilities is obvious but cannot be noticed on large scales, the trajectories on the right can not be distinguished from each other.

This is a very important result. Irrespective of the functional properties of the single step density $\rho_{\mathbf{X}}(x)$, the rescaled sum (2.8) has a Gaussian density, which is why the Gaussian pdf plays such a universal role in stochastics and physics.

The universality of the Gaussian as a limit distribution of a wide class of random walks is depicted graphically in figure 2.1.

2.1.2. The Wiener Process

If the individual steps are associated with time, random walks become stochastic processes. If the requirements for the central limit theorem are fulfilled, the universality of the Gaussian limit distribution leads to a universal stochastic process, known as the Wiener process $W(t)$, named after Norbert Wiener for his mathematical treatment of Brownian motion [132]. Assume that each step in the random walk takes a time Δt such that after N steps the time

$$t = N\Delta t. \quad (2.10)$$



has elapsed. Identifying $W(t)$ with Y_N in (2.1) we have

$$W(t) = \sum_{n=1}^N \Delta W_n \quad \text{with} \quad \Delta W_n = X_n. \quad (2.11)$$

In the limit

$$N \rightarrow \infty \quad \text{and} \quad \Delta t \rightarrow dt, \quad \text{with} \quad t = N\Delta t \quad (2.12)$$

the quantity $W(t)$ becomes a time continuous process, provided we scale the variance σ of single steps ΔW_n appropriately as

$$\sigma = \sqrt{\Delta t} \rightarrow \sqrt{dt}. \quad (2.13)$$

The sum (2.11) becomes an integral in this limit, i.e.

$$W(t) = \int_0^t dW(t'). \quad (2.14)$$

The infinitesimal increments $dW(t)$ are stochastically independent, the moments are given by

$$\begin{aligned} \langle dW^{2n+1} \rangle &= 0 \quad \text{and} \\ \langle dW^{2n+2} \rangle &= \frac{2^{1+n}\Gamma(3/2+n)}{\sqrt{\pi}} dt^{1+n} \quad n \in \mathbb{N}_0. \end{aligned} \quad (2.15)$$

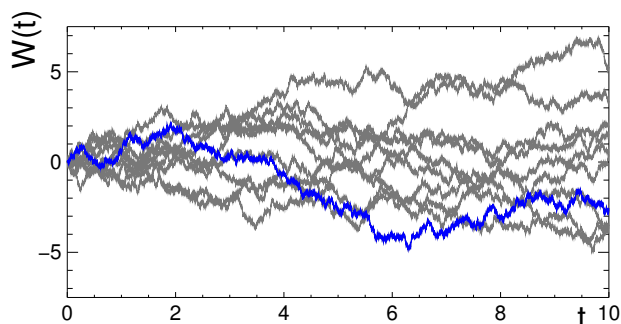
Odd moments vanish, the variance is dt and all higher moments are $\mathcal{O}(dt^2)$. The typical value of a random increment is thus $\mathcal{O}(\sqrt{dt})$. Since the increments are independent, the process $W(t)$ is Markovian and the propagator $p(w, t|w', t')$ of finding a value $W(t) = w$ at time t , provided that $W(t') = w'$, is a spreading Gaussian,

$$p(w, t|w', t') = \frac{1}{\sqrt{2\pi(t-t')}} \exp\left(-\frac{(w-w')^2}{2(t-t')}\right) \quad \text{with} \quad t > t'. \quad (2.16)$$

The process $W(t)$ is known as the Wiener process and plays a very important role in physics. The sample paths of $W(t)$ are continuous but nowhere differentiable.

Figure 2.2 depict a few trajectories of the Wiener process as a function of time. Each curve is very wiggly.

Figure 2.2.: Realizations of the Wiener process $W(t)$ as a function of time with initial condition $W(0) = 0$. Trajectories are continuous but nowhere differentiable. The time evolution of the conditional probability $p(w, t|0, 0)$ is given by equation (2.16).



2.2. Physics

The Wiener process represents the most widely used stochastic process in theoretical physics, but also in many other sciences. And there is a reason for it. Quite often the smooth time evolution of, say, a particle is perturbed by an erratic random force which consists of microscopic, uncorrelated kicks. Whenever the kicks are small enough in magnitude such that on the scale of interest the trajectory of the particle is a continuous function of time, the Wiener process emerges quite naturally in the evolution equations which correctly describe the system. More precisely, let a physical system evolve according to

$$\dot{x} = F(x, t). \quad (2.17)$$

If the system is subjected to a highly irregular non-deterministic fluctuating force $\Gamma(t)$ with zero mean and no temporal correlation relative to the typical observation time, i.e.

$$\langle \Gamma(t) \rangle = 0, \quad \langle \Gamma(t)\Gamma(t') \rangle = \delta(t - t'), \quad (2.18)$$

the complete dynamics is described by the stochastic differential equation also known as a Langevin equation,

$$\dot{x} = F(x, t) + \sqrt{D(x, t)} \Gamma(t). \quad (2.19)$$

The function $D(x, t) > 0$ quantifies the influence of the stochastic force on the dynamics. Usually, the fluctuating force is assumed to be Gaussian white noise. The Gaussian nature of the noise, however, is difficult to extract from the expectation values (2.18). In fact, no Gaussian has an infinite variance. It is a pathological and unattractive property of $\Gamma(t)$. Also, differential equations implicitly contain a limiting procedure which does not have to be defined because everyone knows them anyway. The limiting procedure which leads to (2.19), however, is ambiguous and may lead to trouble, misunderstanding and superfluous discussions with colleagues. For a transparent discussion of the problem of interpreting stochastic differential equations the reader is urged to consult [44].



2.2.1. Diffusion Processes and Langevin Dynamics

The difficulties can be eased by rewriting the the differential equation (2.19) as

$$dX(t) = F(X, t)dt + \sqrt{D(X, t)} dW(t), \quad (2.20)$$

which gives a more intuitive picture of the mathematics, because we can connect it more precisely to the original difference equation

$$\Delta X(t) = X(t + \Delta t) - X(t) = F(X(t), t)\Delta t + \sqrt{D(X(t), t)}\Delta W(t; \Delta t), \quad (2.21)$$

of which (2.20) represents the limit $\Delta t \rightarrow 0$. At each point t in time the increment $\Delta X(t)$ consists of a deterministic drift $F(X(t), t)\Delta t$ proportional to Δt as in any ordinary dynamical system, and a random perturbation $\sqrt{D(X(t), t)}\Delta W(t; \Delta t)$, where

$$\Delta W(t; \Delta t) = W(t + \Delta t) - W(t) \quad (2.22)$$

is the difference of a Wiener process taken at two times separated by Δt . $\Delta W(t; \Delta t)$ is a Gaussian random variable with zero mean and a variance of Δt . Note that the factor $\sqrt{D(X(t), t)}$ is evaluated at the beginning of each time interval in the difference equation (2.21). This is important, because the integration of such an equation gives different results depending on where in the interval $[t, t + \Delta t]$ the function D is evaluated. One must provide this information in order to interpret the stochastic differential equation (2.20) unambiguously. The definition above is known as the Ito-interpretation, and in the following we will cling to it exclusively. The technical treatment of stochastic differential equations in this way is much less prone to errors and easier in many ways. For example one can compute the first two moments of $dX(t)$ without a problem,

$$\begin{aligned} \langle dX(t) \rangle &= \langle F(X(t), t) \rangle dt \quad \text{and} \\ \langle dX(t)^2 \rangle &= \langle D(X(t), t) \rangle dt + \mathcal{O}(dt^2). \end{aligned} \quad (2.23)$$

Therefore, $dX(t) = \mathcal{O}(\sqrt{dt})$ and realizations $X(t)$ are generally non-differentiable.

The evolution of the propagator $p(x, t|x_0, t_0)$ for such processes is governed by the Fokker-Planck equation (FPE)

$$\partial_t p(x, t|x_0, t_0) = \left(-\partial_x F(x, t) + \frac{1}{2}\partial_x^2 D(x, t) \right) p(x, t|x_0, t_0), \quad (2.24)$$

which can be obtained from (2.20) (see Appendix B). Processes $X(t)$ which solve a Langevin equation and possess a propagator solving the FPE are known as diffusion processes. Their realizations are continuous, wiggly functions of time. Observe that when $F \equiv 0$ and $D = D_0$ in the Langevin equation (2.20), we have

$dX(t) = \sqrt{D_0}dW(t)$ and consequently $X(t) = \sqrt{D_0}W(t)$. The variance of the process is

$$\langle X^2(t) \rangle = D_0 t. \quad (2.25)$$

The function $D(x, t)$ is known as the diffusion coefficient. The FPE for the Wiener process ($D_0 = 1$) is given by

$$\partial_t p(x, t|x_0, t_0) = \frac{1}{2} \partial_x^2 p(x, t|x_0, t_0), \quad (2.26)$$

consistent with the explicit form provided by equation (2.16).

2.2.2. Probabilistic Models

The description of a physical system in terms of a Langevin equation and the associated FPE is reasonable whenever the ansatz of deterministic evolution with additive white noise can be made. However, the range of application of these concepts is much wider. If we start with a purely probabilistic model then quite often the system behaves asymptotically as a diffusion process. Say a system is correctly described by a master equation,

$$\partial_t p(x, t|x_0, t_0) = \int dy [w(x|y, t) p(y, t|x_0, t_0) - w(y|x, t) p(x, t|x_0, t_0)], \quad (2.27)$$

where the rate of transition $w(x|y, t)$ from y to x is defined as

$$w(x|y, t) = \lim_{\Delta t \rightarrow 0} \frac{1}{\Delta t} p(x, t + \Delta t|y, t) \quad x \neq y. \quad (2.28)$$

A Kramers-Moyal expansion of the rate yields an evolution equation in terms of differential operators [109],

$$\partial_t p(x, t|x_0, t_0) = \sum_{n=1}^{\infty} \frac{(-\partial_x)^n}{n!} m_n(x, t) p(x, t|x_0, t_0). \quad (2.29)$$

The coefficients $m_n(x, t)$ are the conditional moments of the rate, i.e.

$$m_n(x, t) = \frac{1}{dt} \langle dX(t) | X(t) = x \rangle = \int dy (x - y)^n w(x|y, t). \quad (2.30)$$

In numerous applications the rates possess typical spatial and temporal scales σ and τ , respectively. On scales much larger than these, the coefficients in (2.30) with $n > 2$ become negligible and the series can be approximated by the first two terms,

$$\partial_t p(x, t|x_0, t_0) = \left(-\partial_x m_1(x, t) + \frac{1}{2} \partial_x^2 m_2(x, t) \right) p(x, t|x_0, t_0), \quad (2.31)$$



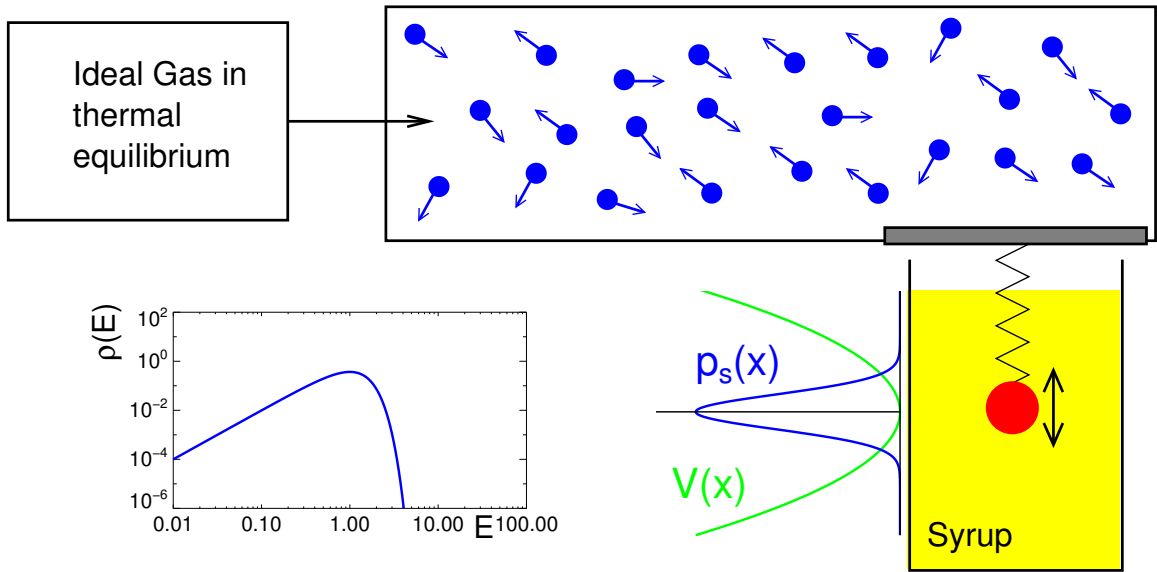


Figure 2.3.: Langevin dynamics in a thermally equilibrated system. A mass (red object) is attached to a Hookean spring and is emerged in a liquid of high viscosity such that the motion is overdamped. The spring is attached to an ideal gas (blue, little objects in container) and energy transfer is permitted by means of a piston or a membrane (gray area). Each degree of freedom in the ideal gas has a typical energy $\langle E \rangle$ which defines the temperature $k_B T = \beta^{-1}$. On a double-logarithmic scale the distribution of energies $\rho(E)$ (qualitative sketch on the lower left) is confined to a range around that value. The harmonic potential $V(x) = x^2$ as a function of displacement is indicated by the green curve. The Gibbs-Boltzmann equilibrium $p_s(x) \propto \exp[-\beta x^2]$ is superimposed in blue.

which is identical to (2.24) if we let $m_1 = F$ and $m_2 = D$. Therefore, even purely stochastic models can be interpreted in terms of deterministic dynamics subjected to Gaussian white noise. On scales for which (2.31) represents an accurate approximation, the trajectories of the process may be considered continuous. An example of this is given in section 3.2.1, in which an FPE for a hopping process along a linear extended hetero-polymer is derived.

2.3. Thermodynamics

Although Langevin equations can be employed for all sorts of systems, they are of particular importance for modeling the influence of a thermal heat bath on deterministic dynamics. A paradigmatic system is depicted in figure 2.3. An overdamped particle is attached to a Hookean spring which interacts with an ideal gas at temperature T . The dynamics of the particle is described by the Langevin



equation

$$dX = -\beta \frac{dV}{dX} dt + \sqrt{2} dW, \quad (2.32)$$

where the potential $V(x) = x^2$ reflects the harmonic potential energy of the spring, $\beta = (k_B T)^{-1}$ is the inverse temperature, and $\sqrt{2}dW$ are random increments induced by momentum transfer from the heat bath in the microscopic time interval dt ¹. The FPE for the stochastic position variable $X(t)$ is given by

$$\partial_t p(x, t|x_0, t_0) = \left(2\beta \partial_x x + \partial_x^2\right) p(x, t|x_0, t_0). \quad (2.33)$$

This process was first investigated by Uhlenbeck and Ornstein in 1930 [124]². Two basic properties of this FPE reflect the underlying thermodynamical properties of the complete system. First, the stationary density is given by the Gibbs-Boltzmann equilibrium,

$$p_s(x) \propto \exp[-\beta V(x)] = \exp[-\beta x^2], \quad (2.34)$$

and detailed balance is fulfilled [109]. The inconspicuous thermal behavior of equation (2.32) and (2.33) is directly linked to the fact that in thermal equilibrium, each degree of freedom has a characteristic typical energy of $\approx k_B T$, reflected in the typical microscopic scale of the noisy increment of the Wiener process dW . This is no longer the case if dW is replaced by a more general type of white noise, as will be revealed below.

2.4. A Tale of Tails

In section 2.1 two basic conditions had to be fulfilled, in order for the central limit theorem to ensure that the properly rescaled sum (2.8) had the Gaussian limiting density (2.9). First, the single steps X_n of the random walk had to be stochastically independent. Furthermore the variance $\langle X_n^2 \rangle$ had to be well defined. Unfortunately, quite a number of densities fail to possess a well defined variance. For instance

$$p_X(x) = \frac{\mu}{2} \begin{cases} \frac{1}{|x|^{1+\mu}} & |x| \geq 1 \\ 0 & |x| < 1 \end{cases} \quad 0 < \mu \leq 2, \quad (2.35)$$

does not. This is not an unusual phenomenon. For example, if we generated a random number Z on a computer by dividing two normally distributed random

¹There is a factor of $\sqrt{2}$ ornamenting the Wiener increment dW in equation (2.32) which seems arbitrary but isn't. It will be useful at later stages of our investigation.

²For some reason the process is known as the Ornstein-Uhlenbeck process and not, as one might expect from the ordering of the authors of the cited paper the Uhlenbeck-Ornstein process.

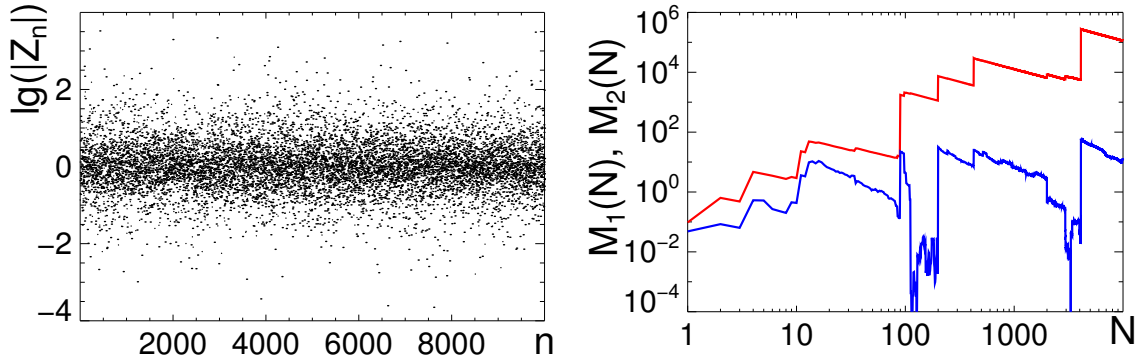


Figure 2.4.: Random numbers with divergent moments. The left panel depicts a sequence of $N = 10,000$ random numbers generated from the density (2.35). In order to estimate the range of values the common logarithm of the absolute value of Z_n is shown. The right panel shows the averages $M_1(N)$ (blue) and $M_2(N)$ (red) defined by equations (2.37) and (2.38) as function of sample size N . With increasing N the averages do not converge.

numbers X and Y the density of the result is given by

$$\langle \delta(X/Y - z) \rangle = \frac{1}{\pi(1 + z^2)}, \quad (2.36)$$

which shows the same asymptotic behavior as (2.35) with $\mu = 1$. More details on how to generate random numbers with power law densities numerically are provided in Appendix E and in [81]. Divergent variances are not just a mathematical peculiarity. In fact if we generated a set $\{Z_n\}_{n=1\dots N}$ of numbers on a computer and tried to estimate the expectation values $\langle Z \rangle^2$ and $\langle Z^2 \rangle$ by a finite sample of size N ,

$$M_1(N) = \overline{Z}_N^2 = \left(\frac{1}{N} \sum_{n=1}^N Z_n \right)^2 \quad (2.37)$$

$$M_2(N) = \overline{Z^2}_N = \frac{1}{N} \sum_{n=1}^N Z_n^2 \quad (2.38)$$

and investigate the averages $M_1(N)$ and $M_2(N)$ as functions of sample size N , we would see that they diverge. The divergence of $M_1(N)$ illustrated in figure 2.4 strikes us as somewhat surprising because the density (2.35) is symmetric and one might guess that $\langle Z \rangle$ vanishes.

All pdfs which behave asymptotically as the inverse power law (2.35) lack a well defined variance. This property implies an absence of scale in random numbers drawn from these pdfs. Scale-free densities appear in many natural system such as income distributions (Pareto's law) [6, 98], the distribution of body sizes of terrestrial animals [84], city sizes [140, 142], and the fluctuation of market indices [49], to



give only a few examples. An interesting collection of power laws in nature can be found in [115].

Of course one could argue that in a realistic system there needs to be a natural cut-off beyond which the inverse algebraic decay no longer holds, and is replaced by a faster decay such that no divergent variance is observed. This argument is a metaphysical one as long as it cannot be repudiated by an experiment. After all, individual measurements give finite values even if the underlying density lacks a scale. Therefore, as long as no evidence for a cut-off is given by experiments, it is safe to assume the absence of one. Furthermore, even when the inverse power law is truncated, the convergence of averages such as (2.37) and (2.38) is very slow [82].

2.4.1. Lévy Flights

Consider now a random walk consisting of independent increments ΔL_n . After N steps the position is denoted by L_N ,

$$L_N = \sum_{n=1}^N \Delta L_n. \quad (2.39)$$

Unlike the random walk defined by (2.1), the increments ΔL_n are drawn from a pdf $\rho_{\Delta L}(l)$ which asymptotically follows a power law,

$$\rho_{\Delta L}(l) \sim \frac{1}{|l|^{1+\mu}}, \quad \text{with } 0 < \mu \leq 2. \quad (2.40)$$

For simplicity we assume that $\rho_{\Delta L}(l)$ is symmetric, i.e.

$$\rho_{\Delta L}(l) = \rho_{\Delta L}(-l). \quad (2.41)$$

For the range of exponents μ given in (2.40), the variance of the location after N steps $\langle L_N^2 \rangle$ is not defined, simply because the variance of each single step $\langle \Delta L_n^2 \rangle$ is not. Note also that although the density $\rho_{\Delta L}(l)$ is symmetric, when $\mu \leq 1$ the expectation value $\langle L_n \rangle$ is divergent despite the symmetry (2.41).

The question is now whether a properly rescaled position variable L_N has a limit distribution, and if so what it is. This question was first thoroughly investigated and answered by Khintchine and Lévy [63, 74]. The answer is a generalization of the central limit theorem discussed above. For a sum (2.39) with symmetrically distributed increments according to (2.40), one can find a number σ such that the random variable

$$Z_N = \frac{L_N}{\sigma N^{1/\mu}} \quad (2.42)$$

has a limit pdf

$$G_\mu(z) = \lim_{N \rightarrow \infty} \langle \delta(Z_N - z) \rangle, \quad (2.43)$$



which depends on the exponent μ . The limit pdf $G_\mu(z)$ is known as the symmetric Lévy stable law of index μ . The index is also commonly referred to as the Lévy exponent. $G_\mu(z)$ has a simple form when expressed as a Fourier integral,

$$G_\mu(z) = \frac{1}{2\pi} \int dk e^{-ikz - |k|^\mu}. \quad (2.44)$$

This holds for all values of $\mu \in (0, 2]$. When $\mu = 1$ the Lévy stable law is the Cauchy pdf (2.36), whereas when $\mu = 2$ the Gaussian pdf is recovered³. Generally, it is difficult to give an explicit expression for $G_\mu(z)$. However, Lévy stable laws can be expressed in terms of Fox H -functions [131]. Asymptotically, the stable laws exhibit the same behavior as their underlying microscopic step pdf $\rho_{\Delta L}(l)$, i.e.

$$G_\mu(z) \sim \frac{1}{|z|^{1+\mu}} \quad |z| \gg 1. \quad (2.45)$$

Therefore, trajectories L_N possess a self-similar geometric structure.

The scaling factor in (2.42) suggests that the location L_N increases with distance as

$$L_N \sim N^{1/\mu}. \quad (2.46)$$

Comparing this to the analogous equation (2.7) for ordinary random walks, we see that L_N increases faster since $\mu < 2$. This is the reason why these types of random walks are known as Lévy flights⁴.

2.4.2. Lévy Stable Processes

Proceeding in the same way as in section 2.1.2, a continuity limit of the sum (2.39) leads to a time-continuous process $L_\mu(t)$ which is a generalization of the Wiener process $W(t)$. Processes $L_\mu(t)$ are known as symmetric Lévy stable processes. We let $t = N\Delta t$ and carry out the limit

$$N \rightarrow \infty, \quad \text{and} \quad \Delta t \rightarrow dt, \quad (2.47)$$

keeping t fixed. The parameter σ in (2.42) must be scaled with Δt according to

$$\sigma = \Delta t^{1/\mu} \rightarrow dt^{1/\mu}, \quad (2.48)$$

³Note that an asymptotic tail with $\mu = 2$ still yields a logarithmically divergent second moment. However, the stable law $G_2(z)$ is still a Gaussian. Thus, for the ordinary central limit theorem a finite variance represents a sufficient but not a necessary condition.

⁴The term *flight* is intended to indicate fast movement as opposed to the word *walk*. However, this can lead to some confusion, because another class of random walks known as Lévy walks [45] are superdiffusive as well. The difference between Lévy flights and Lévy walks is the amount of time that elapses during a displacement. For a Lévy flight this time is zero, whereas for a Lévy walk the time duration of a step is proportional to the distance of the step.



which deviates from the scaling relation (2.13) appropriate for ordinary random walks. With (2.47) and (2.48) the sum (2.39) yields a generalization of the integral (2.14), i.e.

$$L_\mu(t) = \int_0^t dL_\mu(t'). \quad (2.49)$$

Lévy stable processes share a number of features with the Wiener process. For example, the infinitesimal increments are unbiased and independent,

$$\langle \delta(dx - dL_\mu(t)) \rangle = \langle \delta(dx + dL_\mu(t)) \rangle, \quad (2.50)$$

and

$$\begin{aligned} \langle \delta(dx - dL_\mu(t)) \delta(dx' - dL_\mu(t')) \rangle \\ = \langle \delta(dx - dL_\mu(t)) \rangle \langle \delta(dx' - dL_\mu(t')) \rangle \quad t \neq t', \end{aligned} \quad (2.51)$$

respectively. Lévy stable processes are also continuous in probability, that is the probability $P(|L_\mu(t + \Delta t) - L_\mu(t)| > \epsilon)$ of $L_\mu(t)$ exiting an ϵ -ball in the limit $\Delta t \rightarrow 0$ vanishes,

$$\lim_{\Delta t \rightarrow 0} P(|L_\mu(t + \Delta t) - L_\mu(t)| > \epsilon) = 0 \quad \forall \epsilon > 0. \quad (2.52)$$

Symmetric Lévy stable processes are Markovian with a propagator given by a spreading Lévy stable law

$$p(x, t | x_0, t_0) = \frac{1}{2\pi} \int dk e^{-ik(x-x_0) - |k|^\mu(t-t_0)} \quad (2.53)$$

$$= \frac{1}{(t-t_0)^{1/\mu}} G_\mu \left(\frac{x-x_0}{(t-t_0)^{1/\mu}} \right) \quad t > t_0. \quad (2.54)$$

which is a direct consequence of the generalized central limit theorem. The heuristic increase of $L_\mu(t)$ with time

$$L_\mu(t) \sim t^{1/\mu} \quad (2.55)$$

appears in the argument of G_μ in (2.54) and reflects the time-continuous analogous expression to (2.46). When $\mu = 2$ the propagator is Gaussian, and comparing (2.53) with (2.16) we see that $L_2(t)$ is proportional to the Wiener process, i.e.

$$L_2(t) = \sqrt{2}W(t). \quad (2.56)$$

A striking difference between $L_\mu(t)$ for $\mu < 2$ and $W(t)$ is that single realizations of $L_\mu(t)$ are almost certainly discontinuous everywhere. If $\mu < 2$ the propagator violates the Lindberg condition [44], that is the integrated probability of exiting a small ϵ -ball in a small time interval Δt decreases more slowly than Δt and



Figure 2.5.: Realizations of a Lévy stable process $L_\mu(t)$ with intermediate exponent $\mu = 1$ (Cauchy process). Each realization is discontinuous everywhere as opposed to realizations of the Wiener process $W(t)$ (compare to figure 2.2). The conditional pdf $p(x, t|0, 0)$ for this process is given by (2.53)

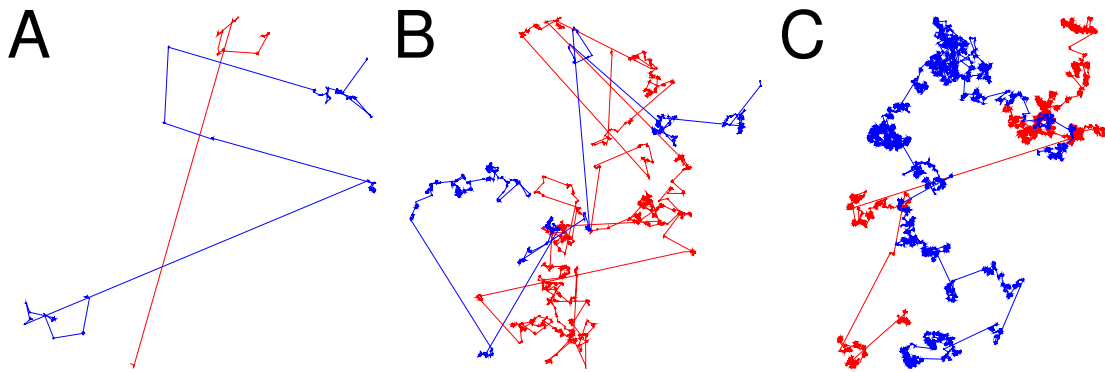
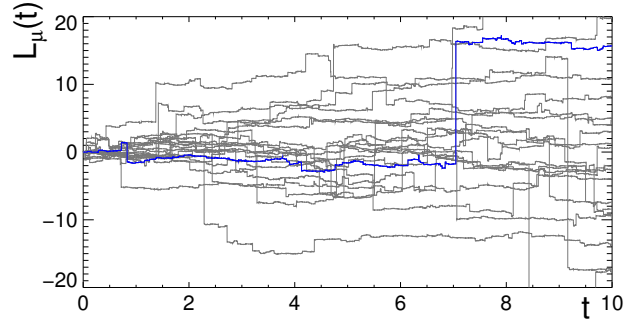


Figure 2.6.: Two dimensional Lévy stable processes with various exponents μ . **A:** A strongly superdiffusive process ($\mu = 3/4$). **B:** the two-dimensional Cauchy process ($\mu = 1$). **C:** A weakly superdiffusive process ($\mu = 3/2$). Each panel shows two realizations in blue and red.

consequently

$$\lim_{\Delta t \rightarrow 0} \frac{1}{\Delta t} \int_{|l-l'| > \epsilon} dl p(l, t + \Delta t | l', t) \neq 0 \quad \forall \epsilon > 0 \quad (2.57)$$

The time evolution of a number of realizations of a Lévy stable process with $\mu = 1$ (Cauchy process) is shown in figure 2.5. As a function of time the trajectories are characterized by discontinuous jumps on all scales, the effect of which increases with decreasing Lévy index μ .

The typical geometry of realizations of two-dimensional Lévy stable processes are depicted in figure 2.6. Three types of processes are compared, a strongly superdiffusive process ($\mu = 3/4$), a process with intermediate exponent ($\mu = 1$), and a weakly superdiffusive process ($\mu = 3/2$). The points visited by a Lévy flight form a fractal with fractal dimension μ if the dimension of the embedding space $d \geq 2$. Typically, Lévy processes consists of clusters connected by large scale jumps (also known as rare events). Clusters consist of smaller cluster which are connected by jumps of the size of the cluster and so on.



2.5. Fractional Calculus

The propagator of a Lévy stable process (2.53) generalizes the Gaussian of the Wiener process. The appropriate generalization of the diffusion equation (2.26) leads to the concept of fractional kinetics, in which ordinary differential operators are replaced by non-local, singular integro-differential operators and the evolution equations are known as fractional diffusion equations, or fractional Fokker-Planck equations (FFPE). The mathematics of fractional integro-differentiation, or fractional calculus is a powerful tool for the study of anomalous diffusion and has contributed considerably to its understanding in the recent past [31, 55, 88, 116, 141]. One can generally distinguish two approaches. The earliest utilization of fractional evolution equations for the description of anomalous transport were phenomenological justified by the fact that they modeled the observed effects sufficiently well [95, 112]. Despite their success, phenomenological models must be scrutinized with care, not only because the underlying physics is often difficult to extract from FFPEs, but also because the implementation of fractional operators introduces a vast variety of often very different possible behaviors. Therefore, a lot of effort has been invested recently in order to establish various FFPEs on solid underlying physical principles, see for example [11, 80, 88].

2.5.1. The Mother of Them All

For simplicity we consider a system which is located at the origin at $t = 0$, and let $p(x, t) = p(x, t|0, 0)$. This implies no loss of generality because the propagator (2.53) is homogeneous in space and time. Its Fourier transform (defined by D.2) attains a very simple form,

$$\tilde{p}(k, t) = e^{-|k|^\mu t}. \quad (2.58)$$

Obviously, $\tilde{p}(k, t)$ fulfills

$$\partial_t \tilde{p}(k, t) = -|k|^\mu \tilde{p}(k, t). \quad (2.59)$$

For $\mu = 2$ equation (2.59) is just an ordinary diffusion equation in Fourier space, because the multiplication by $-k^2$ is equivalent to the Laplacian in position coordinates. But also for $\mu \neq 2$ equations (2.58) and (2.59) appear rather harmless. Notice however, that for $\mu < 2$ the propagator $\tilde{p}(k, t)$ is not analytic at $k = 0$. Since $\tilde{p}(k, t)$ is the characteristic function of $p(x, t)$, this is a signature of the divergent moments of $L_\mu(t)$.

Formally, we may apply the inverse Fourier transform on equation (2.59) and obtain

$$\partial_t p(x, t) = \Delta_x^{\mu/2} p(x, t), \quad (2.60)$$

which defines the operator $\Delta_x^{\mu/2}$ as the inverse Fourier transform of a multiplication by $-|k|^\mu$. The symbol $\Delta_x^{\mu/2}$ indicates that the operator is obtained by raising



the ordinary Laplacian Δ_x to a fractional power $\mu/2$ less than unity. As such, raising the Laplace operator to a fractional power is just a symbolic undertaking. But since Δ is Hermitian on commonly used function spaces, the spectral decomposition theorems of functional analysis imbues $\Delta^{\mu/2}$ with meaning. Still, the physical implication of the generalized diffusion equations (2.59) and (2.60) do not say much about the properties of the processes they describe. These become more obvious when the position representation of the fractional Laplacian is scrutinized. Explicitly, equation (2.60) reads

$$\partial_t p(x, t) = \Delta_x^{\mu/2} p(x, t) = C_\mu \int_{-\infty}^{\infty} dy \frac{p(y, t) - p(x, t)}{|x - y|^{1+\mu}}, \quad (2.61)$$

where $C_\mu = \Gamma(1 + \mu) \sin(\pi\mu/2)/\pi$. The derivation of this representation is provided in Appendix A. Thus, the fractional diffusion equation (2.61) has the form of a master equation

$$\partial_t p(x, t) = \int dy [w(x|y) p(y, t) - w(y|x) p(x, t)], \quad (2.62)$$

with a homogenous non-local transition rate

$$w(x|y) = \frac{C_\mu}{|x - y|^{1+\mu}}. \quad (2.63)$$

The representation (2.61) tells us more about the structure of the process, for example that $L_\mu(t)$ is a jump process. Note also that the rate (2.63) is singular, and that the integral in (2.61) converges because two singularities cancel. The divergence in the rate implies that trajectories are discontinuous everywhere unlike those of pure jump processes which have integrable rates and jumps are interspersed with intervals on which single realizations are constant. Singular rates are typical for processes which are generated from superdiffusive Lévy stable processes. The fractional diffusion equations (2.59) and (2.61) represent the simplest type of superdiffusive FFPE, of which a number of more complicated ones will be investigated in forthcoming chapters.

A few more words need to be said about the fractional Laplacian $\Delta^{\mu/2}$. In the limit $\mu \rightarrow 2$, the fractional Laplacian $\Delta^{\mu/2}$ converges to the ordinary Laplacian Δ , the proof of which is somewhat involved [141]. Also, the square root of the Laplacian $\Delta^{1/2}$ is not to be confused with the first derivative, i.e.

$$\Delta^{1/2} \neq \nabla, \quad (2.64)$$

since

$$-|k| \neq -ik. \quad (2.65)$$



One is tempted to generalize equation (2.61) to exponents μ beyond the interval $(0, 2]$. This is certainly possible for the fractional Laplacian. However, the resultant operator is no longer a stochastic one. In other words, when applied to a probability density, the result will generally violate the requirements of positivity.

2.6. Generalized Langevin Dynamics

A number of physical systems behave superdiffusively because their deterministic evolution is perturbed by an additive, highly fluctuating white noise which lacks a scale, in contrast to the common Gaussian white noise. A change in position ΔX within a small time interval Δt due to the random force follows an inverse power law such that the variance is divergent. Thus, it seems reasonable to generalize the Langevin equation (2.20) by replacing the ordinary Wiener increment with a Lévy stable one, i.e.

$$dX = F(X, t) dt + [D(X, t)]^{1/\mu} dL_\mu. \quad (2.66)$$

The function $D(x, t) > 0$ is the generalized diffusion coefficient and quantifies the influence of the noise as a function of position and time⁵. When $\mu = 2$ equation (2.66) is reduced to an ordinary Langevin equation, since $L_2(t) = \sqrt{2}W(t)$. Again, this stochastic differential equation is the limit of the difference equation

$$X(t + \Delta t) = X(t) + F(X(t), t)\Delta t + [D_\mu(X(t), t)]^{1/\mu} \Delta L_\mu(t, \Delta t), \quad (2.67)$$

in the limit $\Delta t \rightarrow 0$, where

$$\Delta L_\mu(t, \Delta t) = L_\mu(t + \Delta t) - L_\mu(t), \quad (2.68)$$

Hence, equation (2.66) is an Ito-stochastic differential equation. Processes $X(t)$ which can be generated from it share a number of properties with Lévy stable processes. Due to the anomalous increment dL_μ it is clear that $X(t)$ lacks the same moments as $L_\mu(t)$. Consequently, realizations of $X(t)$ are structurally similar to those of $L_\mu(t)$. They possess discontinuous sample paths, a fractal structure and disperse superdiffusively. Since (2.66) represents a generalization of the ordinary Langevin equation, it is reasonable to assume that a generalization of the Fokker-Planck equation governs the evolution of the propagator of the process $X(t)$. The derivation of the ordinary FPE from the underlying Langevin equation given in Appendix B relies on the existence of short time moments of the process and cannot be employed when the noise is Lévy stable. However, the correct generalization can be established by means of characteristic functions. This was done achieved [39] for the special case of non-multiplicative noise, i.e. a constant generalized diffusion coefficient $D(x, t) = D_0$, for alternative approaches see [28, 101].

⁵The power of $1/\mu$ which appears in the random force may seem a bit arbitrary at this point. Don't worry. It isn't.



2.6.1. Mother's Darling

We proceed in a similar fashion, including the more general case of possibly time dependent multiplicative noise. Symmetric Lévy stable processes are Markovian, and from the generalized Langevin equation (2.66) it follows that $X(t)$ is a Markov process as well. Consequently, the conditional pdf obeys the Chapman-Kolmogorov equation

$$p(x, t + \Delta t | x_0, t_0) = \int dy p(x, t + \Delta t | y, t) p(y, t | x_0, t_0). \quad (2.69)$$

We expand $p(x, t + \Delta t | y, t)$ into a Fourier integral,

$$p(x, t + \Delta t | y, t) = \frac{1}{2\pi} \int dk e^{-ik(x-y)} \Phi(k, t + \Delta t | y, t). \quad (2.70)$$

The function

$$\Phi(k, t + \Delta t | y, t) = \int dx e^{ik(x-y)} p(x, t + \Delta t | y, t). \quad (2.71)$$

is the conditional characteristic function of the pdf. The terms $\exp[\pm ik y]$ in equations (2.70) and (2.71) are practical. Because of them, the characteristic function can be expressed as a conditional expectation value of an exponential of the increment $\Delta X(t) = X(t + \Delta t) - X(t)$ as

$$\Phi(k, t + \Delta t | y, t) = \left\langle e^{ik\Delta X(t)} \middle| X(t) = y \right\rangle. \quad (2.72)$$

Inserting (2.70) into (2.69), subtracting $p(x, t | x_0, t_0)$ from both sides, dividing by Δt and performing a Fourier transform with respect to the coordinate x yields

$$\partial_t \tilde{p}(k, t | x_0, t_0) = \lim_{\Delta t \rightarrow 0} \int dy e^{iky} \left[\frac{\Phi(k, t + \Delta t | y, t) - 1}{\Delta t} \right] p(y, t | x_0, t_0). \quad (2.73)$$

It remains to investigate the behavior of the expression in brackets as $\Delta t \rightarrow 0$. To this end, we insert the rhs of the difference equation (2.67) into (2.72) which gives

$$\Phi(k, t + \Delta t | y, t) = \left\langle \exp \left(ik \left[F(X(t), t) \Delta t + [D(X(t), t)]^{1/\mu} \Delta L_\mu(t, \Delta t) \right] \right) \middle| X(t) = y \right\rangle \quad (2.74)$$

Since the process $X(t)$ and the increments $\Delta L_\mu(t, \Delta t)$ are stochastically independent, we can factorize the expectation value,

$$\Phi(k, t + \Delta t | y, t) = \langle \exp(ik F(X(t), t) \Delta t) | X(t) = y \rangle \left\langle \exp \left(ik [D(X(t), t)]^{1/\mu} \Delta L_\mu(t, \Delta t) \right) \middle| X(t) = y \right\rangle. \quad (2.75)$$



The first factor evaluates to

$$\langle \exp(ik F(X(t), t) \Delta t) | X(t) = y \rangle = \exp(ik F(y, t) \Delta t), \quad (2.76)$$

the second one is given by

$$\begin{aligned} \langle \exp(ik [D(X(t), t)]^{1/\mu} \Delta L_\mu(t, \Delta t)) | X(t) = y \rangle = \\ \langle \exp(ik [D(y, t)]^{1/\mu} \Delta L(t, \Delta t)) \rangle. \end{aligned} \quad (2.77)$$

In order to compute the expectation value on the right, we employ the Fourier representation of the conditional pdf (2.53) of the symmetric Lévy stable process and we find

$$\langle \exp(ik [D(y, t)]^{1/\mu} \Delta L(t, \Delta t)) \rangle = \exp(-|k|^\mu D(y, t) \Delta t). \quad (2.78)$$

Combining equations (2.76) and (2.78) the characteristic function reads,

$$\Phi(k, t + \Delta t | y, t) = \exp(ik F(y, t) - |k|^\mu D(y, t) \Delta t) \quad (2.79)$$

$$= 1 + ik F(y, t) \Delta t - |k|^\mu D(y, t) \Delta t + \mathcal{O}(\Delta t^2), \quad (2.80)$$

and thus

$$\lim_{\Delta t \rightarrow 0} \frac{\Phi(k, t + \Delta t | y, t) - 1}{\Delta t} = ik F(y, t) - |k|^\mu D(y, t). \quad (2.81)$$

Substituting into (2.73) we obtain the FFPE in Fourier space, explicitly

$$\partial_t \tilde{p}(k, t | x_0, t_0) = \int dy e^{iky} [ik F(y, t) - |k|^\mu D(y, t)] p(y, t | x_0, t_0). \quad (2.82)$$

An inverse Fourier transformation yields the FFPE in position representation, i.e.

$$\begin{aligned} \partial_t p(x, t | x_0, t_0) = \\ \int dy \left[\int dk e^{ik(y-x)} ik \right] F(y, t) p(y, t | x_0, t_0) \\ - \int dy \left[\int dk e^{ik(y-x)} |k|^\mu \right] D(y, t) p(y, t | x_0, t_0). \end{aligned} \quad (2.83)$$

The terms in brackets can be evaluated by partial integration. They reflect an ordinary first order derivative and a fractional Laplacian of order μ ,

$$\int dk e^{-ik(y-x)} ik = -\delta(y-x) \nabla_x \quad \text{and} \quad (2.84)$$

$$\int dk e^{-ik(y-x)} |k|^\mu = -\delta(y-x) \Delta_x^{\mu/2}. \quad (2.85)$$



With these expression we finally obtain the FFPE for the generalized Langevin equation (2.66),

$$\partial_t p(x, t|x_0, t_0) = \left[-\nabla_x F(x, t) + \Delta_x^{\mu/2} D(x, t) \right] p(x, t|x_0, t_0). \quad (2.86)$$

Both the force coefficient $F(x, t)$ and generalized diffusion coefficient $D(x, t)$ may depend on position x and time t . For $\mu = 2$ the fractional Laplacian is reduced to the ordinary second derivative and we recover an ordinary Fokker-Planck equation (2.24). The factor of $1/2$ present in (2.24) and missing in (2.86) stems from the fact that the diffusive Lévy stable process $L_2(t)$ is not identical to $W(t)$ but rather $L_2(t) = \sqrt{2}W(t)$.

2.6.2. Physics, Again

The FFPE (2.86) is by far the most investigated generalized Fokker-Planck equation for superdiffusive motion [40, 41, 60, 88] which is based on a plausible underlying physical process. Comparing with the ordinary FPE (2.24) we see that Lévy stable white noise introduces an anomalous diffusion term, whereas the drift term remains unaffected. The physical implications of this are revealed most transparently when $D(x, t) = 1$ and in a gradient force field

$$F = -\beta dV/dx,$$

where $V(x)$ is a potential. In this case (2.86) is given by

$$\partial_t p(x, t|x_0, t_0) = \left[\beta \nabla_x \frac{dV}{dx} + \Delta_x^{\mu/2} \right] p(x, t|x_0, t_0). \quad (2.87)$$

The key feature of this type of FFPE is the violation of ordinary Gibbs-Boltzmann thermodynamics. Neither is the stationary solution to (2.87) the Gibbs-Boltzmann equilibrium, i.e.

$$p_s(x) \neq e^{-\beta V(x)}, \quad (2.88)$$

nor is detailed balance fulfilled. Consider the harmonic potential $V(x) = x^2$, which is investigated in detail in section 4.4.3. This system can be solved [60] and the stationary solution is given by the Lévy stable law

$$p_s(x) = \frac{1}{2\pi} \int dk \exp \left(-ikx + \frac{|k|^\mu}{2\mu\beta} \right), \quad (2.89)$$

which is clearly different (for $\mu < 2$) from the Gaussian expected for Gibbs-Boltzmann thermodynamics.

In figure 2.7 the generalization of the physical system discussed in figure 2.3, section 2.2.1 is depicted. As opposed to the ordinary system the ideal gas is prepared

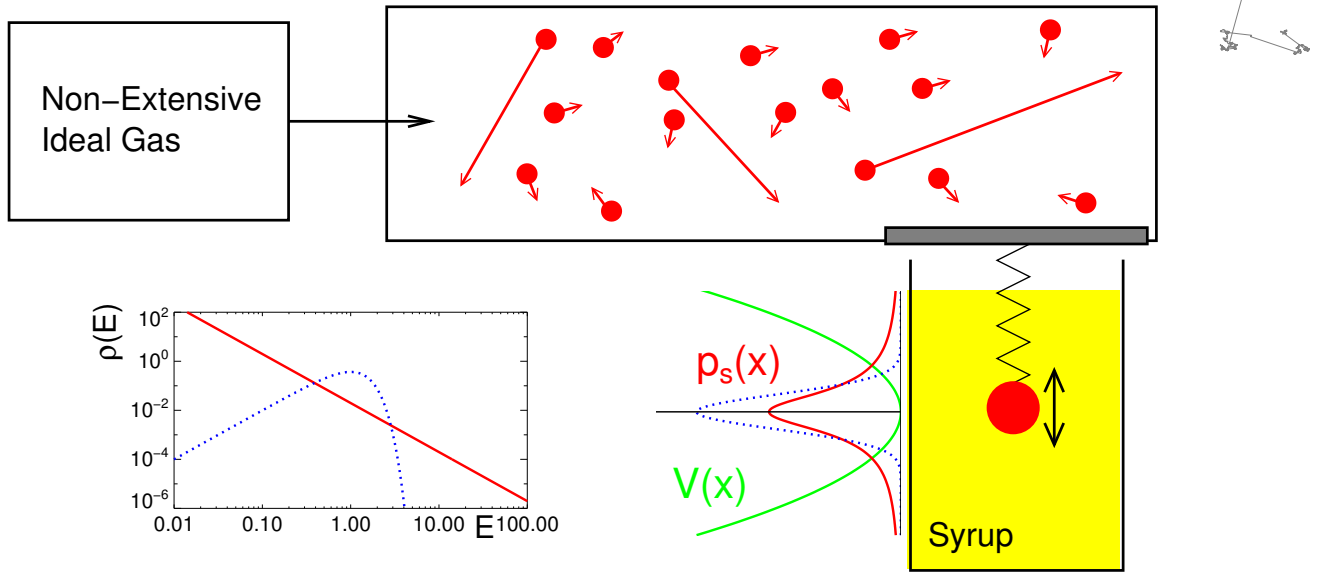


Figure 2.7.: Generalized Langevin dynamics of a mass attached to a harmonic spring coupled to a Lévy ideal gas. The situation is similar to the paradigmatic case depicted in figure 2.3 above. The mass (red object) is submerged in a liquid of high viscosity such that the motion is overdamped. The Lévy ideal gas (red, little objects in container) transfers momentum to the coupled system by means of a piston or a membrane (gray area). In contrast to the ordinary ideal gas in figure 2.3, in the Lévy ideal gas the energies are distributed according to a power law among the degrees of freedom. The pdf of the energies of the Lévy ideal gas (red line) is compared to the pdf of an ordinary ideal gas (blue dotted line). The potential $V(x) = x^2$ (green curve) is the same as in figure 2.3. The stationary pdf $p_s(x)$ of the mass deviates from the Gibbs-Boltzmann equilibrium $\exp(-\beta x^2)$ as is indicated by the superimposed blue dotted curve.

such that the kinetic energy of individual degrees of freedom is distributed according to an inverse power law with divergent variance. Consequently, the energy transfer to the coupled systems is strongly fluctuating. These fluctuations follow an inverse power law as well [42]. Still, individual increments of energy transfer to the coupled system are uncorrelated. Therefore the dynamics of the mass can be modeled by the generalized Langevin equation

$$dX = -2\beta X dt + dL_\mu \quad \text{with} \quad \mu < 2. \quad (2.90)$$

For any initial condition, the mass will equilibrate to the Lévy stable stationary density (2.89). At first glance, this seems paradoxical, because nothing indicates a violation of ordinary statistical physics on the microscopic scale. The reason why ordinary Gibbs-Boltzmann thermodynamics fails here is the non-equilibrated state of the ideal gas in figure 2.7. In thermal equilibrium each degree of freedom has approximately the same amount of energy of the order of $k_B T$ which defines the



temperature as an intensive quantity [107]. This typical energy scale is not well defined for the Lévy gas, hence temperature cannot be defined in the usual way.

2.6.2.1. A Lévy Gas on the Computer

A very simple numerical experiment illustrates this unusual behavior: A set of $N \gg 1$ random numbers $\epsilon_n > 0$ are generated which model the energies of individual degrees of freedom of an ideal gas. The total energy E of the gas is scaled, such that $E = \sum_n \epsilon_n = N$. The temperature T can be defined as the energy per degree of freedom, $T = E/N = 1/N \sum_n \epsilon_n$. The volume containing the gas is split into $N_g = \mathcal{O}(1)$ smaller volumes, each one containing N/N_g degrees of freedom, see figure 2.8. The total energy E and temperature T of the subsystems is computed and compared. First we treat an ordinary, thermally equilibrated ideal gas. Thermal equilibrium implies an equipartition of energy between the degrees of freedom, each one having approximately the same energy $\epsilon_n \approx T$ with some variance [107]. We model this by random numbers ϵ_n which are uniformly distributed in some finite interval. Therefore, the temperature of each subsystem fluctuates around the temperature T of the original system with a standard deviation of proportional to $1/\sqrt{N/N_g}$ which is very small for $N \gg 1$. In this case temperature is an intensive quantity. Likewise, the total energy of each subsystem is approximately E/N_g and thus an extensive quantity.

If we prepare a Lévy ideal gas in a similar fashion, a different behavior is observed. We generate the individual energies ϵ from a scale-free power law and normalize the total energy as above. We define the temperature in the same fashion as the energy per degree of freedom, i.e. $T = 1/N \sum_n \epsilon_n$. However, equipartition of energies ($\epsilon_n \approx T$) is no longer valid, because some degrees of freedom possess an energy of the order of the total energy. Therefore, if we distribute the N degrees of freedom equally into N_g subsystems and compute the total energy and temperature of each one, both quantities fluctuate heavily and are not even remotely the same for each subsystem. The total energy is neither an extensive, nor the temperature an intensive quantity.

This example shows that generalized Langevin equations such as (2.66) and their associated FFPEs describe non-equilibrium phenomena. For these a number of generalizations of Gibbs-Boltzmann thermodynamics have been developed in which entropy is non-extensive and temperature non-intensive [105, 123]. The connection to generalized Langevin dynamics has been discovered recently and is discussed in detail in [14, 26, 80]. The question remains of why the coupled system can equilibrate despite the fact that the thermal bath is not equilibrated. This is a consequence of the idealization of overdamped motion. If the complete Newtonian

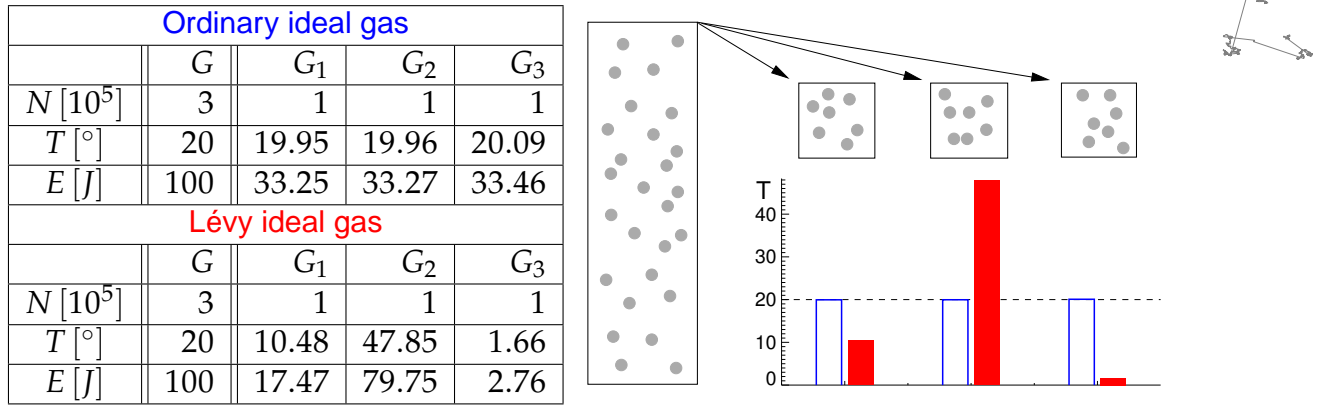


Figure 2.8.: Ordinary thermodynamics is inadequate for Lévy ideal gases. A set of $N = 300,000$ random energies ϵ_n are generated from a uniform distribution $[0, 1]$ reflecting the properties of an ordinary ideal gas (blue) and a scale-free density $\rho(\epsilon) \propto \epsilon^{-1.7}$ (red). The energies ϵ_n represent the microscopic degrees of freedom (gray dots) of the large container. The total energy was normalized to the same value of $E = 100$ in some arbitrary units J . The temperature is defined as the average energy of each degree of freedom $T = 1/N \sum \epsilon_n$ and is defined to be 20° in some arbitrary units. The system is split into three subsystems, each one containing 100,000 degrees of freedom. The total energy and temperature of each subsystem is computed. The subsystems containing an ordinary ideal gas have approximately the same temperature (blue bars) and approximately a third of the total energy (see table), whereas the subsystems containing the Lévy gas have variable temperature (red bars), e.g. the container in the center has a temperature 28 times larger than that of the container on the right.

equations of motion are included, i.e.

$$dU = -2\beta X dt - U dt + dL_\mu \quad (2.91)$$

$$dX = U, \quad (2.92)$$

the system does not possess a stationary state [80].

The reasoning presented above suggests that Lévy flights are generally a non-equilibrium phenomenon. This is certainly true when a system is correctly described by generalized Langevin dynamics in which a segregation of deterministic drift and stochastic force can be motivated. However, due to the non-local nature of Lévy flights, the FFPE (2.86) represents only one out of many possible generalizations of the FPE.

2.6.3. Probabilistic Models, Again

The Langevin approach is suitable whenever a separation of deterministic evolution and additive stochastic force can be justified which is often the case in physical systems. For a number of stochastic phenomena observed in biological, ecological



and econophysical systems, this segregation cannot be easily motivated. Consequently, stochastic models based on the more fundamental master equation are required. However, the expansion ideas of section 2.2.2 showed that rate equations for ordinary random walks can also be interpreted within the ordinary Langevin picture.

Thus it seems natural to address this issue when confronted with superdiffusive rate equations. In other words, does the FFPE for generalized Langevin dynamics represent the canonical limit of underlying superdiffusive rate equations? This question is more difficult to answer. The most prominent probabilistic modeling scheme is the Continuous Time Random Walk (CTRW) introduced by Scher and Montroll in a study of anomalous diffusion in amorphous solids [113]. Since then the CTRW scheme has received a lot of attention and still represents one of the most popular tools for investigating anomalous diffusion phenomena, ranging from transport in intermittent chaotic systems [143] to fluctuation phenomena financial markets [83]. A marvelous overview on CTRWs is provided in [91]⁶. Anomalous CTRW are intimately connected with fractional diffusion equations, and since their invention considerable effort has been devoted to draw a one-to-one correspondence between various CTRW models and analogous fractional evolution equations [88, 89]. For example, when a CTRW evolves in a homogeneous environment, the asymptotic behavior is governed by the FFPE of a free Lévy stable process (2.60). Furthermore, when an external field or an inhomogeneous environment is incorporated into a subdiffusive CTRW model, one can generally establish the equivalence to a subdiffusive FFPE [11].

However, combining superdiffusive CTRW with inhomogeneous environments is a subtle matter and no canonic FFPE can be obtained. This is not surprising, since only in these systems the non-local nature of transitions and the inhomogeneity are found in the spatial domain. Only when the rates which incorporate the spatial inhomogeneity as well as the non-local spatial transitions are fine tuned, can the FFPE (2.86) be derived from an underlying CTRW model [86]. Nonetheless, the generalized Langevin scenario has been regarded as the canonic generalization of the Fokker-Planck equation until very recently, when topological superdiffusion was introduced [22, 24, 25].

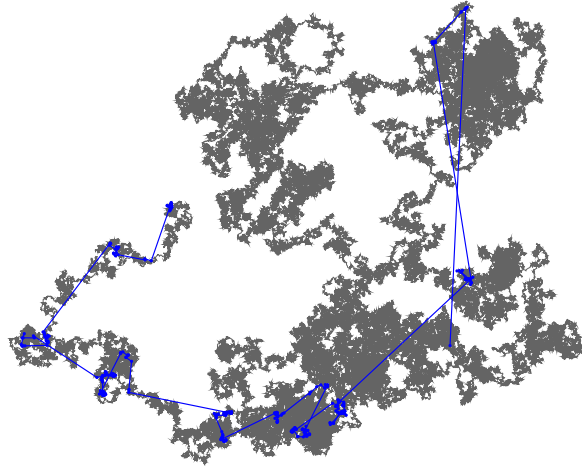
2.7. Fractal Time Processes

Since generalized Langevin dynamics violates ordinary Gibbs-Boltzmann thermodynamics, one may conjecture that Lévy flights are strictly a non-equilibrium phenomenon and that superdiffusion is absent in properly equilibrated systems. This,

⁶This article also contains a greatly entertaining historical synopsis of random walks, stochastics and statistics.



Figure 2.9.: A Lévy stable process (blue) generated by a strongly inhomogeneous temporal sampling of a two-dimensional realization of the Wiener process (gray). The exponent of the operational time density (2.94) is $\mu = 1$.



however, is not so. The first FFPE to describe superdiffusion in Gibbs-Boltzmann equilibrium and which is based on a plausible underlying microscopic dynamics is the subordination idea developed in [119], extended in [120], and thoroughly investigated in [25]. In the subordination scenario, the process $X(t) = \tilde{X}(\tau(t))$ evolves with an operational time $\tau(t)$ which is a strongly fluctuating function of the physical time t [38]. This type of irregular temporal sampling occurs in a number of physical situations, for example temporal fluctuations near phase transitions [54], superdiffusion from anomalous drift [75], and phenomena with scale-free memories, see [55] and references therein. The operational time is a monotonically increasing stochastic process itself. In operational time the dynamics are governed by an ordinary Langevin equation

$$d\tilde{X}(\tau) = F(\tilde{X}(\tau))d\tau + dW(\tau). \quad (2.93)$$

The process $X(t)$ is superdiffusive as a function of physical time t , if the operational time increments $\Delta\tau$ are drawn from an inverse power law defined on the positive real axis such that the first two moments diverge, i.e.

$$\rho(\Delta\tau) \sim \frac{1}{\Delta\tau^{1+\mu/2}} \quad \Delta\tau \gg \Delta t, \quad 0 < \mu \leq 2. \quad (2.94)$$

The case of vanishing force ($F \equiv 0$) in two dimensions is illustrated in figure 2.9. In this case $W(t)$ is simply the Wiener process, but $X(t) = W(\tau(t))$ is a process subordinated to it. The irregular sampling of physical time $\tau(t)$ causes $X(t)$ to be a Lévy stable process with $W(t)$ as a support. In fact, for a density of operational



time increments as (2.94) and $F \equiv 0$ one can show that $X(t) = L_\mu(t)$. The corresponding conditional pdf $p(x, t|x_0, t_0)$ in physical time is governed by the FFPE for symmetric Lévy stable processes [120],

$$\partial_t p(x, t|x_0, t_0) = \Delta_x^{\mu/2} p(x, t|x_0, t_0). \quad (2.95)$$

For non-vanishing force the correct FFPE is given by

$$\partial_t p(x, t|x_0, t_0) = -(-\mathcal{L}_{x,FP})^{\mu/2} p(x, t|x_0, t_0) \quad (2.96)$$

(see [120] for a detailed derivation), where

$$\mathcal{L}_{x,FP} = -\nabla_x F(x, t) + \frac{1}{2} \Delta_x D(x, t) \quad (2.97)$$

is the ordinary Fokker-Planck operator. Comparing with the FFPE for generalized Langevin dynamics (2.86), we see that the FFPEs are only identical in the force free case (free superdiffusion) or when $\mu = 2$ (ordinary diffusion). Raising the entire Fokker-Planck operator to a fractional power may seem a bit unusual. However, since $\mathcal{L}_{x,FP}$ is skew-symmetric it can be spectrally decomposed and functions of $\mathcal{L}_{x,FP}$ can be computed with ease. The eigenvalues $E(k)$ of $\mathcal{L}_{x,FP}$ are non-positive and the spectrum of $-(-\mathcal{L}_{x,FP})^{\mu/2}$ is given by

$$E_s(k) = -(-E(k))^{\mu/2} \leq 0, \quad (2.98)$$

which is non-positive as well. Because the operators $\mathcal{L}_{x,FP}$ and $-(-\mathcal{L}_{x,FP})^{\mu/2}$ commute superdiffusive subordinated processes are consistent with Gibbs-Boltzmann thermodynamics. If, for example, $D(x, t) = 1$ and $F(x, t) = -\beta dV(x)/dx$ the stationary solution $p_s(x) = \exp[-\beta V]$ to $\partial_t p = \mathcal{L}_{FP} p$ it is also the stationary solution to (2.96).

2.8. Summary

Superdiffusive phenomena are accounted for by models based on random walks known as Lévy flights. Unlike ordinary random walks, Lévy flights lack a scale in their jump length statistics. Based on Lévy flights, Lévy stable processes can be defined which serve as an anomalous noise in generalized Langevin dynamics and generalize the Wiener process. In the associated generalization of the Fokker-Planck equation, non-local, fractional integro-differential operators replace the ordinary diffusion term. However, generalized Langevin dynamics violates ordinary Gibbs-Boltzmann thermodynamics and is only valid for systems in which superdiffusion is a consequence of thermal non-equilibrium, corresponding to only a restricted set of physical situations. However, due to its formal similarity to the ordinary Fokker-Planck equation, the appealing concept of additive anomalous noise,

the existence of a microscopic picture, and the fact that all ordinary diffusion processes are governed by a Fokker-Planck equation, generalized Langevin dynamics has been considered the canonic generalization of the Fokker-Planck equation. Consequently, Lévy flights and superdiffusion in general have been stigmatized as non-equilibrium phenomena. The concept of topological superdiffusion, the central idea of this work, will redeem Lévy flights, as will be revealed in the next chapter.



2. Everything You Always Wanted to Know About Superdiffusion, but Were Afraid to Ask





3. Topological Superdiffusion

In this respect the master equation approach is a much more complete description.

(C. W. Gardiner)

In this chapter we will introduce the concept of topological superdiffusion. Based on the paradigmatic case of random motion along a linear folded hetero-polymer, we develop a novel fractional generalization of the Fokker-Planck equation (FPE). Despite the fact that this fractional Fokker-Planck equation (FFPE) describes Lévy flights in an inhomogeneous environment, thermodynamic requirements such as Boltzmann equilibrium and detailed balance are met. We show that only either in the diffusion limit or when the external field vanishes is the FFPE for topological superdiffusion identical to the one which corresponds to generalized Langevin dynamics. We demonstrate that topologically superdiffusive processes can be mapped onto a quantum mechanical system defined by a fractional Hamiltonian consisting of a modified kinetic term and an effective potential, indicating that topological superdiffusion can be understood in terms of quantum mechanical concepts. We briefly discuss the example of topological superdiffusion in the harmonic potential. Finally we introduce further generalizations of the idea and present an FFPE suitable for systems of arbitrary dimension. We summarize with a discussion on Lévy flights in thermal equilibrium, and argue that the FFPE developed in this chapter is applicable to a variety of superdiffusive phenomena in nature which cannot be explained in terms of the generalized Langevin approach, and have so far resisted a description by fractional kinetics.

3.1. Preliminary Considerations

In topologically superdiffusive systems long tailed spatial transitions are generated by the complex topology on which random motion evolves, as opposed to external anomalous Lévy stable white noise present in generalized Langevin dynamics (section 2.6) and fractal temporal sampling observed in the subordination scenario (section 2.7). The concept of topological superdiffusion is best understood in terms of the model systems depicted in figure 3.1.

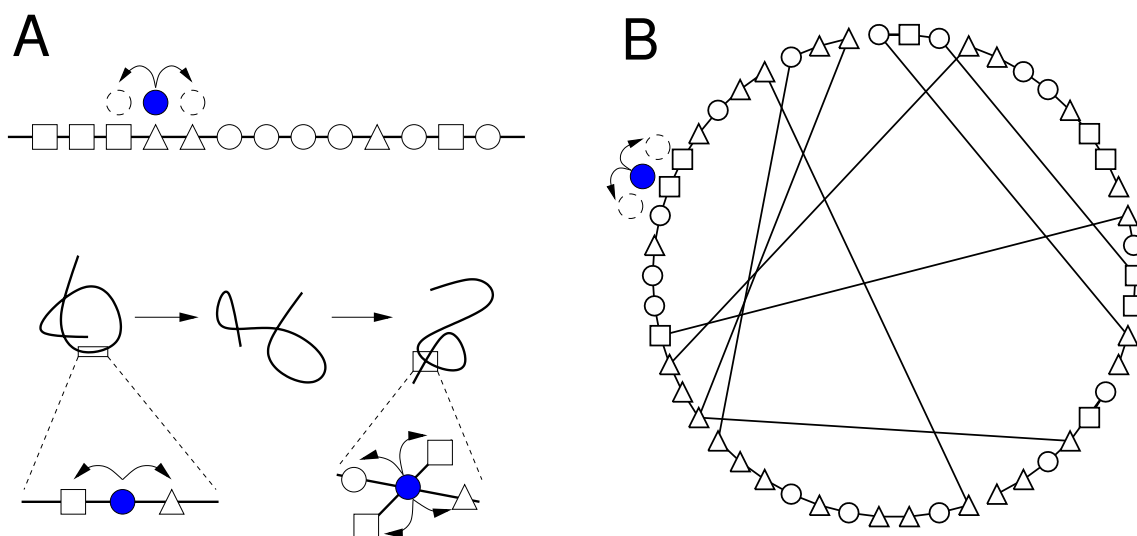


Figure 3.1.: Two examples of superdiffusion arising in complex topologies. **A:** A thermally activated particle (blue circle) performs an ordinary random walk on a hetero-polymer. The chain is submerged in a solvent which serves as a heat bath. Thermal conformational changes locations far apart along the chemical axis of the chain approach each other in Euclidean space. The particle may then initiate a long range jump in chemical coordinates. **B:** A random walker (blue circle) evolves on a small world network [2]. As the process evolves the walker will eventually be located on a site with a long range connection and may jump to a distant region in the network.

On the left a particle is loosely attached to a linear polymer. Thermally activated, the particle performs a next-neighbor random hopping process along the chain. If the polymer is in solution and rapidly changing its conformational state, two positions which are far apart along the chemical axis of the chain may approach in Euclidean space. Due to the folding, long range (measured in chemical coordinates) transitions may occur. This effect enhances the dispersion of a particle along the chain, an effect which is believed to play a role in protein motion along DNA strands [16, 135, 136], active transport on semiflexible intracellular polymers [29] and random walks on cytoskeletal motors [77].

A similar system, known as a small world network (SWN), is depicted in figure 3.1B. Recently, these networks were introduced [130] as models for scale-free real world networks [2] such as metabolic networks [58] and the internet [3], and have also been employed as models for linear folded polymers [62]. The absence of a typical scale arises rather naturally in real world random networks and is not a rare peculiarity [9]. In addition to the uniform local connectivity a small fraction of long range connections are either added to or replace the local connections. Random motion on these structures is important to the understanding of disease spreading in social networks and signal dispersion in biological networks,

see e.g. [92]. In the figure a random walker is moving on a small world network. During the process the walker will eventually be located on a site with a long range connection and may jump to a distant region in the network. Clearly, enhanced diffusion in such a system is caused by the complex connectivity of the structure on which the process evolves. In [69] it was shown that the spatio-temporal scaling of dispersion on small world networks is rather different from that expected for ordinary diffusion.

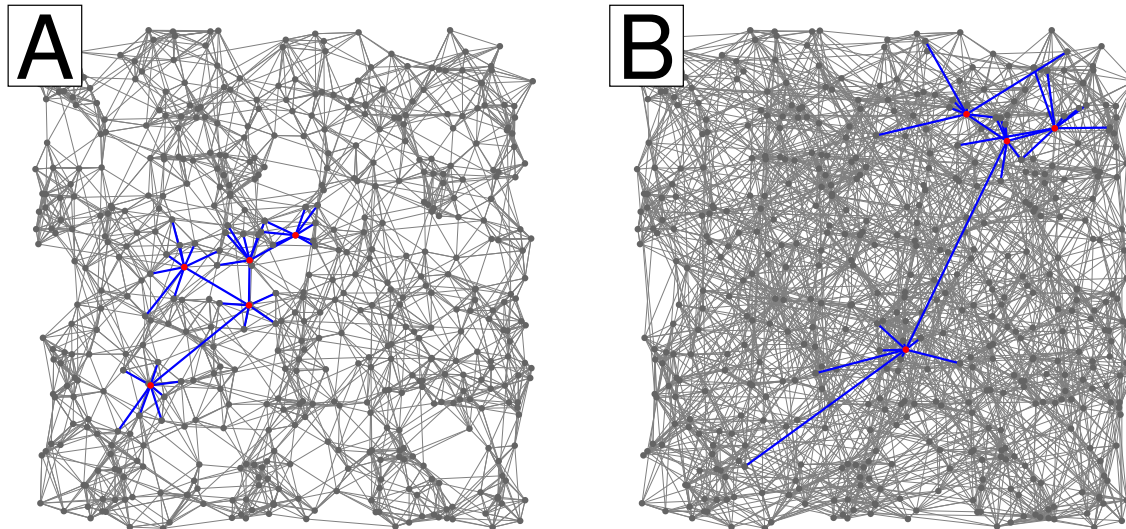


Figure 3.2.: Random motion on two dimensional randomly connected graphs. Depending on the connectivity structure random motion on these graphs exhibits different types of asymptotics. Ordinary as well as enhanced diffusion may occur. The difference in connectivity is highlighted by a subset of vertices (red) and their connections (blue) **A:** On a locally connected graph a random walk is diffusive on scales larger than the typical connection length. **B:** Connection lengths follow an inverse power law with and thus lack a scale. A random walk on this type of graph is superdiffusive on scales greater than the typical inter-vertex spacing.

Figure 3.2 illustrates a two-dimensional system in which enhanced diffusion may be caused by the topological features. Each random graph consists of a number of vertices uniformly distributed in the plane. Each vertex connected to a subset of other vertices by a small number of connections. The number of connections as well as the planar coordinates of the vertices are identical in both graphs. However, the connectivity structure is different. The graph in figure 3.2A is locally connected, i.e connection lengths possess a typical scale. The displacements of a random walk on such a graph have a typical length scale defined by the typical connection length. On large scales, a random walk on such a graph is diffusive. In figure 3.2B connection lengths follow an inverse power law with divergent variance. Connection lengths and consequently jump lengths of a random walk on



such a graph lack a typical scale. A random walk on this type of graph is superdiffusive, a quality caused exclusively by the connectivity properties of the graph.

At first glance, a distinction between the underlying mechanisms (i.e. additive noise vs. topological structure) which cause the stochastic motion may seem unnecessary. Ordinary, run-of-the-mill Markov processes generally possess typical time and length scales. This implies that these processes can either be approximated by or asymptotically converge to ordinary diffusion processes on relevant spatio-temporal scales. The dynamics is always governed by a FPE, regardless of whether the stochastic motion originates in the geometrical complexity of the system or in a rapidly fluctuating external force. Of course, different underlying mechanisms lead to different drift and diffusion coefficients of the FPE. However, the existence of a FPE implies that on relevant scales the dynamics can be interpreted in terms of the associated Langevin equation. That is, on appropriate scales these processes may be understood as evolving according to a deterministic dynamics subjected to an external stochastic force.

Based on this reasoning, we may expect that when Lévy flights evolve in external potentials or inhomogeneities, the appropriate, universal and all encompassing framework of description is the generalized Langevin scheme introduced in section 2.6, or equivalently a FFPE which segregates into deterministic drift and fractional diffusion terms. The success of the Langevin framework for ordinary processes, and the fact that the concept of deterministic dynamics subjected to additive fluctuating forces is so appealing to a physicist's mind, might explain why the fractional Langevin approach has attracted so much attention in recent years [40, 41, 56, 60]. Since generalized Langevin dynamics violates basic principles of thermodynamic equilibrium, it is not surprising that Lévy flights have been categorized as non-equilibrium phenomena, absent in thermally equilibrated systems.

In the following we will show that this reasoning is incautious and hasty. Lévy flights occur in a number of thermally inconspicuous systems. Furthermore, the generalized Langevin approach is inadequate for systems in which enhanced diffusion is caused by the topology of the substrate on which the process evolves. We will demonstrate that when long tailed spatial transitions are possible, a novel fractional generalization of the FPE must be used. The FFPE for topological superdiffusion cannot be separated into deterministic and stochastic components, it is purely probabilistic. Thus, a description in terms of a stochastic differential equation is not possible for these systems. Equipped with the FFPE developed below, a variety of superdiffusive phenomena can be investigated which are known to obey ordinary Gibbs-Boltzmann thermodynamics.



3.2. Random Motion on a Folding Polymer – A Paradigm

Let us begin with a detailed analysis of the model system briefly mentioned above and depicted in figure 3.1A. A particle (e.g. an enzyme, exciton or electron) is loosely attached to an inhomogeneous polymer (e.g. a DNA strand or linear protein) of length L in solution at temperature T . Thermal activation by the environment causes the particle to jump randomly along the chain with a typical waiting time τ at a given site. A potential $V(x)$ at each monomer site x reflects the energetic inhomogeneity of the chain. The potential quantifies the energy of the particle when it is attached to the associated monomer. If the moving particle is thermally equilibrated with its environment, the probability of finding the particle attached to monomer x is proportional to the Boltzmann factor $\exp[-\beta V(x)]$. Note that the coordinate x quantifies distance in *chemical space*, i.e. along the chain, as opposed to distance in Euclidean space. In the following we assume that the microscopic distance between adjacent monomers a is much smaller than the chain length, i.e. $a \ll L$.

The quantity of interest is $p(x, t|x_0, t_0)$, the conditional probability density function (pdf) of finding the particle at site x at time t given that it was initially (t_0) located at x_0 . If we neglect memory effects, we can model the random motion of the particle as a Markovian jump process $X(t)$. The propagator belonging to this type of process is governed by the master equation (for convenience we abbreviate $p(x, t) = p(x, t|x_0, t_0)$)

$$\partial_t p(x, t) = \int dy [w(x|y, t) p(y, t) - w(y|x, t) p(x, t)] \quad (3.1)$$

The rhs of (3.1) defines the linear stochastic operator $\mathcal{L}_M(t)$, i.e. (3.1) can be written as

$$\partial_t p = \mathcal{L}_M(t) p. \quad (3.2)$$

The integral representation $L_M(x|y, t)$ of $\mathcal{L}_M(t)$ in position coordinates is

$$L_M(x|y, t) = w(x|y, t) - \left[\int dy w(y|x, t) \right] \delta(x - y). \quad (3.3)$$

The master equation is defined by the time dependent rate $w(x|y, t)$ of making a transition from a monomer at $y \neq x$ to an adjacent monomer at x within a short time interval Δt at time t , i.e.

$$w(x|y, t) = \lim_{\Delta t \rightarrow 0} \frac{1}{\Delta t} p(x, t + \Delta t|y, t) \quad x \neq y. \quad (3.4)$$

Since we wish to describe a system with Gibbs-Boltzmann statistics, we model thermal transitions between adjacent sites y and x as

$$y \rightarrow x : \quad w(x|y, t) \propto \frac{1}{\tau} e^{-\beta[V(x)-V(y)]/2}. \quad (3.5)$$



The exponential in (3.5) is the consequence of two basic assumptions. We assume that the probability of jumping to a target site x decreases as the potential at that site $V(x)$ increases. Furthermore, we assume that hopping between monomers depends on the energetic difference with respect to the thermal energy scale $k_B T = \beta^{-1}$. A more general approach is discussed in section 3.6 below.

Let us now take into account the geometrical complexity of the system. We assume that transitions may only occur if the corresponding sites are in close proximity in Euclidean space, in other words if

$$|\mathbf{R}(x, t) - \mathbf{R}(y, t)| \leq a, \quad (3.6)$$

where $\mathbf{R}(x, t), \mathbf{R}(y, t) \in \mathbb{R}^3$ denote the Euclidean coordinates of the two monomers x and y . Since the polymer is subjected to conformational changes, the distance between two given sites changes over time. In a nearly linear chain the particle jumps exclusively between neighboring sites along the chemical axis, whereas in a more complex conformational state locations far apart along the chemical coordinate may be contiguous in Euclidean space. In this case long range transitions may occur as well. Incorporating the thermal component of a transition between two sites as well as the topological constraints imposed by the conformational state of the polymer it is reasonable to make the following ansatz for the rate,

$$w(x|y, t) = \frac{1}{\tau} e^{-\beta[V(x)-V(y)]/2} G(x, y; t). \quad (3.7)$$

The function $G(x, y; t)$ takes into account the geometrical constraints imposed by the configuration of the polymer in Euclidean space,

$$G(x, y; t) = \begin{cases} 1 & \text{if } |\mathbf{R}(x, t) - \mathbf{R}(y, t)| \leq a, \\ 0 & \text{otherwise.} \end{cases} \quad (3.8)$$

This definition of the geometrical constraint factor implies a symmetry, namely $G(x, y; t) = G(y, x; t)$. Note that the thermal factor is time independent, reflecting thermal equilibrium with the environment and ordinary thermodynamics, i.e. the stationary solution $p_s(x)$ to (3.1) is the ordinary, off-the-shelf Gibbs-Boltzmann equilibrium,

$$p_s(x) \propto e^{-\beta V(x)}. \quad (3.9)$$

Clearly, at any time the condition of detailed balance is fulfilled,

$$w(x|y, t) e^{-\beta V(y)} = w(y|x, t) e^{-\beta V(x)}. \quad (3.10)$$

The parameter τ in (3.7) is the typical waiting time at a given location. The rate defined by (3.7) together with the master equation (3.1) represent a model for random motion of a particle along a polymer in solution. Although equipped with a fair

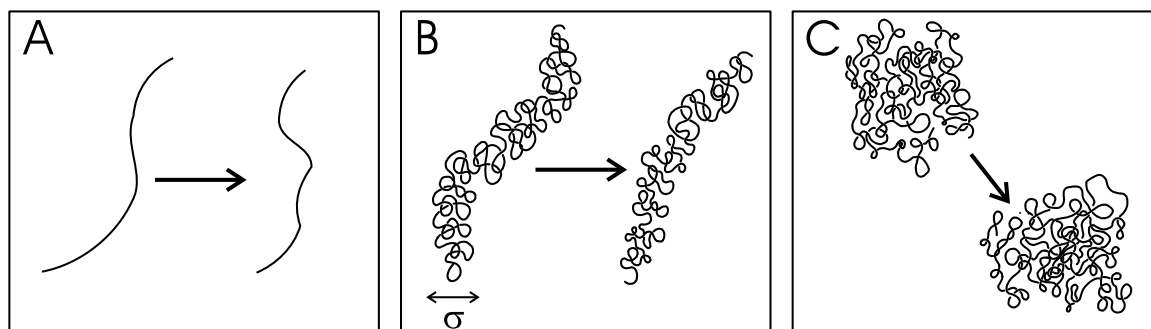


Figure 3.3.: Flexible linear polymers in solution. Depending on the microscopic structure of the polymer and properties of the solvent three qualitatively different conformational dynamics can be distinguished. **A:** A nearly rigid, extended chain makes no long or intermediate range contacts. **B:** A coiled polymers exhibits intermediate connections below a typical length σ . **C:** A completely flexible polymers is typically in conformational states with long range connections on all scales. Arrows indicate conformational changes over time.

amount of appeal and beauty, the model as such defies further investigation. Master equations are generally impossible to solve, with the exception of a few very trivial cases. Furthermore, in the model defined above, the devil is in the details. For a polymer in solution, which is subjected to thermal conformational changes, the geometrical constraint factor $G(x, y; t)$ is extremely complex, especially as a function of time. It is rapidly fluctuating in an unpredictable manner. However, matters can be simplified if the conformational changes occur on a much smaller time scale than the hopping of the particle along the chain, as will be shown below.

Let us first turn our attention to a number of cases which are particularly interesting and important from a physical point of view. These are depicted in figure 3.3. The simplest case is a nearly rigid, extended polymer lacking long range contacts (figure 3.3A). The topology of the coiled polymer in figure 3.3B permits intermediate range transitions below a typical length σ , in addition to nearest neighbor hopping. The fully flexible polymer allows transitions on all scales (figure 3.3C). For each of these systems a useful approximation of the master equation can be obtained.

3.2.1. Rigid chains

Consider the polymer depicted in figure 3.3A. In this case only nearest neighbor hopping occurs. Rigidity and nearest neighbor hopping provide a geometrical constraint factor $G(x, y; t)$ which is time independent and homogeneous in chemical



space,

$$G(x, y; t) = g(x - y) \quad \text{with} \quad (3.11)$$

$$g(x) = \frac{1}{2} (\delta(x - a) + \delta(x + a)). \quad (3.12)$$

Inserted into (3.7), we discover that the master equation (3.1) is simplified slightly. Letting

$$s(x) = e^{-\beta V(x)/2}, \quad \text{and} \quad q_t(x) = e^{\beta V(x)/2} p(x, t) \quad (3.13)$$

we obtain

$$\partial_t p(x, t) = \frac{1}{2\tau} (s(x) [q_t(x + a) + q_t(x - a)] - q_t(x) [s(x + a) + s(x - a)]). \quad (3.14)$$

This can be slightly rearranged as

$$\begin{aligned} \partial_t p(x, t) = \frac{a^2}{2\tau} s(x) \left[\frac{q_t(x + a) + q_t(x - a) - 2q_t(x)}{a^2} \right] \\ - \frac{a^2}{2\tau} q_t(x) \left[\frac{s(x + a) + s(x - a) - 2s(x)}{a^2} \right] \end{aligned} \quad (3.15)$$

On scales much larger than the inter-monomer spacing a and times much larger than the typical waiting time τ , the process is asymptotically governed by the diffusion limit of (3.14), i.e.

$$\tau, a \rightarrow 0 \quad \text{with} \quad D \equiv \frac{a^2}{2\tau}, \quad (3.16)$$

defining the diffusion coefficient D of the system. The diffusion coefficient determines the way spatial and temporal microscopic scales depend on each other in order for the limit to be meaningful. Since the diffusion coefficient appears as a prefactor in both terms of (3.15) it may be absorbed by rescaling time $t \rightarrow t/D$, equivalently and without loss of generality we may set $D = 1$. The terms in square brackets in (3.15) converge to $\partial^2 q_t(x)/\partial x^2$ and $\partial^2 s(x)/\partial x^2$ in this limit. Reinserting (3.13), the master equation reads

$$\partial_t p = e^{-\beta V/2} \Delta e^{\beta V/2} p - p e^{\beta V/2} \Delta e^{-\beta V/2} \quad (3.17)$$

$$\equiv \mathcal{L} p, \quad (3.18)$$

where Δ denotes the Laplace operator. Although structurally similar to the original master equation, the representation of the stochastic operator \mathcal{L} in (3.17) does not



seem very familiar. Yet if we expand both Laplacians, sort terms and scrutinize their relationship, we obtain

$$\mathcal{L} p = (-\nabla F + \Delta) p \quad \text{where} \quad (3.19)$$

$$F(x) = -\beta \frac{dV(x)}{dx}. \quad (3.20)$$

Interestingly, the operator \mathcal{L} is in fact an ordinary Fokker-Planck operator, describing deterministic gradient dynamics in the potential V subjected to Gaussian white noise. Therefore, on scales larger than the inter-monomer spacing, random motion along a inhomogeneous polymer can be modeled by the associated Langevin equation

$$dX(t) = \beta \frac{dV(X)}{dX} dt + dW(t), \quad (3.21)$$

in which $dW(t)$ is the differential of the Wiener process. Asymptotically, the dynamics segregates into additive deterministic and stochastic forces. In the limit given by (3.16) the original jump process $X(t)$ becomes a diffusion process with continuous sample paths. Thermodynamic properties such as detailed balance and Gibbs-Boltzmann equilibrium are still valid in this limit. This can easily be checked by employing the representation of \mathcal{L} in (3.17) instead of the frequently used representation (3.19).

3.3. Mean Field Theory for Non-Local Transitions

Let us now turn our attention to the more interesting cases of rapidly folding polymers, figure 3.2B and C. Because the conformational changes of the polymer in solution are thermal, the time dependent geometrical constraint factor $G(x, y; t)$ can be interpreted as a stochastic process itself. From a physical point of view it is of no use and also impossible to study the microscopic dynamics of $G(x, y; t)$. Instead, we need to think of the system as consisting of an ensemble of N polymers labeled i , each one in a random conformation at time t characterized by $G_i(x, y; t)$. The conformational state represents a disorder implicitly contained in the operator $\mathcal{L}_M(t)$ of the master equation (3.1). Information about the typical behavior of the system can be gained by averaging the master equation over the disorder. In other words, we will study

$$\partial_t \llbracket p \rrbracket = \llbracket \mathcal{L}_M(t) p \rrbracket, \quad (3.22)$$

where $\llbracket \cdot \rrbracket = 1/N \sum_i (\cdot)_i$ denotes the disorder average. The average on the rhs poses a problem because generally the disorder average $\llbracket \mathcal{L}_M(t) p \rrbracket$ does not factorize into $\llbracket \mathcal{L}_M(t) \rrbracket \llbracket p \rrbracket$. However, if the conformational changes of the polymer occur on a much faster time scale than the hopping of the particle, $p(x, t)$ can be assumed to



be approximately constant on time scale typical for $G(x, y; t)$ and we may assume that

$$\llbracket \mathcal{L}_M(t) p \rrbracket \approx \llbracket \mathcal{L}_M(t) \rrbracket \llbracket p \rrbracket. \quad (3.23)$$

This is a mean field approximation. The operator is replaced by its expectation value. Inserted into the master equation (making the notational change $\llbracket p \rrbracket \rightarrow p$) we obtain

$$\partial_t p(x, t) = \int dy \{ \llbracket w(x|y, t) \rrbracket p(y, t) - \llbracket w(y|x, t) \rrbracket p(x, t) \}, \quad (3.24)$$

where

$$\llbracket w(x|y, t) \rrbracket = e^{-\beta[V(x)-V(y)]/2} \llbracket G(x, y; t) \rrbracket. \quad (3.25)$$

The disorder average $\llbracket G(x, y; t) \rrbracket$ is just the probability $P(|\mathbf{R}(x, t) - \mathbf{R}(y, t)| \leq a)$ of finding monomers x and y at a distance from each other less than a in Euclidean space, for

$$\llbracket G(x, y; t) \rrbracket = [\chi(|\mathbf{R}(x, t) - \mathbf{R}(y, t)| - a)] \quad (3.26)$$

$$= P(|\mathbf{R}(x, t) - \mathbf{R}(y, t)| \leq a), \quad (3.27)$$

where $\chi(z)$ is the characteristic function which is unity when $z \in [0, 1]$ and zero otherwise. If the conformational dynamics are equilibrated with respect to the thermal bath, the probability on the rhs of (3.27) does not depend on time. In addition to the symmetry of interchanging x and y we may assume homogeneity along the chemical axis. All this implies that the probability is a function ρ which merely depends on chemical distance $|x - y|$, i.e.

$$P(|\mathbf{R}(x, t) - \mathbf{R}(y, t)| \leq a) \propto \rho(|x - y|). \quad (3.28)$$

Thus, the mean field approximation yields a temporally homogeneous master equation with time independent rates,

$$w(x|y) = \frac{1}{\tau} e^{-\beta[V(x)-V(y)]/2} \rho(|x - y|) \quad (3.29)$$

Although the function $\rho(l)$ with $l = |x - y|$ depends on the folding properties of the polymer, it is reasonable to assume that it decreases monotonically with distance l . A jump process governed by this rate clearly fulfills detailed balance, since

$$w(x|y)e^{-\beta V(y)} = w(y|x)e^{-\beta V(x)}. \quad (3.30)$$



3.3.1. The Coiled Polymer

We ambitiously apply the above reasoning to the coiled polymer depicted in figure 3.3B. Qualitatively, the state of such a polymer is characterized by a typical length scale σ , above which long range transitions are highly unlikely to occur. The length scale σ represents a natural cutoff in the PDF $\rho(l)$ of making a transition of length l in chemical space. We therefore expect all the moments of $\rho(l)$ to exist, i.e.

$$A_m = \langle l^m \rangle \equiv 2 \int_0^{\infty} dl \rho(l) l^m. \quad (3.31)$$

Inserting the mean field rate (3.29) into (3.1) and performing a Kramers-Moyal expansion [109] of the rates we obtain

$$\partial_t p(x, t) = \sum_{n=1}^{\infty} \frac{1}{n!} \left(-\frac{\partial}{\partial x} \right)^n D_n(x) p(x, t), \quad (3.32)$$

where

$$D_n(x) = \frac{1}{\tau} \int dy (y - x)^n e^{-\beta[V(x) - V(y)]/2} \rho(|x - y|). \quad (3.33)$$

Expanding the exponential $\exp[\beta V(y)/2]$ around x , we can express the Kramers-Moyal coefficients $D_n(x)$ in terms of the moments A_m as

$$D_n(x) = \frac{1}{\tau} \sum_{k=0}^{\infty} \frac{A_{n+k}}{k!} e^{\beta V(x)/2} \left[\left(\frac{\partial}{\partial x} \right)^k e^{-\beta V(x)/2} \right]. \quad (3.34)$$

Inserted into (3.32), this gives the evolution equation of the propagator¹,

$$\partial_t p(x, t) = \frac{1}{\tau} \sum_{n=1}^{\infty} \sum_{k=0}^{\infty} \frac{A_{n+k}}{n! k!} \left(-\frac{\partial}{\partial x} \right)^n e^{\beta V(x)/2} \left[\left(\frac{\partial}{\partial x} \right)^k e^{-\beta V(x)/2} \right] p(x, t). \quad (3.35)$$

Apart from the mean field approximation no further approximations have been made so far, the evolution equation (3.35) is equivalent to the disorder averaged master equation.

Irrespective of the exact shape of the jump length probability $\rho(l)$, the situation depicted in figure 3.3.B suggests that the moments depend on the natural length scale σ as

$$A_{2m} = a_{2m} \sigma^{2m}, \quad A_{2m+1} = 0 \quad m \in \mathbb{N}. \quad (3.36)$$

¹Here and in the following we employ brackets $[\cdot]$ to restrict the action of differential operators to whatever functions appear inside the brackets, for example $\partial_x a(x) [\partial_x b(x)] c(x) = a'(x) b'(x) c(x) + a(x) b''(x) c(x) + a(x) b'(x) c'(x)$



Odd moments vanish because $\rho(l)$ is even, the prefactor a_{2m} is independent of σ and is determined by the functional features of $\rho(l)$. Without loss of generality we can assume that the second moment is identical to σ^2 and thus $a_2 = 1$. Again, the dynamics on scales much larger than the natural cutoff σ is governed by the canonical diffusion limit,

$$\sigma, \tau \rightarrow 0 \quad \text{with} \quad D_c \equiv \frac{\sigma^2}{2\tau}. \quad (3.37)$$

In this case, the diffusion coefficient D_c contains the cutoff σ in the numerator as opposed to the inter-monomer spacing a . In the above limit only two terms ($n, k = 1, 1$ and $n, k = 2, 0$) in (3.35) are nonvanishing, because

$$\lim_{\sigma, \tau \rightarrow 0} \frac{A_{2m}}{\tau} = 2 D_c a_{2m} \delta_{m,1}. \quad (3.38)$$

Inserting this into (3.35) yields

$$\begin{aligned} \partial_t p(x, t) &= D_c \left(-2 \frac{\partial}{\partial x} e^{\beta V(x)/2} \left[\frac{\partial}{\partial x} e^{-\beta V(x)/2} \right] + \frac{\partial^2}{\partial x^2} \right) p(x, t) \\ &= D_c \left(-\frac{\partial}{\partial x} F(x) + \frac{\partial^2}{\partial x^2} \right) p(x, t), \end{aligned} \quad (3.39)$$

where $F(x) \equiv -\beta dV(x)/dx$. The disorder averaged master equation for the random walk along coiled polymers with limited long range transitions is asymptotically equivalent to an ordinary FPE identical the one obtained for the linear rigid chain. On scales larger than the cutoff parameter σ the particle becomes diffusive. The possibility of initiating intermediate jumps only increases the effective speed of dispersion quantified by D_c as compared to the diffusion coefficient D of the linear chain. The increase in dispersion speed is proportional to the number of monomers contained within the cutoff length σ as can easily be checked combining equations (3.16) and (3.37), i.e.

$$\frac{D_c}{D} = \left(\frac{\sigma}{a} \right)^2. \quad (3.40)$$

However, the diffusive nature of dispersion is not changed when long range transitions of finite variance come into play.

3.4. The FFPE for Topological Superdiffusion

The situation changes drastically when scale-free long range transitions between monomers can occur. When the polymer is flexible, for example when the chemical



bonds between monomers can be rotated freely, the typical conformational states are more erratic and globular, see figure 3.3C. The 3-dimensional state of such a chain can be regarded as a random walk in Euclidean space [32, 35]. In these random walk models, the probability $\rho(l)$ of finding two distant sites x and $y = x + l$ in close proximity in Euclidian space is related to the return probability of the 3-dimensional random walk. The function $\rho(l)$ is generically an inverse power law, $\rho(l) \propto |l|^{-(1+\mu)}$ for $|l| \gg a$. The exponent depends on the underlying random walk model for the polymer configuration but is typically less than unity [122]. In the following we assume that

$$\rho(l) = \frac{\mu a^\mu}{2} \begin{cases} |l|^{-(1+\mu)} & |l| \geq a, \quad 0 < \mu \leq 2 \\ 0 & \text{otherwise.} \end{cases} \quad (3.41)$$

The prefactor $\mu a^\mu/2$ ensures the proper normalization of $\rho(l)$ to unity. The intermonomer spacing a represents the minimal jump length. If the exponent $\mu \leq 2$, the density $\rho(l)$ lacks a finite variance, even worse, when $\mu \leq 1$ the expectation value $\langle l \rangle$ diverges. The statistics of jump lengths along a random polymer lack a typical scale (see figure 2.4 for consequences of this). We cannot apply the Kramers-Moyal expansion for $\mu < 2$ in order to obtain the asymptotic behavior of the propagator. Instead, we will work with the disorder averaged master equation directly. Inserting the jump length PDF into the rate (3.29), the master equation reads

$$\partial_t p(x, t) = \frac{\mu a^\mu}{2\tau} \left\{ e^{-\beta V(x)/2} \int_{|x-y| \geq a} dy \frac{e^{\beta V(y)/2} p(y, t)}{|x-y|^{1+\mu}} - e^{\beta V(x)/2} p(x, t) \int_{|x-y| \geq a} dy \frac{e^{-\beta V(y)/2}}{|x-y|^{1+\mu}} \right\} \quad (3.42)$$

Note that the integrals are restricted to a region $|x-y| \geq a$. We now investigate the asymptotic limit of (3.42), letting $a, \tau \rightarrow 0$. In order for this to make any sense the ratio a^μ/τ must be kept constant. This scaling relation of the microscopic quantities reflects the underlying fractal structure of the process, which is determined by the exponent in the power law (3.41). The generalized diffusion coefficient D is defined in analogy to (3.16) as

$$\tau, a \rightarrow 0 \quad \text{with} \quad D \equiv \frac{\pi\mu}{2\Gamma(1+\mu)\sin(\pi\mu/2)} \left(\frac{a^\mu}{\tau} \right). \quad (3.43)$$

The choice of the prefactor in the definition of D may seem a bit peculiar and arbitrary at this point. It will become useful below. Note that the units of the generalized diffusion coefficient are not the same as in ordinary diffusion. Substituting



$s(x)$ and $q_t(x)$ as defined in (3.13) we may carry out the limit as follows

$$\partial_t p(x, t) = D \lim_{a \rightarrow 0} C_\mu \left\{ s(x) \int_{|x-y| \geq a} dy \frac{q_t(y)}{|x-y|^{1+\mu}} - q_t(x) \int_{|x-y| > a} dy \frac{s(y)}{|x-y|^{1+\mu}} \right\}, \quad (3.44)$$

where $C_\mu = \Gamma(1 + \mu) \sin(\pi\mu/2)/\pi$. Adding two terms $\pm s(x)q_t(x) \int_{|y-x| > a} dy |y-x|^{-(1+\mu)}$ yields

$$\partial_t p(x, t) = D \lim_{a \rightarrow 0} C_\mu \left\{ s(x) \int_{|x-y| > a} dy \frac{q_t(y) - q_t(x)}{|x-y|^{1+\mu}} - q_t(x) \int_{|x-y| > a} dy \frac{s(y) - s(x)}{|x-y|^{1+\mu}} \right\}. \quad (3.45)$$

Both integrals are now regularized and the limit is well defined, yielding

$$\partial_t p(x, t) = D \left\{ s(x) C_\mu \int dy \frac{q_t(y) - q_t(x)}{|x-y|^{1+\mu}} - q_t(x) C_\mu \int dy \frac{s(y) - s(x)}{|x-y|^{1+\mu}} \right\}. \quad (3.46)$$

Note that in the limit the resulting rates $w(x|y)$ are not normalizable. Therefore, as mentioned earlier, the process is not a pure jump process in this limit. In fact, trajectories become discontinuous almost everywhere in this limit. However, the limit can be carried out since the resultant singularities cancel, and equation (3.46) can be interpreted consistently. The integrals appearing in equation (3.46) are symmetric generalized fractional Laplacians² (see Appendix A.3) defined by

$$\left(\Delta^{\mu/2} f \right) (x) = C_\mu \int dy \frac{f(y) - f(x)}{|x-y|^{1+\mu}}. \quad (3.47)$$

Using this notation and inserting the definitions (3.13) of $s(x)$ and $q_t(x)$, the dynamics of the propagator can be cast into a more concise form:

²The term fractional Laplacian originates in the behavior of that operator in Fourier space, in which $\Delta^{\mu/2}$ is just a multiplication by $-|k|^\mu$ extending the Fourier representation of the ordinary Laplacian ($-k^2$) to exponents $\mu \in (0, 2)$.



$$\begin{aligned} \partial_t p &= \mathcal{L}_\mu p \\ \mathcal{L}_\mu p &= e^{-\beta V/2} \Delta^{\mu/2} e^{\beta V/2} p - p e^{\beta V/2} \Delta^{\mu/2} e^{-\beta V/2}. \end{aligned} \quad (3.48)$$

What you see here is the FFPE for topological superdiffusion. Without a doubt this equation does have esthetic value. In addition, it represents the centerpiece of this work, as everything that we report in forthcoming chapters more or less revolves around it. Again, the similarity to the underlying master equation is obvious. Trivially, in equation (3.48) detailed balance is fulfilled. The solution to $\mathcal{L}_\mu p_s \equiv 0$ is always $p_s \propto \exp[-\beta V]$. If properly normalizable this solution is the stationary state of the system, that is to say Gibbs-Boltzmann equilibrium is retained in the limit (3.43). Since the rhs of (3.48) does not change if a constant offset V_0 is added to the potential, we may always choose V_0 such that the stationary state if it exists is normalized to unity,

$$p_s(x) = e^{-\beta V(x)} \quad \text{with} \quad \int dx p_s(x) = 1. \quad (3.49)$$

Hence topological superdiffusion is thermodynamically sound. For $\mu = 2$ equation (3.48) is identical to (3.17), in other words \mathcal{L}_μ is an ordinary Fokker-Planck operator in this case,

$$\mathcal{L}_\mu = \mathcal{L}_{FP} \quad \text{for} \quad \mu = 2. \quad (3.50)$$

If $\beta V \equiv 0$, that is either in the absence of an external potential or in the high temperature limit $\beta \rightarrow 0$ all the exponentials in (3.48) are unity and \mathcal{L}_μ is reduced to the fractional Laplacian of free superdiffusion,

$$\mathcal{L}_\mu = \Delta^{\mu/2} \quad \text{for} \quad \beta V \equiv 0. \quad (3.51)$$

Equations (3.50) and (3.51) show that the topological FFPE coincides with the FFPE describing additive Lévy stable noise (sections 2.6) and the FFPE associated with highly fluctuating temporal behavior (section 2.7) when either $\mu = 2$ or $\beta V \equiv 0$. However, for $0 < \mu < 2$ and non-vanishing βV the topological superdiffusion does not portray a situation equivalent to any of the FFPE discussed so far. More specifically, the dynamics governed by \mathcal{L}_μ can not be recast into a generalized Langevin description such as

$$dX = F(X, t) dt + D(X, t) dL_\mu(t). \quad (3.52)$$

This can be explained intuitively as follows: In topological superdiffusion, large magnitude jumps are caused by the underlying geometrical constraint of the system, they depend on energetic properties of the target location just as much as on the current position. This is not the case for generalized Langevin dynamics, where



the probability of an additive stochastic increment does not depend on the possible values the process $X(t)$ may acquire in the future.

Although the derivation of the FFPE (3.48) was based on the specific example of random hopping on a rapidly folding hetero-polymer in mean field, the range of its application is much wider. Whenever the probability rate of a master equation can be expressed as

$$w(x|y) \propto e^{-\beta[V(x)-V(y)]/2} f(x-y) \quad \text{with}$$

$$f(l) \propto \frac{1}{|l|^{1+\mu}} \quad \text{for } |l| \gg x_0 \quad \text{and } 0 < \mu \leq 2,$$

the asymptotics is governed by the FFPE given in (3.48). In other words, when thermal and geometrical components of the probability of making a transition $y \rightarrow x$ represent independent factors, the geometrical component decays according to an inverse power law as a function of distance with divergent variance, and the thermal factor describes ordinary Gibbs-Boltzmann thermodynamics the FPE must be generalized as above.

Mathematically, the FFPE describing topological superdiffusion is different from the FFPEs associated with generalized Langevin dynamics and subordination, compare equation (3.48) to equations (2.86) and (2.96) in sections 2.6 and 2.7, respectively. Yet the question must be addressed of whether all these generalizations imply substantial deviations in their dynamical properties, apart from the fact that the generalized Langevin approach violates Gibbs-Boltzmann thermodynamics. In chapter 4 the various FFPEs are compared in the paradigm of superdiffusion in the harmonic potential and escape dynamics in a double well potential. It will be shown that the dynamical properties of topological superdiffusion are indeed very different from any of the other superdiffusion models encountered so far.

The most drastic difference occurs when superdiffusion is modulated by an external potential with variable but limited magnitude. These type of potentials are frequently encountered in physical systems. The hetero-polymer in figure 3.1 is a good example. If each monomer type has a particular energy associated with it, the potential as a function of chemical coordinates is clearly a potential with variable but limited magnitude. Another example we mentioned earlier is the dispersion of foraging animals in their habitat, which can be successfully described by Lévy flight models [30, 73, 127, 128]. Usually, an animal's habitat is inhomogeneous and this inhomogeneity must be taken into consideration by a modulation of the dynamics [85]. We will show in section 4.3.4 that the asymptotics of generalized Langevin dynamics is trivial in any bounded potential, an indication that this modeling scheme fails for these type of systems. On the contrary, in topologically superdiffusive systems bounded potentials do have a significant impact on the dynamics. This will be discussed in chapters 5 and 6 on superdiffusion in periodic and quenched random phase potentials, respectively.



3.5. The Fractional Schrödinger Equation

The operator \mathcal{L}_μ defined in (3.48) is not symmetric, for the probability rate $w(x|y)$ of making a transition $y \rightarrow x$ is not necessarily the same as the probability rate $w(y|x)$ of making a transition in the reverse direction,

$$w(x|y) \neq w(y|x) \quad (3.53)$$

However, the property of detailed balance (3.30) provides us with a transformation $S^{1/2}$, by which the evolution equation can be cast into symmetric form (see Appendix C). In fact, any stochastic evolution equation of the type $\partial_t p = \mathcal{L} p$ can be recast into symmetric form, as long as a solution to $\mathcal{L} p = 0$ exists and detailed balance is fulfilled. Despite the fact that a symmetrization introduces a number of analytical techniques by which the problem is more likely to be bludgeoned into submission, one does not usually gain a deeper understanding of the dynamics by this, see for example section 3.6 on generalizations of topological superdiffusion. However, recasting the FFPE (3.48) into symmetric form yields a fractional Schrödinger equation which consists of two terms, an anomalous kinetic term and an effective potential term. This formal equivalence to quantum mechanical wave propagation entails a number of valuable analogies which promote the understanding of topological superdiffusion.

Adopting Dirac notation from quantum mechanics, the transformation we seek may be expressed as

$$S^{1/2} = \exp[-\beta V(X)/2] \quad (3.54)$$

$$= \int dx e^{-\beta V(x)/2} |x\rangle \langle x|. \quad (3.55)$$

The position operator X is simply a multiplication by x , i.e.

$$X = \int dx x |x\rangle \langle x|. \quad (3.56)$$

Since X is symmetric $S^{1/2}$ is, too. It represents a multiplication by the function $\exp[-\beta V(x)/2]$, the “square root” of the solution to $\mathcal{L}_\mu p_s \equiv 0$. The integral kernel of $S^{1/2}$ is given by

$$\langle x | S^{1/2} | y \rangle = e^{-\beta V(x)/2} \delta(x - y). \quad (3.57)$$

Normalizability of $\exp[-\beta V]$ is not required for the transformation to be applicable. Now we insert

$$p = S^{1/2} |\psi\rangle \quad \text{and} \quad (3.58)$$

$$\mathcal{L}_\mu = -S^{1/2} H S^{-1/2} \quad (3.59)$$



into (3.48), obtaining a fractional Schrödinger equation for the wave function $|\psi\rangle$,

$$\partial_t |\psi\rangle = -H |\psi\rangle. \quad (3.60)$$

The Hamiltonian H in (3.60) is indeed symmetric. Note, however, that this Schrödinger equation is missing the factor $i\hbar$, which we could formally introduce by mapping time on the imaginary axis, $t \rightarrow i\hbar t$. In terms of momentum and position operators the Hamiltonian reads

$$H = |P|^\mu + U_\mu(X). \quad (3.61)$$

This Hamiltonian describes the motion of a particle with an anomalous kinetic term $|P|^\mu$ in an effective potential $U_\mu(x)$. The anomalous kinetic term is an imprint of the superdiffusive nature of the original process. Intuitively, for a given kinetic energy the momentum increases when μ is decreased. The original potential $V(x)$ determines the effective potential

$$U_\mu(x) = e^{\beta V(x)/2} \Delta^{\mu/2} e^{-\beta V(x)/2}, \quad (3.62)$$

which also depends on the Lévy index μ . If we modify the kinetic term by varying μ the effect is balanced by a change of the effective potential. This is plausible, because Gibbs-Boltzmann equilibrium, i.e.

$$p_s(x) = e^{-\beta V(x)}, \quad (3.63)$$

does not depend on μ . In the ordinary diffusion limit the effective potential can be computed easily,

$$U = \frac{\beta}{2} \left[\frac{\beta}{2} (V')^2 - V'' \right]. \quad (3.64)$$

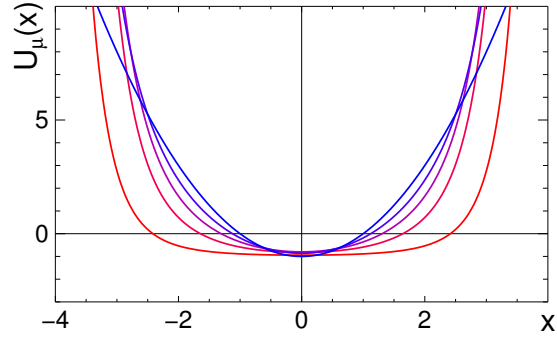
When $\mu \neq 2$ matters are more involved. The equivalence of the FFPE for topological superdiffusion and the fractional Schrödinger equation is more than formal. In fact, fractional Schrödinger equations have just recently been introduced to quantum mechanics and have been investigated in detail by Laskin [67, 68].

3.5.1. Topological Superdiffusion in the Harmonic Potential

The interplay between the anomalous kinetic term $|P|^\mu$ and effective potential term $U_\mu(X)$ is most transparent in the harmonic potential, which we will discuss in more detail in section 4.4. If $V(x) = x^2$ the effective potential is

$$U_\mu(x) = -\frac{1}{\sqrt{\pi}} (2\beta)^{\mu/2} \Gamma\left(\frac{1+\mu}{2}\right) \Phi\left(-\frac{\mu}{2}, \frac{1}{2}; \frac{\beta x^2}{2}\right), \quad (3.65)$$

Figure 3.4.: The effective potential $U_\mu(x)$ for superdiffusion in the harmonic potential $V(x) = x^2$ for $\beta = 1$. The curves represent effective potentials for a set of values of the Lévy index $\mu = \{0.1, 0.5, 1.0, 1.5, 2.0\}$. The red and blue curves correspond to $\mu = 0.1$ and $\mu = 2$, respectively, the intermediate hues to the intermediate Lévy indices.



where

$$\Phi(\alpha, \gamma; z) = 1 + \frac{\alpha z}{\gamma 1!} + \frac{\alpha(\alpha+1) z^2}{\gamma(\gamma+1) 2!} + \frac{\alpha(\alpha+1)(\alpha+2) z^3}{\gamma(\gamma+1)(\gamma+2) 3!} + \dots \quad (3.66)$$

The function Φ is a confluent hypergeometric function [50, pp. 1013]. When $\mu = 2$ the effective potential is quadratic in x , because all terms in the series expansion vanish due to the factor $\alpha + 1 = 0$ in the numerator in each term, and (3.65) reduces to

$$U_2(x) = \beta \left[\beta x^2 - 1 \right], \quad (3.67)$$

consistent with (3.64). When $\mu \in (0, 2)$ the series expansion cannot be truncated and the effective potentials contains terms of all orders of x^2 . The effective potential for a set of Lévy exponents μ for³ $\beta = 1$ is depicted in figure 3.4. For superdiffusive systems the effective potentials possess a more pronounced trough at the origin and a greater increase as $x \rightarrow \pm\infty$. The smaller the exponent μ , the stronger the effect, exactly balancing the superdiffusive kinetic term such that the Gaussian

$$\psi_s(x) = e^{-\beta x^2/2} \quad (3.68)$$

is the stationary state and identical for all superdiffusive systems in the harmonic potential. This is in sharp contrast to generalized Langevin dynamics in the harmonic potential [60] in which the stationary state does depend on the Lévy index μ and is a Gaussian only when $\mu = 2$ (see section 4.4). The dynamical properties of topological superdiffusion on one hand and generalized Langevin dynamics on the other are compared in detail in the next chapter.

³The value $\beta = 1$ can be considered without loss of generality, since a coordinate transformation $x \rightarrow \beta^{-1/2}x$, $t \rightarrow \beta^{-\mu/2}t$ yields an Schrödinger equation for the wave function $\phi(x, t) = \beta^{-1/2}\psi(\beta^{-1/2}x, \beta^{-\mu/2}t)$ with an effective potential $\hat{U}(x) = \beta^{-\mu/2}U(\beta^{-1/2}x)$ independent of β .



3.5.2. Perturbation Theory for Weak Potentials

Generally, it is very difficult to solve the fractional Schrödinger equation (3.60) for a given potential. Even the simpler task of finding the spectral decomposition of H is generally a hopeless enterprise. An method which often yields useful results is the perturbation expansion of the Hamiltonian in the vicinity of some H_0 for which the spectral decomposition is known. The example of the harmonic potential given above represents the simplest case of an external potential without bounds. Whenever V is unbounded, so is the effective potential U_μ in the fractional Hamiltonian (3.61), and $U_\mu(X)$ cannot be considered as a small perturbation of free superdiffusion, i.e.

$$H_0 = |P|^\mu. \quad (3.69)$$

However, in a variety of physical applications the potential $V(x)$ varies as a function of position but is bounded in magnitude, $|V| \leq V_0$, or possesses a typical variance,

$$\lim_{L \rightarrow \infty} \frac{1}{L} \int_L dx V^2(x) = V_0^2, \quad (3.70)$$

where we set the spatial average of $V(x)$ to zero, which we may, because an offset to $V(x)$ does not change the effective potential $U_\mu(x)$. Furthermore, we may set

$$V_0 = 1, \quad (3.71)$$

without loss of generality (this can be accomplished by the appropriate rescaling of the inverse temperature $\beta \rightarrow \beta/V_0$). Potentials of this type are appropriate for models in which spatial inhomogeneities need to be taken into account, such as the hetero-polymer discussed above. As opposed to generalized Langevin dynamics, which is trivial in these types of potentials (see section 4.3.4), they reflect the most interesting class of potentials for topologically superdiffusive systems.

Examples of potentials of this kind are periodic potentials (chapter 5) and random phase potentials (chapter 6), two examples of which are schematically depicted in figure 3.5. For various values of β and μ , the associated effective potentials are shown as well. The effective potential decreases in magnitude with β . Also, just as in the case for the harmonic potential, $U_\mu(x)$ differs for various values of μ . Nonetheless, the qualitative shape differs only little. When $V(x)$ is bounded, so is the effective potential U_μ . In this case the effective potential can be treated as a perturbation to (3.69), the magnitude of which is quantified by the perturbation parameter β . If β is small the effective potential $U_\mu(x)$ is approximately given by

$$U_\mu \approx -\frac{\beta}{2} \Delta^{\mu/2} V + \frac{\beta^2}{8} \left\{ \Delta^{\mu/2} V^2 - 2V \Delta^{\mu/2} V \right\}. \quad (3.72)$$

When $\beta \ll 1$, the effective potential is small and the fractional Hamiltonian can be treated by perturbation theory. The approximation (3.72) is superimposed on the

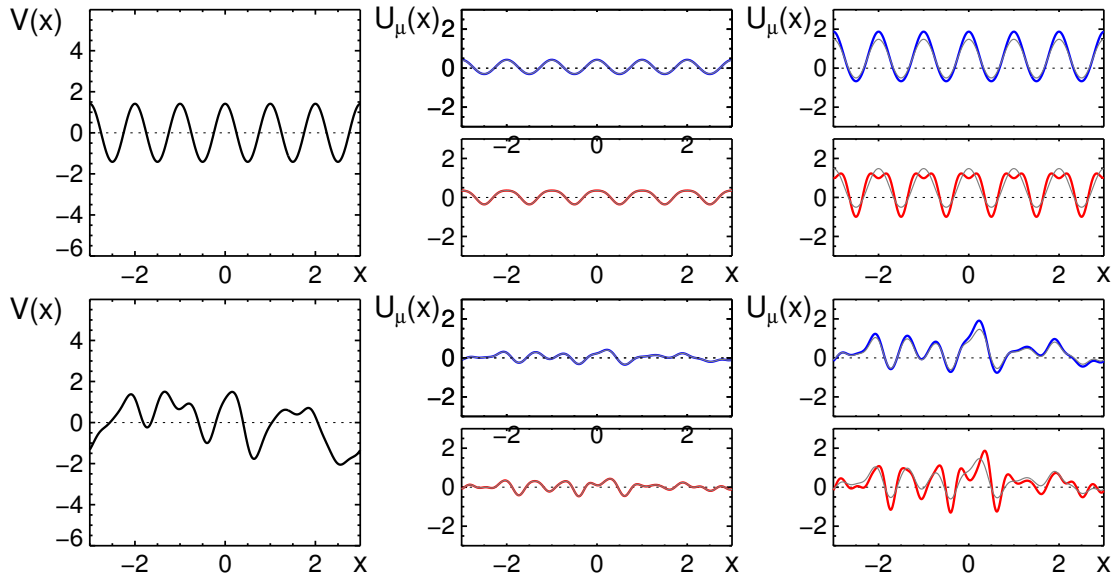


Figure 3.5.: Two examples of bounded potentials $V(x)$ with limited variance and their associated effective potentials $U_\mu(x)$. **Top:** $V(x) = \sqrt{2} \cos(x)$, **bottom:** a potential with a Gaussian power spectrum, uncorrelated random phases and unit variance. Effective potentials $U_\mu(x)$ are shown in the middle and right column for $\beta = 0.5$ and $\beta = 1.4$, respectively. Two values for the Lévy exponent were chosen and are distinguished by color, $\mu = 1$ (blue) and 2 (red). The high temperature approximation for $U_\mu(x)$, equation (3.72) is superimposed in grey.

effective potentials depicted in figure (3.5). The agreement with the exact effective potential is still satisfactory even when $\beta \approx 1$. Since β is an inverse temperature, the results obtained from (3.72) and (3.61) will be valid in the high temperature regime.

3.6. Generalizations of the Approach

The fractional generalization of the FPE derived and discussed above rests on a number of assumptions made for the transition rate $w(x|y)$ of the underlying master equation. First, the rate segregates into independent thermal and topological components,

$$w(x|y) = \frac{1}{\tau} e^{-\beta[V(x)-V(y)]/2} \rho(|x-y|). \quad (3.73)$$

If the topological factor $\rho(l)$ decreases with distance asymptotically as $|l|^{-(1+\mu)}$ the fundamental FFPE (3.48) is obtained. The thermal component of the rate, $\exp(-\beta[V(x) - V(y)]/2)$, fulfills two basic requirements often met in physical situations, namely that the probability of initiating a jump $y \rightarrow x$ decreases with increasing potential at the target location, and that it increases with increasing po-



tential at the source location y . The degree to which the potential at the source and target location contribute to the probability is balanced in the thermal factor in equation (3.73). Source and target locations contribute only by their difference,

$$\Delta V = \frac{1}{2}[V(x) - V(y)], \quad (3.74)$$

a potential offset is irrelevant. This last assumption may be relaxed while retaining the other features of the dynamics. If in the exponential in (3.73) instead of ΔV we insert

$$\Delta V_c = cV(x) - (1 - c)V(y) \quad \text{with} \quad c \in [0, 1], \quad (3.75)$$

a more general rate is obtained,

$$w(x|y) = \frac{1}{\tau} e^{-\beta c V(x)} \rho(|x - y|) e^{\beta(1-c)V(y)}. \quad (3.76)$$

The parameter c controls the influence of source and target location on the rate. When $c = 0$, the rate is independent of the potential at the target location. The opposite extreme case $c = 1$ depicts a situation in which the transition depends solely on the target location. When $c = 1/2$ the offset invariant rate (3.73) is recovered. The dynamics defined through (3.76) still fulfills detailed balance, the associated master equation possesses Boltzmann equilibrium, and transition rates increase with increasing potential at the source location and decrease with increasing potential at the target location.

When $c \neq 1/2$ the rate depends on the potential offset. If the entire potential is increased by a constant V_0 the $w(x|y)$ retains the same form, however the waiting time constant τ is effectively changed,

$$V \rightarrow V + V_0 \quad \Rightarrow \quad \tau \rightarrow \frac{\tau}{\exp[\beta V_0(2c - 1)]}. \quad (3.77)$$

Thus, when $c < 1/2$ (higher influence of the source location) an increase of the potential increases the typical rate at which transitions occur, whereas when $c > 1/2$ an increase of the potential by V_0 decreases the rate.

When $c \neq 1/2$ a fractional generalization of the FPE can be obtained in a manner analogous to the one by which we obtained the FFPE for $c = 1/2$. It is instructive to treat the case $\mu = 2$ (ordinary diffusion) first. In this case we must replace $\rho(|x - y|)$ in (3.76) by $\delta(x - y) \Delta_y$ and substitute the rate into the master equation which gives the following diffusion equation,

$$\partial_t p = e^{-c\beta V} \Delta e^{(1-c)\beta V} p - p e^{(1-c)\beta V} \Delta e^{-c\beta V}. \quad (3.78)$$

Expanding the sandwiched Laplacians, this equation can be recast into the familiar shape of an FPE,

$$\partial_t p = \left\{ -\nabla F + \frac{1}{2} \Delta D \right\} p. \quad (3.79)$$

Drift and diffusion coefficients can be expressed in terms of the potential $V(x)$, inverse temperature β and parameter c as



$$F(x) = -c\beta \frac{dV}{dx} D(x) \quad \text{and} \quad (3.80)$$

$$D(x) = 2 \exp[-\beta(2c - 1)V(x)]. \quad (3.81)$$

Two particular cases are of special interest. If we let $c = 1/2$ we recover the usual diffusion equation in a gradient force field,

$$c = 1/2 \quad \Rightarrow \quad \begin{cases} F & = -\beta \frac{dV}{dx} \\ D & = 2 \\ \partial_t p & = \left\{ \beta \nabla \frac{dV}{dx} + \Delta \right\} p, \end{cases} \quad (3.82)$$

which we have met in sections 3.2.1 and 3.3.1. When transitional rates are solely determined by the potential at the source site ($c = 0$), we obtain an evolution equation without drift term. The inhomogeneity of the environment is entirely incorporated in the position dependent diffusion coefficient $D(x)$,

$$c = 0 \quad \Rightarrow \quad \begin{cases} F & = 0 \\ D & = 2 \exp[\beta V] \\ \partial_t p & = \frac{1}{2} \Delta D p. \end{cases} \quad (3.83)$$

The Ito-stochastic differential equation for the process with a propagator evolving according to equation (3.83) reads (see Appendix B)

$$dX(t) = \sqrt{D(X)} dW(t). \quad (3.84)$$

Intuitively this is clear. The diffusion coefficient increases with the potential at a given location. The local speed of dispersion increases with the local diffusion coefficient, which in terms of Langevin dynamics is equivalent to an increased variance of the noise.

Proceeding along the same lines of reasoning, we may generalize equation (3.78) for topologically superdiffusive systems. For these systems the Laplacian must be replaced by its fractional generalization $\Delta^{\mu/2}$. The generalization thus obtained is

$$\partial_t p = e^{-c\beta V} \Delta^{\mu/2} e^{(1-c)\beta V} p - p e^{(1-c)\beta V} \Delta^{\mu/2} e^{-c\beta V}. \quad (3.85)$$

When $\mu = 2$ we recover the diffusion equation (3.19). Basic thermal properties, Boltzmann equilibrium, detailed balance etc., of the ordinary FPE remain unchanged, only the topological features of the evolution equation are altered in equation (3.85). A more careful procedure analogous to the one presented in section 3.4



leads to the same equation. Clearly, when $c = 1/2$ equation (3.85) is identical to (3.48), corresponding to thermal transitions which depend on potential differences only. In this case a description in terms of a stochastic differential equation fails to exist.

However, when $c = 0$ the second term on the rhs of equation (3.85) vanishes, since $\Delta^{\mu/2} 1 = 0$, and the generalized FFPE becomes

$$\partial_t p = \Delta^{\mu/2} D p \quad \text{with} \quad D(x) = e^{\beta V(x)}. \quad (3.86)$$

Again, a drift term is missing and the generalized diffusion coefficient is not constant. As opposed to the general case $c \neq 0$ and the most interesting case in terms of applications, $c = 1/2$, the generalized FFPE for topological superdiffusion is in fact equivalent to a generalized Langevin equation when $c = 0$,

$$dX(t) = [D(x)]^{1/\mu} dL_\mu(t), \quad (3.87)$$

since (3.86) and (3.87) are special cases of equations (2.86) and (2.66). In other words, the marginal case $c = 0$ of topological superdiffusion is equivalent to generalized Langevin dynamics with multiplicative Lévy stable noise.

The transition properties of the physical system one wishes to describe determine the correct choice of $c \in [0, 1]$. While the values $c = 1/2$ and $c = 0$ depict situations which one frequently encounters in physics, other values may be the correct choice in biological, econophysical, optimal search algorithms and various other systems. The intermediate case is of pronounced importance, since it reflects the situation in which transitions depend on potential differences only. It is also the only situation for which an alternative description in terms of a fractional Hamiltonian of the form

$$H = |P|^\mu + U_\mu \quad (3.88)$$

exists. Despite the fact that for any value of $c \in [0, 1]$ detailed balance is fulfilled and the problems can be recast into symmetrical form by the transformation (3.54), the resulting evolution equation for the field $|\psi\rangle$ is different, especially the appealing separation into kinetic and potential term in (3.88) and the quantum mechanical interpretation this entails are only valid when $c = 1/2$.

3.6.1. Higher Dimensions

The FFPE (3.48) is suitable for one-dimensional systems, examples of which are depicted in figure 3.1. Many other systems exist, such as the random graph in figure 3.2, for which a higher dimensional variant of the FFPE is called for. As a matter of fact, this generalization is straightforward and can be obtained in a similar fashion as the one presented above.



When the process $\mathbf{X}(t)$ evolves in \mathbb{R}^n and is subjected to a potential $V(\mathbf{x})$ with $\mathbf{x} \in \mathbb{R}^n$ the FFPE for the PDF $p(\mathbf{x}, t)$ is obtained when the topological component of the transition probability $\mathbf{x} \rightarrow \mathbf{y}$ asymptotically follows an inverse power law,

$$w(\mathbf{y}|\mathbf{x}) \propto |\mathbf{x} - \mathbf{y}|^{-(n+\mu)} \quad \mu \in (0, 2]. \quad (3.89)$$

In this case the probability $p(l)$ of initiating a jump of length l obeys a power law as well,

$$p(l) \propto l^{-(1+\mu)}. \quad (3.90)$$

The generalization of (3.48) to higher dimensions then reads

$$\partial_t p(\mathbf{x}, t) = e^{-\beta V(\mathbf{x})/2} \Delta_{\mathbf{x}}^{\mu/2} e^{\beta V(\mathbf{x})/2} p(\mathbf{x}, t) - p(\mathbf{x}, t) e^{\beta V(\mathbf{x})/2} \Delta_{\mathbf{x}}^{\mu/2} e^{-\beta V(\mathbf{x})/2}. \quad (3.91)$$

The n -dimensional generalization of the Laplacian in (3.91) is defined by

$$\Delta_{\mathbf{x}}^{\mu/2} f(\mathbf{x}) = -\frac{2^\mu \Gamma((\mu + n)/2)}{\pi^{n/2} \Gamma(-\mu/2)} \int_{-\infty}^{\infty} d^n y \frac{[f(\mathbf{y}) - f(\mathbf{x})]}{|\mathbf{x} - \mathbf{y}|^{\mu+n}}. \quad (3.92)$$

In Fourier space it reflects a multiplication by $-|\mathbf{k}|^\mu$, a behavior identical in all dimensions.

3.7. Discussion

When random walks with a well defined variance of step size or ordinary diffusion processes are subjected to an external field, or evolve in an inhomogeneous environment, the dynamics of the propagator is always governed by the FPE. Consequently, the dynamics can always be interpreted as evolving according to some deterministic dynamics perturbed by a stochastic noisy force. For a physicist, this is a very pleasant way to think about things. Thus, the first attempts and by far most frequently encountered generalizations of the FPE suitable for superdiffusive processes under the influence of an external force follow the same lines of reasoning, the generalized Langevin scheme discussed in the previous chapter.

However, the concept of topological superdiffusion, in which the topological complexity is responsible for enhanced transport, shows that the stochastic force picture is not only false in a number of situations, but also a very restrictive way of thinking. Depending on the physical situation, other generalizations of the FPE are appropriate. In particular, systems which are known to evolve in thermodynamics equilibrium cannot be successfully described by generalized Langevin dynamics.

The FFPE derived above is suitable for a number of systems which are superdiffusive, their thermal inconspicuousness notwithstanding. Not only does this new framework represent a new technique to analyze a great class of superdiffusive



systems which evolve in inhomogeneous environments, it also clears away the common misunderstanding that superdiffusive phenomena are a non-equilibrium phenomenon. Topologically superdiffusive systems can generally not be treated in terms of stochastic differential equations, the dynamics cannot be interpreted as being deterministic, perturbed by a possibly non generic noisy force. The interpretation is purely probabilistic. Consequently, whenever superdiffusion occurs in an inhomogeneous environment, the correct choice of FFPE depends on the underlying cause of enhanced transport, and the generalized Langevin scheme is not necessarily the appropriate modeling framework. In fact all models in which an ad hoc separation of deterministic evolution and fluctuating force are made are an embarrassment, and can only be trusted if fluctuation dissipation arguments can be relied upon to gain information about the noise. Recalling a number of situation which are known to be superdiffusive, namely dispersion on foraging animals in their habitat [30, 73, 127], stock price dynamics [102, 103], millennial climate changes [34], random walks on linear polymers [22, 24, 25, 122] and human eye-movements [23], to mention only a few, it is rather questionable whether a separation into independent deterministic and fluctuating forces can be made for these systems. These systems can be accounted for more plausibly by purely probabilistic models of the type developed in above.



3. Topological Superdiffusion





4. Comparison of Models

"The time has come," the
Walrus said, "To talk of many
things."

(Lewis Carroll)

This chapter is devoted to a detailed comparison of the various mechanisms which lead to superdiffusive behavior. We compare diffusion on scale free inhomogeneous structures (topological superdiffusion) with superdiffusion induced by anomalous noise (generalized Langevin dynamics) and by strong temporal fluctuations (subordinated superdiffusion). A scaling analysis is applied to the associated fractional Fokker-Planck equations (FFPEs). Not only does this type of analysis fortify our intuition about different superdiffusive mechanisms, it also reveals general properties of the dynamics, irrespective of the chosen external potential. Whereas topological and subordinated superdiffusion respond identically to spatio-temporal scaling, generalized Langevin dynamics exhibits a different response. The scaling analysis exposes a crucial difference between topological superdiffusion and generalized Langevin dynamics in bounded potentials. Although generalized Langevin dynamics is asymptotically trivial in these types of potentials, topological superdiffusion exhibits non-trivial behavior. We investigate the paradigmatic case of superdiffusion in the harmonic potential and escape dynamics in a double-well potential.

4.1. Motivation

In chapters 2 and 3 we showed that when Lévy flights evolve in external potentials, the type of fractional evolution equation to govern the dynamics depends on the underlying physical model. The non-local nature of Lévy flights requires different FFPEs for the description of topologically superdiffusive motion, subordinated processes and generalized Langevin dynamics. However, the formal differences between the FFPEs do not automatically imply essential differences in the dynamics. In the following we will investigate and compare all FFPEs by means of scaling techniques, and show that they possess strikingly different properties.



4.2. Of Apples, Pears and Potatoes

Let us recall the different principles which lead to superdiffusion and the associated FFPEs introduced in previous chapters. All FFPEs permit the incorporation of an external inhomogeneity. In topological superdiffusion this inhomogeneity is modeled by a potential $V(x)$, in generalized Langevin dynamics and subordinated superdiffusion by an external force $F(x)$. We will focus on gradient forces $F(x) = -dV(x)/dx$ and compare the different dynamics for specific choices of $V(x)$.

I: Topological Superdiffusion

<ul style="list-style-type: none"> • Scale free topologies • Gibbs-Boltzmann thermodynamics 	$\partial_t p(x, t) = \int dy [w(x y) p(y, t) - w(y x) p(x, t)]$ $w(x y) \sim e^{-\beta[V(x)-V(y)]/2} x - y ^{-(1+\mu)}$ <p style="text-align: center;">↓</p> $\partial_t p = e^{-\beta V/2} \Delta^{\mu/2} e^{\beta V/2} p - p e^{\beta V/2} \Delta^{\mu/2} e^{-\beta V/2} \quad (4.1)$ $\partial_t p = \mathcal{L}_T p$
---	--

The key characteristics of topological superdiffusion are summarized in the box above. The FFPE originates from an underlying master equation describing a jump process in which the probability rate $w(x|y)$ of jumping from y to x segregates into independent thermal and geometrical components. Topological superdiffusion is caused by an underlying scale-free topology and obeys ordinary thermodynamics. In the following we will refer to the operator describing topological superdiffusion as \mathcal{L}_T .

On the other hand, the FFPE for generalized Langevin dynamics describes superdiffusion due to anomalous Lévy stable white noise. It is obtained from a stochastic differential equation in which the ordinary Wiener increment dW is replaced by the differential dL_μ of the symmetric Lévy stable process of index μ , i.e.

$$\langle \delta(l - L_\mu(t)) \rangle = \frac{1}{2\pi} \int dk e^{-ikl - |k|^\mu t} \quad (4.2)$$



II: Generalized Langevin Dynamics

- Anomalous Lévy stable noise

$$dX = -\beta \frac{dV}{dX} dt + dL_\mu$$

$$\Downarrow$$

- Non-extensive thermodynamics

$$\partial_t p = \left(\beta \nabla V' + \Delta^{\mu/2} \right) p \quad (4.3)$$

$$\partial_t p = \mathcal{L}_N p$$

The operator describing generalized Langevin dynamics in an external potential $V(x)$ will be denoted by \mathcal{L}_N . Ordinary Gibbs-Boltzmann thermodynamics is generally violated by generalized Langevin dynamics.

III: Subordinated Superdiffusion

- strong temporal fluctuations

$$d\tilde{X}(\tau) = -\beta \frac{dV(\tilde{X}(\tau))}{d\tilde{X}} d\tau + dW(\tau)$$

$$\tau = \tau(t) \quad \rho(\Delta\tau) \sim (\Delta\tau)^{-(1+\mu/2)}$$

- Gibbs-Boltzmann thermodynamics

$$\Downarrow$$

$$\partial_t p = - \left(-\beta \nabla V' - \Delta \right)^{\mu/2} p \quad (4.4)$$

$$\partial_t p = \mathcal{L}_S p, \quad \mathcal{L}_S = - \left(-\mathcal{L}_{FP} \right)^{\mu/2}$$

Similar to generalized Langevin dynamics, subordinated superdiffusion is governed by a stochastic differential equation. However, superdiffusion is a result of strong temporal fluctuations. The associated evolution operator \mathcal{L}_S is obtained by raising the ordinary Fokker-Planck operator \mathcal{L}_{FP} to a fractional power of $\mu/2$. Like its topological sibling, subordinated superdiffusion obeys ordinary Gibbs-Boltzmann statistics.

4.2.1. Sometimes They Agree, But Mostly They Do Not

Comparing the definition of the stochastic operators defined in the boxes above, we see that they generally differ, i.e

$$\mathcal{L}_T \neq \mathcal{L}_N \neq \mathcal{L}_S. \quad (4.5)$$



Only for vanishing potential ($V \equiv 0$), or equivalently if $\beta = 0$ do all three operators describe free superdiffusion,

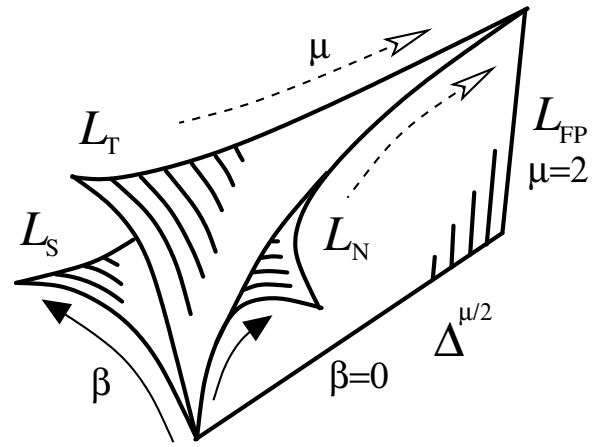
$$\beta V = 0 \quad \Rightarrow \quad \mathcal{L}_T = \mathcal{L}_N = \mathcal{L}_S = \Delta^{\mu/2}. \quad (4.6)$$

Likewise, in the ordinary diffusion limit ($\mu = 2$) they all coincide with ordinary Fokker-Planck operator \mathcal{L}_{FP} ,

$$\mu = 2 \quad \Rightarrow \quad \mathcal{L}_T = \mathcal{L}_N = \mathcal{L}_S = \beta \nabla V' + \Delta. \quad (4.7)$$

The situation is sketched qualitatively in figure 4.1. The operators are depicted as

Figure 4.1.: Qualitative comparison of the operators \mathcal{L}_T , \mathcal{L}_N and \mathcal{L}_S . Each operator is represented by a sheet in an “operator space”. The sheets are spanned by varying the parameters μ and β . On the boundary $\mu = 2$ all three operators are identical to the ordinary Fokker-Planck operator $\mathcal{L}_{FP} \beta \nabla V' + \Delta$. When $\beta = 0$ they coincide with the free superdiffusive fractional Laplacian $\Delta^{\mu/2}$. The “difference” between \mathcal{L}_T , \mathcal{L}_N and \mathcal{L}_S increases as β increases and μ decreases.



sheets in an abstract operator space parameterized by β and μ . The sheets coincide when $\beta = 0$ and/or when $\mu = 2$. The figure also indicates that the “difference” between \mathcal{L}_T , \mathcal{L}_S and \mathcal{L}_N increases either when β increases and/or when μ decreases.

4.3. Scaling Laws

In the following we will investigate the behavior of the FFPEs (4.1), (4.3) and (4.4) when the original spatio-temporal coordinates (x, t) are transformed to new ones, (z, τ) . Suppose we have a stochastic operator $\mathcal{L}(\alpha)$, a parameter set denoted by α , and an evolution equation

$$\partial_t p = \mathcal{L}(\alpha) p. \quad (4.8)$$

When the system is transformed into the new coordinate system by

$$z = x/\gamma \quad \text{and} \quad (4.9)$$

$$\tau = t/g(\gamma), \quad (4.10)$$

the relation

$$q(z, t) = \gamma p(\gamma z, g(\gamma) \tau) \quad (4.11)$$

between the original probability density function (pdf) $p(x, t)$ and the pdf $q(z, \tau)$ in the new coordinates induces a map

$$\mathcal{L}(\alpha) \mapsto \widehat{\mathcal{L}}(\widehat{\alpha}) \quad (4.12)$$

between the former operator $\mathcal{L}(\alpha)$ and the operator $\widehat{\mathcal{L}}(\widehat{\alpha})$ governing the evolution of $q(z, \tau)$ in the new coordinate system, i.e.

$$\partial_\tau q = \widehat{\mathcal{L}}(\widehat{\alpha}) q. \quad (4.13)$$

If the temporal scaling function $g_1(\gamma)$ is chosen appropriately, the transformation may leave the operator form invariant. Form invariance implies that only the parameters are changed by the transformation, i.e.

$$\widehat{\mathcal{L}}(\widehat{\alpha}) = \mathcal{L}(\widehat{\alpha}), \quad (4.14)$$

a relation from which useful dynamical properties can be obtained. When even the parameters remain unchanged under the transformation, i.e.

$$\widehat{\alpha} = \alpha \quad (4.15)$$

we speak of invariance under scaling or symmetry with respect to it.

Often, particular scaling regimes are of more interest than others. For example, one frequently wishes to investigate the behavior on large spatial scales. This corresponds to the study of the rescaled operator for a scaling factor $\gamma \gg 1$.

4.3.1. Ordinary Diffusion

For $\mu = 2$ all superdiffusive FFPEs coincide with the common FPE describing diffusion in an external potential, i.e.

$$\partial_t p(x, t) = \left(\beta \nabla_x \frac{dV(x)}{dx} + \Delta_x \right) p(x, t). \quad (4.16)$$

With $g(\gamma) = \gamma^2$ in equation (4.10) we find a form invariant description in the new coordinates,

$$\partial_\tau q(z, \tau) = \left(\beta \nabla_z \frac{d\widehat{V}(z)}{dz} + \Delta_z \right) q(z, \tau), \quad (4.17)$$

where the potential \widehat{V} is expressed in terms of V and z as

$$\widehat{V}(z) = V(\gamma z). \quad (4.18)$$





In other words \widehat{V} is just V at the different location. The magnitude of the potential remains unaltered. The potential cannot be “scaled away”. The spatio-temporal scaling

$$z = x/\gamma \quad \text{and} \quad \tau = t/\gamma^2 \quad (4.19)$$

is typical for ordinary diffusive motion.

4.3.2. Free Superdiffusion

When $\beta V \equiv 0$ all FPPEs are reduced to

$$\partial_t p(x, t) = \Delta_x^{\mu/2} p(x, t). \quad (4.20)$$

The behavior of the generalized Laplacian $\Delta^{\mu/2}$ under scaling is given by

$$\Delta_{\gamma z}^{\mu/2} = \frac{1}{\gamma^\mu} \Delta_z^{\mu/2}, \quad (4.21)$$

which can be obtained from the definition

$$\Delta_x^{\mu/2} f(x) = \frac{\Gamma(1 + \mu) \sin(\pi\mu/2)}{\pi} \int_{-\infty}^{\infty} dy \frac{[f(y) - f(x)]}{|x - y|^{1+\mu}}. \quad (4.22)$$

Thus, the coordinate transformation appropriate for (4.20) is

$$z = x/\gamma \quad \text{and} \quad (4.23)$$

$$\tau = t/\gamma^\mu, \quad (4.24)$$

which yields an invariant evolution equation for the new density $q(z, \tau)$, i.e.

$$\partial_\tau q(z, \tau) = \Delta_z^{\mu/2} q(z, \tau). \quad (4.25)$$

Comparing the coordinate scaling for superdiffusion with that appropriate for ordinary diffusion, we see that the temporal scaling function $g(\gamma)$ is proportional to γ^μ as opposed to the γ^2 -scaling in (4.19). Since equations (4.20) and (4.25) are identical, and $p(x, t)$ and $q(z, \tau)$ are related according to (4.11), the pdf $p(x, t)$ must satisfy

$$p(x, t) = \gamma p(\gamma x, \gamma^\mu t). \quad (4.26)$$

The rhs of (4.26) must be independent of γ , hence $p(x, t)$ can only depend on the ratio $x/t^{1/\mu}$. More specifically, letting $\gamma = (Dt)^{-\frac{1}{\mu}}$ we can write

$$p(x, t) = (Dt)^{-1/\mu} L_\mu \left(x/(Dt)^{1/\mu} \right), \quad (4.27)$$

with $\int dx L_\mu(x) = 1$ and some constant D . Without having to compute time dependent expectation values or even giving an explicit expression for the function L_μ , the canonical spatio-temporal behavior of superdiffusion is given by the argument of L_μ in (4.27), i.e.

$$X(t) \sim (Dt)^{1/\mu} \quad (4.28)$$

The parameter D is the generalized diffusion coefficient with units $[\text{length}]^\mu / [\text{time}]$. The function L_μ is the symmetric Lévy-stable law of index μ , i.e.

$$L_\mu(x) = \frac{1}{2\pi} \int dk e^{-ikx - |k|^\mu}. \quad (4.29)$$

4.3.3. Topological Superdiffusion

Proceeding swiftly, we examine the scaling properties of topological superdiffusion and investigate the FFPE (4.1). Without loss of generality, we examine the scaling properties of the equivalent fractional Schrödinger equation (see section 3.5) for the wave function

$$\psi(x, t) = e^{\beta V(x)/2} p(x, t). \quad (4.30)$$

From (4.1) we obtain

$$\partial_t \psi(x, t) = -\mathcal{H}_T \psi(x, t), \quad (4.31)$$

where the Hamiltonian

$$\mathcal{H}_T = -\Delta_x^{\mu/2} + U(x) \quad (4.32)$$

is symmetric and the effective potential $U(x)$ is given by

$$U(x) = e^{\beta V(x)/2} \Delta_x^{\mu/2} e^{-\beta V(x)/2}. \quad (4.33)$$

Rescaling the spatial coordinate x according to (4.9) and combining equations (4.31), (4.32) and (4.33) yields

$$\partial_t \psi(\gamma z, t) = \frac{1}{\gamma^\mu} \left[\Delta_z^{\mu/2} - e^{\beta V(\gamma z)/2} \Delta_z^{\mu/2} e^{-\beta V(\gamma z)/2} \right] \psi(\gamma z, t). \quad (4.34)$$

The prefactor $1/\gamma^\mu$ can be absorbed by the appropriate scaling of time (i.e. equation (4.24)). Thus, in the new coordinate system the process is governed by a form invariant FFPE,

$$\partial_\tau \phi = \left[\Delta^{\mu/2} - e^{\beta \hat{V}/2} \Delta^{\mu/2} e^{-\beta \hat{V}/2} \right] \phi. \quad (4.35)$$

The rescaled wave function ϕ is expressed in terms of ψ by

$$\phi(z, \tau) = \gamma \psi(\gamma z, \gamma^\mu \tau). \quad (4.36)$$





The potential appearing in \widehat{V} in (4.35) is the same as V in (4.33) at the rescaled location, i.e.

$$\widehat{V}(z) = V(\gamma z). \quad (4.37)$$

Although the exponent in the spatio-temporal scaling differs from the canonical scaling of ordinary diffusion, the relation between the potentials is the same as in ordinary diffusion, i.e. there is no prefactor depending on scaling factor γ . This implies that the potential V has an impact on the dynamics on all spatio-temporal scales. Since the potential quantifies an energy in many applications, equation (4.37) can be interpreted as a signature of the extensive nature of the energy in topologically superdiffusive systems.

4.3.3.1. Potentials with a Length Scale

In a number of physical situations external potentials are of finite variation and exhibit a typical length scale ξ . This implies that the potential depends solely on the ratio x/ξ , i.e. $V = V(x/\xi)$. Examples are periodic potentials for which ξ reflects the wavelength. A periodic potential of wavelength ξ can be expanded into a Fourier series

$$V(x/\xi) = \sum_n \widehat{V}_n \exp [2\pi i x/\xi], \quad (4.38)$$

in which the dependence on x/ξ is rather obvious. Note however that periodicity is not necessary. In chapter 6 random phase potentials are investigated which are nonperiodic but nevertheless possess a length scale defined by the correlation length also denoted by ξ . These potentials are frequently defined as

$$V(x/\xi) = \int dk \phi(k) e^{i\vartheta(k) + ikx/\xi}. \quad (4.39)$$

where the phases $\vartheta(k) = -\vartheta(-k)$ are uncorrelated random variables and the function $\phi(k)$ is related to the power spectrum $S(k)$ by

$$\phi(k)\overline{\phi(k')} = 2\pi S(k)\delta(k - k'). \quad (4.40)$$

The scaling analysis above suggests a choice of $\gamma = \xi$ which yields an FFPE (4.35) independent of ξ . The solution of the original equation $\psi(x, t)$ may then be expressed in terms of $\phi(z, \tau)$ as

$$\psi(x, t) = \xi^{-1} \phi(x/\xi, t/\xi^\mu), \quad (4.41)$$

in which the function ϕ is ξ -independent. Hence, in topological superdiffusion a typical length scale ξ drops out as a parameter.



4.3.3.2. x^n -Potentials

Often, randomly moving particles are bound by potentials which increase with increasing distance from the origin. These types of potentials are usually modeled by an even power of x as

$$V(x) = x^n \quad \text{with even } n. \quad (4.42)$$

In this situation the choice

$$\gamma = \beta^{-\frac{1}{n}} \quad (4.43)$$

is wise, because it yields a fractional Schrödinger equation (4.32) with an effective potential $U(z)$ in the new coordinates, which is independent of the parameter β , i.e.

$$U(z) = e^{z^n/2} \Delta_z^{\mu/2} e^{-z^n/2}, \quad (4.44)$$

and we can express $\psi(x, t)$ in terms of $\phi(z, \tau)$ as

$$\psi(x, t) = \beta^{\frac{1}{n}} \phi\left(\beta^{1/n} x, \beta^{\mu/n} t\right). \quad (4.45)$$

Consequently it suffices to investigate a system with $\beta = 1$ and subsequently employ equation (4.45) for the complete range of β .

4.3.4. Generalized Langevin Dynamics

When scaled, generalized Langevin dynamics exhibits a rather different behavior. In (x, t) -coordinates the FFPE (4.3) reads

$$\partial_t p(x, t) = \left(\beta \nabla_x \frac{dV}{dx} + \Delta_x^{\mu/2} \right) p(x, t). \quad (4.46)$$

In this equation, a clash occurs. The drift and anomalous diffusion terms possess a different natural response to spatial scaling. Substituting the spatio-temporal scaling relation for superdiffusion ($z = x/\gamma$, $\tau = t/\gamma^\mu$) we obtain in (z, τ) -coordinates

$$\partial_t q(z, \tau) = \left(\beta \nabla_z \frac{d\hat{V}}{dz} + \Delta_z^{\mu/2} \right) q(z, \tau), \quad (4.47)$$

which is form invariant to (4.46). However, the potential in the new coordinates $\hat{V}(z)$ is given by

$$\hat{V}(z) = \frac{V(\gamma z)}{\gamma^{2-\mu}}. \quad (4.48)$$

As opposed to the analogous relation (4.37) derived for topological superdiffusion, a μ -dependent factor $\gamma^{2-\mu}$ in the denominator of (4.48) effectively changes



the magnitude of the potential. Therefore, different superdiffusion processes see different potentials on different scales. For example, if we investigate the system on a coarser scale ($\gamma > 1$), we must choose a potential with a lowered magnitude if we wish to utilize a form invariant FFPE. In topologically superdiffusive systems, a length scale ξ of the potential effectively drops out as a parameter of the system by choosing the appropriate value $\gamma = \xi$. In generalized Langevin dynamics this is generally impossible, and the wavelength of a periodic potential or the correlation length of a random phase potential represents an essential parameter of the system.

Taking this train of thought a bit further, we discover that the seemingly harmless factor $\gamma^{2-\mu}$ implies a rather far reaching consequence. If the potential is of finite variation, i.e.

$$|V(x)| \leq V_0, \quad (4.49)$$

the impact of the potential on the asymptotics of the process vanishes, because as $\gamma \rightarrow \infty$ the potential tends to zero. Only in the diffusion limit ($\mu = 2$) is equation (4.48) reduced to (4.18). Alternatively, one may incorporate the factor $\gamma^{\mu-2}$ into the parameter β as

$$\hat{\beta} = \beta/\gamma^{2-\mu}, \quad (4.50)$$

and leave the potential V unchanged. For systems coupled to a heat bath, this can be interpreted as follows. When $\mu = 2$ the parameter β is an inverse energy and represents an inverse temperature, i.e. $\beta = (k_B T)^{-1}$. The temperature T is an intensive quantity in ordinary Gibbs-Boltzmann thermodynamics, and remains unchanged under scaling, in other words $\hat{\beta} = \beta$. In systems driven by Lévy stable white noise ($\mu < 2$), the temperature is affected by scaling and is no longer an intensive quantity. Therefore, these systems describe situations which violate ordinary thermodynamics. However, generalizations of ordinary Gibbs-Boltzmann statistics exists in which requirements on thermodynamics quantities are relaxed and which can be related to generalized Langevin dynamics [26, 105, 123].

Equivalently, one can deduce the behavior under coordinate transformation in terms of the stochastic differential equation

$$dX = -\beta \frac{dV}{dX} dt - dL_\mu. \quad (4.51)$$

To this end we compute the scaling behavior

$$dL_\mu(\gamma^\mu \tau) = \gamma dL_\mu(\tau) \quad (4.52)$$

of the Lévy stable differential $dL_\mu(t)$, which is easily obtained from the pdf for $L_\mu(t)$, i.e.

$$p(x, t) = \langle \delta(L_\mu(t) - x) \rangle = \frac{1}{2\pi} \int dk e^{-ikx - |k|^\mu t} \quad t > 0. \quad (4.53)$$

Rescaling spatial and temporal coordinates as above, the generalized Langevin equation for the new process



$$Y(\tau) = \gamma^{-1}X(\gamma^\mu\tau) \quad (4.54)$$

has the same form as (4.51), i.e.

$$dY = -\hat{\beta}\frac{d\hat{V}}{dY}d\tau - dL_\mu. \quad (4.55)$$

The potential \hat{V} and parameter $\hat{\beta}$ are

$$\hat{V}(z) = V(\gamma z) \quad \text{and} \quad (4.56)$$

$$\hat{\beta} = \gamma^{\mu-2}\beta. \quad (4.57)$$

which is equivalent to the rescaled FFPE (4.47). In rescaled coordinates, the influence of the potential becomes smaller on larger scales. Intuitively, as we observe the system on increasing spatial scales, the likelihood of extreme kicks by the anomalous Lévy stable noise is increased. With respect to the noisy influence the deterministic drift becomes less important.

4.3.5. Subordinated Superdiffusion

The scaling behavior of subordinated superdiffusion is easily obtained by combining the associated FFPE in (x, t) -coordinates

$$\partial_t p(x, t) = -(-\mathcal{L}_{x,FP})^{\mu/2} p(x, t) \quad (4.58)$$

with the scaling behavior of the ordinary diffusion processes (4.19). The subscript x in the Fokker-Planck operator denotes the current coordinate. With $z = x/\gamma$ and $\tau = t/\gamma^\mu$, the FFPE for the pdf in the new coordinates is given by

$$\partial_\tau q(z, \tau) = -(-\mathcal{L}_{z,FP})^{\mu/2} q(z, \tau), \quad (4.59)$$

where the operator $\mathcal{L}_{z,FP}$ is defined by the rhs of (4.17), i.e.

$$\mathcal{L}_{z,FP} = \frac{1}{\gamma^2}\mathcal{L}_{\gamma z,FP}. \quad (4.60)$$

The exponent $\mu/2$ in the FFPE (4.58) ensures the appropriate superdiffusive scaling, so the prefactor γ^{-2} is transformed into $\gamma^{-\mu}$. The relation (4.60) implies for subordinated processes

$$\hat{V}(z) = V(\gamma z), \quad (4.61)$$



the same result we obtained for ordinary diffusion and topological superdiffusion. Consequently, external potentials acquire the same importance for subordinated processes as for topological superdiffusion. The scaling analysis alone cannot extract dynamical differences of both types of superdiffusion. On the other hand, subordinated superdiffusion is similar to generalized Langevin dynamics in the sense that both are derived from underlying stochastic differential equations which seem mathematically akin.

4.4. Relaxation in the Harmonic Potential

The dynamical differences of various types of superdiffusion become particularly transparent in the paradigmatic case of the harmonic potential $V(x) = x^2$. Relaxation properties in the harmonic potential are universal in the sense that many potentials can be locally approximated by them. Ordinary diffusion in this type of potential is known as the Ornstein-Uhlenbeck process [124]. We compare relaxation dynamics of topological superdiffusion, generalized Langevin dynamics and subordinated superdiffusion. Although the parameter β may represent different physical quantities in different models and FFPEs, in the following we will interpret β as an inverse temperature $\beta \propto T^{-1}$, and concentrate on the differences in spatio-temporal scaling with respect to changes in the temperature T .

4.4.1. Topological Superdiffusion

Topological superdiffusion in the harmonic potential is governed by the fractional Schrödinger equation

$$\partial_t \psi(x, t) = - \left(\Delta_x^{\mu/2} + U_\mu(x) \right) \psi(x, t) \quad (4.62)$$

with an effective potential $U(x)$ which can be expressed in terms of the confluent hypergeometric function $\Phi(\alpha, \gamma; z)$ as

$$U_\mu(x) = -\frac{1}{\sqrt{\pi}} (2\beta)^{\mu/2} \Gamma\left(\frac{1+\mu}{2}\right) \Phi\left(-\frac{\mu}{2}, \frac{1}{2}; \frac{\beta x^2}{2}\right) \quad \text{where} \quad (4.63)$$

$$\Phi(\alpha, \gamma; z) = 1 + \frac{\alpha z}{\gamma 1!} + \frac{\alpha(\alpha+1) z^2}{\gamma(\gamma+1) 2!} + \frac{\alpha(\alpha+1)(\alpha+2) z^3}{\gamma(\gamma+1)(\gamma+2) 3!} + \dots \quad (4.64)$$

The effective potential depends on the Lévy exponent μ such that the anomaly in the kinetic term is exactly balanced in Gibbs-Boltzmann equilibrium. The stationary state is

$$\psi_s(x) = e^{-\beta x^2/2}, \quad (4.65)$$



which is independent of μ . For a set of Lévy exponents μ the corresponding effective potentials are depicted in figure 3.4. Although it is impossible to solve (4.62) exactly, we may employ the scaling properties of section 4.3.3.2. Equation (4.45) with $n = 2$ yields

$$\psi(x, t) = \beta^{\frac{1}{2}} \phi\left(\beta^{1/2} x, \beta^{\mu/2} t\right). \quad (4.66)$$

Denoting typical spatial and temporal scales by ξ and τ , respectively, one readily infers from (4.66) how ξ and τ scale with the parameter β , or alternatively the temperature T ,

$$\xi \propto \beta^{-1/2} \propto T^{1/2} \quad \text{and} \quad (4.67)$$

$$\tau \propto \beta^{-\mu/2} \propto T^{\mu/2}. \quad (4.68)$$

The temperature dependence (4.67) of the spatial scale ξ can also be extracted from the stationary solution (4.65). Since topological superdiffusion always implies ordinary thermodynamics, the energy scale ($E = \xi^2$ in the harmonic potential) is always proportional to the temperature T , i.e.

$$E = \xi^2 \propto T. \quad (4.69)$$

Thus, the exponent μ does not appear in (4.67). Only the temperature dependence of the temporal scale τ is affected by the exponent μ , the anomaly of the process is a temporal one. The ordinary Ornstein-Uhlenbeck process ($\mu = 2$) is characterized by a relaxation time linear in T . If $\mu < 2$, relaxation to the stationary state is faster at high relative temperatures, i.e.

$$T^{\mu/2} < T \quad \text{for} \quad T > 1 \quad (4.70)$$

and slower when the temperature is low,

$$T^{\mu/2} > T \quad \text{for} \quad T < 1. \quad (4.71)$$

Clearly, the typical time scale τ as well as the typical energy scale $E = \xi^2$ increase with temperature. Their ratio τ/ξ^2 as a function of T quantifies in terms of ξ^2 how much time elapses until energy is distributed within this typical energy range,

$$\frac{\tau}{\xi^2} \propto T^\eta \quad \text{with} \quad \eta = \frac{\mu}{2} - 1. \quad (4.72)$$

If $\mu = 2$ then η vanishes and in units of ξ^2 the typical time scale of equilibration is temperature independent. On the other hand, $\mu < 2$ implies that $\eta < 0$. Thus, relaxation in terms of energy is faster for high and slower for low temperatures. Note, however, that the canonical relation

$$\frac{\xi^\mu}{\tau} = \text{const.} \quad (4.73)$$

is fulfilled for topological superdiffusion in the harmonic potential.



4.4.2. Subordination

Of course, all of the above applies to subordinated superdiffusion as well, since it exhibits a scaling behavior identical to that of topological superdiffusion. Because \mathcal{L}_S is just a power of the ordinary Fokker-Planck operator, the solution $p(x, t)$ for subordinated superdiffusion in the harmonic potential can be computed in a straightforward fashion. Since the ordinary Fokker-Planck operator fulfills detailed balance, we can map the FPE onto the symmetric Schrödinger equation,

$$\partial_t \psi = -\mathcal{H}_{FP} \psi \quad \text{where} \quad (4.74)$$

$$\mathcal{H}_{FP} = -\Delta + U \quad \text{and} \quad (4.75)$$

$$U(x) = \beta(\beta x^2 - 2). \quad (4.76)$$

The Hamiltonian \mathcal{H}_{FP} has a discrete spectrum and can be decomposed according to

$$\mathcal{H}_{FP} = \sum_n \lambda_n \mathcal{P}_n. \quad (4.77)$$

The eigenvalues depend linearly on the label n and are given by [109]

$$\lambda_n = 4\beta n \quad \text{with} \quad n \in \mathbb{N}. \quad (4.78)$$

The Hamiltonian \mathcal{H}_S associated with \mathcal{L}_S has the same spectral measure as \mathcal{H}_{FP} (the operators commute) and the spectral decomposition of \mathcal{H}_S reads

$$\mathcal{H}_S = \sum_n (\lambda_n)^{\mu/2} \mathcal{P}_n. \quad (4.79)$$

Following the lines of reasoning explained in detail in Appendix C and utilizing equation (C.52), we can express the conditional pdf $p(x, t) = p(x, t|x_0, t_0)$ in terms of eigenvalues λ_n and eigenstates $\psi_n(x)$ of \mathcal{H}_{FP} as

$$p(x, t) = e^{-\beta x^2} + e^{-\beta x^2/2} \sum_{n=1} \exp \left[- (4\beta n)^{\mu/2} t \right] \psi_n(x) \psi_n(0), \quad (4.80)$$

where the eigenfunctions $\psi_n(x)$ can be expressed in terms of Hermite polynomials [43, pp. 143],

$$\psi_n(x) = \frac{1}{2^n n!} \left(\frac{2\beta}{\pi} \right)^{1/2} H_n(\sqrt{2\beta}x) e^{-\beta x^2}. \quad (4.81)$$

The only difference from the ordinary Ornstein-Uhlenbeck process is an anomalous, sublinear dependence of the relaxation times on the label n (see the exponential in (4.80)).



4.4.3. Generalized Langevin Dynamics

Generalized Langevin dynamics in the harmonic potential is one of the rare cases for which an explicit solution of the FFPE can be computed [60]. The generalized Langevin equation

$$dX = -2\beta X dt + dL_\mu \quad (4.82)$$

is linear and the associated FFPE is given by

$$\partial_t p(x, t) = \left(2\beta \nabla_x x + \Delta_x^{\mu/2} \right) p(x, t). \quad (4.83)$$

For the initial condition

$$p(x, 0) = \delta(x). \quad (4.84)$$

the solution $p(x, t)$ can be expressed as a Fourier integral, i.e.

$$p(x, t) = \frac{1}{2\pi} \int dk \exp \left(-ikx - \xi^\mu |k|^\mu \left[1 - e^{-t/\tau} \right] \right). \quad (4.85)$$

Comparing to (4.29) we see that $p(x, t)$ is at all times a Lévy stable law of index μ with time dependent generalized diffusion coefficient $D(t)$, i.e.

$$p(x, t) = D^{-1/\mu}(t) L_\mu \left(x/D^{1/\mu}(t) \right) \quad \text{with} \quad (4.86)$$

$$D(t) = \xi^\mu \left[1 - e^{-t/\tau} \right]. \quad (4.87)$$

For all $\mu \in (0, 2]$ a stationary solution exists and is given by

$$p_s(x) = \frac{1}{2\pi} \int dk \exp \left(-ikx + \xi^\mu |k|^\mu \right). \quad (4.88)$$

The stationary state depends on μ and is only identical to Gibbs-Boltzmann equilibrium for the boundary case of ordinary diffusion ($\mu = 2$). The spatial and temporal scales ξ and τ in equations (4.86) and (4.88) in terms of μ and β are

$$\xi^\mu = \tau = \frac{1}{2\mu\beta}. \quad (4.89)$$

From this we obtain their scaling with T , i.e.

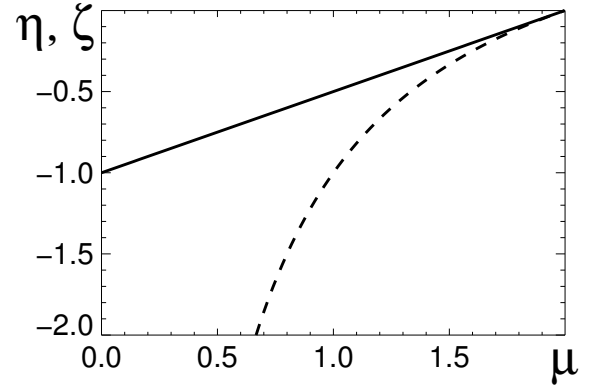
$$\xi \propto \beta^{-1/\mu} \propto T^{\frac{1}{\mu}} \quad (4.90)$$

$$\tau \propto \beta^{-1} \propto T. \quad (4.91)$$

Comparing to the analogous expressions derived for topological superdiffusion, i.e. equations (4.67) and (4.68), we discover a totally different scaling with T . The



Figure 4.2.: The scaling exponents η (solid line) and ζ (dashed line) of dispersion time per energy (τ/ξ^2) as functions of the Lévy exponent μ in topological superdiffusion (and subordinated superdiffusion) and generalized Langevin dynamics in the harmonic potential as defined by equations (4.72) and (4.93).



scaling relations (4.90) and (4.91) inform us that the temporal scale τ is unaffected by the anomalous exponent μ , and the linear temperature dependence is identical to the one of the ordinary Ornstein-Uhlenbeck process. However, $p(x, t)$ as well as the stationary solution $p_s(x)$ possess algebraic tails depending on μ . Therefore, in contrast to the situation previously discussed, the anomaly in systems described by (4.83) resides in the spatial domain. Intuitively this is clear, the anomalous increments dL_μ are “added” to the stochastic quantity $X(t)$ in the generalized Langevin equation (4.82).

The relation (4.90) restates the nonlinear temperature dependence of energy, i.e.

$$E = \xi^2 \propto T^{2/\mu}, \quad (4.92)$$

which is to be compared to the thermally inconspicuous relation (4.69) observed in topologically superdiffusive systems. Equation (4.92) states that the formal identification of the parameter β with an inverse temperature remains a formal one in generalized Langevin dynamics, since T is not an energy. Combining (4.90) and (4.91) we obtain the ratio τ/ξ^2 of dispersion time per energy, i.e.

$$\frac{\tau}{\xi^2} \propto T^\zeta \quad \text{with} \quad \zeta = 1 - \frac{2}{\mu}. \quad (4.93)$$

The temperature scaling is determined by the exponent ζ which is quite different from the exponent η observed in topologically superdiffusive systems, see equation (4.72). As expected, for $\mu = 2$ the ratio τ/ξ^2 is independent of T . Similar to the exponent η (i.e. equation 4.72)) the exponent ζ is negative for $\mu < 2$. However, the physical consequences are more pronounced since $\zeta < \eta$, in fact as $\mu \rightarrow 0$ the exponent ζ diverges. Both exponents η and ζ as functions of the Lévy exponent μ are shown in figure 4.2.

Note, however, that the canonical relation (4.73) also holds in systems described by generalized Langevin dynamics. In table 4.1, the various scaling behaviors with



temperature T of different quantities of topological superdiffusion, subordinated superdiffusion and generalized Langevin dynamics in the harmonic potential are summarized.

	$\xi \propto T^p$	$\tau \propto T^p$	$\tau/\xi^\mu \propto T^p$	$\tau/\xi^2 \propto T^p$
\mathcal{L}_{FP} $p =$	1/2	1	0	0
\mathcal{L}_T $p =$	1/2	$\mu/2$	0	$\mu/2 - 1$
\mathcal{L}_S $p =$	1/2	$\mu/2$	0	$\mu/2 - 1$
\mathcal{L}_N $p =$	$1/\mu$	1	0	$1 - 2/\mu$

Table 4.1.: Scaling behavior of various quantities with temperature. Topological and subordinated superdiffusion (\mathcal{L}_T and \mathcal{L}_S) and generalized Langevin dynamics (\mathcal{L}_N) in the harmonic potential are compared to the ordinary Ornstein-Uhlenbeck process (\mathcal{L}_{FP}). Spatial and temporal scales are denoted by ξ and τ , respectively. The quantity ξ^μ/τ reflects the canonical quotient of superdiffusion and τ/ξ^2 dispersion time per energy in the harmonic potential. All quantities scale with T as T^p where p is different in each case. For topological superdiffusion, the anomalous exponent μ appears in the time scale, as opposed to generalized Langevin dynamics where only ξ depends on it.

4.4.4. Trajectories, Relaxation and Spectra

The analysis above showed that the spatio-temporal scaling behavior and the scaling with the parameter β differs considerably in various superdiffusive processes. Geometrical differences are particularly obvious when single realizations $X(t)$ of all types of processes are compared. For $\mu = 2$ realizations $X(t)$ are continuous (Ornstein-Uhlenbeck process), and the stationary density is Gaussian, i.e.

$$p_s(x) = e^{-\beta x^2}. \quad (4.94)$$

Since the fractional generalizations involve non-local fractional operators, the trajectories are discontinuous.

In figure 4.3, a number of trajectories of the Ornstein-Uhlenbeck process are compared to realizations of generalized Langevin dynamics, topological and subordinated superdiffusion. Generalized Langevin dynamics is characterized by fre-

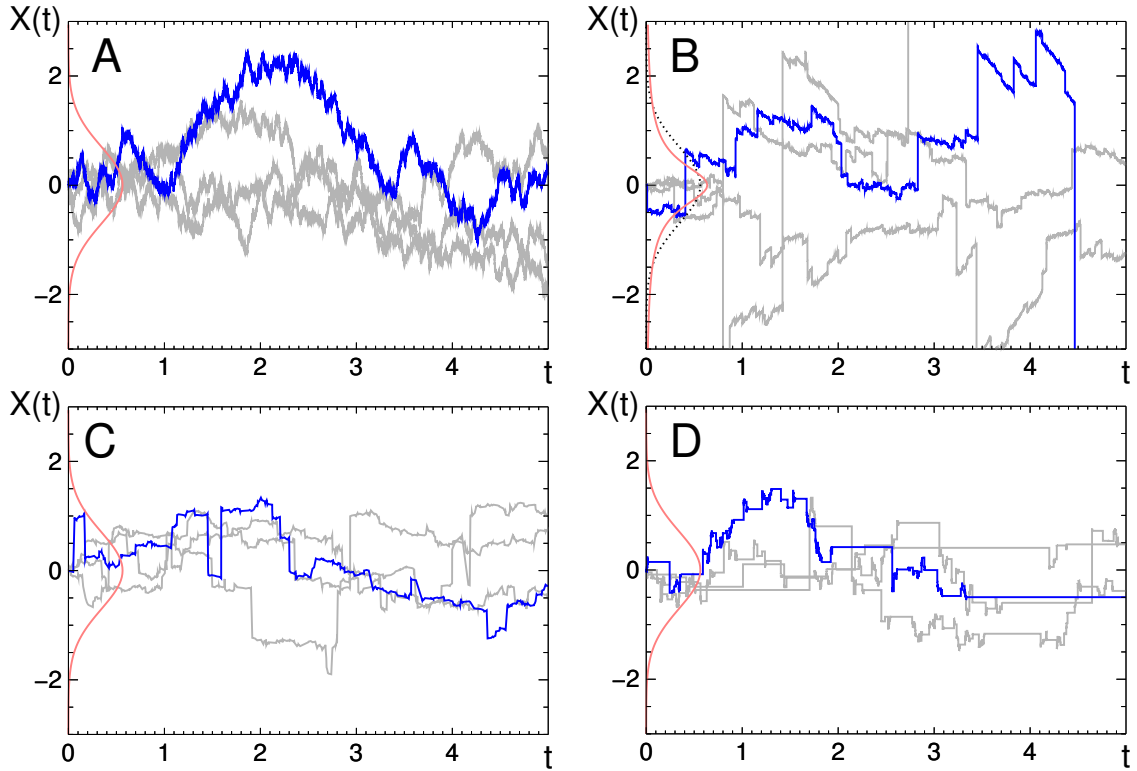


Figure 4.3.: Realizations $X(t)$ of the Ornstein-Uhlenbeck process (A) compared to generalized Langevin dynamics (B) topological superdiffusion (C) and subordinated superdiffusion (D) in the harmonic potential. The Lévy exponent for the superdiffusive processes was set to $\mu = 1$ the parameter β was set to unity. The red curves indicate the stationary density $p_s(x)$, the Gibbs-Boltzmann equilibrium $\exp(-\beta x^2)$ in (A), (C) and (D) and the Lévy stable law (equation (4.88)) in (B). The dotted line in (B) is identical to the Gaussian and serves as a reference.

quent, large excursions, taking the system to a position distant from the equilibrium value $x = 0$. Large kicks are interspersed with relaxation periods in which the linear Hookean force in (4.82) takes the system back to the equilibrium value. Note that the stationary state for generalized Langevin dynamics is no longer Gaussian but a Lévy stable law given by equation (4.88).

The topologically superdiffusive process exhibits large scale trajectory excursions as well, but they are restricted to an interval approximately given by the width of the Gaussian stationary state. Furthermore, the trajectories do not display periods of linear relaxation towards the origin. Intuitively this is clear, since in topological superdiffusion no segregation into deterministic drift and anomalous additive noise can be made. Qualitatively, the trajectories evolve similarly to free superdiffusion in the interval defined by the length scale $\xi \approx \sqrt{\beta}$. The subordination process exhibits long waiting times and infrequent but large scale jumps.

Figure 4.4 depicts the solutions $p(x, t)$ of the FFPEs for $\mu = 1$ and the FPE of the

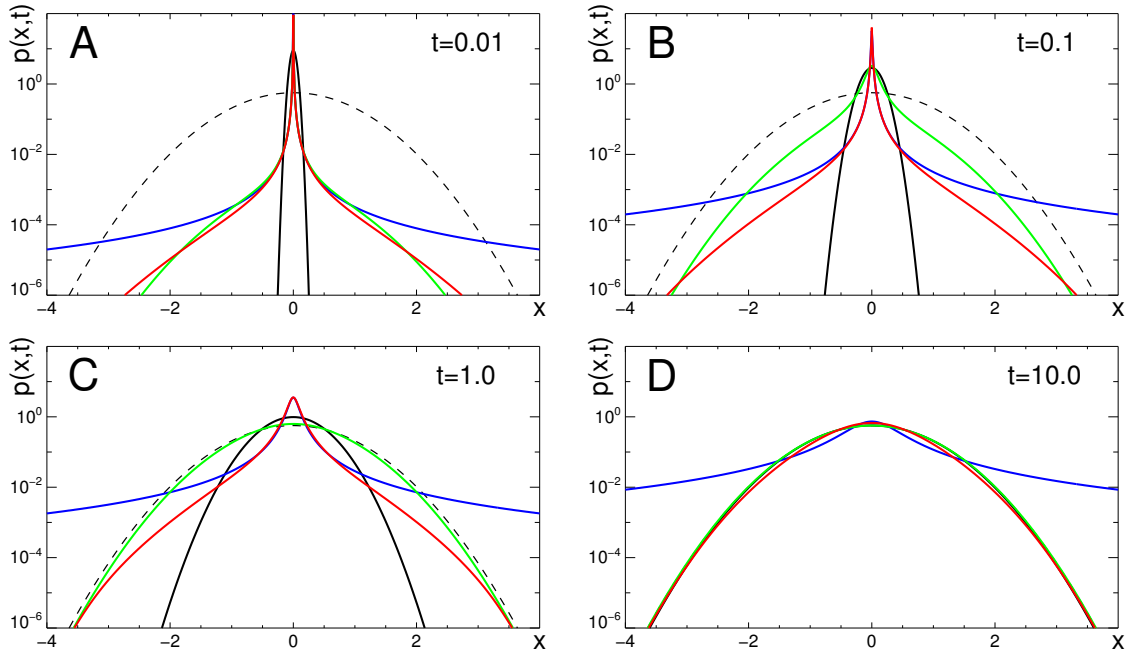


Figure 4.4.: Temporal evolution of the propagator $p(x, t)$ of the Ornstein-Uhlenbeck process (black line), generalized Langevin dynamics (blue line), topological superdiffusion (red line) and subordinated superdiffusion (green line). Parameters were $\beta = 1$ for each process and $\mu = 1$ for the superdiffusive processes. The Gaussian stationary density of the Ornstein-Uhlenbeck process is given by the dashed line. Each panel shows $p(x, t)$ at different times t , which are to be compared to the typical relaxation time of the diffusion process, $\tau = 1/4$.

Ornstein-Uhlenbeck process. The inverse temperature is identical for all systems ($\beta = 1$). On small spatial scales and for small times, the pdfs of the superdiffusive processes coincide and display a pronounced cusp at the origin as opposed to the Gaussian shape of the Ornstein-Uhlenbeck density. On large spatial and small temporal scales all processes deviate from one another considerably. As time evolves, $p(x, t)$ of the topological and subordinated superdiffusive processes attain Gaussian shape, whereas the $p(x, t)$ of generalized Langevin dynamics remains Lévy stable at all times.

Dynamical differences of the three types of superdiffusion are also visible in the spectra of \mathcal{L}_T , \mathcal{L}_S and \mathcal{L}_N . The eigenvalues λ_n are given by,

$$(\mathcal{L} - \lambda_n) \theta_n = 0, \quad (4.95)$$

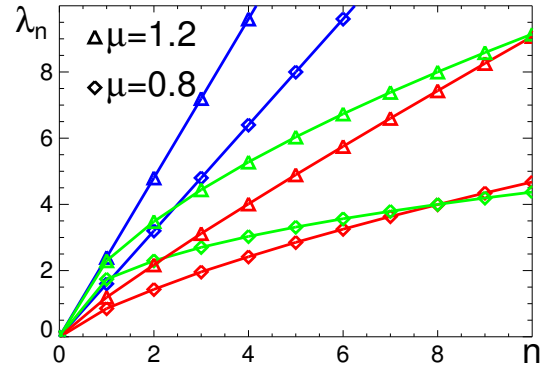
in which \mathcal{L} is one of the above operators and the θ_n denote the corresponding eigenstates. In all cases the spectrum is discrete.

The spectrum of \mathcal{L}_N can be computed for the harmonic potential [60]. It is given by

$$\mathcal{L}_N : \quad \lambda_n = 2\beta\mu n. \quad (4.96)$$



Figure 4.5.: Spectrum of eigenvalues λ_n for the three kinds of superdiffusion in the harmonic potential. Blue, red and green symbols show the eigenvalues of generalized Langevin dynamics, topological superdiffusion and subordinated superdiffusion, respectively. Symbols differentiate between the two Lévy exponents $\mu = 6/5$ and $4/5$. The parameter β was set to 1.



For all Lévy exponents μ the eigenvalues increase linearly with n . Furthermore, λ_n is proportional to β , consistent with the expected temporal behavior of generalized Langevin dynamics (see equation (4.91)).

Since \mathcal{L}_S is a fractional power of the ordinary Fokker-Planck operator \mathcal{L}_{FP} the spectrum of the former is easily computed from the the spectrum of the latter (4.78) and reads

$$\mathcal{L}_S : \quad \lambda_n = (4\beta n)^{\mu/2}. \quad (4.97)$$

It is a matter of misfortune and lack of dexterity that the author was unable to determine the eigenvalues of \mathcal{L}_T analytically. However, the scaling relation (4.66) states that

$$\mathcal{L}_T : \quad \lambda_n = \beta^{\mu/2} \Lambda_n, \quad (4.98)$$

where Λ_n is independent of β . The $\beta^{\mu/2}$ behavior of λ_n in (4.97) and (4.98) reflects the anomalous temporal behavior of subordinated and topological superdiffusion with respect to temperature scaling, which we have already encountered in equation (4.68). Comparing the spectra, we deduce that each superdiffusive process can be faster than the other two, depending on the temperature regime. In figure 4.5, the first few eigenvalues for the processes are depicted. The spectra for two Lévy exponents, $\mu = 6/5$ and $4/5$, are shown.

Concluding, we can say that the different types of mechanisms which induce superdiffusive motion exhibit strong dynamical differences in the paradigmatic example of the harmonic potential, and we expect that these differences will also be present in more complicated external fields.

4.5. Escape Dynamics in a Double Well

An important concept for modeling a variety of physical systems is escape dynamics over a potential barrier. In a number of physical situations a system may reside in either of two potentially favorable states and move from one to the other by crossing the barrier which separates the potential minima. This type of system

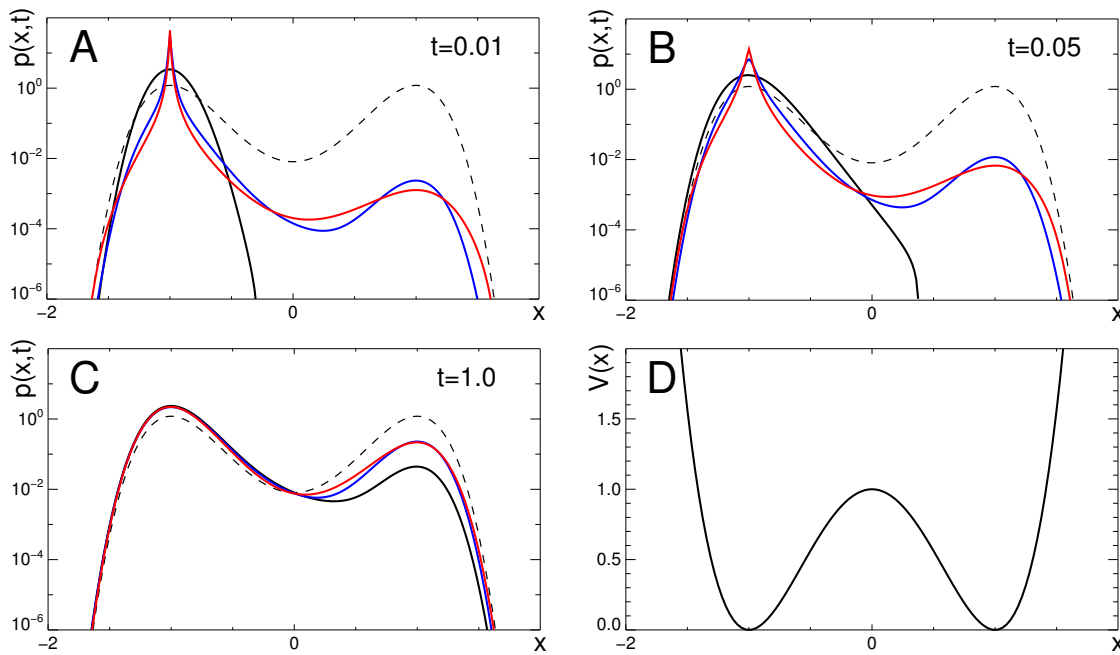


Figure 4.6.: Evolution of the pdf $p(x, t)$ in the double well potential $V(x)$ (D) at three different times: $t = 0.01$ (A), 0.05 (B) and 1.0 (C) for $\beta = 5.0$ and $\mu = 1$. Ordinary diffusion (black) is compared to topological (red) and subordinated (blue) superdiffusion. Initially the pdf is centered in the left minimum, i.e. $p(x, 0) = \delta(x + 1)$. The stationary state is represented by the dashed line. The diffusion process equilibrates quickly within the left potential well and does not pass the barrier for short times. In contrast, the superdiffusive processes transfer probability even for small times and remain peaked at $x = -1$ for much longer.

has served as a paradigm for a number of ordinary diffusion processes [109]. In a model for millennial climate changes Ditlevsen investigated generalized Langevin dynamics in a double well potential [33], and showed that the escape rate over the barrier depends on the spatial separation of the potential minima, unlike ordinary diffusion which is affected only by the difference between potential extrema. The results obtained by Ditlevsen are consistent with the scaling analysis of generalized Langevin dynamics, which showed that a typical length scale (in a double well the distance between potential minima) represents an important parameter (see section 4.3.4).

Here, we will compare topological and subordinated superdiffusion to ordinary diffusion in the escape dynamics scenario. Recall that both superdiffusive mechanisms obey ordinary Gibbs-Boltzmann statistics and possess the same spatio-temporal scaling behavior.

We proceed by showing that both processes differ strongly in their relaxation in

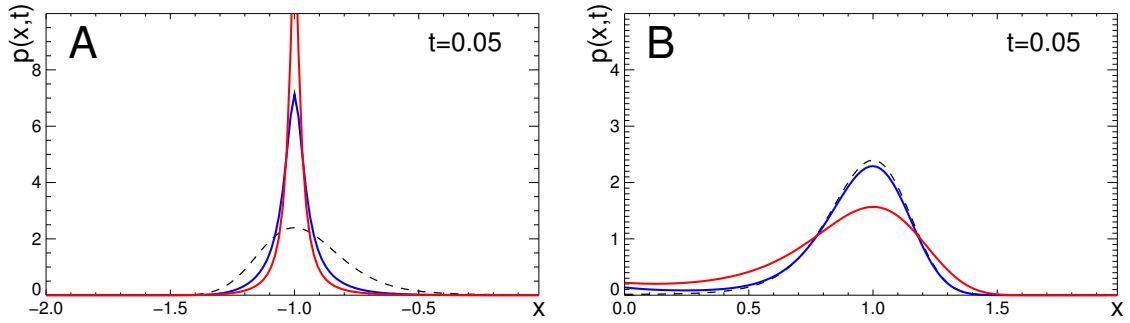


Figure 4.7.: The shape of $p_L(x, t)$ (left) and $p_R(x, t)$ (right) for subordinated (blue) and topological (red) superdiffusion at $t = 0.05$, $\beta = 5.0$ and Lévy exponent $\mu = 1$.

the same kind of potential. As a generic double well potential we choose

$$V(x) = x^4 - 4x^2 + 1 \quad (4.99)$$

depicted on the lower right in figure 4.6. Initially a particle is placed at the potential minimum at $x = -1$, i.e. $p(x, 0) = \delta(x + 1)$. The solutions $p(x, t)$ are depicted at three different times ($t = 0.01, 0.05, 1.0$) in figure 4.6 for a value $\beta = 5.0$ and an exponent $\mu = 1$. The fractional diffusion equations are mapped onto the corresponding Hamiltonian \mathcal{H} and subsequent spectral decomposition $\mathcal{H} = \sum_n \lambda_n \mathcal{P}_n$ where the λ_n and \mathcal{P}_n are eigenvalues and projectors onto the corresponding eigenspaces. Solutions $p(x, t)$ were then expressed in term of these quantities.

Let us first note that the time-scales of the relaxation processes for the case of normal diffusion and for Lévy-processes differ vastly. The typical times of the concentration equilibration (being the inverse of the largest nonzero eigenvalue) are: $\tau_C = 20.36$ for the diffusion process, $\tau_C = 4.51$ for subordinated superdiffusion ($\mu = 1$) and $\tau_C = 3.93$ for topological superdiffusion ($\mu = 1$). A much greater value of τ_C for the ordinary diffusion process is not surprising. In a short time it equilibrates within the left potential well. However, due to the continuity of its sample paths, the diffusion process accumulates probability in the right potential well only after a long time. In comparison, the subordinated process can pass the potential maximum at $x = 0$ even for short times, a direct consequence of the possibility of initiating a long jump from left to right. The transmission of probability through the potential barrier is compensated by a slower equilibration within the left potential well, in which $p(x, t)$ for both subordinated and topological superdiffusion stays sharply peaked around $x = -1$.

Despite their qualitative similarities in the overall shape of $p(x, t)$, subordination and topological superdiffusion are quite distinct on close inspection, as is shown in figure 4.7. To illustrate the difference between the processes the densities $p_L(x, t)$ and $p_R(x, t)$ are depicted on the left and right potential well normalized to unity

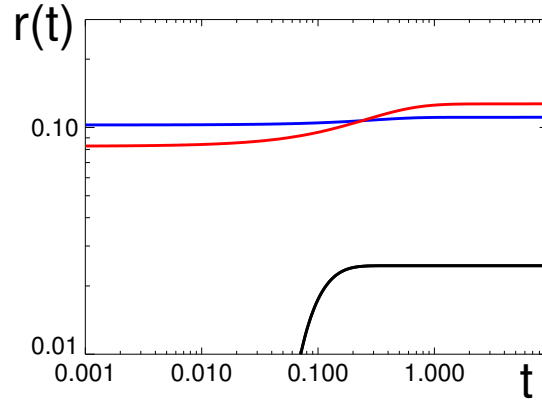


Figure 4.8.: The time dependent rate $r(t)$ of probability transfer from one potential well to the other. The curves correspond to ordinary diffusion (black), subordinated superdiffusion (blue) and topological superdiffusion (red). Parameters are $\beta = 5$ and $\mu = 1$, the initial condition is $p(x, 0) = \delta(x + 1)$.

on the corresponding sub-interval, i.e.

$$p_L(x, t) = \frac{p(x, t)}{\int_{-\infty}^0 dy p(y, t)} \quad \text{and} \quad (4.100)$$

$$p_R(x, t) = \frac{p(x, t)}{\int_0^{\infty} dy p(y, t)}. \quad (4.101)$$

Clearly, the shapes differ strongly on the two sides of the potential. The subordination process equilibrates faster on both sides of the potential barrier. The topological process attains a comparatively higher probability in regions of high potential.

In order to reveal the differences in barrier penetration, we consider the time dependent total probability in the right potential well, i.e.

$$Q(t) = \int_0^{\infty} dx p(x, t), \quad (4.102)$$

and the time dependent rate $r(t)$ of probability transfer which is defined as

$$r(t) = -\frac{1}{2} \frac{d}{dt} \ln [1/2 - Q(t)]. \quad (4.103)$$

In the limit $t \rightarrow \infty$, the pdfs approach the equilibrium according to

$$p(x, t) \approx p_s(x) - (p_s(x) - p_0(x)) e^{-\lambda_1 t} \quad \text{with} \quad \lambda_1 > 0. \quad (4.104)$$

where $p_s(x)$ and $p_0(x)$ denote the stationary and initial states of the system, respectively. Therefore, the rate approaches the lowest eigenvalues as $t \rightarrow \infty$, i.e. $r(t) \rightarrow \lambda_1$ the inverse of which quantifies the relaxation time. In other words, the function $r(t)$ measures how fast the probability transfer across the barrier approaches the its quasi-equilibrium value. For the same parameters as in figures 4.6 and 4.7 the rate $r(t)$ is depicted in figure 4.8. For ordinary diffusion the rate is initially zero and increases as soon as the process equilibrates within the left potential



well. It then levels off to a constant value proportional to the probability flux across the barrier. In contrast, if the system is superdiffusive, the probability transfer rate is nonzero even for small times. Note that the subordinated process penetrates the barrier at relatively high but almost constant rate for the entire time, whereas for topological superdiffusion the rate is initially smaller but increases for large times beyond the rate of the subordinated process.

4.6. Discussion

The detailed comparison of various superdiffusive fractional Fokker-Planck equations revealed important dynamical differences between generalized Langevin dynamics, topological and subordinated superdiffusion. The respective underlying physical principles which cause the enhanced diffusion, i.e. anomalous additive noise, scale-free topologies and strong temporal fluctuations, exhibit different dispersion characteristic when an external potential is present, although their behavior is identical when the potential is absent. Consequently, one is advised to be cautious and take into account the underlying physics when employing the fractional approach. Topological and subordinated superdiffusion are adequate for situations in which the stationary state is independent of the Lévy exponent μ , and both FFPEs respond identically to spatio-temporal scaling. However, the relaxation properties of topological superdiffusion on one hand and subordinated superdiffusion on the other in the harmonic potential as well as in the double well deviate from one another considerably.

In generalized Langevin equations bounded potentials can be effectively scaled away and play no role on large scales, which is the reason why Lévy flights in these potentials have attracted no attention in the past. However, in topological superdiffusion these potentials cannot be scaled away, and it is reasonable to assume that they influence the dynamics globally. We therefore predict that, if random motion on scale-free topologies is modulated by a variable and bounded external field, the dispersion properties will be changed in an essential fashion.



5. Periodic Potentials

On 31 December 1970, the
band officially split.

(The Beatles Anthology)

In this chapter we investigate the impact of external periodic potentials on superdiffusive motion. We develop a Bloch theory for Lévy flights, based on the fractional Schrödinger equation introduced in section 3.5. We show that a number of interesting and bizarre phenomena occur when Lévy flights evolve in periodic potentials, contrasting with generalized Langevin dynamics which is trivial in bounded potentials. A systematic study of the spectral band structure as a function of Lévy exponent, inverse temperature and Bloch phase shows that superdiffusion is remarkably different from ordinary diffusion in periodic potentials. Lévy flights are strongly affected by the specific functional shape of the potential, as opposed to ordinary diffusion processes which respond primarily to the magnitude variation of the potential. We demonstrate that even strongly superdiffusive processes are highly susceptible to external periodic potentials. The asymptotic behavior is quantified by the generalized diffusion coefficient as a function of inverse temperature, Lévy exponent and type of potential. At low temperatures, the generalized diffusion coefficient exhibits a significant dependence on the shape of the potential. Counterintuitively, the asymptotic behavior does not depend on the Lévy exponent, except in the ordinary diffusion limit in which the generalized diffusion coefficient as a function of Lévy exponent is discontinuous. The high temperature regime is treated by perturbation theory, which reveals a universal behavior for all periodic potentials. Finally, we examine relaxation in finite systems. We show that the effect of the potential on the relaxation time is least pronounced for intermediate values of the Lévy exponent, which may explain why these types of Lévy flights are observed in target location strategies of foraging animals and human visual search.

The results we present are a first step towards an understanding of superdiffusive dynamics on topologically complex structures exposed to external inhomogeneities, such as random motion of particles on complex polymeric media and random motion on scale-free networks.



5.1. Motivation

Why study random motion in periodic potentials at all? There are countless phenomena in physics and biology, which are successfully described by random walk models. In many of these systems the quantity of interest, e.g. a diffusive particle, a foraging animal, or a fluctuating stock price evolves in an inhomogeneous environment which has an influence on the dynamics. For instance, a foraging animal which intends to survive is more likely to remain in a habitat offering safety and food; the animal is less attracted by regions without these resources. Quite often the degree of inhomogeneity as a function of position fluctuates around some average value and possesses a typical variance. Furthermore, it is frequently equipped with a typical length scale. When the external inhomogeneity has some degree of regularity, it can be modeled by a periodic potential, which combines the properties of boundedness, typical magnitude variability and length scale.

What happens when Lévy flights evolve in external periodic potentials? We must answer this question in order to understand the dynamic properties of a large class of systems. A number of examples from physics and biology which fall into this class are schematically depicted in figure 5.1. The first system is a special case of a hetero-polymer, introduced in sections 3.1 and 3.2, and figure 3.1. If the hetero-polymer consists of a small number of monomer types arranged regularly along the chain, the external potential $V(x)$ of the chain will be periodic. In the example depicted in figure 5.1A, the polymer consists mainly of one type of monomer interspersed at regular intervals with another type of monomer at a lower potential. When a particle randomly hops along such a chain, it will eventually be trapped for some time in a potential minimum. Compared to random motion along a homogeneous chain, the dispersion is slowed down. When configurational changes permit long range transitions, the dispersion of the particle along the chain is governed by the fractional Fokker-Planck equation (FFPE) (3.48) for topological superdiffusion derived in the last chapter. The interplay between local trapping in potential minima and long range transitions due to configurational changes of the chain can be investigated quantitatively based on this FFPE.

Two-dimensional examples of topologically superdiffusion in periodic environments are sketched in figure 5.1B and C. In one panel a random graph is depicted, similar to the one shown in 3.2B. The distribution of connection lengths in the graph follows a power law and lacks a well defined variance. In contrast to the graph in 3.2B, the vertices in figure 5.1B are not scattered uniformly in the plane but concentrate periodically in clusters. This affects the asymptotic spreading of a particle which randomly moves on such a graph.

It is particularly important to understand the interplay between anomalous dispersion and inhomogeneous environments in a great class of biological systems, such as the spreading of foraging animals in their habitat and the dispersion of an epidemic in an ecosystem. On one hand, a number of species are known to

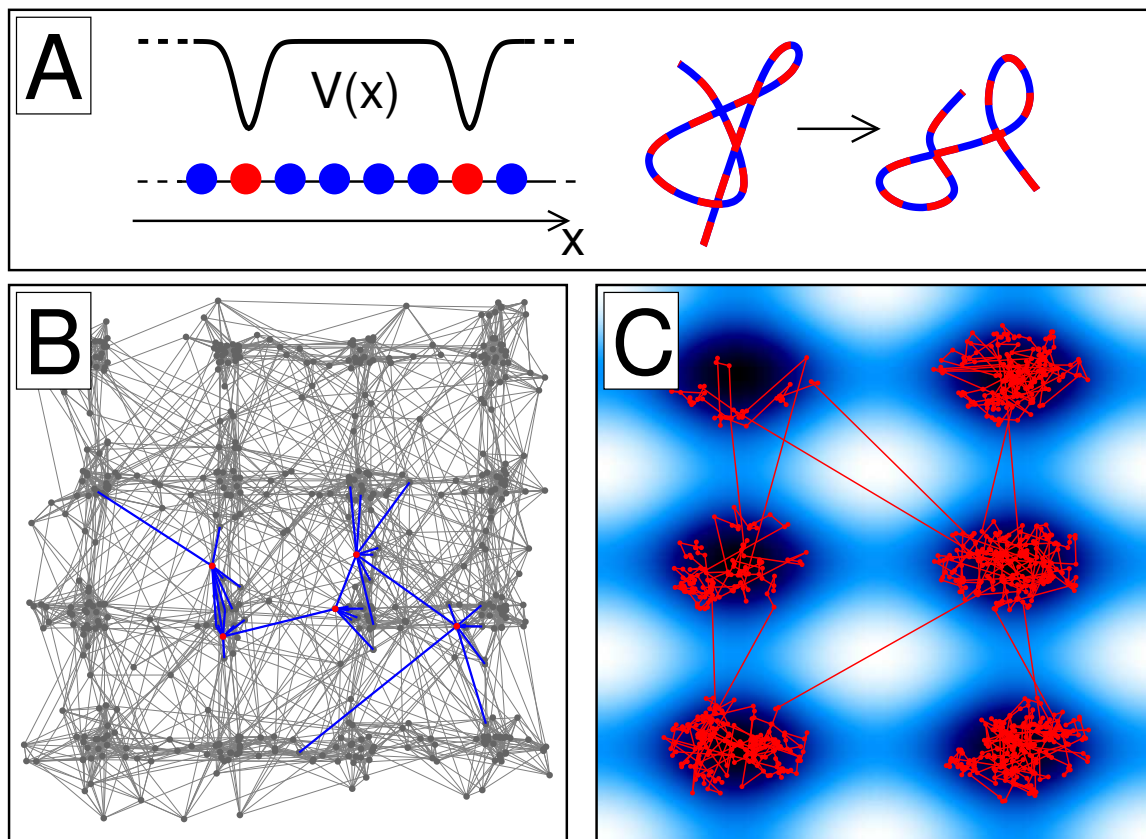


Figure 5.1.: Three examples of topological superdiffusion in periodic potentials. **A:** A polymer which consists mainly of one type of monomer (blue) interspersed at regular intervals with an energetically more favorable monomer (red). **B:** A random graph with scale-free connection lengths and periodically modulated vertex concentration. **C:** A Lévy flight evolving in a two dimensional periodic potential, schematically describing animal foraging in an inhomogeneous resource landscape.

spread superdiffusively in their habitat, examples of which are the albatross [127], oceanic microzooplankton [72], soil amoebas [73], fruit flies [30] and even spider monkeys[106]. On the other hand, resources which are crucial to an animal's survival are generally not concentrated uniformly in the environment. Experiments show that resource inhomogeneities determine to a large extent the spreading behavior of some life forms [52, 85]. From a population dynamics perspective, it is essential to investigate the impact of external inhomogeneities on the dispersion of animal specimens theoretically, especially in the light of extinction probabilities of endangered species due to habitat fragmentation [133]. The FFPE developed in the previous chapter offers a means to study these effects. Resource inhomogeneities can be modeled by the variability of the external potential. An idealized trajec-



tory of a superdiffusive model specimen in an inhomogeneous two-dimensional resource distribution is depicted in figure 5.1C.

Most certainly, resource inhomogeneities in an animal's habitat and monomer types along a real hetero-polymer are not strictly periodic. However, trapping in potential minima or inhabitation of regions with a high level of resources does occur in periodic potentials just as much as in potentials with a higher degree of irregularity. Therefore, any insight which is gained from studying topological superdiffusion in periodic potentials will be applicable to more realistic inhomogeneities as well. A detailed and more complicated investigation of random potentials is given in chapter 6.

Inhomogeneities in superdiffusive processes have received little attention in the past, partially because generalized Langevin dynamics is trivial in bounded potentials (see section 4.3.4), and these types of potentials were regarded as an inconsequential perturbation of free superdiffusion, but also because no other straightforward and physically plausible way of incorporating these potentials into known models existed.

5.2. Bloch Theory for Superdiffusive Processes

In the following we will generalize ideas originally obtained for the quantum mechanical description of electrons in periodic crystal lattices. When a free electron is subjected to a periodic potential, the combination of translation invariance of the kinetic energy term in the Hamiltonian with the periodicity of the potential energy term leads to a number of general properties of the spectral decomposition of the associated Hamiltonian. The eigenstates as well as the spectra of such Hamiltonians fulfill certain requirements, all of which are embraced in what is usually known as Bloch theory, see for example [7]. It will become clear below that a generalization for topologically superdiffusive processes in periodic potentials is straightforward.

Let us begin with the FFPE for a topologically superdiffusive process evolving in an external potential, i.e.

$$\partial_t p = e^{-\beta V/2} \Delta^{\mu/2} e^{\beta V/2} p - p e^{\beta V/2} \Delta^{\mu/2} e^{-\beta V/2}, \quad 0 < \mu \leq 2. \quad (5.1)$$

Ordinary diffusion is recovered for $\mu = 2$. In section 3.5 we showed that under a suitable transformation (3.54) the FFPE turns into a fractional Schrödinger equation (FSE) for the wave function $|\psi\rangle$, i.e.

$$\begin{aligned} \partial_t |\psi\rangle &= -(|P|^\mu + U(X)) |\psi\rangle \quad \text{where} \\ \langle x|\psi\rangle &= \psi(x, t) = \exp(\beta V(x)/2) p(x, t). \end{aligned} \quad (5.2)$$

Clearly, the anomalous kinetic term $|P|^\mu = -\Delta^{\mu/2}$ is translation invariant for all

values of $\mu \in (0, 2]$. The effective potential $U(x)$ is obtained from $V(x)$ by

$$U(x) = e^{\beta V(x)/2} \Delta^{\mu/2} e^{-\beta V(x)/2}. \quad (5.3)$$

A separation ansatz for the wave function

$$\langle x | \psi \rangle = \psi(x, t) = e^{-Et} \phi(x), \quad (5.4)$$

yields the stationary fractional Schrödinger equation (SFSE) for the eigenfunction $|\phi\rangle$ with energy E ,

$$(|P|^\mu + U(X) - E) |\phi\rangle = 0. \quad (5.5)$$

This is the equation that we must solve.

We wish to investigate periodic potentials of wavelength $2\pi\lambda$, i.e.

$$V(x) = V(x + 2\pi n\lambda) \quad \text{with } n \in \mathbb{Z}. \quad (5.6)$$

Furthermore, we assume that V is bounded and without loss of generality we let

$$\frac{1}{2\pi\lambda} \int_{2\pi\lambda} dx V(x) = 0 \quad \text{and} \quad \frac{1}{2\pi\lambda} \int_{2\pi\lambda} dx V^2(x) = V_0^2. \quad (5.7)$$

The quantity V_0 reflects the typical magnitude variation over one period. For convenience we will work with a dimensionless version

$$v(x) = V(x)/V_0 \quad (5.8)$$

of the potential and an effective potential strength ε which quantifies the magnitude variations of the potential in units of $k_B T$, i.e.

$$\varepsilon = \frac{1}{2} V_0 \beta = \frac{V_0}{2k_B T}. \quad (5.9)$$

For example, when the effective potential is much less than unity, $\varepsilon \ll 1$, the situation corresponds to either a weak potential or a high temperature. When $\varepsilon \gg 1$ the opposite is the case. The effective potential in (5.3) then depends only on two parameters, the Lévy exponent μ and the effective potential strength defined above,

$$U(x) = e^{\varepsilon v(x)} \Delta^{\mu/2} e^{-\varepsilon v(x)}. \quad (5.10)$$

The periodicity requirement (5.6) entails that the effective potential is also $2\pi\lambda$ -periodic, i.e.

$$U(x) = U(x + 2\pi n\lambda), \quad \text{with } n \in \mathbb{Z}. \quad (5.11)$$





Therefore, the FSE (5.2) consists of a translation invariant anomalous kinetic term and a periodic potential term, and a Bloch theoretic treatment sounds promising. Defining the “bra” $\langle k|$ by

$$\langle k|f\rangle = \tilde{f}(k) = \int dx e^{ikx} f(x), \quad (5.12)$$

and multiplying equation (5.5) by it from the left yields the stationary FSE in Fourier representation,

$$(E - |k|^\mu) \tilde{\phi}(k) - \int dk' \tilde{U}(k - k') \tilde{\phi}(k') = 0. \quad (5.13)$$

Since the effective potential is a periodic function, we may express the Fourier transform of it as a discrete sum of Dirac δ -functions,

$$\tilde{U}(k) = 2\pi \sum_n \delta(k - k_n) \hat{U}_n \quad \text{with } k_n = n/\lambda, \quad n \in \mathbb{Z}. \quad (5.14)$$

The Fourier coefficients \hat{U}_n are defined by (see Appendix D)

$$\hat{U}_n = \frac{1}{2\pi\lambda} \int_{2\pi\lambda} dx U(x) e^{-inx/\lambda}. \quad (5.15)$$

The central merit of Bloch theory is the fact that any solution to (5.13) is of the form

$$\phi(x) = e^{iqx/\lambda} \theta(x) \quad \text{with } q \in [0, 1]. \quad (5.16)$$

The quantity q is referred to as the Bloch phase and the function $\theta(x)$ has the same period as the effective potential, i.e.

$$\theta(x) = \theta(x + 2\pi n\lambda), \quad \text{with } n \in \mathbb{Z}. \quad (5.17)$$

The Fourier transform $\tilde{\phi}(k)$ of the wave function $\phi(x)$ can be expressed in terms of the Fourier coefficients $\hat{\theta}_n$ of the periodic component $\theta(x)$ as

$$\tilde{\phi}(k) = 2\pi \sum_n \delta(k + (q - n)/\lambda) \hat{\theta}_n, \quad (5.18)$$

where

$$\hat{\theta}_n = \frac{1}{2\pi\lambda} \int_{2\pi\lambda} dx \theta(x) e^{-inx/\lambda}. \quad (5.19)$$

Substituting the expansion (5.14) of the effective potential and the expansion (5.18) of the wave function into equation (5.13) yields a sum (after a somewhat cumbersome rearrangement of indices)

$$\left(E - |n/\lambda - q/\lambda|^\mu - \hat{U}_0\right) \hat{\theta}_n - \sum_{m \neq n} \hat{U}_{n-m} \hat{\theta}_m = 0. \quad (5.20)$$



Letting

$$\langle n | \theta \rangle = \widehat{\theta}_n, \quad (5.21)$$

we immediately see that (5.20) is a discrete stationary Schrödinger equation defined by a Hamiltonian $H(q)$ which is parameterized by the Bloch phase q , more precisely,

$$H(q) | \theta \rangle = E(q) | \theta \rangle. \quad (5.22)$$

The matrix elements of the Hamiltonian read

$$\langle n | H(q) | m \rangle = H_{nm}(q) = \frac{1}{\lambda^\mu} |m - q|^\mu \delta_{nm} + \widehat{U}_{n-m}. \quad (5.23)$$

Since (5.20) is a discrete matrix equation, the eigenvalues and eigenstates can be labeled by a discrete index n . However, since $H_{nm}(q)$ depends on the Bloch phase, so do the energy levels, i.e.

$$E = E_n(q) \quad \text{with} \quad n \in \mathbb{Z}, \quad q \in [0, 1]. \quad (5.24)$$

The functions $E_n(q)$ are commonly referred to as the energy bands of the original SFE (5.5). When the effective potential strength ε vanishes, the FSE (5.2) is equivalent to unperturbed superdiffusion, and the energy bands $E_n^0(q)$ and eigenfunctions $\phi_n^0(q)$ are given by

$$E_n^0(q) = \left| \frac{n - q}{\lambda} \right|^\mu \quad \text{and} \quad \phi_n^0(q) = e^{i(n-q)x/\lambda}. \quad (5.25)$$

The combination of discrete level index n and continuous Bloch phase $q \in [0, 1]$ spans the entire real axis \mathbb{R} in this case. With $k = (n - q)/\lambda$ the well known result for the spectral decomposition of $|P|^\mu$ alias $\Delta^{\mu/2}$ is obtained,

$$E^0(k) = |k|^\mu \quad \text{and} \quad \phi_k(x) = e^{ikx}, \quad \text{with} \quad k \in \mathbb{R}. \quad (5.26)$$

In the discrete Schrödinger equation (5.20) the Fourier coefficients of the effective potential can be expressed as a function of Fourier coefficients

$$\widehat{s}_n(\varepsilon) = \frac{1}{2\pi\lambda} \int_{2\pi\lambda} dx e^{\varepsilon v(x) - inx/\lambda} \quad (5.27)$$

of the exponential $\exp[\varepsilon v(x)]$. These coefficients can either be evaluated analytically, or an expansion of the exponential of the integrand leads to a series in powers of effective potential strength ε weighted by the Fourier coefficients of powers of the original potential $v(x)$, i.e.

$$\widehat{s}_n(\varepsilon) = 1 + \sum_{k=1} \frac{\varepsilon^k}{k!} \widehat{v}_n^k. \quad (5.28)$$



The coefficients \widehat{U}_n are obtained by Fourier expansion of the definition of $U(x)$,

$$\widehat{U}_n = -\frac{1}{\lambda^\mu} \sum_m \widehat{s}_{n-m}(\varepsilon) |m|^\mu \widehat{s}_m(-\varepsilon). \quad (5.29)$$

Denoting complex conjugation by $\overline{(\cdot)}$, the coefficients appearing in equation (5.20) are given by

$$\widehat{U}_{n-m} = -\frac{1}{\lambda^\mu} \sum_l \widehat{s}_{n-l}(\varepsilon) |l-m|^\mu \widehat{s}_{l-m}(-\varepsilon) \quad (5.30)$$

and

$$\widehat{U}_0 = -\frac{2}{\lambda^\mu} \sum_{m>0} |m|^\mu \operatorname{Re} \left[\widehat{s}_m(-\varepsilon) \overline{\widehat{s}_m(\varepsilon)} \right]. \quad (5.31)$$

In the following we wish to compare the properties of the band spectra of various superdiffusive processes, each defined by a Lévy exponent μ . For a comparison the energy is not a suitable quantity, because it represents a different physical quantity for different values of μ . In other words, depending on μ , the quantity E has different units. Therefore, it is more sensible to compute the generalized crystal momentum defined by

$$\kappa_n(q) = \lambda E_n(q)^{1/\mu}, \quad (5.32)$$

since this quantity is dimensionless and independent of λ , irrespective of the specific value of μ chosen. Furthermore, it is identical in all freely superdiffusive processes,

$$\kappa_n^0(q) = |n-q| \quad n \in \mathbb{Z}, \quad q \in [0, 1], \quad \mu \in (0, 2] \quad (5.33)$$

When inserted into equation (5.20) along with the expressions (5.30) and (5.31), the Schrödinger equation is given in terms of the functions $\widehat{s}_n(\varepsilon)$,

$$\left((\kappa_n(q))^\mu - (\kappa_n^0(q))^\mu + 2 \sum_{m>0} |m|^\mu \operatorname{Re} \left[\widehat{s}_m(-\varepsilon) \overline{\widehat{s}_m(\varepsilon)} \right] \right) \widehat{\theta}_n + \sum_{m \neq n, l} \widehat{s}_{n-l}(\varepsilon) |l-m|^\mu \widehat{s}_{l-m}(-\varepsilon) \widehat{\theta}_m = 0. \quad (5.34)$$

The investigation below will be based on this equation. Parameters of this equation are the Lévy index μ and the effective potential strength ε . It is generally very difficult if not impossible to solve this equation for a given external potential $V(x)$. We must rely on the numerical diagonalization of the associated matrix and approximation methods in order to obtain the generalized crystal momentum $\kappa_n(q)$ as a function of the Bloch phase q and for a given set of parameters μ and ε . From a numerical point of view, equation (5.34) is a much better starting point than the original SFSE. In addition, a perturbation theoretic treatment, valid for weak effective potentials, can be carried out more easily on (5.34).



5.3. Bands

We investigate in detail the quantity $\kappa_n(q)$ for four paradigmatic potentials $V(x)$. Each potential reflects a situation frequently encountered in physical modeling. The potentials are qualitatively sketched in figure 5.2. The simplest type of potential is the cosine, shown in figure 5.2A.

In contrast to the cosine, the square wave potential (figure 5.2B) is characterized by sharp boundaries between two constant potential levels. In terms of the copolymer example discussed in chapter 3, we expect the square wave potential to be an appropriate choice for a chain which consists of two monomer types arranged in alternating segments of fixed length.

Two additional typical potentials are depicted in figures 5.2C and 5.2D. These types of potentials are adequate for polymers consisting of one type of monomer interspersed at regular intervals with a different type of monomer. When the rare type is energetically higher, the potential along the chain will possess localized peaks (figure 5.2C). Conversely, if the interspersed monomers are energetically more favorable, then $V(x)$ will consist of a succession of localized potential troughs (figure 5.2D).

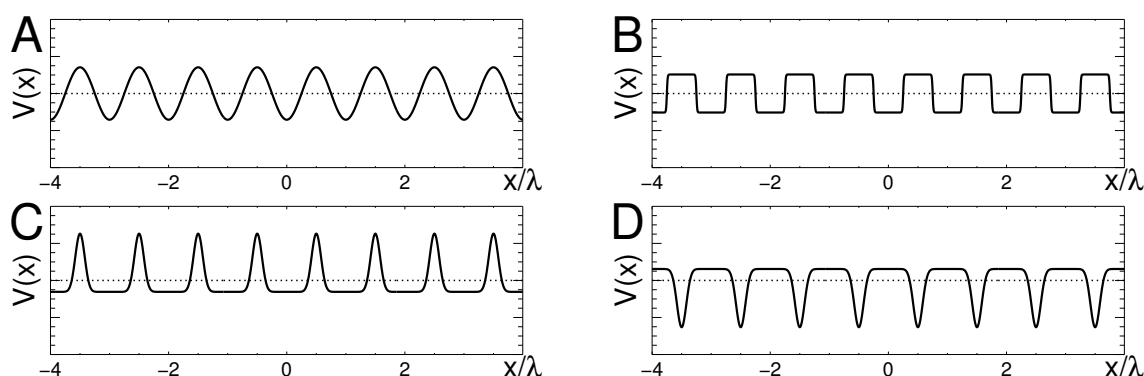


Figure 5.2.: Periodic potentials frequently encountered in physical systems. The simple cosine (A), the square wave potential (B), a potential possessing localized peaks (C), and the same potential with opposite bias, the localized trough potential. (D) Each potential has zero mean and unit variance.

5.3.1. Band Gaps Everywhere

We begin with the simplest type of potential, the cosine of wavelength $2\pi\lambda$, zero offset and unit variance, i.e.

$$v(x) = \sqrt{2} \cos(x/\lambda). \quad (5.35)$$

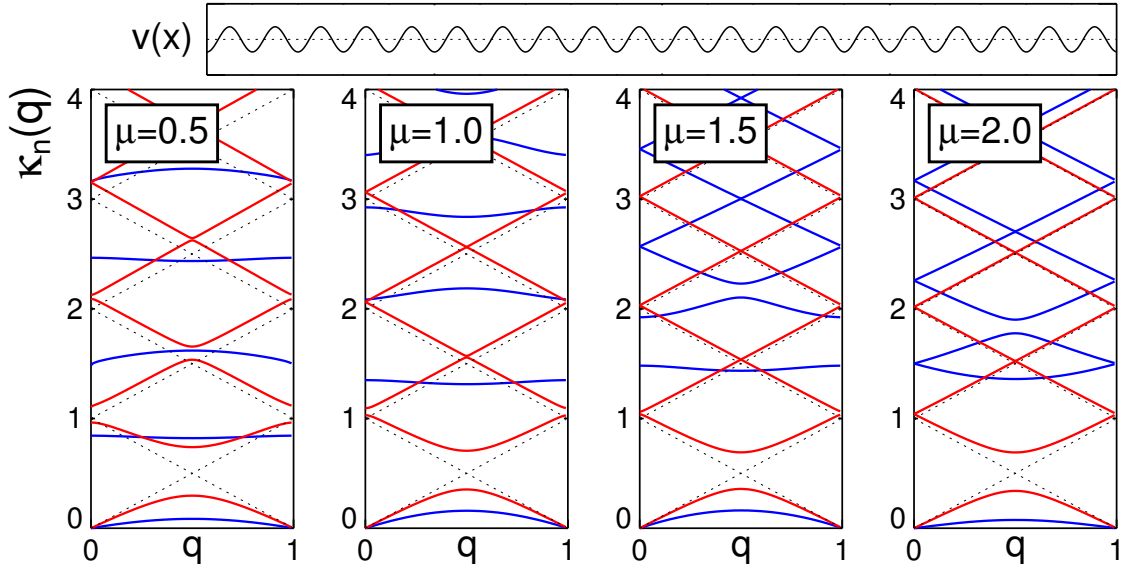


Figure 5.3.: Superdiffusion in the cosine potential. The generalized crystal momentum $\kappa_n(q)$ (defined by (5.32)) as a function of the Bloch phase q . Each panel depicts the structure of the first few bands for various Lévy exponents ($\mu = 1/2, 1, 3/2, 2$). Linestyles label the effective potential strength, $\varepsilon = 0$ (dashed line), $\varepsilon = 1/4$ (—) and $\varepsilon = 1$ (—).

Inserted into equations (5.27), the Fourier coefficients $\hat{s}_n(\varepsilon)$ appearing in (5.34) can be expressed in terms of the Bessel functions $I_n(z)$ [50, p. 900 ff],

$$\hat{s}_n(\varepsilon) = I_n(\sqrt{2\varepsilon}). \quad (5.36)$$

After substitution into the Schrödinger equation (5.34), the generalized crystal momentum $\kappa_n(q)$ can be computed numerically for a given set of parameters $\{\mu, \varepsilon\}$.

Figure 5.3 depicts $\kappa_n(q)$ for a number of Lévy exponents μ and two effective potential strengths ε . The limiting case of ordinary diffusion ($\mu = 2$) is shown in the right panel of the figure. Clearly, the band structure depends strongly on the Lévy exponent μ . Therefore the transient dynamics is different for various values of μ . The lowest band $\kappa_0(q)$ determines the dispersion in the potential on scales larger than the wavelength of the potential. When the effective potential strength is low (red bands), only the lowest band is affected by the potential, because a band gap of approximately the same magnitude appears in every system. The upwards shift of $\kappa_n(q)$ in the upper bands is most pronounced when the process is strongly superdiffusive ($\mu = 1/2$). This implies that on small scales these highly superdiffusive processes relax faster. When the effective potential strength is increased, the band structure differs vastly for different values of μ . On one hand, higher bands of the ordinary diffusion process are nearly unaffected by a strong potential. On the other hand, the same bands in the strongly superdiffusive systems are almost independent of the Bloch phase q . However, the decrease of the lowest band is



strongest in both the ordinary diffusion process and the strongly superdiffusive process. It is least pronounced for intermediate values of the Lévy exponent μ . Thus, moderately superdiffusive processes are least slowed down by the external potential, a matter investigated in detail in section 5.4.

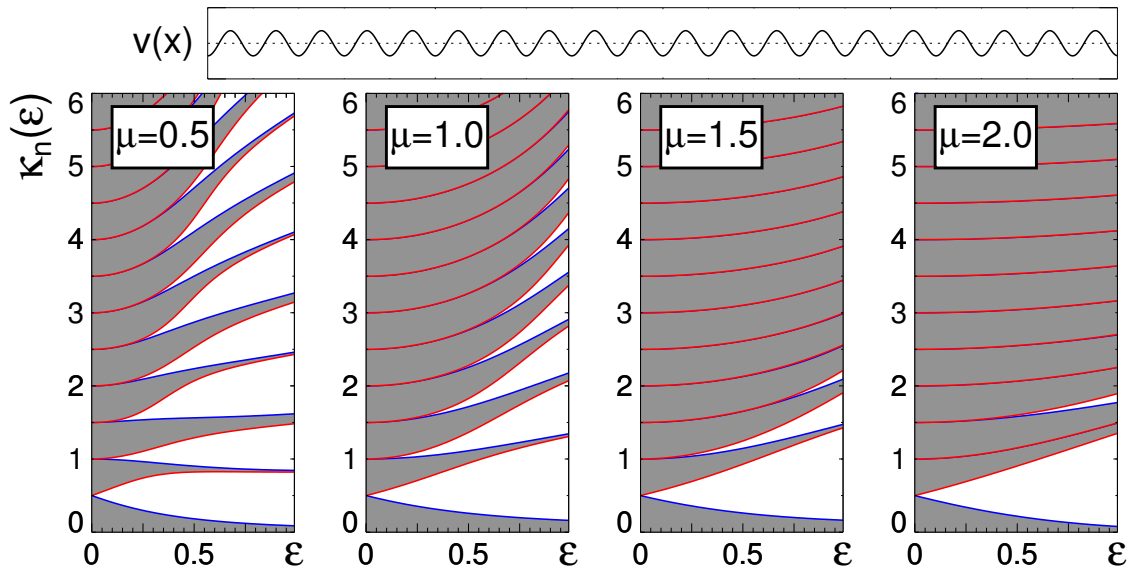


Figure 5.4.: Superdiffusion in the cosine potential. The quantity $\kappa_n(\varepsilon)$ as a function of effective potential strength ε . The panels depict the band structure of systems defined by Lévy exponents $\mu = 1/2, 1, 3/2$ and 2 . Upper and lower boundaries of the bands are marked by blue and red lines, respectively. The spectral measure vanishes in the gaps (white zones).

These effects are particularly visible in figure 5.4 which depicts $\kappa_n(q)$ as a function of potential strength ε for the same set of Lévy exponents. Each band n is bounded by the upper and lower values $\kappa_n(0)$ and $\kappa_n(1)$. When q spans the interval $[0, 1]$, the gray area is filled. Increasing the potential strength leads to band splitting, the degree of which is most pronounced for low Lévy exponents. Obviously, relaxation is different for various types of Lévy flights in the cosine potential. However, given a fixed Lévy exponent μ , the effect of band width reduction increases smoothly as the effective potential strength is increased. Intuitively speaking, the transient dynamics of superdiffusion in the cosine potential does not hold any surprises with increasing effective potential.

5.3.2. Dancing Bands

In more complicated and realistic potentials this simple response to increasing effective potential strength vanishes into thin air. Consider the square wave potential

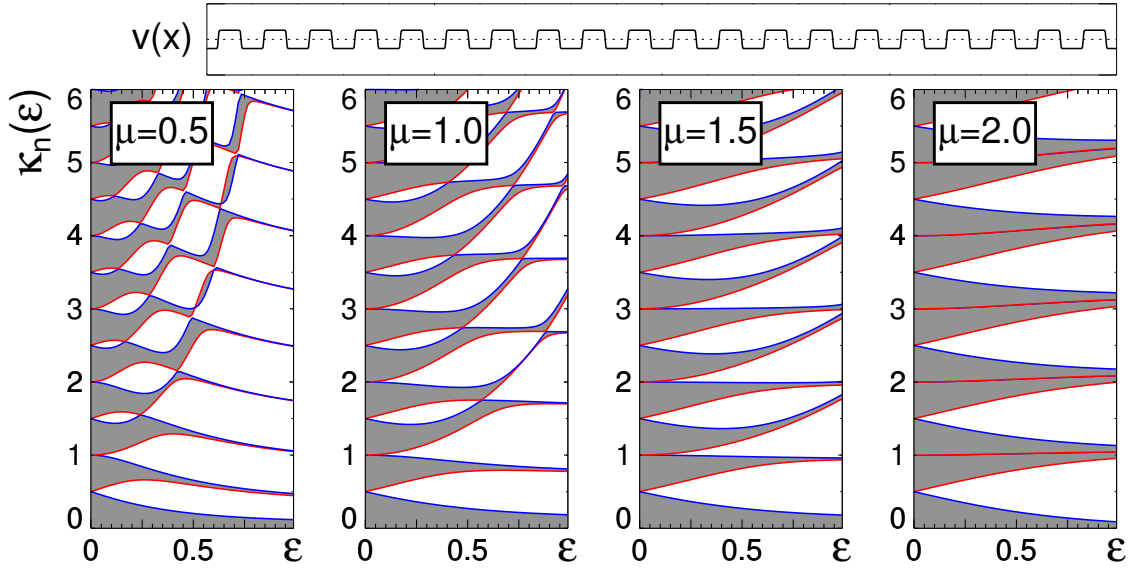


Figure 5.5.: Superdiffusion in the square wave potential. $\kappa_n(\varepsilon)$ as a function of effective potential strength ε . A detailed description of the figure is provided in the caption of figure 5.4.

defined by

$$v(x) = \begin{cases} +1 & \frac{2n-1}{4} < x/\lambda < \frac{2n+1}{4} \\ -1 & \text{otherwise.} \end{cases} \quad \text{with } n \in \mathbb{Z} \quad (5.37)$$

The Fourier coefficients

$$\hat{s}_{2n}(\varepsilon) = 0 \quad \text{and} \quad (5.38)$$

$$\hat{s}_{2n+1}(\varepsilon) = \frac{2(-1)^n}{\pi(2n+1)} \sinh(\varepsilon) \quad (5.39)$$

can be computed in a flash.

This potential exhibits a far more complicated band structure than the softly varying cosine. The bands $\kappa_n(q)$ for the square wave potential as a function of potential strength are shown in figure 5.5. The choice of Lévy exponents is the same as for the cosine spectra. The band structure of the ordinary diffusion displays the most transparent response to increasing effective potential strength. Due to the high abundance of harmonic frequencies in the square wave, the effect of mode coupling leads to increasing gaps between all neighboring bands. Thinning of bands increases smoothly as the effective potential strength is increased.

Contrasting with this simple behavior, the band structure of the superdiffusive processes is far more complicated. Neighboring bands approach and repel each other. Band twists occur, and the global structure is rather complex. The effect is most pronounced for small Lévy exponents.

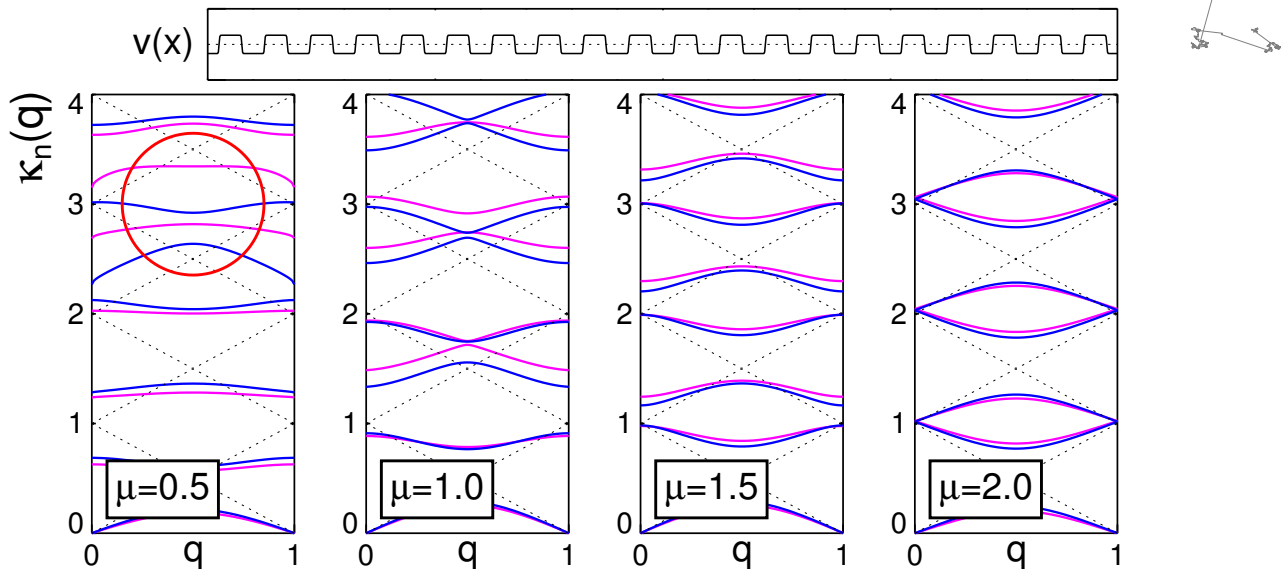


Figure 5.6.: Superdiffusion in the square wave potential. The crystal momentum $\kappa_n(q)$ as a function of the Bloch phase q is shown for two, only slightly different effective potential strengths, $\varepsilon = 0.45$ (blue) and $\varepsilon = 0.55$ (purple). The red circle indicates the region of high susceptibility towards changes in potential strength.

Consequently, the transient dynamics of superdiffusive processes is strongly susceptible to changes in effective potential strength. That is, for a given potential strength ε , only a slight increase by $\delta\varepsilon$ may change $\kappa_n(q)$ extensively. Figure 5.6 shows the crystal momentum as a function of the Bloch phase q at two similar potential strengths, $\varepsilon = 0.45$ and $\varepsilon = 0.55$. A change in potential strength of small magnitude affects the band structure of ordinary diffusion only slightly, whereas the superdiffusive system with $\mu = 1/2$ displays a striking difference in the area indicated by the red circle.

5.3.3. The Ups and Downs

A rather bizarre phenomenon occurs when Lévy flights evolve in potentials in which the periodic inhomogeneity is localized in a small region relative to the wavelength, such as the localized peak and trough potentials shown in figure 5.2C and 5.2D. In order to compute the quantity $\kappa_n(q)$, we model these potentials as

$$v_{\pm}(x) = \pm a (\cos(x/2\lambda))^{2\gamma} + b. \quad (5.40)$$

The relevant parameter in (5.40) is the exponent γ which controls the degree of localization of the peaks and troughs. The parameters a and b are chosen such that the potentials $v_{\pm}(x)$ have zero mean and unit variance. The \pm sign determines the bias of the potential, i.e. potential peaks (+) or potential troughs (-).

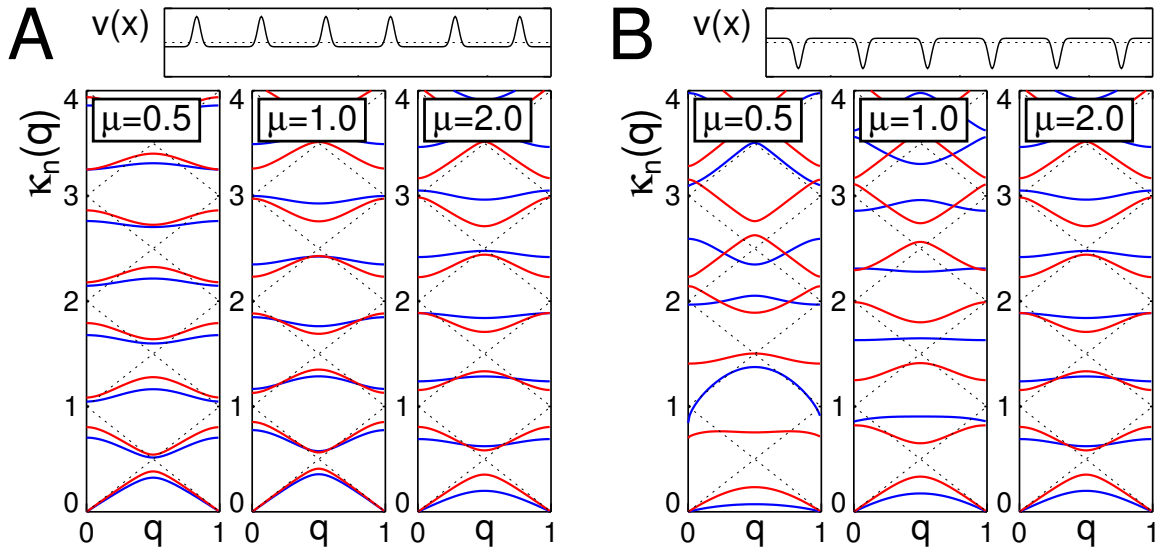


Figure 5.7.: A comparison of the band structure of the crystal momentum $\kappa_n(q)$ as a function of the Bloch phase in the localized peak (**A**) and localized trough (**B**) potentials. Lévy exponents are $\mu = 1/2, 1$ and 2 . The effective potential strengths ε are 0 (dashed line), $1/4$ (—) and 1 (—). The potentials $v(x)$ depicted above the band panels are given by equation (5.40) for a peak parameter $\gamma = 32$ and bias ± 1 .

In figure 5.7 the band structure of Lévy flights in potentials of identical shape but opposite bias are compared. The effective potential strength ε was set to $1/4$ (blue bands) and 1 (red bands).

The effect of the localized peak potential (figure 5.7A) is similar for all values of the Lévy exponent. Gaps are present between all adjacent bands, their size increases with increasing potential strength. However, the dynamics on scales larger than the wavelength of the potential differs for each μ . The arc of the lowest band is reduced most strongly in the diffusive system, whereas when $\mu = 1/2$ nearly no response of the lowest band occurs. This is plausible, since potential peaks only pose an obstacle for the ordinary diffusion process, which is local and needs to overcome each peak diffusively. Lévy flights, which are intrinsically non-local, possess a non zero probability of jumping past a potential peak without even sensing its presence.

Comparing this to the localized trough potential (figure 5.7B), we see that the effect on the lowest band is reversed. A superdiffusive particle is trapped in the potential troughs more strongly than an ordinary diffusive one. At first sight this is a rather counterintuitive phenomenon. We will attempt to give a physical explanation of this in section 5.4 on asymptotics. Furthermore, the band structure is far more complicated when $\mu = 1/2$, observe for instance $\kappa_n(q)$ for $n = 2, 3$ in panels A and B. Note also that the shape of the bands varies substantially when the

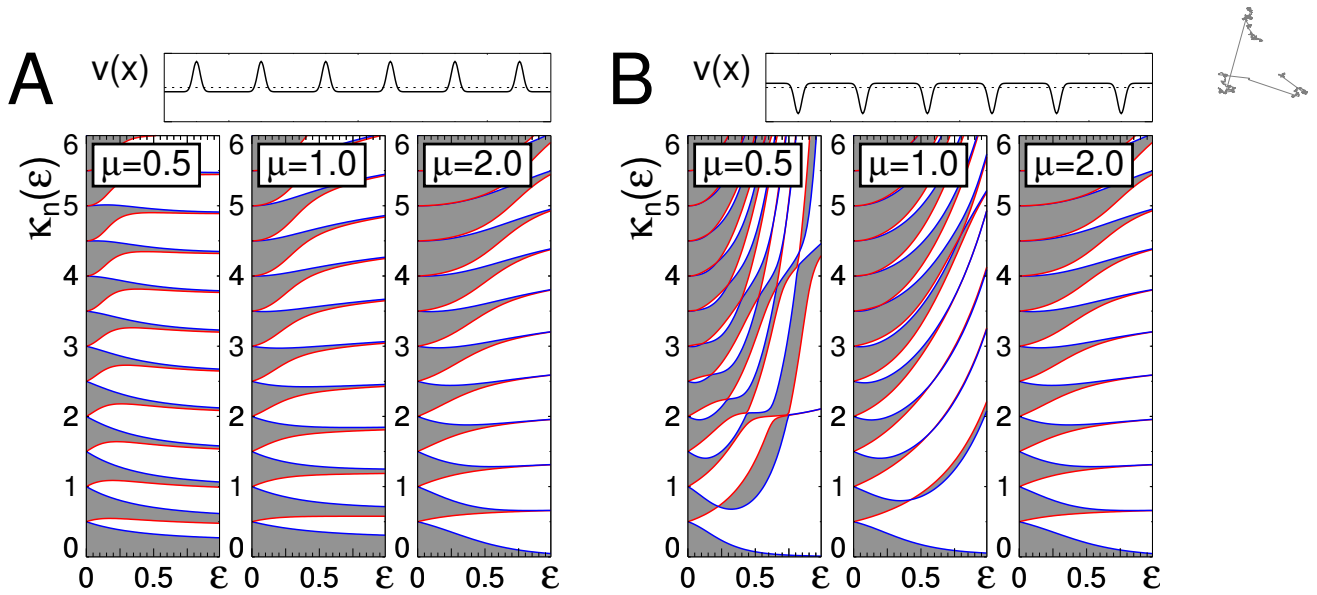
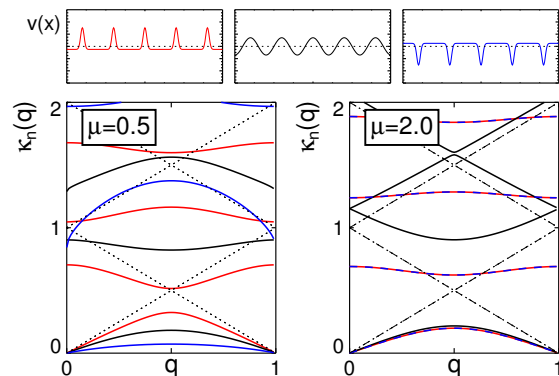


Figure 5.8.: A comparison of the band structures of $\kappa_n(\varepsilon)$ as a function of ε in the localized peak (A) and localized trough (B) potentials. Lévy exponent, peak and parity parameters for the potentials are identical to the ones chosen in figure 5.7 (refer to for more details).

potential strength is changed. Figure 5.8 illustrates this fact even better. Increasing ε leads to a smooth thinning of bands in the localized peak potential, and a complex structure of $\kappa_n(q)$ in the localized trough potential, including avoided band crossings and twists.

However, the limiting case of ordinary diffusion shows identical bands in either potential, which is not surprising. When $\mu = 2$ the evolution equation (5.1) is local. A diffusive particle has only the choice of making a transition to the neighboring locations; it can not differentiate between potential troughs and peaks. The bias of the potential is only crucial for superdiffusive motion. Transition probabilities of a

Figure 5.9.: The structure of $\kappa_n(q)$ for a superdiffusive process ($\mu = 1/2$, left panel) compared to ordinary diffusion ($\mu = 2$, right panel) for the potentials depicted in the top row. The bands corresponding to the given potentials are depicted in the same color. The effective potential strength ε is $1/2$. The dashed line shows the situation of vanishing potential. Potential parameters are identical to those chosen in figure 5.7.



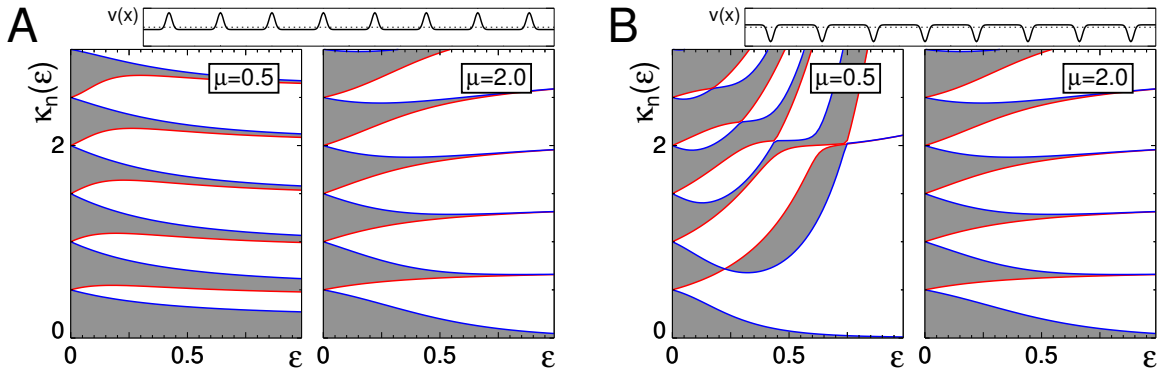


Figure 5.10.: $\kappa_n(\varepsilon)$ as a function of effective potential strength ε for $\mu = 1/2$ (left panels) compared to ordinary diffusion ($\mu = 2$) in the localized peak potential (**A**) and the localized trough potential with the same shape and opposite bias (**B**). Potential parameters are identical to those chosen in figure 5.7.

Lévy flight are determined by the interplay of the non-local jump statistics with the specific shape of the potential. Localized potential peaks are largely ignored by a Lévy flight if the peaks have a small width relative to the wavelength of the potential; the particle tunnels through them. In the localized trough potential, however, possible low energy target sites of hopping are sparse, and the dispersion of Lévy flights in such potentials is strongly affected.

This is an important result. In terms of the model of a randomly hopping particle on a hetero-polymer, it implies that as soon as long range transitions are permitted due to folding, the specific structure of the potential has a large effect on the dispersion of the particle.

5.4. Asymptotics

Let us now focus on the asymptotics of topological superdiffusion in periodic potentials. The dynamics on large spatial scales relative to the wavelength of the potential ($x \gg \lambda$) is governed by the crystal momentum κ at small values of the associated wave number, i.e. $k \ll \lambda^{-1}$. In terms of the Bloch phase, this is equivalent to $q \ll 1$. The dynamics on large temporal scales is dominated by the small energies E and hence the spectrum of κ near the origin. Therefore, it suffices to investigate the properties of the lowest band $\kappa_0(q)$ for $q \ll 1$.

In figure 5.11 the crystal momentum $\kappa_0(q)$ for superdiffusion and ordinary diffusion is compared in the four potentials given in the top row. The dashed line in each panel is the dispersion relation of a freely moving particle, i.e. $\kappa_0(q) = q$. Recall that a linear q -dependence implies that the propagator of the process is Lévy

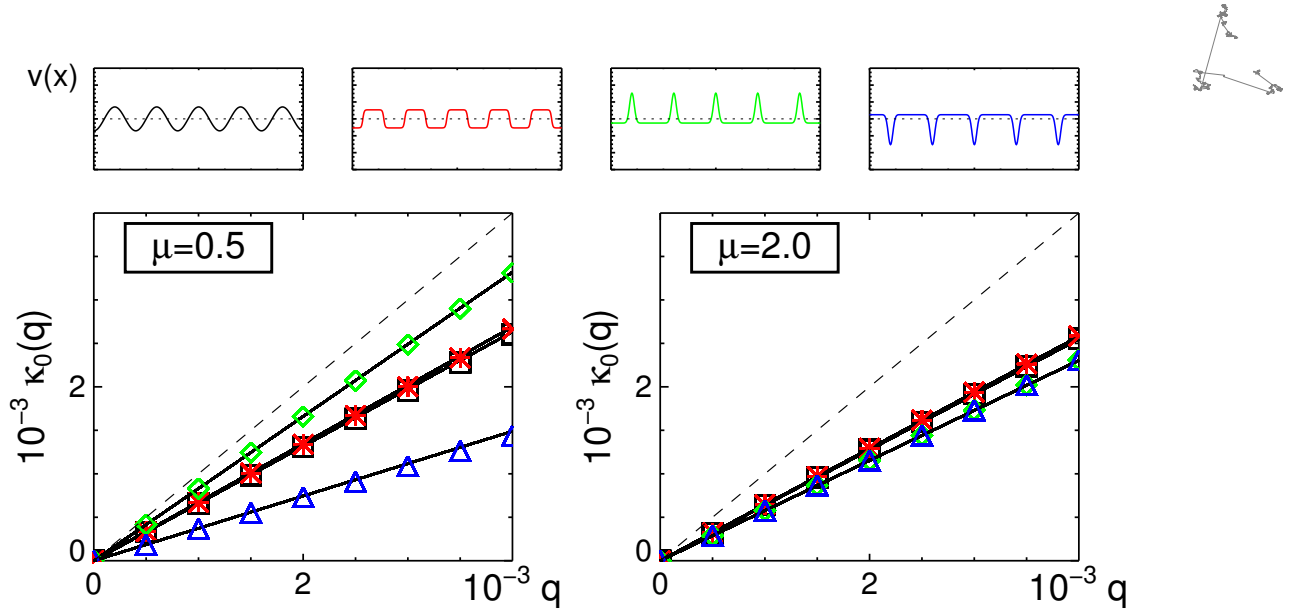


Figure 5.11.: Asymptotic behavior of superdiffusion ($\mu = 1/2$) and ordinary diffusion ($\mu = 2$) in the potentials displayed in the top row. The asymptotics is governed by the behavior of the lowest band $\kappa_0(q)$ for $q \ll 1$. Symbol type and color are associated with the color of the potentials. The slope of $\kappa_0(q)$ is the effective length ξ which is related to the generalized diffusion coefficient and defined by equation (5.43). The effective potential strength ε is set to $1/2$.

stable, since $E_0(q) = \kappa_0(q)^\mu = q^\mu$ and thus

$$\tilde{p}(q, t) \approx e^{-q^\mu t}. \quad (5.41)$$

Figure 5.11 shows that for the chosen potential strength ε , both Lévy exponents μ and all the potentials, the asymptotic q -dependence is still linear. However, the slope ξ of the curves is decreased by the potential, i.e.

$$\kappa_0(q) = \xi q \quad \text{and} \quad E_0(q) = \xi^\mu q^\mu. \quad (5.42)$$

The quantity ξ can be interpreted as a typical length scale of the system. Because of the second equation in (5.42), it is related to the generalized diffusion coefficient by

$$\xi^\mu = D_\mu. \quad (5.43)$$

Since the length scale (and consequently D_μ) is decreased by an external potential, each process is slowed down. However, since the q -dependence remains the same, the propagator is still Lévy stable on large scales. One can think of the process on large scales as evolving in a homogeneous environment of which the position coordinate is rescaled by a factor ξ .

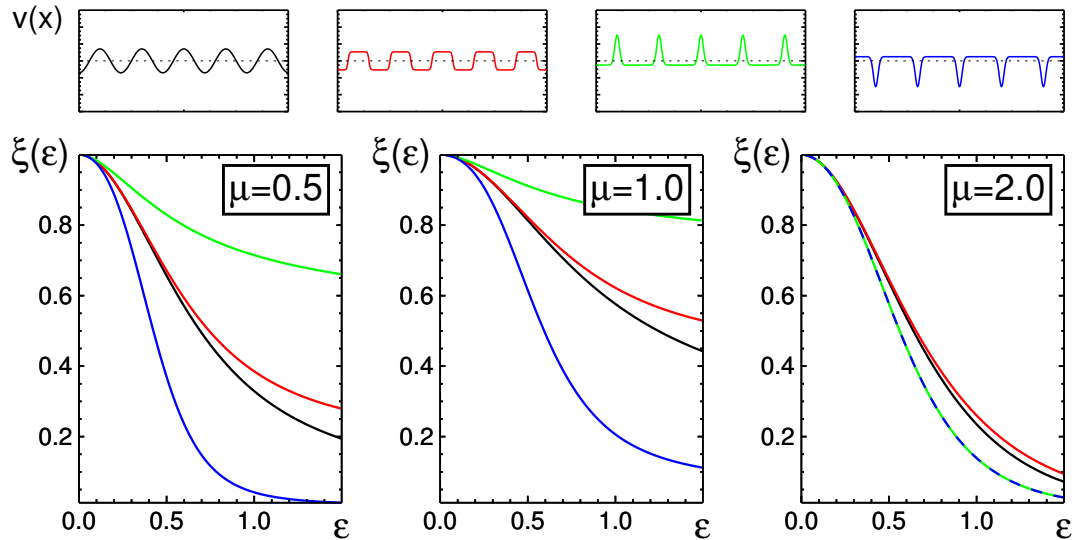


Figure 5.12.: The effective length scale $\xi(\varepsilon)$ in the asymptotic limit as a function of the potential strength ε . Two superdiffusive processes ($\mu = 1/2$ and 1) are compared to ordinary diffusion ($\mu = 2$). Each curve corresponds to the potential depicted in the top row in the same color.

Comparing the change of effective length scales ξ in various external potentials, we see that Lévy flights respond strongly to the bias of the potential. The curves of the square wave and the cosine potential are nearly identical. ξ is decreased only slightly by the localized peak potential and strongly affected by the localized trough potential. In contrast, the asymptotics of ordinary diffusion is nearly unaffected by the potential shape, consistent with Kramers escape theory [44].

Figure 5.12 shows the length scale ξ as a function of effective potential strength ε in an ordinary diffusion process, a moderately superdiffusive process and a strongly superdiffusive process in the aforementioned potentials. The ordinary diffusion process displays a similar decrease of $\xi(\varepsilon)$ for all potentials. Conversely, both superdiffusive processes exhibit substantial differences in $\xi(\varepsilon)$ which increase for increasing potential strength.

Comparing the effective length scales for each μ in the localized trough potential (blue lines), we see that the moderately superdiffusive process ($\mu = 1$) is least affected by the potential. When $\mu = 1/2$ a particle is bound to spend more time in the potential minima, when $\mu = 2$ it is less able to overcome the potential barrier. The intermediate case ($\mu = 1$) represents a compromise in terms of least impact of an external field on the dynamics. This may explain why Lévy flights with intermediate exponents $\mu \approx 1$ are predominantly observed in foraging strategies of animal species [30, 72, 73, 127] and human visual search [23].



5.5. Universal Behavior in Weak Potentials

The results presented in the previous sections relied on the numerical diagonalization of the Schrödinger equation (5.34). The low temperature and the weak potential regime can be treated by a perturbation expansion in the effective potential strength, since

$$\frac{V_0}{2k_B T} = \varepsilon \ll 1. \quad (5.44)$$

In this case, the effective potential U (5.3) can be approximated as

$$U \approx -\varepsilon \Delta^{\mu/2} v + \frac{1}{2} \varepsilon^2 \left(\Delta^{\mu/2} v^2 - 2v \Delta^{\mu/2} v \right), \quad (5.45)$$

which is correct to second order in ε . Expanding the potential $v(x)$ in a Fourier series yields approximate expressions for the Fourier coefficients,

$$\hat{U}_n \approx \frac{1}{\lambda^\mu} \varepsilon \left(|n|^\mu \hat{v}_n - \frac{1}{2} \varepsilon \sum_m \hat{v}_{n-m} (|n|^\mu - 2|m|^\mu) \hat{v}_m \right). \quad (5.46)$$

The energy bands $E_n(q)$ of a Schrödinger equation such as (5.5) can be expanded in the neighborhood of the energy bands $E_n^0(q) = |n/\lambda - q/\lambda|^\mu$ of the free Hamiltonian $H^0 = |P|^\mu$ as a perturbation series [7]. Depending on whether the Bloch phase q is near the Bragg plane (i.e. $q \approx 1/2$), two different expressions are obtained for the energy levels of the perturbed Hamiltonian.

5.5.1. Energy Levels Distant to the Bragg Planes

When $q \not\approx 1/2$, the energy difference $E_n^0(q) - E_m^0(q)$ of two arbitrary levels $n \neq m$ of the free Hamiltonian is of $\mathcal{O}(1)$. In this case the energy levels of the perturbed system can be expressed in terms of quantities belonging to the unperturbed system by

$$E_n(q) = E_n^0(q) + \hat{U}_0 + \sum_{m \neq n} \frac{|\hat{U}_{m-n}|^2}{E_n^0(q) - E_m^0(q)} + \mathcal{O}(U^3). \quad (5.47)$$

For $|U| \ll 1$ the $\mathcal{O}(U^3)$ -term can be neglected. The Fourier coefficients of the effective potential on the rhs of equation (5.47) are obtained from (5.46), and read

$$|\hat{U}_n|^2 \approx \frac{1}{\lambda^{2\mu}} \varepsilon^2 |n|^{2\mu} |\hat{v}_n|^2, \quad (5.48)$$

and

$$\hat{U}_0 = \frac{1}{\lambda^\mu} \varepsilon^2 \sum_m |m|^\mu |\hat{v}_m|^2. \quad (5.49)$$

Thus, the modification of the levels due to the weak potential is of the second order in the effective potential strength ε .



5.5.2. Energy Levels Near the Bragg Planes

When $q \approx 0, 1/2$ or 1 the degenerate energy levels n and $1 - n$ of free propagation, namely $E_n^0(q) = |n/\lambda - q/\lambda|^\mu$ and $E_{1-n}^0(q) = |n/\lambda - (q - 1)/\lambda|^\mu$ cause a divergence in the denominator in the expansion (5.47) which is no longer valid in this case. Instead, the energy levels near a Bragg plane become non-degenerate and split into two levels linearly in U [7],

$$E_n^0(q) \rightarrow E_n^-(q) \quad \text{and} \quad E_{1-n}^0(q) \rightarrow E_{1-n}^+(q), \quad (5.50)$$

where the correct modification in terms of the energies of the free systems is given by

$$\begin{aligned} E_n^\pm(q) &\approx E_n^0(q) \pm |\widehat{U}_{2n-1}| + \widehat{U}_0 \\ &\approx E_n^0(q) \pm \frac{1}{\lambda^\mu} \left(\varepsilon |2n - 1|^\mu |\widehat{v}_{2n-1}| + \varepsilon^2 \sum_m |m|^\mu |\widehat{v}_m|^2 \right) \end{aligned} \quad (5.51)$$

The second term explains why a band split linear in ε is only observed for the lowest two bands in the cosine potential (figure 5.4), since the Fourier coefficients \widehat{v}_{2n-1} vanish except for $2n - 1 = \pm 1$. Potentials with higher non-vanishing modes possess a linear split between additional bands, see for example the band structure of the localized peak and trough potentials in figure 5.8. Although the bias of the potentials influences the band structure of these potentials on the entire range of potential strengths, the behavior is identical in the weak potential regime, since the additional terms in equation (5.51) depend only on the absolute value of the Fourier coefficients of the potential.

5.5.3. Asymptotic Behavior in Weak Potentials

The asymptotic behavior in weak periodic potentials is determined by the lowest band ($n = 0$) and small values of the Bloch phase ($q \ll 1$). Combining equations (5.48) and (5.49) with equation (5.47) yields

$$E_n(q) \approx E_n^0(q) - \frac{1}{\lambda^\mu} \varepsilon^2 \sum_{m \neq n} \left(\frac{|n - m|^{2\mu}}{|m - q|^\mu - |n - q|^\mu} |\widehat{v}_{n-m}|^2 - |m|^\mu |\widehat{v}_m|^2 \right) \quad (5.52)$$

for all bands. Substituting $n = 0$ and rearranging the sum gives

$$E_0(q) \approx E_0^0(q) - \frac{1}{\lambda^\mu} \varepsilon^2 \sum_{m>0} |\widehat{v}_m|^2 \left(\frac{m^{2\mu}}{(m - q)^\mu - q^\mu} + \frac{m^{2\mu}}{(m + q)^\mu - q^\mu} - 2m^\mu \right). \quad (5.53)$$

With $E_0^0(q) = (q/\lambda)^\mu$ we obtain

$$E_0(q) = E_0^0(q) \left[1 - 8 \varepsilon^2 \sum_{m>0} |\widehat{v}_m|^2 g_\mu(q/m) \right], \quad (5.54)$$



in which the function $g_\mu(z)$ is given by

$$g_\mu(z) = \frac{1}{8z^\mu} \left(\frac{1}{(1-z)^\mu - z^\mu} + \frac{1}{(1+z)^\mu - z^\mu} - 2 \right). \quad (5.55)$$

Equation (5.54) states that a weak periodic potential decreases the dispersion speed by a factor proportional to ε^2 , so the characteristics of the dispersion are not changed since $E_0(q) \sim E_0^0(q)$. The degree to which the term in brackets in (5.54) is decreased depends on the structure of the potential represented by the Fourier coefficients \hat{v}_m as well as the Lévy exponent μ in the factor $g_\mu(q/m)$.

Consider now the asymptotic limit $q \rightarrow 0$. This limit is equivalent to $z \rightarrow 0$ in equation (5.55), i.e.

$$\lim_{z \rightarrow 0} g_\mu(z) = \begin{cases} 1 & \mu = 2 \\ \frac{1}{4} & 0 < \mu < 2. \end{cases} \quad (5.56)$$

As $z \rightarrow 0$ the function $g_\mu(z)$ does not converge uniformly on the interval of Lévy exponents $(0, 2]$. The Lévy exponent $\mu = 2$ describes ordinary diffusion possesses an exceptional limit. The effect on the generalized diffusion coefficient

$$D_\mu = \lim_{k \rightarrow 0} \frac{E_0(\lambda k)}{k^\mu} \quad (5.57)$$

is quantified by relative difference to the unperturbed dynamics, i.e.

$$\delta D_\mu = 1 - D_\mu^0. \quad (5.58)$$

The rescaled potentials $v(x)$ have unit variance and thus

$$2 \sum_{m>0} |\hat{v}_m|^2 = 1. \quad (5.59)$$

Inserting the limit of $g_\mu(z)$ into (5.56), taking (5.59) into account and replacing the effective potential strengths by the original physical quantities V_0 and $k_B T$ yields

$$\lim_{k \rightarrow 0} \delta D_\mu = \left(\frac{V_0}{k_B T} \right)^2 \begin{cases} 1 & \mu = 2 \\ \frac{1}{4} & 0 < \mu < 2. \end{cases} \quad (5.60)$$

This is a rather interesting result. The dispersion speed of all processes is decreased quadratically by a weak periodic potential in the ratio $V_0/k_B T$. Furthermore, on large scales the magnitude is independent of the Lévy exponent μ , and hence universal for all Lévy flights. Only the marginal case of ordinary diffusion is an exception, being slowed down by a factor of 4. The response to an external potential displays a discontinuity at $\mu = 2$. In terms of the physical example of random motion on a hetero-polymer, this result implies that as soon as folding dynamics permit

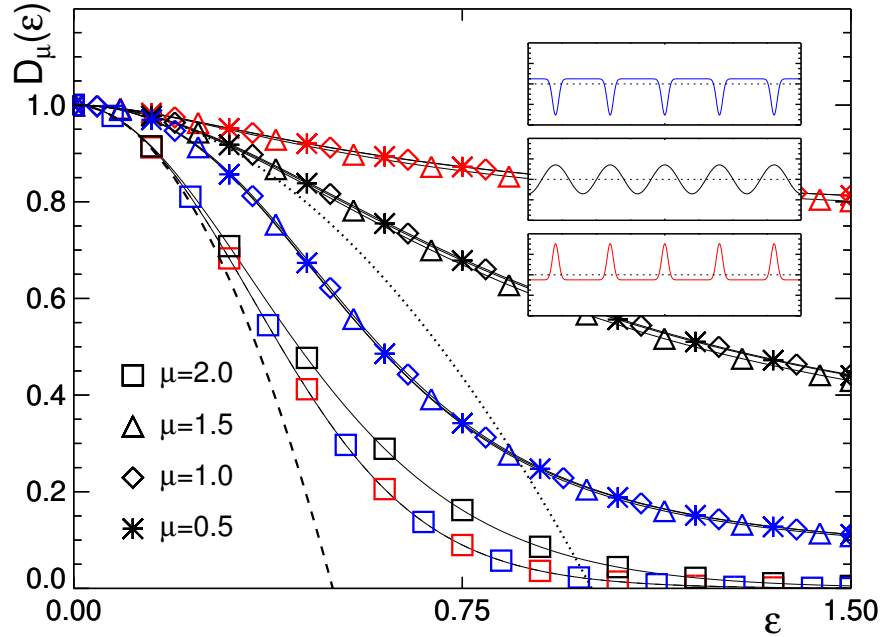


Figure 5.13.: The generalized diffusion coefficient $D_\mu(\varepsilon)$ as a function of effective potential strength ε for a chosen set of Lévy exponents listed in the lower left corner and assigned different symbols. For each Lévy exponent three potentials (inset) are compared and labeled by color. The dashed and dotted lines represent the results obtained from perturbation theory (equations (5.60) and (5.58)), for superdiffusion and ordinary diffusion, respectively.

long range transitions, a quantitatively different dispersion speed is predicted by equation (5.60). However, changing the exponent of long range transition probabilities by different folding dynamics does not alter the dispersion speed as long the effective strength of the potential on the polymer remains the same.

The universal behavior for $\mu < 2$ seems to be contradicting the results obtained above, namely the strong dependence of band structures on properties of the potentials, such as the bias and shape, as well as strong variation as a function μ . Actually, the universal behavior is only observed for weak potentials and in the asymptotic limit. In figure 5.13 the generalized diffusion coefficient is shown as a function of effective potential strength for the set of potentials sketched in the insets. The results obtained by perturbation theory (i.e. equation (5.57)) are represented by the dotted ($\mu < 2$) and dashed ($\mu = 2$) lines. For the set of Lévy exponents listed in the lower left corner, the generalized diffusion coefficient was computed numerically. In the weak potential regime the numerics coincide nicely with the predictions given by perturbation theory. For all Lévy exponents $\mu < 2$ the generalized diffusion coefficient as a function of ε is identical. The marginal case of

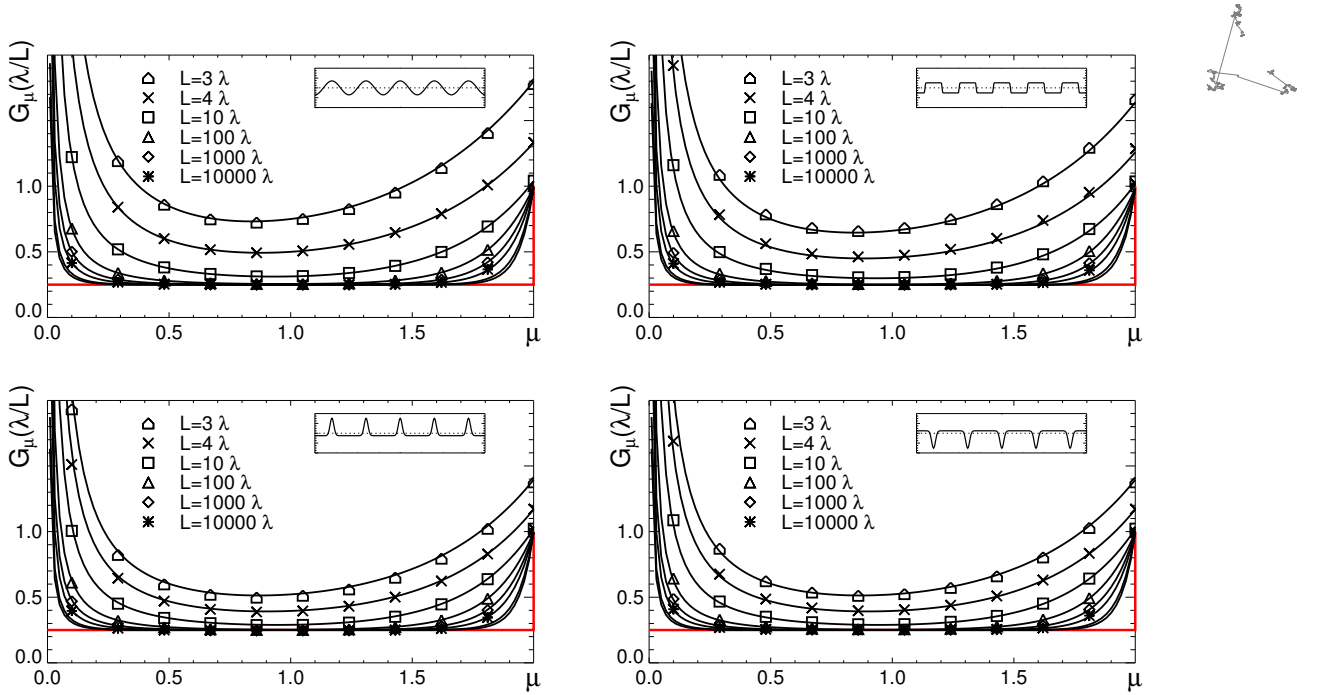


Figure 5.14.: Relaxation properties of superdiffusion processes in finite systems. The quantity $G_\mu(\lambda/L)$ (see equation (5.55)) is depicted for various system sizes L in units of wavelength λ as a function of Lévy exponent μ (solid lines). Each panel corresponds to the potential shown in the inset. The symbols depict the results obtained from numerical diagonalization of equation (5.34). The non-uniform limit $L \rightarrow \infty$ is shown in red.

ordinary diffusion $\mu = 2$ is an exception. For strong effective potential strengths, ordinary diffusion and Lévy flights behave in a somewhat complementary fashion. For the Lévy flights the curves still coincide for a given potential. The behavior is still universal in that respect. Yet each curve differs for each potential, reflecting the sensitivity of Lévy flights to potential shape. When $\mu = 2$ the situation is reversed. While $D_\mu(\varepsilon)$ of the ordinary diffusion process fails to coincide with the rest of the curves, it remains largely the same when the potential is changed.

Recently, a number of studies [12, 126, 128] proposed that Lévy flights with intermediate exponents $\mu \approx 1$ are optimal when employed in search strategies of foraging animals. The results obtain above suggests that on large scales, the specific choice of exponent is irrelevant to the dispersion speed, as long as $\mu < 2$. However, our results are a consequence of a limiting procedure, the physical plausibility of which needs to be investigated with care, especially because the limit is attained non-uniformly. In the next section we show that the idea of optimal intermediate Lévy exponents is still valid in finite systems, even if they span orders of magnitude of the typical wavelength of the potential.

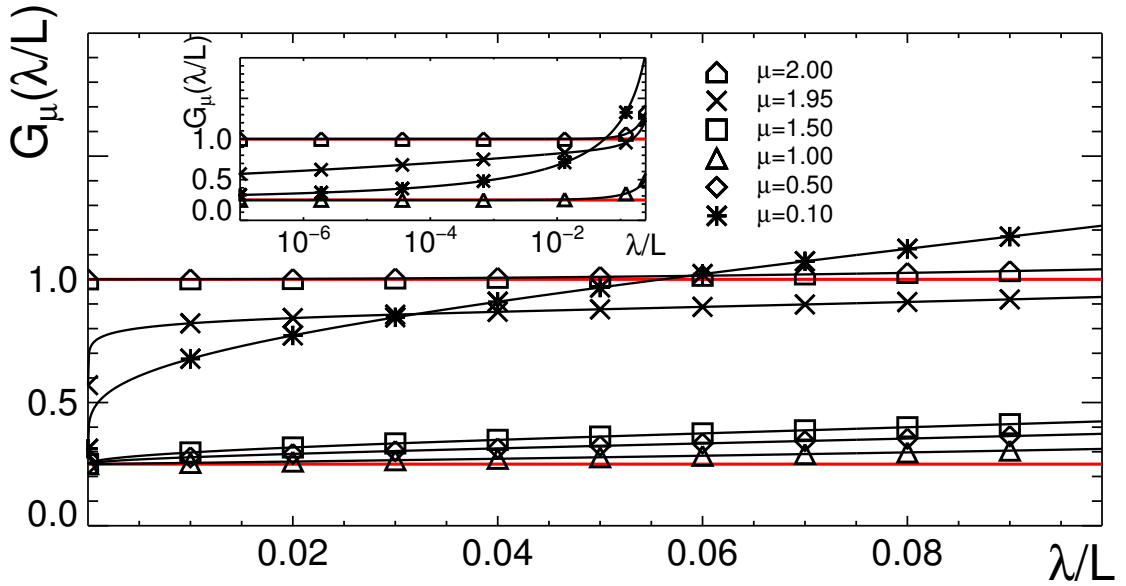


Figure 5.15.: For the set of Lévy exponents listed in the upper right the quantity $G_\mu(\lambda/L)$ is shown as a function of relative inverse system size λ/L for the cosine potential. The inset shows the same curves on a semi-logarithmic scale. The red lines depict the limits $\lim_{\lambda/L \rightarrow 0} G_\mu(\lambda/L)$ for $\mu = 2$ (upper line) and $\mu < 2$ (lower line).

5.6. Finite Systems

So far we have considered systems of infinite physical extent. In the study of ordinary diffusion processes this usually poses no problem. The evolution operators involved are local, and boundary effects can be neglected on relevant spatio-temporal scales. In the realm of superdiffusion more care is appropriate, since fractional operators are non-local and may respond to the system's boundary more strongly. In fact, boundary effects come in various shapes in superdiffusive systems, see for example [27, 36, 87, 144].

We consider a finite system of length $2\pi L$ which is modulated by a periodic potential of much shorter wavelength $2\pi\lambda$, i.e.

$$\lambda \ll L. \quad (5.61)$$

In a finite system the Hamiltonian in equation (5.5) has a discrete spectrum. Each continuous band $E_n(q)$ splits into $M = L/\lambda$ discrete energy eigenvalues, which are obtained by evaluating $E_n(q)$ at $q_m = m\lambda/L$ with $m = 1 \dots M$. The lowest wave number in a finite system is given by

$$k_1 = L^{-1}, \quad (5.62)$$

the smallest value of the Bloch phase q_1 is thus given by the ratio of wavelength and system size, i.e.

$$q_1 = \frac{\lambda}{L}. \quad (5.63)$$

The relaxation time of the process is related to the lowest eigenvalue of the spectrum by

$$\tau_c = \frac{1}{E_0(q_1)} = \frac{1}{E_0(\lambda/L)}, \quad (5.64)$$

and quantifies the amount of time that elapses until a localized initial density spreads over the entire system. We define the relative change in relaxation time compared to the unperturbed system as

$$\delta\tau_c = \tau_c/\tau_c^0 - 1, \quad (5.65)$$

where $\tau_c^0 = L^\mu$ denotes the relaxation time of a freely moving particle. Applying the results obtained from perturbation theory we obtain

$$\delta\tau_c \approx \varepsilon^2 G_\mu(\lambda/L) \quad \text{where} \quad (5.66)$$

$$G_\mu(\lambda/L) = 2 \sum_{m>0} g_\mu(\lambda/Lm) |\widehat{v}_m|^2. \quad (5.67)$$

Since $g_\mu(z)$ and $|\widehat{v}_m|^2$ are non-negative and $g_\mu(z)$ is monotonically decreasing with decreasing z , the function $G_\mu(\lambda/L)$ is certainly larger than the first summand, and a lower bound to $\delta\tau_c$ is given by

$$\delta\tau_c \approx \varepsilon^2 g_\mu(\lambda/L). \quad (5.68)$$

Note that $G_\mu(z) = g_\mu(z)$ for the cosine potential which has only one non-vanishing Fourier component.

The relative increase in relaxation time $\delta\tau_c$ is thus determined by the value of the function $G_\mu(z)$ at small but non-zero arguments $z = \lambda/L$. Figure 5.14 depicts $G_\mu(\lambda/L)$ as a function of Lévy exponent μ for a given set of system size wavelength ratios. Each panel gives the results for the one of the potentials. Superimposed and denoted by symbols are the numerical results for $G_\mu(\lambda/L)$. The red line indicates the limit (5.56) obtained above. Note the discontinuity at $\mu = 2$. As opposed to the behavior in an infinite system, the curves corresponding to large but finite systems show a pronounced minimum at intermediate values of μ . Even for very large systems, the function $G_\mu(z)$ diverges beyond any value as $\mu \rightarrow 0$.

The rate of convergence is very different for various Lévy exponents, as is indicated in figure 5.15 for the cosine potential. The figure shows the behavior of $G_\mu(\lambda/L)$ as a function of λ/L for a set of exponents μ . The limits of 1/4 for the Lévy flights and 1 for ordinary diffusion are indicated by the red lines. All processes attain their limit quickly, except for those which are nearly diffusive ($\mu \lesssim 2$)





and those which are extremely superdiffusive ($\mu \approx 0$). The semi-logarithmic plot (inset) shows that a convergence of these processes is very slow.

Consequently, in any real and hence finite system, the effect of an external potential on the speed of dispersion is least pronounced for Lévy flights with $\mu \approx 1$, consistent with the observation that these type of Lévy flights are employed as search strategies.

5.7. Discussion

The investigation of topological superdiffusion in periodic potentials revealed a number of interesting and important effects. The spectral band structure which we obtained by means of a Bloch theory for superdiffusion strongly depends on the Lévy exponent as well as the functional form of the periodic potential. The superdiffusive processes ($\mu < 2$) generally possess band structures with greater complexity than ordinary diffusion processes ($\mu = 2$). Consequently, the transient dynamics of superdiffusion in periodic potentials exhibits a higher degree of variability. Even small changes in the effective potential strength can change the relaxation properties of the superdiffusive processes, whereas ordinary diffusion responds smoothly to parameter changes.

The comparison of a potential with localized peaks on one hand, and localized troughs on the other, showed that superdiffusion is rather different in each potential, although ordinary diffusive dispersion is identical in both potentials. Therefore, unlike ordinary diffusion processes which are solely affected by magnitude variations of the external potential, superdiffusion processes are susceptible to the precise shape of the potential. These results are relevant to a number of systems in which scale-free topologies induce enhanced diffusion, such as random motion of regulatory proteins on folded DNA strands and other intracellular translocation processes, and we predict that these systems possess a rich variety of relaxation dynamics.

The perturbation analysis revealed two key properties of the asymptotics of topological superdiffusion. Although the transient dynamics in a given external potential varies with μ , the asymptotic behavior is universal for all superdiffusive processes ($\mu < 2$) in a given potential, because the generalized diffusion coefficients for various Lévy exponents are identical in the perturbative regime. An exception is the limiting case of ordinary diffusion ($\mu = 2$). In terms of the physical example of random motion on a folding polymer, this result implies that the folding statistics of the chain play no role for the dispersion speed along a chain, as long as scale-free transition occur. Conversely, the generalized diffusion coefficient for superdiffusion depends on the form of the potential, and does not depend on it for ordinary diffusion. Compared to the unbiased cosine potential, superdiffusive processes are slowed down strongly by periodic trough potentials, and are least

affected by potential peaks.

The investigation of relaxation to the stationary state in finite systems demonstrated that processes with intermediate Lévy exponents are least affected by external potentials. The reduction of dispersion speed is greatest for nearly diffusive processes but also for processes with small exponents (strong superdiffusion). Based on this result, we predict that Lévy flights with intermediate exponents are optimal when employed for target location strategies in variable environments. This is supported by the observation that foraging animals perform Lévy flights with exponents near unity. We speculate that Lévy strategies may be a useful tool in computational search strategies as well, and that Lévy flights with $\mu \approx 1$ will be most efficient.

We believe that our analysis of topological superdiffusion in periodic potentials is not only important for the reasons given above, but also because in the popular modeling framework of generalized Langevin dynamics, periodic potentials do not give interesting results, and have thus not been considered a source of interesting dynamical behaviors. Furthermore, the results presented will be valid for the wide range of rate models which are asymptotically governed by the fractional Fokker-Planck equation studied here.



5. Periodic Potentials





6. Random Environments

All generalizations are false.
Including this one.

(Mark Twain)

We extend the analysis presented in the last chapter to random potentials. First we investigate topological superdiffusion in random phase potentials, which represent a popular model for random environments with typical variance and correlation length. We compute the density of states for the generalized crystal momentum and compare the dynamics in four typical potentials with different power spectra. We show that the density of states depends on the statistical properties of the random potential, and generally exhibits a complex behavior as a function of effective potential strength. As opposed to the dynamics in periodic potentials for which the complexity of the spectral band structure increases with decreasing Lévy exponent μ , the density of states for random potentials exhibits the highest degree of complexity for diffusive processes. Concerning relaxation speed on finite scales, we demonstrate that moderately superdiffusive processes are least affected by external potentials. Ordinary diffusion and superdiffusion with a Lévy exponent above a critical value μ_c are slowed down on large scales and sped up on scales smaller than the correlation length of the external potential. Surprisingly, strongly superdiffusive processes are slowed down even on small scales. We show that the generalized diffusion coefficient, which quantifies the asymptotic dispersion speed, is independent of the type of potential and identical for all superdiffusive processes ($\mu < 2$) but different for ordinary diffusion ($\mu = 2$). A perturbation theoretic treatment predicts that in weak random potentials transient dynamics differs considerably for various Lévy exponents, the greatest deviations from the typical behavior being observed for nearly diffusive ($\mu \approx 2$) as well as strongly superdiffusive ($\mu \approx 0$) processes. In a simple model for topological superdiffusion on a random co-polymer, we investigate the influence of relative monomer concentration on the dynamics. Unlike ordinary diffusion which is independent of the relative abundance of each monomer type, the dispersion speed of a superdiffusive particle is considerably affected. Consequently, when polymer folding permits scale-free transitions along the chain, more information than the relative abundance of monomer types is needed to correctly estimate dispersion speeds. We believe that this insight will be relevant for the understanding of random motion on biological



macromolecules, such as protein dynamics on DNA strands.

6.1. Motivation

Investigating topological superdiffusion in random environments is important for a number of reasons. The periodic potentials studied in chapter 5 certainly represent an idealized scenario. There is no such thing as a perfectly periodic polymer or resource distribution in an animal's habitat. Even though external forces may fluctuate around a typical value with a typical degree of variability and possess a typical length scale, they usually exhibit a certain degree of irregularity.

A number of prominent systems possess dynamical properties which are rather different in regular and random environments, even when the degree of external irregularity is small. For example, a one-dimensional ordinary random walk in a periodically modulated environment is recurrent, but transient if a small random perturbation is added [118]. A similar effect occurs in disordered one-dimensional quantum mechanical systems, which exhibit spectral properties absent in regular potentials [5].

From a modeling point of view, it is crucial to understand which phenomena are linked to what specific ingredients of the model. Are the predictions of the generalized Bloch theory for periodic environments also accurate in random environments for which the theory is inappropriate?

Generalized Langevin dynamics in quenched random force fields has been studied extensively in recent years [40, 41, 56]. However, the quenched fields considered were unbounded, and in chapter 4 we saw that generalized Langevin dynamics is asymptotically trivial in bounded potentials.

How does the random environment interfere with superdiffusion on scale-free topologies, how can it be quantified and how does it depend on the potential strength and the Lévy exponent μ ? These questions will be addressed below. The results will not only be essential to the understanding of particle dynamics on folding hetero-polymers but also to ecological processes such as foraging strategies of animals in inhomogeneous resource environments, which have attracted much attention recently [12, 76, 134].

Figure 6.1 depicts a situation analogous to that depicted in figure 5.1A. Instead of a periodically arranged set of monomers of variable energies, a random sequence of monomers results in a random potential defined along the chemical axis of the chain. The folding dynamics permits long range transitions, and at each point in time the neighborhood topology has a structure qualitatively sketched on the right in figure 6.1. The arcs between two pairs of monomers indicate that they are adjacent in Euclidean space.

In figure 6.2 two-dimensional examples of topological superdiffusion in inhomogeneous random environments are depicted. The random graph in figure 6.2A is

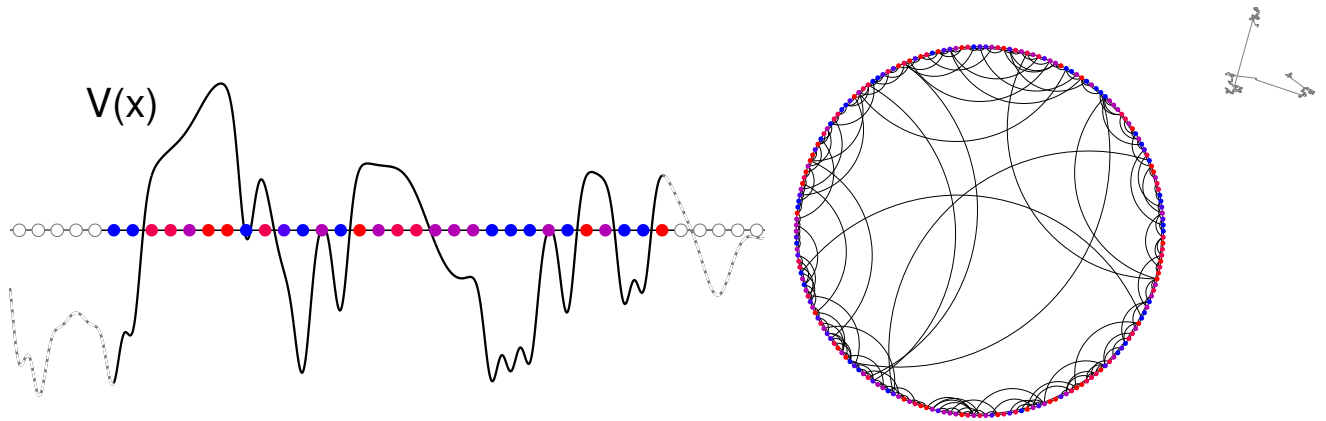


Figure 6.1.: **Left:** A random hetero-polymer, consisting of randomly arranged monomers. The types of monomers are distinguished by color and reflect the local potential. The random arrangement of monomer leads to a random potential $V(x)$ defined along the chemical axis of the chain. **Right:** The neighborhood topology of a random hetero-polymer in a folded conformation. Circular arcs indicate proximity in Euclidean space.

similar to the scale-free graphs depicted in figures 3.2B and 5.1B. The probability of finding a connection of a certain length lacks a scale. As opposed to the previous systems, the graph in figure 6.2A has a random inhomogeneous vertex concentration in the plane.

A model trajectory of a foraging animal in a inhomogeneous resource landscape is shown in figure 6.2B. Unlike the strongly idealized periodic landscape in figure 5.1C, the landscape depicted here is more irregular as a function of position.

In the following we investigate the fractional Fokker-Planck equation (FFPE) for topological superdiffusion

$$\partial_t p = e^{-\beta V/2} \Delta^{\mu/2} e^{\beta V/2} p - p e^{\beta V/2} \Delta^{\mu/2} e^{-\beta V/2}, \quad 0 < \mu \leq 2 \quad (6.1)$$

for random potentials V . As in the previous chapter, our analysis is based on the spectral properties of the fractional Hamiltonian

$$H = |P|^\mu + U(X), \quad \text{with} \quad (6.2)$$

$$U(x) = e^{\beta V/2} \Delta^{\mu/2} e^{-\beta V/2}. \quad (6.3)$$

Since V is a random quantity, so is the effective potential U . The spectral properties of the Hamiltonian are different for every realization in the potential ensemble. Typical spectral properties of the system are given by the potential ensemble average, denoted by $\langle \cdot \rangle_V$. Since the random potential reflects a quenched disorder which does not change over time, the ensemble average does not commute with the expectation value for the stochastic process, and must be carried out as the final step in the computation.

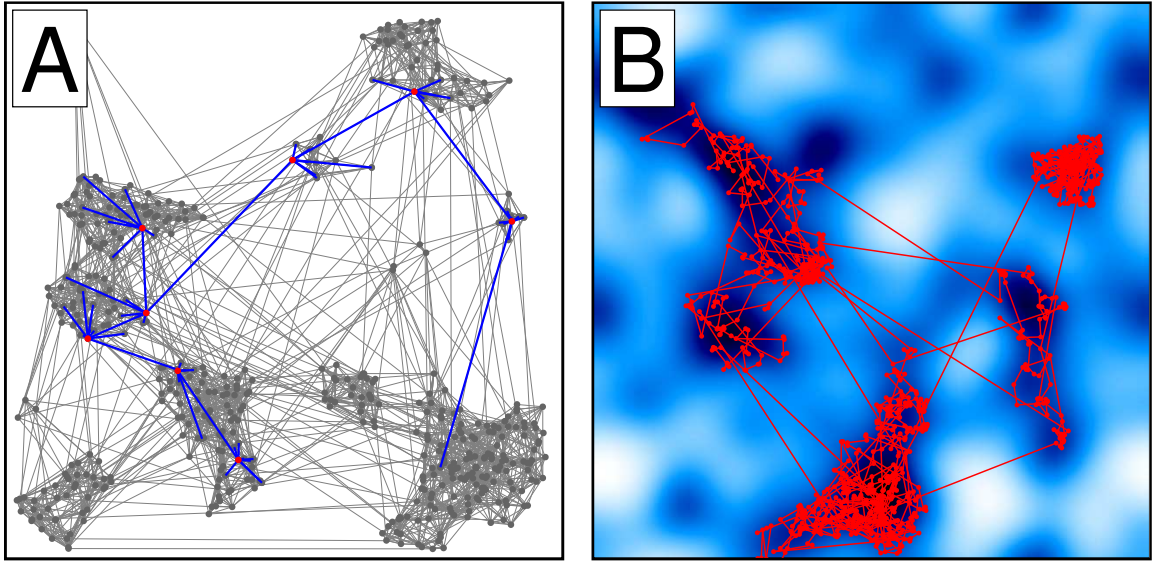


Figure 6.2.: Topological superdiffusion in random environments. **A:** A random graph with scale-free connection lengths and inhomogeneous vertex concentration in the plane. **B:** A model trajectory of a foraging animal in an inhomogeneous resource landscape. Dark regions reflect a high abundance of resources, bright regions a low abundance.

6.2. Random Potentials

We consider random potentials with vanishing mean and a variance V_0^2 , i.e.

$$\langle V(x) \rangle_V = 0 \quad \text{and} \quad \langle V^2(x) \rangle_V = V_0^2. \quad (6.4)$$

Furthermore, we assume a stationary potential ensemble which implies that the correlation function $C(x)$ depends only on distance, i.e.

$$\langle V(x)V(y) \rangle_V = C(|x - y|). \quad (6.5)$$

The power spectrum $S(k)$ is defined as the Fourier transform of the correlation function,

$$S(k) = \int dx e^{ikx} C(x). \quad (6.6)$$

Stationarity entails that the Fourier transform

$$\tilde{V}(k) = \int dx e^{ikx} V(x) \quad (6.7)$$

of the potential itself is uncorrelated and related to the power spectrum by

$$\langle \tilde{V}(k) \overline{\tilde{V}(k')} \rangle_V = 2\pi S(k) \delta(k - k'), \quad (6.8)$$

where $\overline{(\cdot)}$ denotes complex conjugation. The spatial scale is quantified by the correlation length



$$\xi = \frac{1}{\langle (V(x) - \langle V \rangle)^2 \rangle} \int_0^\infty dx \langle (V(x) - \langle V \rangle)(V(0) - \langle V \rangle) \rangle_V. \quad (6.9)$$

Since $\langle V \rangle = 0$, the correlation length is just the integrated correlation function, normalized by V_0^2 , i.e.

$$\xi = \frac{1}{V_0^2} \int_0^\infty dx C(x). \quad (6.10)$$

Equation (6.6) implies that the variance V_0^2 is proportional to the total power in the potential, and the power spectrum at $k = 0$ can be related to the correlation length,

$$2\pi V_0^2 = \int dk S(k) \quad \text{and} \quad 2\xi V_0^2 = S(0). \quad (6.11)$$

This yields an equation for the correlation length in terms of the power spectrum,

$$\xi = \frac{\pi S(0)}{2 \int_0^\infty dk S(k)}. \quad (6.12)$$

In the comparison between potential types we will investigate different power spectra with equal variances and correlation lengths.

6.2.1. Modeling Random Environments with Random Phases

A simple, straightforward and elegant way of modeling random potentials retaining the attributes of amplitude variability and typical spatial scale is the random phase scheme. The Fourier transform of the potential can be separated into its absolute value $\phi(k)$ and a phase factor, i.e.

$$\tilde{V}(k) = \phi(k) e^{i\vartheta(k)} \quad \text{with} \quad \phi(k) > 0. \quad (6.13)$$

Generally, $\phi(k)$ and $\vartheta(k)$ are random functions of k . A random phase potential is generated by a deterministic $\phi(k)$ and uncorrelated random phases $\vartheta(k)$ which are uniformly distributed in the interval $[0, 2\pi)$,

$$\rho(\vartheta) = \begin{cases} 1/2\pi & \vartheta \in [0, 2\pi) \\ 0 & \text{otherwise.} \end{cases} \quad (6.14)$$

Since $V(x)$ is real, the random phases $\vartheta(k)$ fulfill

$$-\vartheta(k) = \vartheta(-k). \quad (6.15)$$

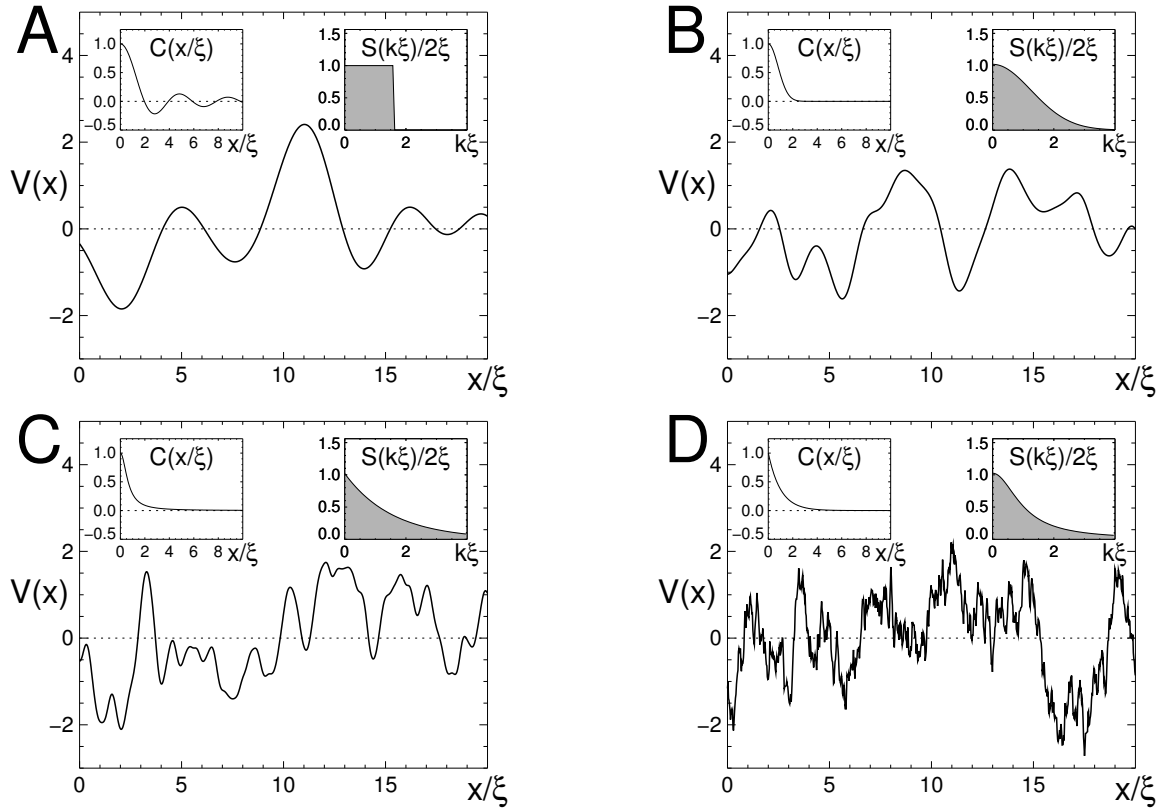


Figure 6.3.: Various types of random phase potentials with unit variance ($V_0 = 1$) and correlation length ξ . Each panel depicts a realization of $V(x)$ derived from a power spectrum $S(k)$ shown in the upper right inset. The associated correlation function $C(x)$ is shown in the upper left inset. **A:** A potential with Heaviside power spectrum and oscillatory correlation function. **B:** A potential with Gaussian spectrum and correlation function. **C:** A potential with exponentially decreasing spectrum **D:** A potential with an exponentially decreasing correlation function. The analytic expressions for $S(k)$ and $C(x)$ are provided in table 6.1.

A realization of a random phase potential can be obtained from a realization of the random phases $\vartheta(k)$ and a prespecified power spectrum, because $\phi(k)$ can be obtained from $S(k)$ by

$$\phi(k)\overline{\phi(k')} = 2\pi S(k)\delta(k - k'), \quad (6.16)$$

and $V(x)$ is obtained by an inverse Fourier transformation,

$$V(x) = \frac{1}{2\pi} \int dk \phi(k) e^{-i(kx + \vartheta(k))}. \quad (6.17)$$

A universal feature of these potentials is that at any position the potential values are evenly distributed around the expectation value. The integral on the rhs of (6.17)

is a sum over independent random variables, and the probability density function (pdf) for $V(x)$ at any point must be a Gaussian centered at $\langle V \rangle_V = 0$,



$$\langle \delta(v - V(x)) \rangle_V = \frac{1}{\sqrt{2\pi V_0^2}} \exp \left[-\frac{v^2}{2V_0^2} \right], \quad (6.18)$$

a consequence of the central limit theorem.

Table 6.1.: Four types of power spectra $S(k)$ and correlation functions $C(x)$ yielding random potentials $V(x)$ appropriate for the description of various physical systems. **A:** A Heaviside spectrum **B:** A Gaussian spectrum, **C:** An exponentially decreasing spectrum **D:** An exponentially decreasing correlation function.

	$S(k)$	$C(x)$
A	$2\xi \Theta(k - \pi/2\xi)$	$\frac{2}{\pi(x/\xi)^2} \sin(\pi x/2\xi)$
B	$2\xi \exp \left[-\frac{k^2 \xi^2}{\pi} \right]$	$\exp \left[-\frac{\pi x^2}{4\xi^2} \right]$
C	$2\xi \exp \left[-\frac{2\xi k }{\pi} \right]$	$\frac{1}{1 + \left(\frac{\pi x}{2\xi}\right)^2}$
D	$\frac{2\xi}{1 + (k\xi)^2}$	$\exp \left[-\frac{ x }{\xi} \right]$

In the following we concentrate on four different types of random phase potentials, each one defined by a specific power spectrum. The spectra are gauged such that the variance of the potentials V_0^2 and the correlation length ξ are identical for all potentials. Expressions for the power spectra and correlation functions are listed in table 6.1; the potentials are labeled by A, B, C, and D. A realization of each potential is depicted in figure 6.3 as well as the associated spectra and correlation functions. The power spectrum in A is given by a Heaviside function Θ with a cut-off at $k = \pi/2\xi$. The correlation function decays in an oscillatory fashion and the potential has a random wavelike shape with a wavelength of approximately 4ξ . System B describes a potential type frequently encountered in physical modeling. The power spectrum and correlation function are Gaussian. Systems C and D represent complementary situations. In each system either the power spectrum (C) or the correlation function (D) decrease exponentially with $k\xi$ or x/ξ , respectively. The potentials in D possess non-differentiable realizations, because the correlation function is not analytic at the origin. Note that from A to D the potentials possess a higher degree of structure on smaller scales due to higher amounts of power in the tails of the spectrum, although in each case the correlation length as defined by equation (6.9) is the same.



6.3. Density of States and Return Probability

In chapter 5 important aspects of the transient dynamics of topological superdiffusion in periodic potentials were revealed by the band structure of the crystal momentum $\kappa_n(q)$. The emergence of bands and gaps in the spectrum is a consequence of the periodicity of the potentials. For random potentials the spectrum does not split into bands. The analogous quantity in this case is the density of crystal momenta $\rho_\kappa(\kappa)$ which is related to the density of energy eigenvalues $\rho_E(E)$. The Laplace transform of $\rho_E(E)$ is the return probability $P_0(t)$ of being at the initial location averaged over all possible initial locations. These quantities will be defined and computed for various random phase potentials below.

We begin with the fractional Schrödinger equation

$$\partial_t |\psi\rangle = -H |\psi\rangle. \quad (6.19)$$

where the Hamiltonian is given by (6.2). Formally, equation (6.19) is solved by

$$|\psi_t\rangle = e^{-Ht} |\psi_0\rangle. \quad (6.20)$$

The spectral decomposition of H can be applied to the operator $\exp[-Ht]$, i.e.

$$e^{-Ht} = \int_0^\infty e^{-Et} dP_E \quad (6.21)$$

in which $\{P_\Delta\}_{\Delta \in \mathcal{B}(\mathbb{R})}$ is the spectral family of H . Equation (6.21) is a generalization of the expansion of a bounded operator into a countable set of eigenvalues and eigenvectors. More details on spectral decomposition of operators with continuous spectra are provided in Appendix C. The conditional pdf $p(x, t|y, 0)$ of the process can be expressed in terms of the spectral family as

$$p(x, t|y, 0) = e^{-\beta[V(x)-V(y)]/2} \int_0^\infty e^{-Et} dP_E(x, y), \quad (6.22)$$

where

$$P_E(x, y) = \langle x|P_E|y\rangle \quad (6.23)$$

is the position representation of the projector P_E . We define a density operator

$$\rho = \lim_{L \rightarrow \infty} \frac{1}{L} \int dx |x\rangle \langle x| \quad (6.24)$$

where the limit is to be understood as the last step of any computation that involves ρ . What is the use of this? With ρ we can express positional averages easily as

brackets. For example, the trace

$$\mathrm{Tr} \left(e^{-Ht} \rho \right) = \int_0^{\infty} e^{-Et} d\mathrm{Tr} (P_E \rho) \quad (6.25)$$

leads to

$$\mathrm{Tr} (P_E \rho) = \lim_{L \rightarrow \infty} \frac{1}{L} \int dx P_E(x, x). \quad (6.26)$$

This trace defines a measure

$$\mu(E) = \mathrm{Tr} (P_E \rho) \quad (6.27)$$

on the positive real axis which is independent of the initial condition. Alternatively, one could have obtained this measure by averaging over an ensemble of random potentials. The measure defined by (6.27) reflects statistical properties of the ensemble of random potentials as opposed to properties of a single realization. The density of states $\rho(E)$ is defined as the concentration of energies in an infinitesimal interval dE in the vicinity of E ,

$$\rho(E) dE = \mu(E + dE) - \mu(E). \quad (6.28)$$

A quantity of interest in the theory of random walks is the probability $P_0(t)$ of being located at the initial location x after time t , averaged over all possible initial locations, i.e.

$$P_0(t) = \lim_{L \rightarrow \infty} \frac{1}{L} \int dx p(x, t | x, 0). \quad (6.29)$$

The asymptotic behavior of $P_0(t)$ determines a number of properties of the process, such as whether the process is recurrent or transient [91]. Combining equation (6.22) with (6.30) and (6.29) gives

$$P_0(t) = \lim_{L \rightarrow \infty} \int_0^{\infty} e^{-Et} \frac{1}{L} \int dx dP(x, x). \quad (6.30)$$

Therefore, the return probability is just the Laplace transform of the density of eigenvalues, i.e.

$$P_0(t) = \int_0^{\infty} dE e^{-Et} \rho(E). \quad (6.31)$$

Before we compute the density of states, we need to establish the reference point of free superdiffusion. A freely superdiffusive particle is governed by the conditional pdf (see section 2.5)

$$p(x, t | y) = \frac{1}{2\pi} \int_{-\infty}^{\infty} dk e^{-ik(x-y) - |k|^\mu t}. \quad (6.32)$$





Equation (6.29) yields for the return probability

$$P_0(t) = \frac{1}{2\pi} \int_{-\infty}^{\infty} dk e^{-|k|^\mu t}. \quad (6.33)$$

Substituting $E = |k|^\mu$, changing the integration variable and comparing with (6.31) we obtain for the density of eigenvalues of a symmetric Lévy stable process,

$$\rho^0(E) = \frac{1}{\mu\pi} E^{1/\mu-1}. \quad (6.34)$$

Depending on the Lévy exponent μ , the density of eigenvalues is either an increasing or decreasing function of E or constant for the intermediate case $\mu = 1$. Performing a Laplace transform on (6.34) with respect to E , we obtain

$$P_0(t) = \frac{1}{\pi} \Gamma(1 + 1/\mu) t^{-\frac{1}{\mu}}. \quad (6.35)$$

Since the functional form of $\rho(E)$ depends on the Lévy exponent μ , the density of the crystal momentum

$$\kappa = E^{1/\mu} \quad (6.36)$$

is more suitable for a comparison between different superdiffusive systems. The density of crystal momenta is expressed in terms of the density of eigenvalues as

$$\rho_\kappa(\kappa) = \mu\kappa^{\mu-1} \rho_E(\kappa^\mu). \quad (6.37)$$

Inserting (6.34) into (6.37), we see that irrespective of the value of μ , this density is constant for all free Lévy stable processes, i.e.

$$\rho_\kappa^0(\kappa) = \frac{1}{\pi}. \quad (6.38)$$

In the following we drop the subscript κ and refer to the density of crystal momentum $\rho(\kappa)$ as the density of states. External random potentials will change the properties of $\rho(\kappa)$. We investigate this quantity as a function of Lévy exponent μ and effective potential strength

$$\varepsilon = \frac{V_0}{2k_B T}. \quad (6.39)$$

Figure 6.4 depicts $\rho(\kappa)$ for strong ($\mu = 1/2$) and intermediate ($\mu = 1$) superdiffusion and ordinary diffusion ($\mu = 2$) in potentials with Heaviside and Gaussian power spectra and two effective potential strengths, $\varepsilon = 0.5$ and $\varepsilon = 1$. As a function of κ , all densities display a pronounced trough (relative to free superdiffusion) on length scales of the order of the correlation length, i.e. $\kappa \approx 1/\xi$. Furthermore,

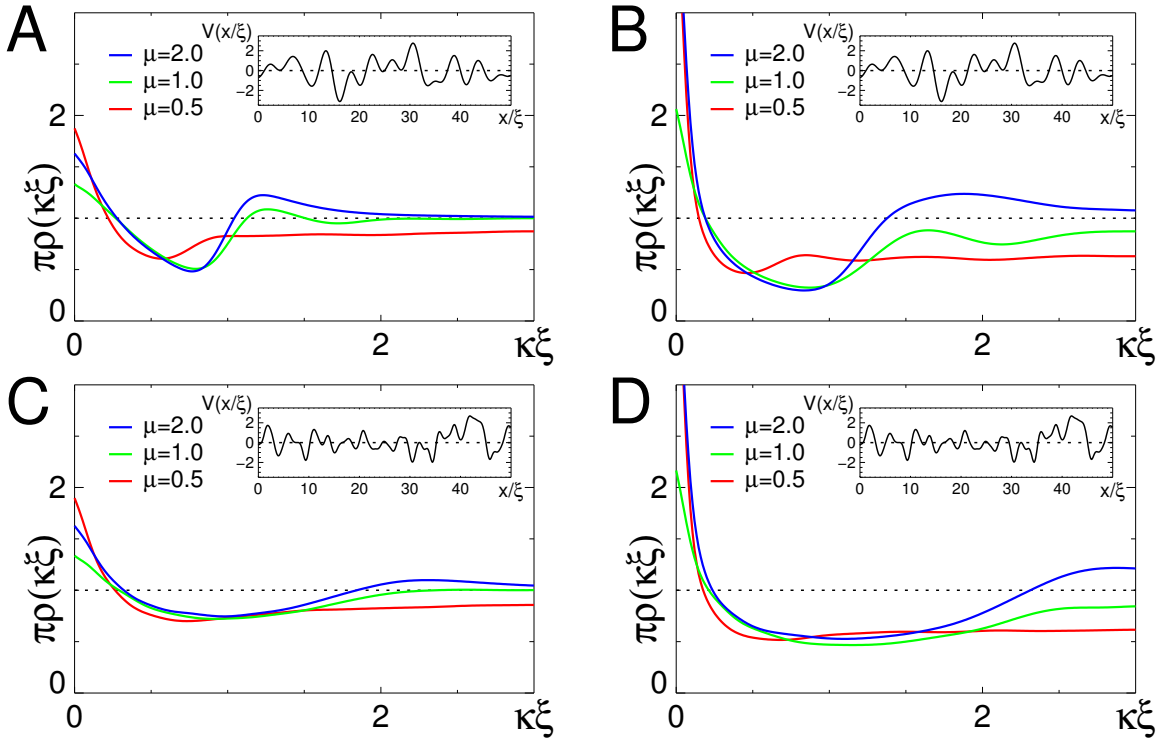


Figure 6.4.: Density of states $\rho(\kappa)$ for processes with exponents $\mu = 1/2, 1$ and 2 . Effective potential strengths are $\varepsilon = 0.5$ (**A** and **C**) and 1.0 (**B** and **D**). A realization of each type of random potentials is shown in the insets. **A** and **B** correspond to potentials with flat power spectrum $S(k)$, **C** and **D** to potentials with Gaussian power spectrum (see table 6.1). The constant density $\rho^0(\kappa) = 1/\pi$ corresponding to vanishing potential is indicated by the dashed line.

$\rho(k)$ increases in the asymptotic regime $\kappa \ll 1/\xi$, because all processes are slowed down on scales larger than the correlation length ξ . The magnitude of this effect is quantified by the density at $\kappa = 0$. For a given effective potential strength ε , the value $\rho(0)$ is the same for all types of random potentials, and the details of the potentials become irrelevant on large scales. Figure 6.5 depicts $\rho(\kappa)$ for all four types of potentials, which serves to illustrate this fact.

Compared to superdiffusion, ordinary diffusion exhibits the most complex shape of $\rho(k)$ and is thus most susceptible to the detailed structure of the potential. The opposite behavior was observed in periodic potentials. While $\rho(k)$ for superdiffusive processes depends only weakly on the potential type (figure 6.5A), the densities of ordinary diffusion processes vary strongly with potential type (figure 6.5B).

Figure 6.6 depicts the density of states for various values of the effective potential strength ε . A superdiffusive process ($\mu = 1$) is compared to ordinary diffusion ($\mu = 2$) in potentials with Heaviside and Gaussian power spectra. The complexity of $\rho(k)$ increases with increasing effective potential strength ε . The magnitude of

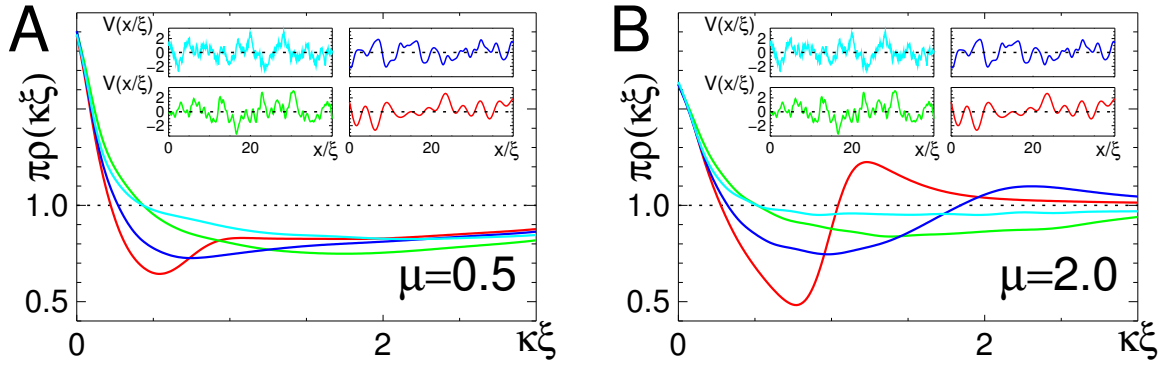


Figure 6.5.: The density of states $\rho(\kappa)$ at an effective potential strength $\varepsilon = 0.5$ in all four types of potentials provided in table 6.1. A superdiffusive process (**A**) is compared to ordinary diffusion (**B**). The dotted lines indicates the density $\rho^0(\kappa) = 1/\pi$ corresponding to vanishing potential strength.

response is greater for ordinary diffusion.

6.4. Dynamics in Weak Potentials

The weak potential (and equivalently high temperature) regime corresponds to effective potential strengths much smaller than unity,

$$\frac{V_0}{2k_B T} = \varepsilon \ll 1, \quad (6.40)$$

and can be treated by perturbation theory. The quantity ε will serve as the perturbation parameter. Introducing a rescaled potential

$$v(x) = \frac{1}{V_0} V(x), \quad (6.41)$$

we may approximate the effective potential U (equation (6.3)) in terms of v by

$$U \approx -\varepsilon \Delta^{\mu/2} v + \frac{1}{2} \varepsilon^2 \left(\Delta^{\mu/2} v^2 - 2v \Delta^{\mu/2} v \right), \quad (6.42)$$

which is correct to second order in ε . First, we consider a process on a finite support of size $2\pi L$. In this case the potentials v and U can be expanded into a Fourier series, whereby the respective Fourier coefficients read

$$\hat{v}_n = \frac{1}{2\pi L} \int_{2\pi L} dx e^{inx/L} v(x) \quad \text{and} \quad (6.43)$$

$$\hat{U}_n = \frac{1}{2\pi L} \int_{2\pi L} dx e^{inx/L} U(x). \quad (6.44)$$

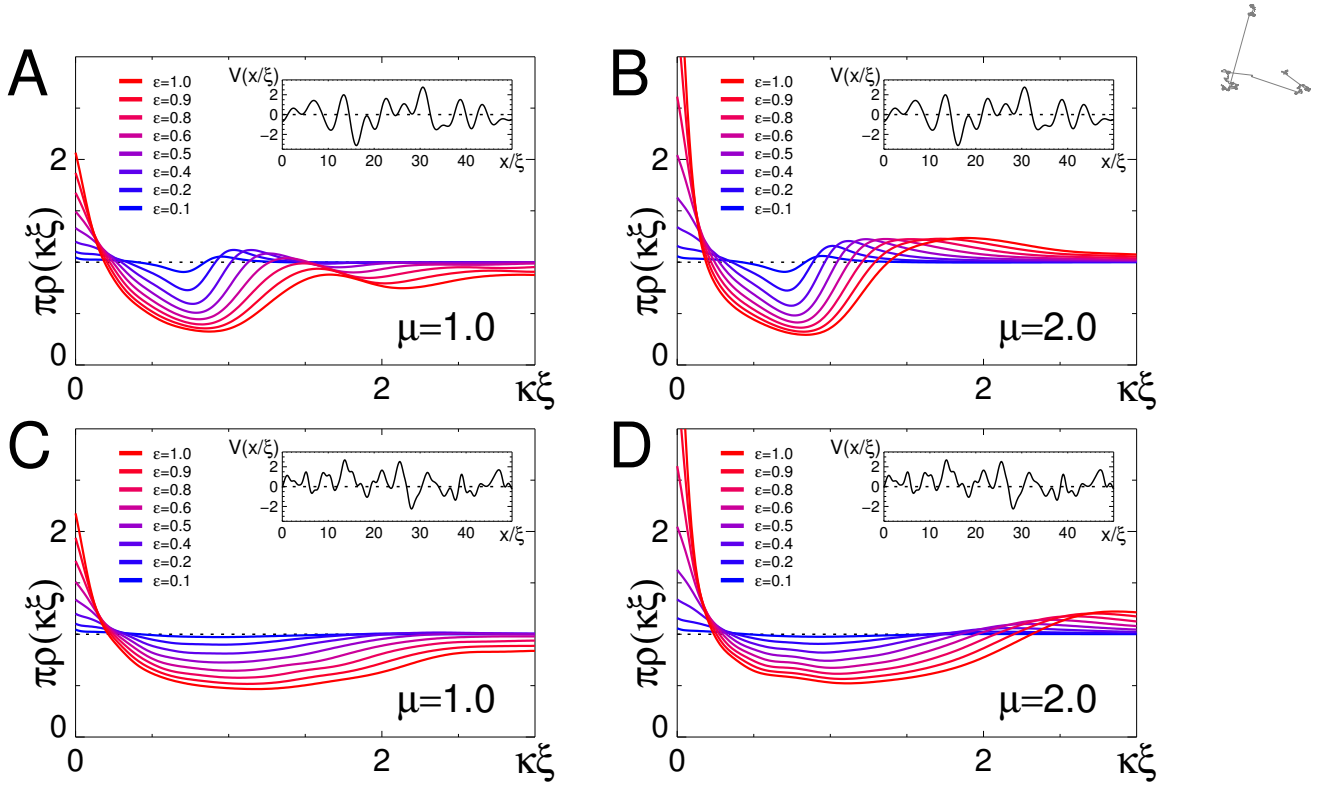


Figure 6.6.: The density of states $\rho(\kappa)$ for a range of effective potential strengths ε , two values of μ and two types of potentials. **A:** $\mu = 1$ and Heaviside $S(k)$, **B:** $\mu = 2$ and Heaviside $S(k)$, **C:** $\mu = 1$ and Gaussian $S(k)$, **D:** $\mu = 2$ and Gaussian $S(k)$. The dotted line represents $\rho^0(\kappa) = 1/\pi$.

By (6.42) they are related according to

$$\hat{U}_n \approx \frac{1}{L^\mu} \varepsilon \left(|n|^\mu \hat{v}_n - \frac{1}{2} \varepsilon \sum_m \hat{v}_{n-m} (|n|^\mu - 2|m|^\mu) \hat{v}_m \right). \quad (6.45)$$

The coefficients \hat{v}_n can be written as

$$\hat{v}_n = \phi_n e^{-\vartheta_n} \quad \text{with } \phi_n > 0 \quad \text{and } \vartheta_n \in [0, 2\pi). \quad (6.46)$$

For a random phase potential, the discrete set of phases ϑ_n constitutes the randomness. The positive components ϕ_n are identical for each realization in the ensemble. The eigenvalues of the Hamiltonian (6.2) for a small effective potential U are approximately given by

$$E_n \approx E_n^0 + \hat{U}_0 + \sum_{m \neq n} \frac{|\hat{U}_{m-n}|^2}{E_n^0 - E_m^0} \quad \text{with } n \in \mathbb{Z}, \quad (6.47)$$

where

$$E_n^0 = |k_n|^\mu \quad \text{with } k_n = n/L, \quad n \in \mathbb{Z}, \quad (6.48)$$



denote the eigenvalues of the unperturbed process. Since the rhs of (6.47) is identical for n and $-n$, it is sufficient to consider positive indices only. Inserting equations (6.45) and (6.46) into (6.47) we find a second order ε correction to E_n^0 , i.e.

$$E_n = k_n^\mu - \varepsilon^2 \left[\sum_{m \neq n} \frac{|k_m - k_n|^{2\mu}}{|k_m|^\mu - |k_n|^\mu} \phi_{n-m}^2 - \sum_m |k_m|^\mu \phi_n^2 \right]. \quad (6.49)$$

This equation announces an interesting albeit subtle implication. The correction term on the right contains only the non-random components ϕ_n of the potential (6.46). Up to second order in the effective potential strength, the randomness of the potential does not contribute and E_n is the same for each realization of v . The quantities ϕ_n are related to the power spectrum by

$$\phi_n^2 = \frac{1}{2\pi L} S(n/L), \quad (6.50)$$

and the eigenvalues E_n can be expressed in terms of S as

$$E_n = k_n^\mu - \frac{\varepsilon^2}{2\pi L} \sum_{m \neq 0, 2n} \frac{|k_m|^{2\mu}}{|k_n + k_m|^\mu - k_n^\mu} S(k_m) - \sum_m |k_m|^\mu S(k_m). \quad (6.51)$$

Note that the indices 0 and $2n$ are excluded from the first sum over m in (6.51). The denominator is zero for these values of m and the limit $L \rightarrow \infty$ must be taken with care, if we wish to remain unshocked by singular integral kernels. We split up the integral into a harmless part and a more sensitive one,

$$\begin{aligned} E(k_n) &= k_n^\mu \\ &+ \frac{\varepsilon^2}{2\pi} \sum_{m>0} \Delta k S(k_n) \left\{ \frac{k_m^{2\mu}}{(k_n + k_m)^\mu - k_n^\mu} - 2k_m^\mu \right\} \\ &+ \frac{\varepsilon^2}{2\pi} \sum_{0 < m \neq 2n} \Delta k S(k_n) \left\{ \frac{k_m^{2\mu}}{|k_n - k_m|^\mu - k_n^\mu} \right\}, \end{aligned} \quad (6.52)$$

where $\Delta k = 1/L$. We may now carry out the limit $\Delta k \rightarrow 0$. The first sum in (6.52) becomes an ordinary Riemann integral, whereas the second one is to be understood as a Cauchy integral due to the singularity. However, the singularity poses no problem as the integral is convergent. The limit yields

$$\begin{aligned} E(k) &= k^\mu \\ &- \frac{\varepsilon^2}{2\pi} \int_0^\infty dq S(q) q^\mu \left\{ \frac{1}{(1 + k/q)^\mu - (k/q)^\mu} + \frac{1}{|1 - k/q|^\mu - (k/q)^\mu} - 2 \right\}. \end{aligned} \quad (6.53)$$



The ε^2 -term represents the weak potential modification of the k^μ -behavior of the unperturbed system. It consists of the total power $S(q)$ of the random phase potential weighted by the strange function in curly brackets which is singular at $q = 2k$. The correlation length ξ of the random phase potential is implicitly contained in the power spectrum $S(q)$. We can express the power spectrum in terms of a rescaled dimensionless power spectrum $s(k)$ as

$$S(q) = 2\pi \xi s(q\xi). \quad (6.54)$$

This is useful, for $s(q)$ does not depend on ξ . The power spectrum $s(k)$ fulfills

$$s(0) = \frac{1}{\pi} \quad \text{and} \quad \int_0^\infty dk s(k) = \frac{1}{2}. \quad (6.55)$$

Inserting (6.54) into (6.53), we can express $E(k)$ as

$$E(k) = k^\mu \left(1 - 8\varepsilon^2 \int_0^\infty dx s(x) g_\mu(k\xi/x) \right), \quad (6.56)$$

where

$$g_\mu(z) = \frac{1}{8z^\mu} \left(\frac{1}{(1+z)^\mu - z^\mu} + \frac{1}{|1-z|^\mu - z^\mu} - 2 \right). \quad (6.57)$$

Equations (6.56) and (6.57) are generalizations of the analogous expressions derived for the asymptotic band for periodic potentials, i.e. equations (5.54) and (5.55) in section 5.5.3. Annoyingly, the eigenvalues $E(k)$ still depend on the correlation length ξ . Defining the dimensionless energy $e(k)$ by

$$E(k) = e(k\xi)/\xi^\mu, \quad (6.58)$$

the correlation length finally drops out as a parameter. We have

$$e(k) = k^\mu \left(1 - 4\varepsilon^2 G_\mu(k) \right), \quad (6.59)$$

with

$$G_\mu(k) = 2 \int_0^\infty dq s(q) g_\mu(k/q). \quad (6.60)$$

The function $G_\mu(k)$ quantifies the effect of the external potential on the spectrum and depends solely on the rescaled power spectrum $s(q)$ weighted by the singular part of the integrand, i.e. $g_\mu(k/q)$.



6.4.1. Asymptotics in Weak Potentials

The asymptotic regime is governed by the behavior of $e(k)$ for $k \ll 1$. The values of $G_\mu(k)$ in this limit are given by

$$\lim_{k \rightarrow 0} G_\mu(k) = \begin{cases} 1 & \mu = 2 \\ 1/4 & \mu < 2, \end{cases} \quad (6.61)$$

because

$$\lim_{z \rightarrow 0} g_\mu(z) = \begin{cases} 1 & \mu = 2 \\ 1/4 & \mu < 2 \end{cases} \quad \text{and} \quad \int_0^\infty dq s(q) = \frac{1}{2}. \quad (6.62)$$

Consequently, neither the statistical properties of the potential ensemble reflected by the power spectrum $s(k)$ nor the choice of Lévy exponents μ have an impact on the dynamics on large scales. The exception is the diffusion limit ($\mu = 2$), for which the modification differs by a factor of 4. This is precisely the same result which we obtained for the asymptotic behavior for weak periodic potentials, see equations (5.54) and (5.55), section 5.5.3.

6.4.2. Transient Dynamics

Equation (6.58) states that the dynamics on a given length scale $x \approx k^{-1}$ deviates from free evolution by a factor proportional to the square of the effective potential ε , weighted by a factor $G_\mu(k)$ which is associated with that length scale. For example, when $G_\mu(k) > 0$ the dispersion speed on length scales $x \approx k^{-1}$ is slowed down, whereas when $G_\mu(k) < 0$ dispersion speed is increased.

Figure 6.7 depicts both integrands in (6.60), the power spectrum $s(q)$ and the singular quantity $g_\mu(k/q)$ as a function of q on a semi-logarithmic scale. The power spectra shown correspond to the random phase potential types shown in figure 6.3, and listed in table 6.1. The function $g_\mu(k/q)$ is shown for a set of Lévy exponents μ . The singularity $q = 2k$ is denoted by the gray dashed line. The value of $G_\mu(k)$ depends strongly on the location of the singularity with respect to the region in which the power spectra display a high degree of variability.

Qualitatively, three regimes can be distinguished. On scales much larger than the correlation length ($k \ll 1$), the left branch of $g_\mu(k/q)$ (i.e. $q < 2k$) does not contribute to the integral, only the limiting behavior of the right branch (i.e. $q > 2k$) does. Since $g_\mu(k/q)$ is positive for $q > 2k$, the dispersion is slowed down on scales much larger than the correlation length. The limits of $g_\mu(k/q)$ given in (6.62) are attained for values of $q \gg k$. Note, however, that the convergence differs for various Lévy exponents μ . Convergence is weak for exponents slightly less than 2 (quasi-diffusive processes) and slightly larger than 0 (extremely superdiffusive

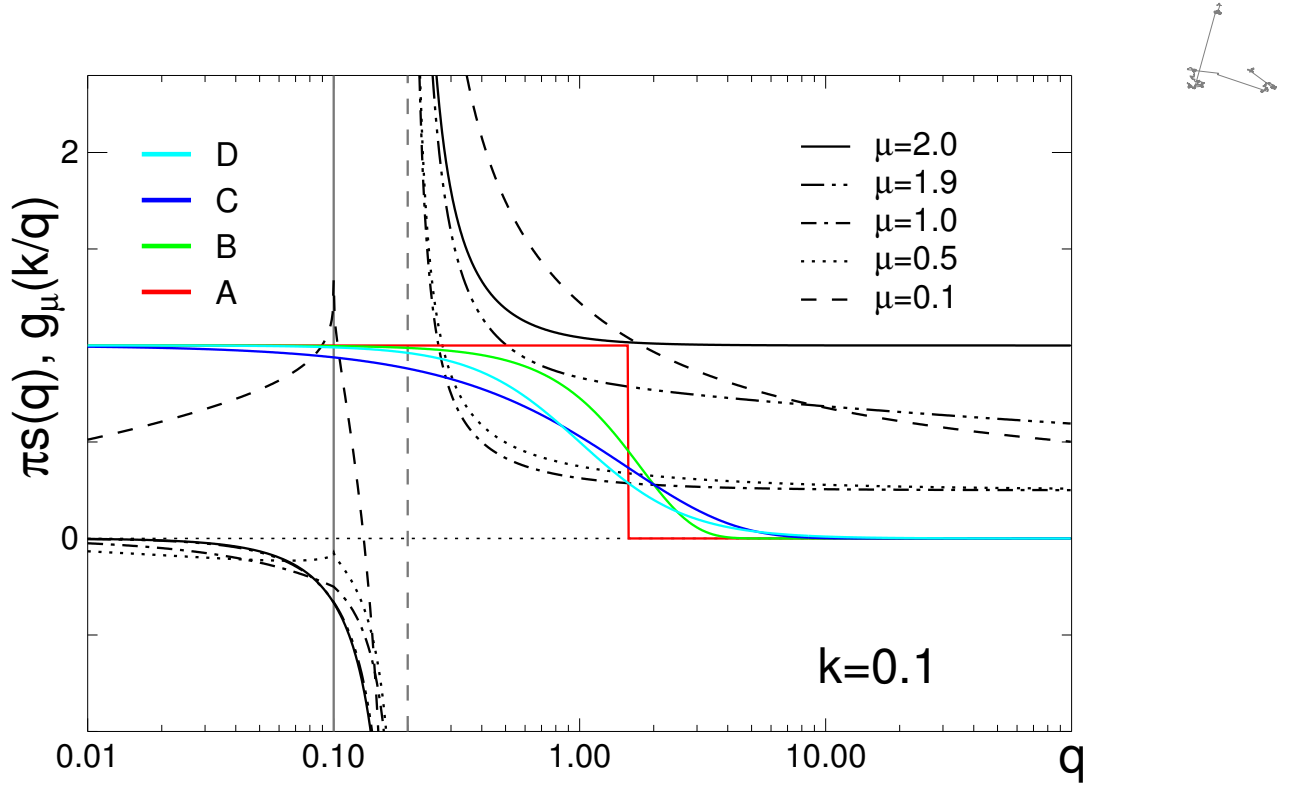


Figure 6.7.: Power spectra $s(q)$ and the weight $g_\mu(k/q)$ as a function of wave number q at $k = 0.1$ corresponding to the relaxation properties on scales an order of magnitude larger than the correlation length ξ . Power spectra for the paradigmatic potentials (table 6.1) are shown in color. For the Lévy exponents listed in the upper right the function $g_\mu(k/q)$ is superimposed. The singularity at $q = 2k$ and the chosen value for k are indicated by the dashed grey and solid gray line, respectively.

processes). Therefore, the range of validity of the limits computed for $G_\mu(k)$ is small for these marginal values of the Lévy exponent.

On scales much smaller than the correlation length ($k \gg 1$), the singularity is located in a q -range in which the power spectra $s(q)$ nearly vanish. Only the product of the left branch of $g_\mu(k/q)$ with $s(q)$ contributes to the integral. The functional form of $g_\mu(k/q)$ on the left of the singularity signals an interesting effect. For Lévy exponents greater than some critical value μ_c , the function $g_\mu(k/q)$ is negative, i.e. relaxation is enhanced on small scales. However, strongly superdiffusive processes (e.g. $\mu = 0.1$) exhibit a positive left branch of $g_\mu(k/q)$. As a result, these processes are slowed down even on small scales. A possible explanation of this phenomenon is a pronounced pinning effect exerted by potential minima which outweighs the enhanced sampling of the vicinity of potential minima. The critical Lévy exponent μ_c can be computed from equation (6.57). With $z = 1$ and $g_\mu(1) = 0$ we may solve

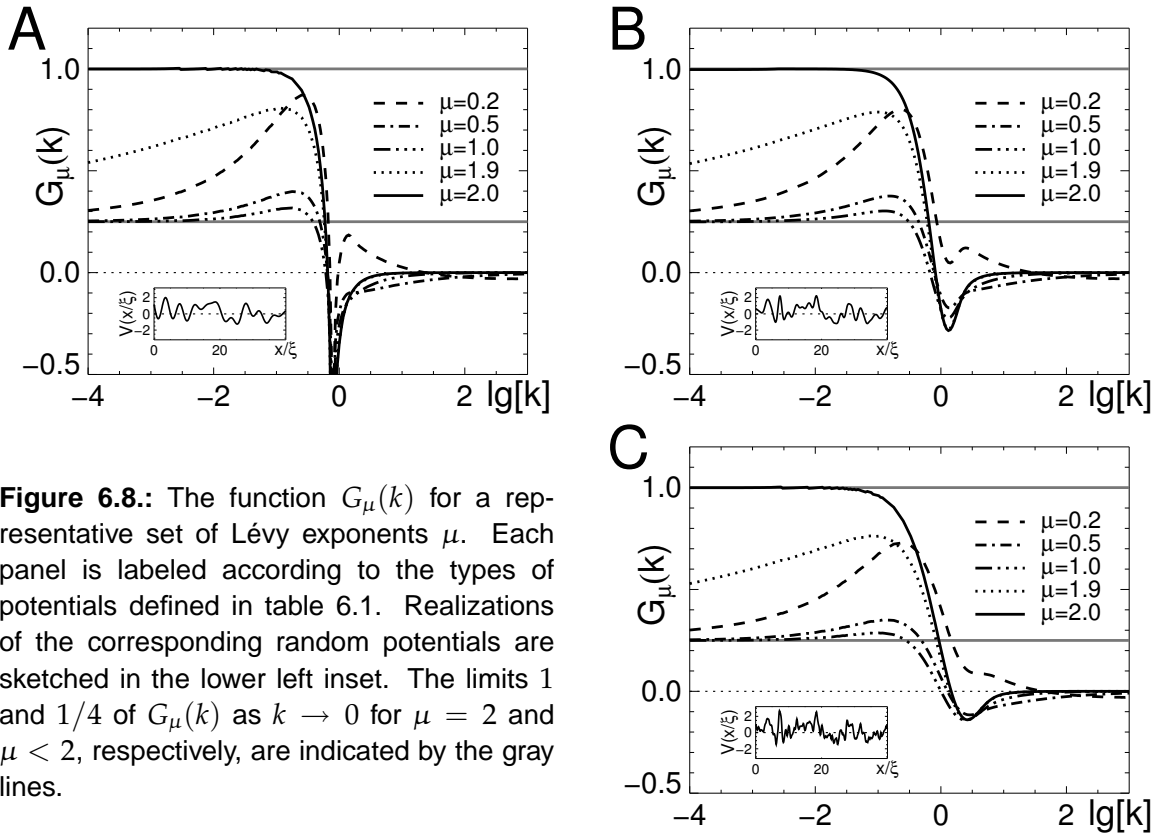


Figure 6.8.: The function $G_\mu(k)$ for a representative set of Lévy exponents μ . Each panel is labeled according to the types of potentials defined in table 6.1. Realizations of the corresponding random potentials are sketched in the lower left inset. The limits 1 and $1/4$ of $G_\mu(k)$ as $k \rightarrow 0$ for $\mu = 2$ and $\mu < 2$, respectively, are indicated by the gray lines.

for μ_c ,

$$\mu_c = 2 - \ln 3 / \ln 2 \approx 0.415. \quad (6.63)$$

For Lévy exponents $\mu > \mu_c$ the function $g_\mu(k/q)$ possesses a strictly negative left branch. When $\mu < \mu_c$ this is no longer the case. On very small scales all processes evolve quasi-free, since as $k/q \rightarrow \infty$ the function $g_\mu(k/q)$ approaches zero.

The greatest variability of $G_\mu(k)$ occurs on length scales of the order of the correlation length ξ , i.e. $k \approx 1$. In this regime the singularity of $g_\mu(k/q)$ coincides with the region in which the power spectra exhibit the highest degree of variation. Generally, the interplay of both integrands in (6.60) leads to negative values of $G_\mu(k)$ in this regime. As a consequence, relaxation is most enhanced on length scales of the order of the correlation length.

Figure 6.8 illustrates the various behaviors in all three regimes. The factor $G_\mu(k)$ is shown on a semi-logarithmic scale for three of the four paradigmatic random potentials. Qualitatively, the curves are similar for each type of potential. As $k \rightarrow 0$ the asymptotic values of equation (6.61) are attained, and a pronounced trough exists for values $k \approx 1$. This is also the region of greatest difference between potentials. As $k \rightarrow \infty$ the function $G_\mu(k)$ vanishes in all cases. Comparing between



potential types, we see that processes evolving in the potential with a Heaviside power spectrum (figure 6.8A) display the highest degree of variation as a function of scale k . Note also that for the marginal processes of quasi-diffusion (μ slightly less than 2) and strong superdiffusion (μ slightly greater than zero), the functions $G_\mu(k)$ do not approach their asymptotic value even on scales orders of magnitude greater than the correlation length. Consequently, these marginal processes are sensitive to the boundaries of the system even if the size of the systems is many orders of magnitude larger than their correlation lengths.

6.5. Asymptotics

The results obtained in the previous section are correct for small effective potential strengths ε . For greater values of the effective potential strengths we expect deviations from the predictions made by perturbation theory. In order to investigate the effect of external random potentials of arbitrary strength, we diagonalize the Hamiltonian in (6.2) numerically for an ensemble of random potentials. Analogous to the procedure introduced in section 5.4, we compute the generalized diffusion coefficient

$$D_\mu(\varepsilon) = \lim_{k \rightarrow 0} \frac{E(k; \varepsilon)}{k^\mu} \quad (6.64)$$

as a function of effective potential strength ε .

The generalized diffusion coefficient $D_\mu(\varepsilon)$ is shown in figure 6.9. Two superdiffusive processes ($\mu = 1/2$ and 1) are compared to ordinary diffusion ($\mu = 2$) in the four potential types shown in the lower left inset. Symbols differentiate between the generalized diffusion coefficients associated with potential types, colors indicate the corresponding Lévy exponent. The results obtained from perturbation theory are superimposed as dashed ($\mu = 2$) and dotted ($\mu < 2$) lines. The figure shows that the asymptotics are independent of the small scale details of the potentials, i.e. for a given process the functions $D_\mu(\varepsilon)$ coincide. Furthermore, $D_\mu(\varepsilon)$ is nearly the same for the superdiffusive processes. The boundary case of ordinary diffusion represents an exception and exhibits a different ε -dependence. In the weak potential limit ($\varepsilon \rightarrow 0$), the curves coincide with the predictions provided by perturbation theory. Thus, the qualitative features predicted by the perturbation theoretic treatment can be extrapolated to the regime of higher effective potential strengths.

6.6. Strange Kinetics on Co-Polymers

In random phase potentials values are distributed symmetrically with respect to the mean $\langle V \rangle = 0$, i.e. a potential of a given value V is just as likely to occur as $-V$,

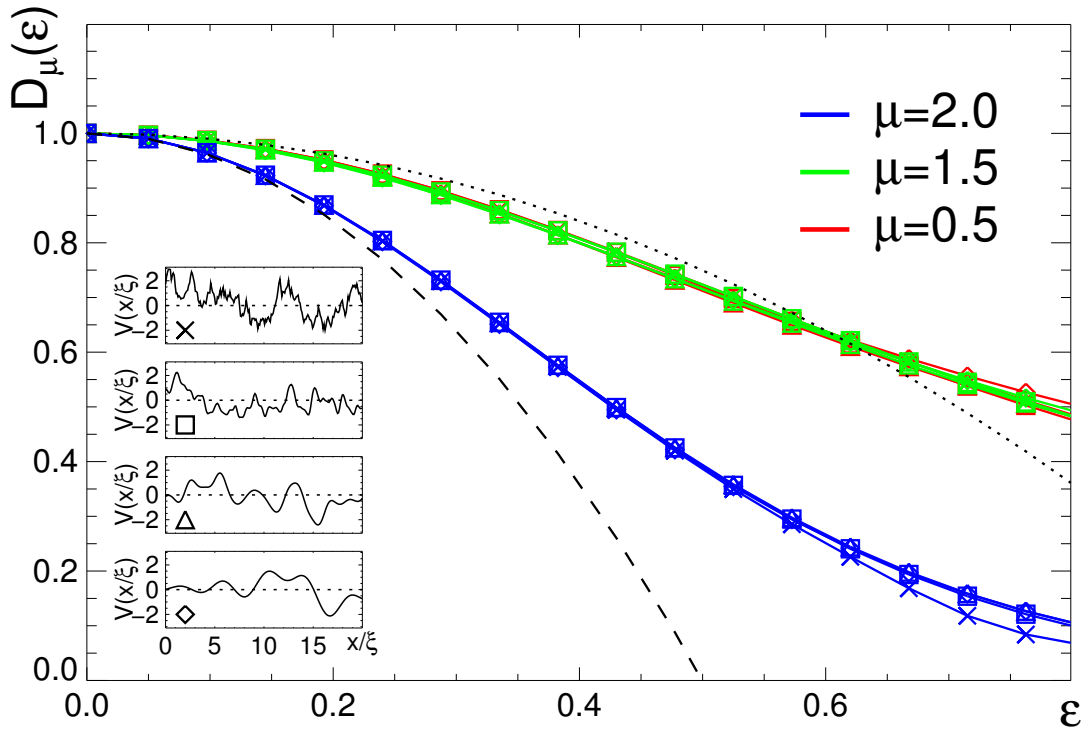


Figure 6.9.: The generalized diffusion coefficient $D_\mu(\varepsilon)$ as a function of effective potential strength ε . Ordinary diffusion ($\mu = 2$) is compared to a moderately ($\mu = 3/2$) and a strongly ($\mu = 1/2$) superdiffusive process in the four types of random phase potentials depicted in the lower left. The data are distinguished by color (Lévy exponent) and symbols (type of potential).

due to the Gaussian density of potential values. Although random phase potentials are a realistic model for a number of inhomogeneous environments, they are not appropriate when the distribution of potential values possess a bias towards higher or lower values with respect to the mean. In the following we investigate to what extent a bias in the external potential impacts on topological superdiffusion. We base our analysis on the simplest possible system of a polymer in which a potential bias is directly connected to the relative concentration of two types of monomers which are randomly arranged along the chain.

Here comes the model. We define the potential along the polymer chain in the following fashion,

$$V(x) = \sum_{n=1}^N v_n f(x - x_n). \quad (6.65)$$

The x_n denote the positions of the monomers in chemical coordinates. The coeffi-

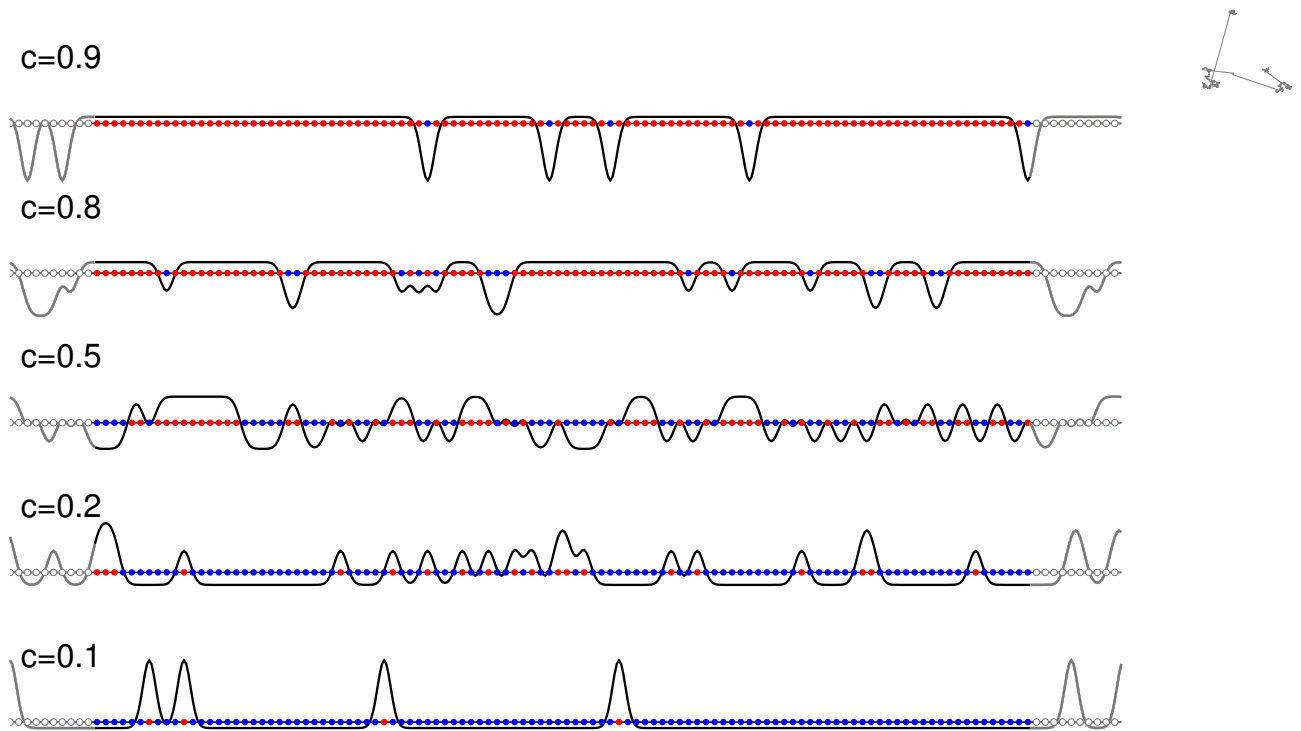


Figure 6.10.: Model copolymers consisting of two types of monomers (red and blue dots) of variable relative abundance c . Red and blue monomers are associated with high (v_+) and low (v_-) potentials.

coefficients v_n are random numbers drawn from the pdf

$$p(v) = (1 - c) \delta(v - v_-) + c \delta(v - v_+). \quad (6.66)$$

Thus, the potential can only acquire the two values v_- and v_+ , representing a chain which consists of two types of monomer only. The parameter c is the relative concentration of monomers with a potential v_- . The term $f(x - x_n)$ in equation (6.65) represents the microscopic spatial range σ of the potential. This factor is assumed to be a Gaussian with a width of σ , i.e.

$$f(x) = \exp\left(-x^2/2\sigma^2\right). \quad (6.67)$$

The situation is depicted in figure 6.10. A number of model co-polymers are shown, each with a different value of c . The red and blue dots represent monomer types of high (v_+) and low (v_-) potential. At low c the chain is nearly homogeneous, consisting of the blue type of monomer interspersed with red monomer impurities leading to potential barriers along the chain. The opposite scenario is described by a high value of c . In this case the low abundance of the blue type of monomer yields

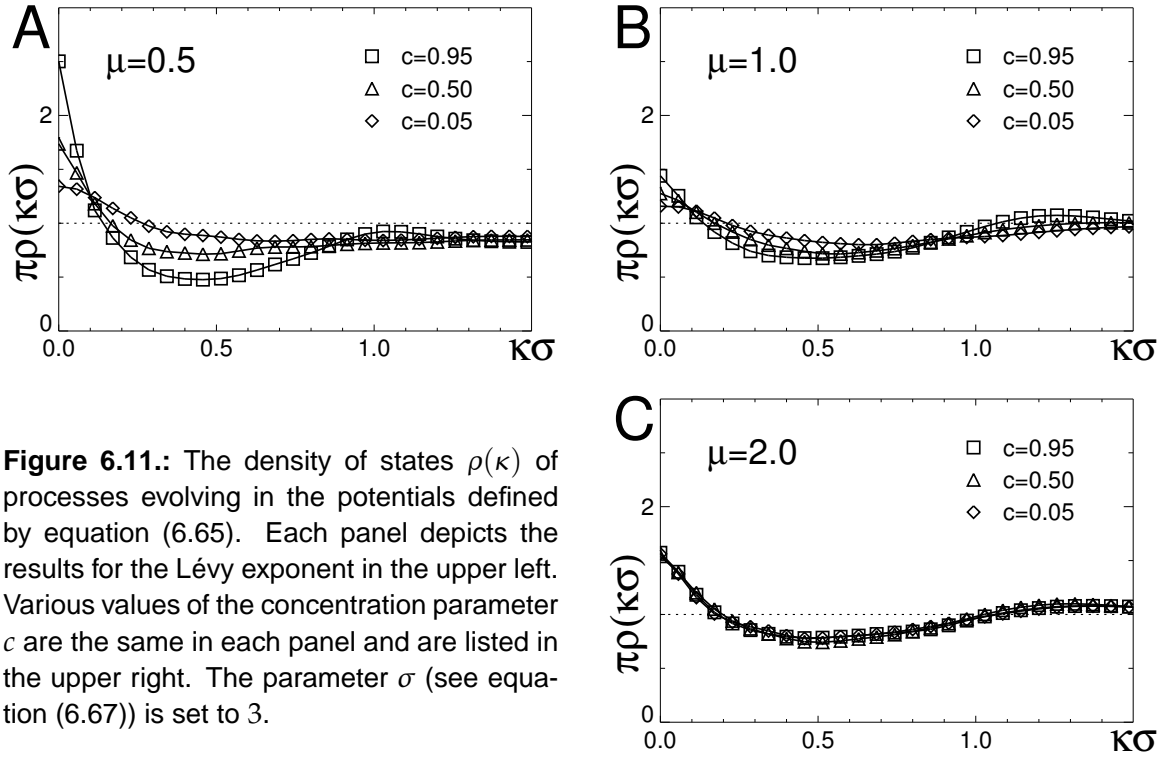


Figure 6.11.: The density of states $\rho(\kappa)$ of processes evolving in the potentials defined by equation (6.65). Each panel depicts the results for the Lévy exponent in the upper left. Various values of the concentration parameter c are the same in each panel and are listed in the upper right. The parameter σ (see equation (6.67)) is set to 3.

sparingly distributed potential troughs along the chain. The average and variance of the potential depend on the relative concentration $c \in [0, 1]$ and the potential difference, i.e.

$$\langle v \rangle = (1 - c) v_- + c v_+ \quad (6.68)$$

$$\langle (v - \langle v \rangle)^2 \rangle = (1 - c) c \delta v^2, \quad (6.69)$$

where

$$\delta v = v_+ - v_-. \quad (6.70)$$

The quantities c and δv are the parameters of the system. In section 6.2 we showed that the relaxation depends only on the effective potential strength $\varepsilon = V_0/2k_B T$, where V_0^2 is the variance of the potential. Since we wish to investigate relaxation dynamics as a function of the relative abundance c , we gauge the potential difference δv such that the variance in equation (6.69) is unity,

$$\delta v = \frac{1}{\sqrt{(1 - c) c}}. \quad (6.71)$$

Proceeding along the same lines as in section 6.3, we compute the density $\rho(\kappa)$ of the crystal momentum κ (equation (6.37)). We choose an intermediate effective



potential strength $\varepsilon = 0.5$ and compare the properties of $\rho(\kappa)$ as a function of the concentration parameter c for a set of Lévy exponents μ . The results are depicted in figure 6.11. Each panel shows the crystal momentum densities $\rho(\kappa)$ computed for the Lévy exponent μ shown in the upper left. In each panel the results obtained for low, intermediate and high values of the concentration c are plotted with different symbols. The functions $\rho(\kappa)$ for the ordinary diffusion process (panel C) are nearly indistinguishable. Therefore, the influence of the potential bias is negligible; relaxation dynamics solely depends on the overall variance of the potential. This result is in accordance with the behavior in periodic potentials with non-zero bias. The ordinary diffusion process is insensitive to the particular shape of the potential.

This behavior is not observed for the superdiffusive processes (panels A and B). The shape of the function $\rho(\kappa)$ depends on the value of the relative concentration c . This dependence is most pronounced for strongly superdiffusive processes. Note also that the highest response to the external potential is observed for high values of c , i.e. potentials with sparsely distributed potential troughs, whereas low values of c (potential peaks) induce the least pronounced response. The highest deviations occur in the asymptotic regime $\kappa\sigma \ll 1$. Since a high density implies a decrease in dispersion speed, Lévy flights are slowed down more efficiently by potential troughs than by potential peaks.

The effect of potential bias on the asymptotics of superdiffusive random motion on the co-polymer is best quantified by the generalized diffusion coefficient $D_\mu(\varepsilon)$ defined in the previous section (6.64). For the same set of values for the relative concentration parameter c , the quantity $D_\mu(\varepsilon)$ as a function of effective potential strength is shown in figure 6.12. The blue curves (ordinary diffusion) are identical for all values of c . They coincide with the predictions made by perturbation theory in the small ε -regime (dashed line). The generalized diffusion coefficients of the superdiffusive process ($\mu = 1$) are different for each value of c . For $c = 0.05$ (sparse potential peaks) the decrease of $D_\mu(\varepsilon)$ with increasing ε is least pronounced, whereas when $c = 0.95$ (sparse potential troughs) the process is slowed down most severely. Only in the weak potential regime ($\varepsilon \ll 1$) do the curves coincide with the perturbation theoretic prediction (dotted line).

For a fixed value of effective potential strength $\varepsilon = 0.5$, the c -dependence of the generalized diffusion coefficient $D_\mu(c)$ is depicted in figure 6.13. Three processes are compared, $\mu = 1/2, 1$ and 2 . The ordinary diffusion remains nearly unaltered when c is changed, contrasting with the generalized diffusion coefficient of the Lévy flights, which are monotonically decreasing with the abundance of potential troughs. Furthermore, the generalized diffusion coefficients for the superdiffusive processes are nearly identical.

We conclude that the dynamics of superdiffusive processes in random potentials does depend on the specific structure of the potentials involved, in particular the potential bias plays an important role for the dispersion speed. In order to make predictions for the relaxation properties of these processes, higher order statistical

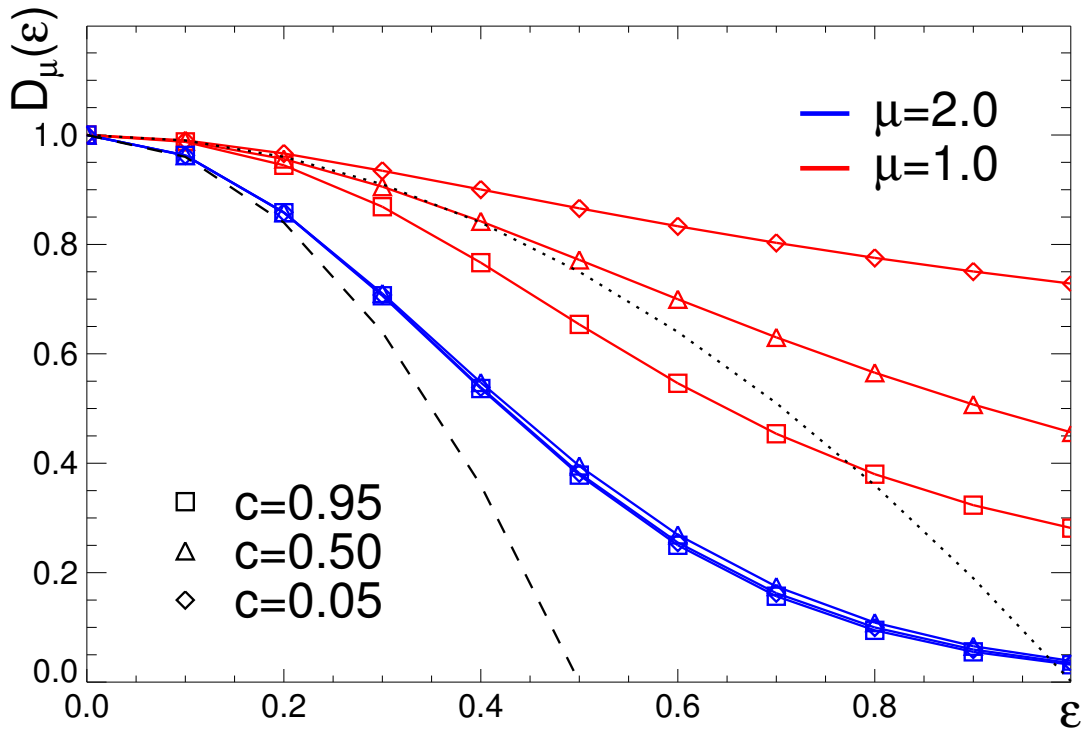
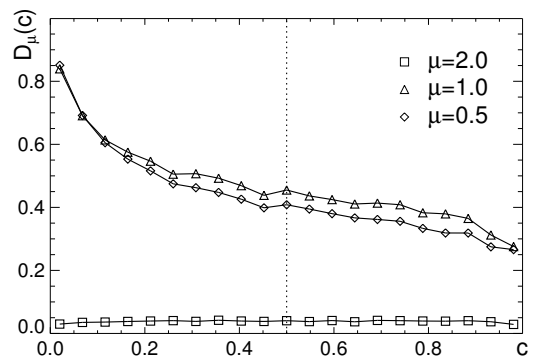


Figure 6.12.: The generalized diffusion coefficient $D_\mu(\varepsilon)$ as a function of effective potential strength. Ordinary diffusion (blue) is compared to a superdiffusive process (red) in potentials with variable concentration parameter c . The choice of values of c represents potentials with sparse potential peaks ($c = 0.05$), sparse potential troughs ($c = 0.95$) and with vanishing parity ($c = 0.5$). The dashed ($\mu = 2$) and dotted ($\mu < 2$) lines indicate the results obtained from perturbation theory.

Figure 6.13.: The generalized diffusion coefficient $D_\mu(c)$ as a function of the relative concentration parameter c . Two superdiffusive processes ($\mu = 1/2$ and 1) are compared to ordinary diffusion ($\mu = 2$). The effective potential strength is $\varepsilon = 0.5$.



properties need to be taken into account. Knowledge of the variance of the potential, which is the only crucial attribute when the effective potential strength is small, is insufficient.



6.7. Discussion

In this chapter we have provided a detailed analysis of the interplay between enhanced diffusion on scale-free topologies and random inhomogeneous environments. The results are relevant to a number of anomalous dispersion phenomena, for instance intracellular translocation processes such as protein dynamics on DNA strands. Our analysis revealed that a number of results obtained for periodic potentials are also valid for random phase potentials, for instance a universal asymptotic behavior for all superdiffusive processes which is different from that of ordinary diffusion. Therefore, these properties can be considered a universal feature of topological superdiffusion in bounded potentials in general. On the other hand, some crucial differences appear when the external potential is irregular. For example, strongly superdiffusive processes with a Lévy exponent less than the critical value $\mu_c \approx 0.415$ are slowed down in their relaxation even on scales smaller than the correlation length ξ , a behavior not observed in ordinary diffusion and moderately superdiffusive processes.

The very simple model for enhanced diffusion on a random co-polymer showed that superdiffusive motion strongly depends on the relative concentration of monomer types, a behavior absent in ordinary diffusion which depends solely on the overall variance of the random potential. Consequently, in order to fully understand the impact of the random potential on superdiffusive motion on folded hetero-polymers, one is required to take the relative abundance of different types of monomers into account.

6. Random Environments





7. The Ecology of Visual Search

And these visions of Joanna
are now all that remain.

(B.D.)

In this chapter we present a phenomenological model for the generation of human saccadic eye movements. We show that human visual scanpaths exemplify the idea of optimal superdiffusive search in inhomogeneous environments. In the model saccadic scanpaths are described as Lévy flights which evolve in an inhomogeneous salience field. Our model successfully accounts for the geometry of visual scanpaths, although neither memory mechanisms nor spatially hierarchical processing is involved. The model is supported by measurements on the saccadic magnitude distribution which follows an inverse power law with an exponent $\mu = 0.73$. We compute the relaxation time as a function of the Lévy exponent μ , and show that the geometry of human visual scanpaths can be interpreted in terms of an optimal search strategy.

7.1. Human Eye Movements

When humans, primates and various other mammals visually investigate their environments, they actively reposition their gaze in a combination of head and eye movements. This is necessary because the visual resolution required for detailed visual processing is sufficiently high in only a small central area of the retina known as the fovea. The diameter of the fovea in humans is approximately 1° of visual angle. In the periphery of the visual field the resolution is poor, because the density of photo receptors and ganglion cells is comparatively small. Qualitatively, peripheral vision is used for detection and foveal visual for recognition. This kind of architecture is a trade-off between the required degree of resolution for detailed visual analysis of objects in focus, and the amount of visual information that can be processed by the visual system. In fact, if the resolution of the retina were as high as in the fovea everywhere, the optic nerve would have a diameter greater than the diameter of the human brain. The transition between foveal vision and peripheral vision has no sharp boundary. Retinal resolution decreases continuously as a function of distance from the fovea.



Figure 7.1.: A topographic map of the visual semi-field onto the superior colliculus of a monkey (left). Small areas near the fovea and large areas in the periphery are mapped onto equal areas in the superior colliculus (after [110]). This topographic map can be modeled by a complex logarithm (right) of the visual semi-field (after [13]).

This is illustrated in figure 7.1, which depicts a topographic map of a polar coordinate grid on one half of the visual field onto the superior colliculus, a brain area which encodes visual information and is involved in the programming of saccadic eye moments [137]. The visual resolution is proportional to the inverse of the area of visual field which is contained in the associated area in the superior colliculus. The map of the visual field onto visual areas in the brain can be modeled by the complex logarithm of the visual field. An image on the visual field is distorted by this map such that regions near the fovea are magnified and peripheral areas shrink (see right panel in figure 7.1).

The loss of visual acuity is compensated by a succession of rapid eye movements known as saccades [138]. Saccades actively reposition the center of gaze in order to foveate regions of interest in the visual environment. The succession of gaze shifts is referred to as a scanpath. The eyes are held relatively stable during fixations which last until the next saccade occurs. The magnitude of saccades ranges from $\approx 0.1^\circ$ of visual angle to 100° with an average of approximately 5° . Gaze shifts of higher magnitude are usually accompanied by head movements. The duration of a typical saccade is approximately 20 – 50 ms which is small compared to the duration of a fixation, which is typically 50 – 500 ms. The scanpaths of two subjects scanning the image of a party scene are depicted in figure 7.2.

Usually the gaze is attracted by regions of high visual salience, and scanpaths connect these regions. A number of factors determine the degree of visual salience, ranging from low level image properties such as high contrast and contour lines

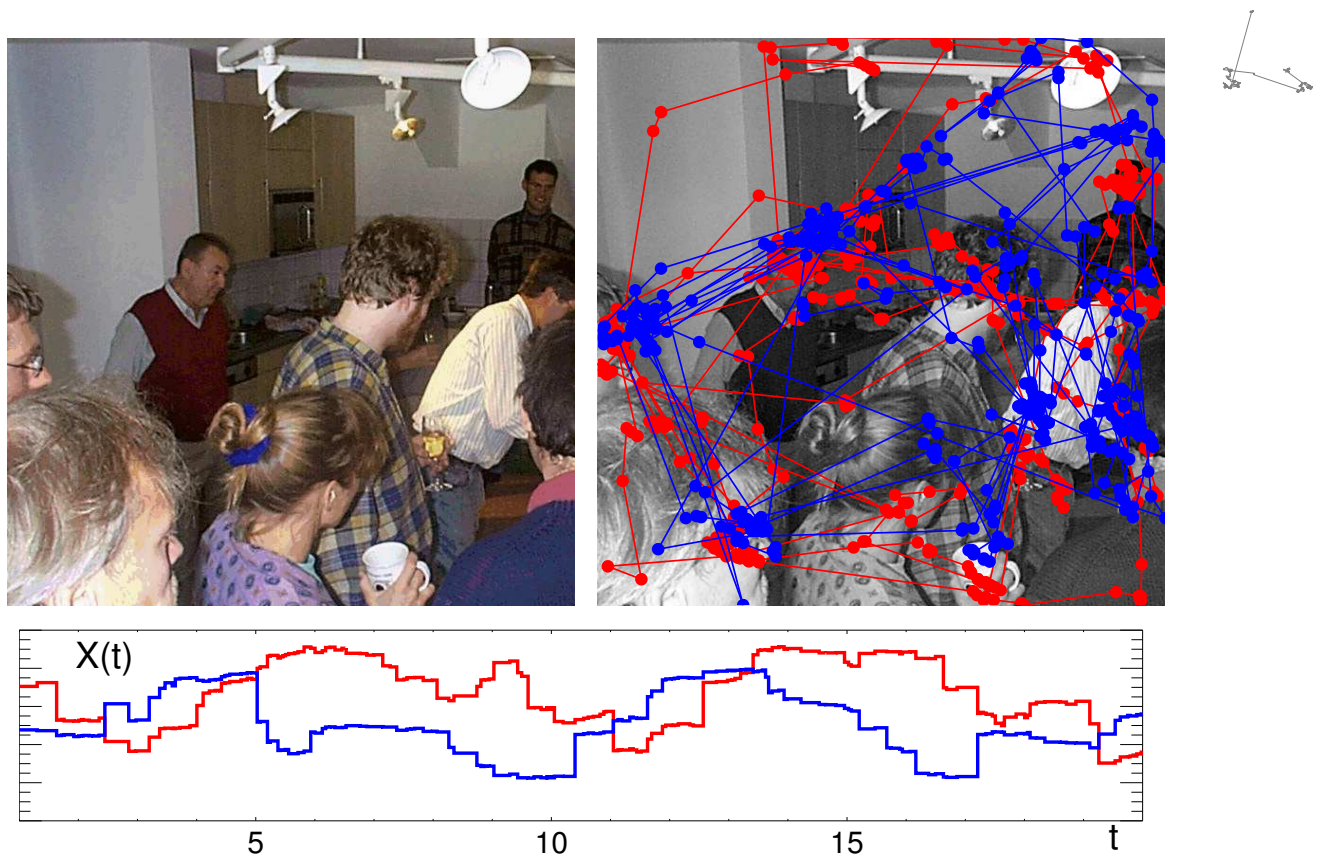


Figure 7.2.: Human saccadic eye movements. **Upper left:** The visual stimulus, an image of various physicists attending a party at the Department of Nonlinear Dynamics, Max-Planck Institut für Strömungsforschung, Göttingen, Germany. **Upper right:** Eye movements of two subjects (also physicists) were recorded for 20 seconds and superimposed on the image in blue and red. Fixations are indicated by dots. **Bottom:** Vertical (blue) and horizontal (red) components of one of the scanpaths as a function of time.

to high level semantic properties of the scene such as faces, food and (generically) opposite sex.

Two more common features of human scanpaths can be observed in figure 7.2. When a subject is confronted with a natural image more than once, the scanpaths observed in each trial are not the same. Although salient regions remain salient in successive trials, the paths connecting them differ between trials and cannot be predicted. They are stochastic. Figure 7.3 shows the beginning of a number of scanpaths on the same image. In each trial the subject was fixating the center of the image.

Furthermore, saccades of small lengths are more frequent than long saccades. A histogram of saccadic magnitudes is depicted on the right in figure 7.3. The frequency decreases monotonically as a function of saccadic magnitude.

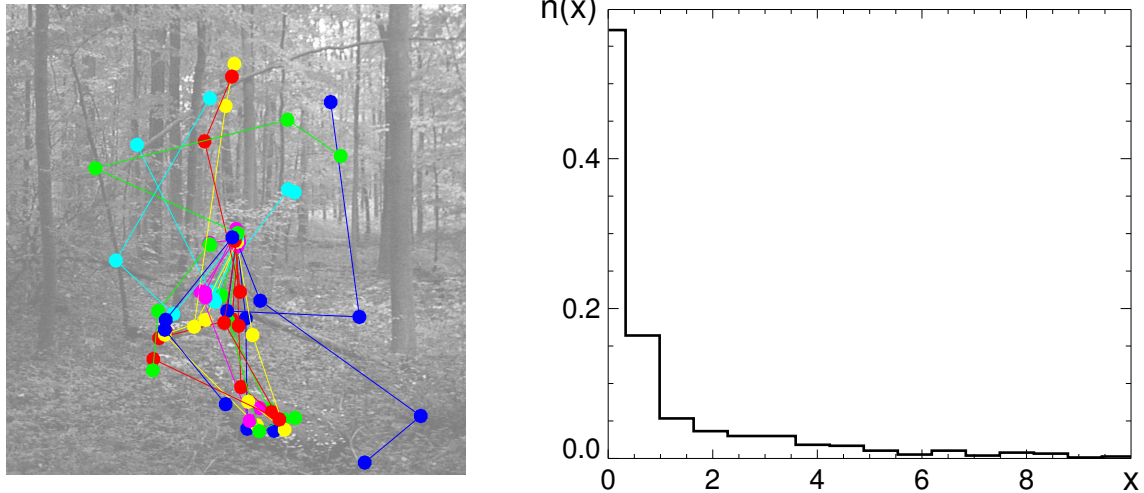


Figure 7.3.: Typical properties of human saccadic eye movements on natural scenes. **Left:** When presented with an identical natural scene individual scanpaths (distinguished by color) differ from trial to trial. They are stochastic. **Right:** Short saccades are more frequent than long ones. The relative frequency $n(x) = N(x)/N_{\text{tot}}$ of saccadic magnitudes x measured in degrees of visual angle decreases monotonically with x . The total number of saccades was $N_{\text{tot}} = 791$ and $N(x)$ denotes the number of saccades in a bin of size $\Delta x = 0.64^\circ$.

7.2. Contemporary Theories

The factors which determine whether a saccade is initiated towards a specific location in the visual field are numerous. The scanpaths depicted in figure 7.2 suggest that visual processing can be split into local processing by small saccadic eye movements, interspersed with long range saccades which govern the global processing of the scene. Two possible complementary theories have been devised to explain these observations. On one hand, memory effects may play a role. If the visual system remembers what areas of the visual field have been processed and decreases the probability of initiating saccades to that region, it will eventually initiate a long saccade to a distant salient region. On the other hand, a hierarchy of spatial scales may explain the structure of human scanpaths. For instance, if two independent neural architectures govern local and global processing and trigger short and long saccades with low and high frequencies respectively, the resultant scanpath would consist of small clusters of local trajectories connected by long range transitions. Either theory is attractive and one or both effects seem to be a necessary ingredient for generating scanpaths with the observed properties. However, a recent study suggested that memory effects play no role in covert visual attention, which is believed to feed peripheral information to brain areas responsible for eye movements [57]. Furthermore, no evidence presently exists for spatially hierarchical

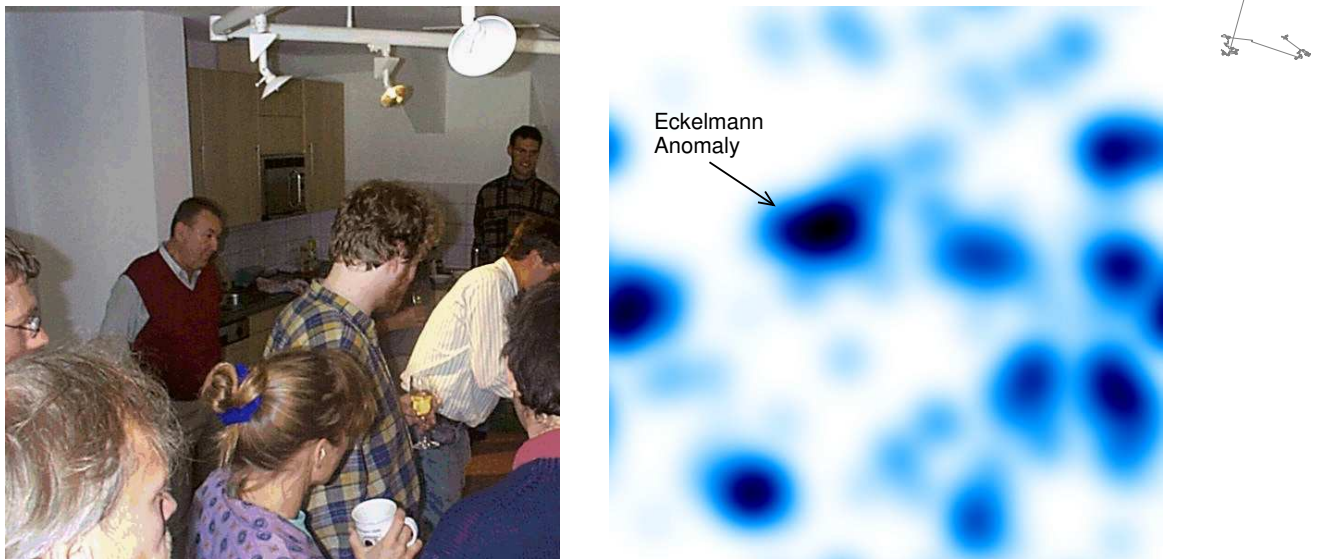


Figure 7.4.: Operational definition of visual saliency by eye movements. The saliency field $s(x)$ can be defined on the image as the approximate density of fixation points. The fixations of the scanpaths depicted in figure 7.2 lead to the saliency field shown on the right. Dark and bright areas indicate regions of high and low visual saliency, respectively. The number of fixations was $N = 1475$.

processing of visual information. Below, we will introduce a model for saccadic human eye movements in which neither memory effects nor a segregation into spatial hierarchies is necessary. Nevertheless the structure of saccadic scanpaths our model predicts is strikingly realistic.

7.3. A Phenomenological Model

We wish to devise a model which takes into account three essential facts about human scanpaths. In the model, scanpaths are realizations of a stochastic process which evolves in a variable saliency landscape. First we assume that saccadic transitions from a position y in the two-dimensional visual field to a position x are stochastic and occur with a transition rate $w(x|y)$. This rate depends on the visual saliency at the target location $s(x)$ and the current position $s(y)$. A number of factors determine the saliency of a visual input, ranging from low level characteristics such as contrast and contours to high level semantic contents. Thus, it is difficult to quantify visual saliency of a natural scene in terms of properties of the stimulus alone. In our model we take an operational approach. We quantify visual saliency $s(x)$ by the probability of finding the gaze of a human subject at the location x . This idea is depicted in figure 7.4.

We assume that the transition rate $y \rightarrow x$ is proportional to the saliency at the



target location $s(\mathbf{x})$ and inversely proportional to the salience at the current position, i.e. $s(\mathbf{y})$. Furthermore, we assume that the probability of initiating a saccade decreases with distance $|\mathbf{x} - \mathbf{y}|$. We assume that memory effects can be neglected. Therefore, the probability density function (pdf) $p(\mathbf{x}, t)$ of finding the gaze at a position \mathbf{x} at time t for an initial condition $p(\mathbf{x}, 0) = \delta(\mathbf{x})$ is governed by the master equation

$$\partial_t p(\mathbf{x}, t) = \int d\mathbf{x} [w(\mathbf{x}|\mathbf{y}) p(\mathbf{y}, t) - w(\mathbf{y}|\mathbf{x}) p(\mathbf{x}, t)] \quad (7.1)$$

with a rate

$$w(\mathbf{x}|\mathbf{y}) = s(\mathbf{x}) f(|\mathbf{x} - \mathbf{y}|) s^{-1}(\mathbf{y}). \quad (7.2)$$

The inverse proportionality of the salience at the current position \mathbf{y} takes into account the assumption that the duration of a fixation at the position \mathbf{y} is proportional to the salience $s(\mathbf{y})$, because the mean waiting time $\tau(\mathbf{y})$ is given by

$$\tau(\mathbf{y}) = \frac{1}{\int d\mathbf{x} w(\mathbf{x}|\mathbf{y})} = \frac{s(\mathbf{y})}{\int d\mathbf{x} s(\mathbf{x}) f(|\mathbf{x} - \mathbf{y}|)}. \quad (7.3)$$

If the salience $s(\mathbf{x})$ fluctuates on scales smaller than the function $f(|\mathbf{x} - \mathbf{y}|)$, the denominator in (7.3) can be approximated by the average salience $\langle s(\mathbf{x}) \rangle$. Without loss of generality we assume that $\langle s(\mathbf{x}) \rangle = 1$, in which case equation (7.3) implies that

$$\tau(\mathbf{y}) \approx s(\mathbf{y}). \quad (7.4)$$

The stationary pdf $p_s(\mathbf{x})$ can be computed from the rate (7.2) because detailed balance is fulfilled. We obtain

$$p_s(\mathbf{x}) \propto s^2(\mathbf{x}). \quad (7.5)$$

Thus, one can obtain the salience by measuring the stationary pdf of saccadic scanpaths. In equilibrium, the pdf of finding the gaze at a location \mathbf{x} increases quadratically with the salience at that location. In our model the frequency of saccadic magnitudes is reflected by the function $f(|\mathbf{x} - \mathbf{y}|)$ which appears in the rate (7.2). Averaging the dynamics over a number of salience fields, we see that this function is proportional to the probability of initiating a saccade of length $x = |\mathbf{x} - \mathbf{y}|$.

Although probabilistic approaches have been applied to various problems in eye movement research such as the perception of ambiguous figures [8], the specific functional form of saccadic magnitude distributions has attracted surprisingly little attention. However, this form has a profound impact on the geometry of scanpaths. The simple model defined above is able to generate model scanpaths which appear strikingly similar to realistic scanpaths if the appropriate choice for the function $f(|\mathbf{x} - \mathbf{y}|)$ is made.



Figure 7.5.: Model scanpath on the saliency field depicted in figure 7.4. **Left:** A scanpath with a magnitude distribution which follows an inverse power law (equation (7.6)) with a Lévy exponent $\mu = 1$. **Center:** A model scanpath with exponentially distributed saccadic magnitudes with a small average magnitude. **Right:** A model scanpath with exponentially distributed saccadic magnitudes with a large average magnitude.

7.4. The Lévy Flight Nature of Saccadic Eye Movements

Saccadic magnitudes x range between $x_0 \approx 0.1^\circ$ and $x_1 \approx 100^\circ$ of visual angle with an average of $x_a \approx 5^\circ$. These numbers show already that the monotonically decreasing function depicted in figure 7.3 cannot be a function with a typical width such as a Gaussian or an exponential. For instance, if the pdf for saccadic magnitudes were an exponential $p(x) = x_a^{-1} \exp(-x/x_a)$, the probability $P(x > 75^\circ)$ of observing a saccadic length greater than 75° would be less than one in a million (i.e. $P(x > 75^\circ) = 3.05 \times 10^{-7}$), a situation clearly not observed in reality. If, on the other hand, the pdf for saccadic magnitudes decreases as an inverse power, then long range saccades are more likely to occur. Thus it is reasonable to investigate the model with a function

$$f(|\mathbf{x} - \mathbf{y}|) \propto \frac{1}{|\mathbf{x} - \mathbf{y}|^{2+\mu}} \quad \text{with } \mu \in (0, 2) \quad \text{for } |\mathbf{x} - \mathbf{y}| > x_0, \quad (7.6)$$

which yields a pdf

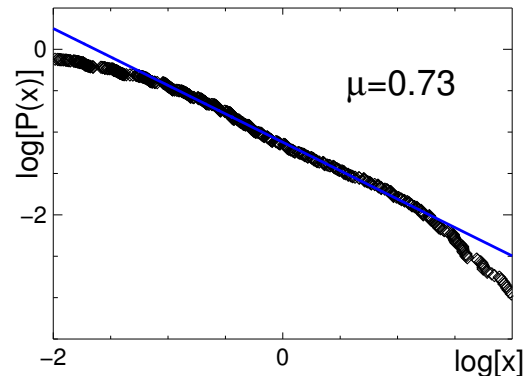
$$\rho(x) \propto \frac{1}{x^{1+\mu}} \quad \text{with } \mu \in (0, 2) \quad \text{for } |\mathbf{x} - \mathbf{y}| > x_0. \quad (7.7)$$

for the saccadic length x .

For exponents μ in the given interval and a constant saliency $s(x) = s_0$, the model scanpaths are Lévy flights with Lévy exponent μ . In figure 7.5 model scanpaths for various choices for the saccadic magnitude statistics are compared. The saliency field is the one depicted in figure 7.4. The red curve shows a Lévy flight scanpath with $\mu = 1$. Without memory effects and without hierarchical processing the scanpath has a geometry very similar to the observed scanpaths shown in figure 7.2.



Figure 7.6.: The probability $P(x)$ of finding a saccadic magnitude larger than a value x as a function of x on a double-logarithmic scale. The blue line is a fit with a slope of $m = -0.73$. The integrated density decreases as $P(x) \sim x^{-0.73}$, which implies that the pdf is given by equation (7.7) with a Lévy exponent of $\mu = 0.73$. The function $P(x)$ was computed from 1791 real saccadic magnitudes. The deviation for large magnitudes is a boundary effect caused by the limited size of the image displayed on the computer screen.



The scanpath evolves in local regions of high salience and jumps from one salient region to a distant region, thereby efficiently scanning the entire salience field. The Lévy flight nature is essential for this geometry, as is easily conceived when a different type of saccadic magnitude pdf is assumed. In the central panel in figure 7.5 model scanpaths possess a pdf for saccadic magnitudes with a small typical scale. As expected, the trajectory never leaves the localized region of high salience (in this case the Eckelmann anomaly mentioned in figure 7.4) and never reaches distant salient regions. The right panel illustrates the situation that emerges when the pdf for saccadic magnitudes has a typical but larger scale. The resultant scanpath jumps erratically between salient regions but spends no time in them for local processing.

The Lévy flight nature of human saccadic eye movements is confirmed by the data depicted in figure 7.6. We collected saccadic magnitudes from scanpaths measured for a number of images and estimated the probability $P(x)$ of initiating a saccade with a magnitude large than x . On a double-logarithmic scale $P(x)$ is well approximated by a line with a slope of -0.73 . This slope implies for the pdf $\rho(x)$ for saccadic magnitudes (equation (7.7)) a Lévy exponent $\mu = 0.73$. Consequently, the data support the Lévy flight theory for human scanpaths.

7.5. Temporal Optimization

What is a possible explanation of this? We will try to answer this question in the light of temporal optimization. A temporal optimization strategy for scanning the visual field is plausible, because under natural conditions speed is a crucial ingredient for survival. A recent experiment supports the assumption of an optimization strategy for visual scanpaths [48]. In this experiment a subject who was not able to move her eyes had to compensate for the deficiency by rapid head movements. The resultant saccadic head movements had a remarkably similar structure to natural

saccadic eye movements of healthy subjects.

Why do we observe an intermediate value of μ in human visual scanpaths? By means of the model introduced above and the concept of topological superdiffusion we can provide an answer to this question. The typical time needed to distribute an ensemble of scanpaths over the entire visual field is given by the relaxation time τ_c of the stochastic evolution operator defined by the rhs of the master equation (7.1) and the rate (7.2). This relaxation time is related to the largest eigenvalue $E_1 < 0$ of the operator, i.e.

$$\tau_c = -\frac{1}{E_1}. \quad (7.8)$$

The spectrum of eigenvalues depends on the statistical properties of the salience $s(\mathbf{x})$ and the Lévy exponent μ . Defining a potential $V(\mathbf{x})$ by

$$V(\mathbf{x}) = -2 \log[s(\mathbf{x})], \quad (7.9)$$

the master equation (7.1) in combination with the rate (7.2) and the pdf for saccadic magnitudes (7.6) is identical to the fractional Fokker-Planck equation (FFPE) for topological superdiffusion,

$$\partial_t p = e^{-V/2} \Delta^{\mu/2} e^{V/2} p - p e^{V/2} \Delta^{\mu/2} e^{-V/2} \quad (7.10)$$

$$= \mathcal{L}_\mu p \quad (7.11)$$

with $\mu \in (0, 2]$ which is valid on scales larger than the minimal saccadic length x_0 . Equation (7.9) states that regions of high visual salience correspond to low potentials $V(\mathbf{x})$ and vice versa. The spectrum of \mathcal{L}_μ can be computed by first mapping the FFPE onto a fractional Schrödinger equation. The transformation is given by (3.58) and (3.59) and yields

$$\partial_t |\psi\rangle = -H |\psi\rangle$$

with a symmetric Hamiltonian

$$H = |\mathbf{P}|^\mu + U(\mathbf{X}) \quad \text{where}$$

$$U(\mathbf{x}) = e^{V(\mathbf{x})/2} \Delta_{\mathbf{x}}^{\mu/2} e^{-V(\mathbf{x})/2},$$

with the same spectrum as \mathcal{L}_μ (apart from a minus sign). Human eye movements can thus be described by fractional quantum mechanics, which is charming.

Figure 7.7 depicts histograms of the relaxation times τ_c for an ensemble of 500 salience fields $s(x)$ and different values of the Lévy exponent μ . Instead of salience fields extracted from experimental data, we chose model salience fields similar to the random phase potentials studied in chapter 6 with a Gaussian power spectrum.



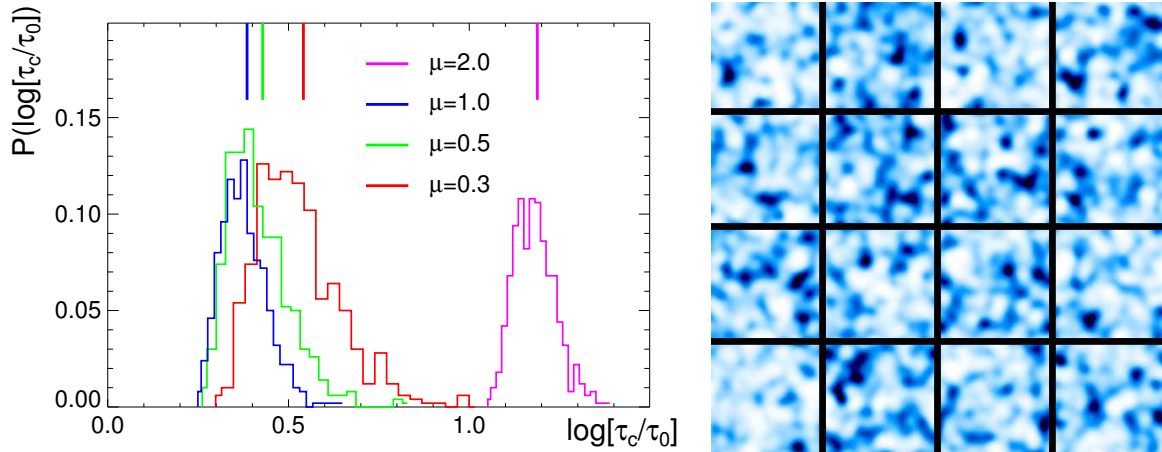


Figure 7.7.: Histograms of relaxation times τ_c for different Lévy exponents μ on a semi-logarithmic scale. The mean of each histogram is indicated by the vertical line segments in the respective color on the upper boundary. τ_0 denotes the relaxation time for a system with uniform salience $s(x) = 1$. Histograms were computed for an ensemble of 500 model salience fields 16 samples of which are shown on the right.

The correlation length of the salience fields was chosen to coincide with the typical spatial scale of salient regions in natural images. The parameter τ_0 in the figure is the relaxation time for a uniform salience field ($s(x) = 1$).

The histograms show that scanpaths with intermediate Lévy exponents ($\mu = 1/2$ and 1) relax most efficiently in the ensemble of salience fields. The average relaxation time $\langle \tau_c \rangle$ is smallest for these scanpaths. The scanpaths with marginal Lévy exponents ($\mu = 0.3$ and 2) are affected more strongly by the salience fields. This confirms the results obtained chapters 5 and 6 for topological superdiffusion in periodic and random phase potentials, respectively. The histograms are shown on a semi-logarithmic scale. Therefore, the standard deviation from the mean strongly depends on the Lévy exponent μ . The standard deviation is smallest for intermediate values of μ and greatest for the marginal values. This implies that these scanpaths are least robust to statistical fluctuations in the salience ensemble.

7.6. Discussion

We showed that a simple phenomenological model for the generation of saccadic eye movements is able to reproduce scanpaths with a geometry very similar to scanpaths observed in experiments. The crucial ingredient in this model is the inverse power law in the frequency of saccadic magnitudes which implies that scanpaths are Lévy flights. The model does not rely on memory effects or hierarchical processing of visual information and supports the idea that neither of these mechanisms play an important role the generation of saccadic eye movements.

In the light of temporal optimization our model predicts an intermediate Lévy exponent μ in the saccadic magnitude distribution. This is confirmed by our data. Furthermore, scanpaths with $\mu \approx 1$ are more robust against statistical fluctuations in the visual environment. We conclude that Lévy flights represent an efficient strategy for visual search.







8. Perspectives

Look out kid.

(Bob Dylan)

We investigated superdiffusive motion in inhomogeneous environments. Based on a plausible underlying Lévy flight model, we devised a novel fractional generalization of the Fokker-Planck equation suitable for systems in which superdiffusion is caused by scale-free topological features of the system. This fractional Fokker-Planck equation combines the anomalous dispersion characterized by the Lévy exponent μ with external inhomogeneities represented by an external potential $V(x)$. The interplay between long range scale-free transitions and the influence of the external potential is modeled such that the requirements of ordinary Gibbs-Boltzmann statistics are met. Consequently, our approach is appropriate for a variety of systems in which the stationary state is solely determined by the external potential and is independent of the topological features of the system.

The fractional generalization of the Fokker-Planck equation unifies a number of models which exhibit similar behaviors despite their differences in detail. Moreover, the approach permits a treatment within the framework of fractional calculus by which a deeper understanding of the dynamics can be gained, and results can be extracted from the model which are not readily available in more complicated microscopic rate models. The equivalence to a fractional Schrödinger equation provides an interpretation in terms of concepts known from quantum mechanics.

Unlike ordinary random walk models, which generically lead to a description in terms of an ordinary Fokker-Planck equation, scale-free non-local transitions lead to different fractional generalizations, depending on the underlying physics. In a detailed comparison of topological superdiffusion to the popular approach of generalized Langevin dynamics and subordinated superdiffusion, we showed that the various generalizations exhibit considerable dynamical differences in the paradigmatic case of the harmonic potential and escape dynamics in the double well scenario.

In a great variety of physical systems potentials are encountered which possess a limited variability and a typical length scale. Examples are resource distributions in the habitats of foraging animals and the potentials defined along inhomogeneous polymers. Generalized Langevin dynamics is asymptotically trivial in bounded potentials, a possible reason why superdiffusive processes in these types of poten-



tials have received no attention in the past.

We investigated topological superdiffusion in periodic potentials and random phase potentials. This study revealed a number of interesting phenomena. The spectral bands and consequently the transient dynamics of superdiffusive processes in periodic potentials, which we obtained by a generalized Bloch theory, exhibit a far more complex structure than the spectrum of ordinary diffusion in the same potentials. The susceptibility to changes in temperature or effective potential strength is much higher for superdiffusive processes. Surprisingly, the asymptotic spreading speed as quantified by the generalized diffusion coefficient is universal for all superdiffusive processes, with the exception of the boundary case of ordinary diffusion. Furthermore, the asymptotics is independent of the functional form of the external potential, as long potential values are distributed symmetrically about the mean. When potential values possess a bias, for example when the potential consists of localized peaks or localized troughs, this has a profound effect on the dispersion speeds of superdiffusive processes unlike those of ordinary diffusion which are only affected by the variance of the potential.

These results cast a new light on enhanced dispersion phenomena observed in translocation of intracellular proteins along polymeric media with complex topologies. On one hand, the generalized diffusion coefficient does not depend on the Lévy exponent μ and thus the topological features of the system. On the other hand, a detailed knowledge of the potential shape of the polymeric medium is required in order to fully understand the dynamics.

Another important aspect is relaxation in finite systems. The universal asymptotic behavior mentioned earlier is valid only in the idealized case of an infinite system. Our analysis of relaxation in finite systems showed that an external inhomogeneity has the least effect on moderately superdiffusive processes characterized by intermediate Lévy exponents, whereas quasi-diffusive processes with a Lévy exponent slightly less than 2, and strongly superdiffusive processes with very small Lévy exponents exhibit a relatively strong response. These results suggest that Lévy flights with the appropriate tail may play a role in search strategies employed in nature.

We addressed the issue in a study of human saccadic eye movements. Within a simple phenomenological model we were able to show that saccadic eye movements can be described as Lévy flights in an inhomogeneous landscape of visual salience. The similarity between model trajectories and real saccadic trajectories is striking, despite the fact that neither memory effects nor spatial hierarchies of processing are involved. We showed that the typical relaxation time for an ensemble of salience fields is smallest for intermediate Lévy exponents, and that the robustness with respect to statistical fluctuations in salience is highest for these processes.

Concerning optimal search strategies, our approach represents a promising candidate for efficient minima search in complex energy landscapes, which may be applied to problems frequently encountered in the statistical mechanics of disordered

and frustrated systems. One cannot generally determine the absolute minimum of the energy in these systems, because the number of possible configurational states increases exponentially with system size and the energy hyper-surface is ragged. A number of random walk strategies have been devised and optimized in the past in order to obtain valuable estimates on the absolute potential minima of such systems. In these strategies, a walker in configurational space randomly picks a new target location. If the energy at the chosen location is smaller than the energy at the current location, the move is accepted. If, on the other hand, the target energy is higher, the move is only accepted with a small probability. This way the walker can overcome local potential barriers. In all of these strategies an annealing procedure, a “cooling” of the system with time, plays a role, effectively decreasing the acceptance rate of higher energies. A strategy based on Lévy flights evolving in a ragged energy landscape is plausible, because large potential barriers can be overcome by long range transitions in configuration space. However, contemporary models for Lévy flights in external potentials violate Gibbs-Boltzmann thermodynamics and the stationary state depends on the Lévy exponent μ . More crucially, temperature is not well defined and the simulated annealing procedures are ambiguous. Due to these drawbacks, Lévy flight algorithms have never been employed in this context. In our approach, however, temperature is well defined, and we conjecture that the concept of topological superdiffusion may serve as a source for new and more efficient search strategies for minima localization in frustrated systems such as spin glasses.



We are convinced that our fractional approach represents a useful framework for the study of random motion on scale-free networks. Contemporary models lack a straightforward way of incorporating external inhomogeneities, yet our results suggest that these inhomogeneities play an important role for the dynamics.

The fractional Fokker-Planck equation for topological superdiffusion is a stochastic evolution equation. In reaction-diffusion equations, spatio-temporal patterns emerge due to the interaction of local nonlinear dynamics with spatial dispersion, generally modeled by a Laplacian. These types of models have been used for a number of ecological systems. A paradigmatic system is local predator prey dynamics combined with diffusive dispersion in a two-dimensional homogeneous habitat. Since the dispersion of a number of animal species cannot be modeled correctly by ordinary diffusion, it seems plausible to generalize common reaction diffusion equations, and include the possibility of enhanced diffusion as well as the inhomogeneity of the environment. The concept of topological superdiffusion introduces a very natural way of taking these properties into account, simply by replacing the ordinary Laplacian in ordinary reaction-diffusion equations by the stochastic operator for topological superdiffusion. We believe that these types of models not only possess a rich palette of behaviors, but may also provide the ground for raising questions concerning optimal survival strategies in competitive ecological networks. We reckon that these models offer new perspectives



on robustness of ecological networks against external perturbations such as habitat fragmentation and pollution, the effects of which are poorly understood in our day.



A. Fractional Calculus

In 1695, only shortly after Leibniz and Newton had developed standard calculus, Leibniz wrote in a letter to l'Hospital: "Thus it follows that $d^{1/2}x$ will be equal to $x \sqrt{dx} : x$, an apparent paradox, from which one day useful consequences will be drawn." Nearly 300 years had to pass until these useful consequences were discovered by physicists who were trying to find a suitable framework for the description of anomalous diffusion processes [88] and other fields of physics [55]. The concept of differentiation to fractional order was employed somewhat earlier by mathematicians, especially complex analysts, because, as is indicated below fractional integrals and differentials behave elegantly under common integral transforms, see e.g. [94].

A.1. Fractional Integration

Incidentally, the most natural way to introduce fractional differentiation is based on the generalization of the n -fold iterated integral of a function $f(x)$ which can be expressed as

$${}_a I_x^n f(x) = \frac{1}{(n-1)!} \int_a^x dy f(y) (x-y)^{n-1}. \quad (\text{A.1})$$

Clearly, if the expression on the right hand side of (A.1) is differentiated n times we recover $f(x)$, i.e.

$$\frac{d^n}{dx^n} {}_a I_x^n f(x) = f(x). \quad (\text{A.2})$$

The prefactor $1/(n-1)!$ in the definition (A.1) can be replaced by $1/\Gamma(n)$. Substituting any positive real number $\alpha > 0$ for the integer n , one obtains a straightforward generalization of n -fold integration to fractional order,

$${}_a I_x^\alpha f(x) \equiv \frac{1}{\Gamma(\alpha)} \int_a^x dy f(y) (x-y)^{\alpha-1} \quad \text{and} \quad (\text{A.3})$$

$${}_x I_a^\alpha f(x) \equiv \frac{1}{\Gamma(\alpha)} \int_x^a dy f(y) (y-x)^{\alpha-1}, \quad (\text{A.4})$$



where we distinguish between the right- and left-handed fractional integrals ${}_a I_x^\alpha$ and ${}_x I_a^\alpha$, respectively. These fractional integral operators are defined for suitable functions $f(x)$. In physical applications one frequently encounters fractional integrals with specific boundary values, for example the Riesz-Weyl fractional integral operators ${}_{-\infty} I_x^\alpha$ and ${}_x I_\infty^\alpha$ on one hand and the Riemann-Liouville operator ${}_0 I_x^\alpha$ on the other.

The generalization of n -fold integration to fractional order α is far more than just a well defined mathematical peculiarity. It can be employed as a useful tool when integral transforms aid the solution of a mathematical problem. Numerous properties of n -fold integration are conserved by their fractional generalization, such as their behavior under composition and differentiation, for example

$${}_a I_x^\alpha {}_a I_x^\beta = {}_a I_x^{\alpha+\beta} \quad \text{and} \quad (\text{A.5})$$

$$\frac{d^n}{dx^n} {}_a I_x^{n+\alpha} = {}_a I_x^\alpha. \quad (\text{A.6})$$

A.2. Fractional Differentiation

A fractional differential operator ${}_a D_x^\mu$ of order μ which is frequently used in the theory of anomalous diffusion is given by the n^{th} ordinary derivative of the fractional integral of order $0 < n - \mu \leq 1$, where $n = [\mu] + 1$, and $[\mu]$ denotes the integer part of μ , in other words

$${}_a D_x^\mu f(x) = \frac{d^n}{dx^n} {}_a I_x^{n-\mu} f(x) \quad \text{and} \quad (\text{A.7})$$

$${}_x D_a^\mu f(x) = \frac{d^n}{dx^n} {}_x I_a^{n-\mu} f(x). \quad (\text{A.8})$$

Note that the distinction between left- and right-handed fractional integration is passed on to fractional differentiation, fractional derivatives are not symmetric with respect to interchanging their subscripts. The definitions (A.7) and (A.8) imply that

$${}_a D_x^m = \frac{d^m}{dx^m} = (-1)^m {}_x D_a^m \quad \text{with} \quad m = 0, 1, 2, \dots \quad (\text{A.9})$$

Hence, fractional differentiation for integer m is proportional to ordinary differentiation¹. By sequential partial integration equation (A.7) can be written as

$${}_a D_x^\mu f(x) = \sum_{k=0}^{n-1} \frac{f^{(k)}(a)}{\Gamma(1+k-\mu)} (x-a)^{k-\mu} + {}_a I_x^{n-\mu} \frac{d^n}{dx^n} f(x). \quad (\text{A.10})$$

¹In order to recover symmetry for integer values of the exponent m one frequently encounters an alternative definition of the left-handed fractional derivative, namely ${}_x D_a^\mu \equiv (-1)^n \frac{d^n}{dx^n} {}_x I_a^{n-\mu}$ which includes the prefactor $(-1)^n$ in the definition.

Therefore, the operations of fractional differentiation and integration generally do not commute.



A.2.1. Examples

An interesting property of fractional differentiation can be read off equation (A.10) directly, namely that the fractional derivative of a constant does not vanish, for example the “square root” derivative of 1 is

$${}_0D_x^{1/2} 1 = \frac{1}{\sqrt{\pi}} x^{-1/2}. \quad (\text{A.11})$$

More generally, we have

$${}_0D_x^\mu x^b = \frac{\Gamma(b+1)}{\Gamma(b-\mu+1)} x^{b-\mu}, \quad (\text{A.12})$$

the fractional derivative of a pure polynomial is a pure polynomial. The fractional derivative of an exponential function e^{-px} is given by

$${}_xD_\infty^\mu e^{-px} = \frac{1}{p^\mu} e^{-px}, \quad (\text{A.13})$$

aside from the pre-factor, fractional differentiation has no effect on the exponential. The examples given above coincide with the well known results of ordinary differentiation when μ is an integer.

A.3. The Fractional Laplacian $\Delta^{\mu/2}$

As noted earlier one distinguishes between left and right handed fractional derivatives. This distinction is necessary and not surprising because fractional differentiation is intrinsically nonlocal as opposed to ordinary differentiation. However, countless physical models are symmetric with respect to coordinate reversal. The regular Laplacian Δ appearing in a diffusion equation is left unaltered by the coordinate reversal. What is the fractional generalization of Δ ? Consider the set of functions which possess bounded derivatives at infinity, i.e. $\lim_{a \rightarrow \pm\infty} f^{(k)}(a) < \infty$. Letting $a \rightarrow \pm\infty$ equations (A.7) and (A.8) yield

$${}_{-\infty}D_x^\mu f(x) = \frac{1}{\Gamma(n-\mu)} \int_{-\infty}^x dy \frac{f^{(n)}(y)}{(x-y)^{\mu+1-n}} \quad \text{and} \quad (\text{A.14})$$

$${}_xD_\infty^\mu f(x) = \frac{1}{\Gamma(n-\mu)} \int_x^\infty dy \frac{f^{(n)}(y)}{(y-x)^{\mu+1-n}}. \quad (\text{A.15})$$



In the derivation of the fractional Laplacian we restrict ourselves to fractional exponents μ in the following interval

$$\mu \in (0, 2]. \quad (\text{A.16})$$

The fractional Laplace operator $\Delta_x^{\mu/2}$ is defined by

$$\Delta_x^{\mu/2} \equiv -\frac{1}{2 \cos(\pi\mu/2)} (-_{-\infty}D_x^\mu + {}_xD_\infty^\mu) \quad \text{with } 0 < \mu \leq 2. \quad (\text{A.17})$$

The prefactor in (A.17) ensures that the operator has a simple representation in Fourier space and that it coincides with the ordinary Laplacian when $\mu \rightarrow 2$. In order to derive an integral representation of $\Delta^{\mu/2}$ it is instructive to treat the cases $0 < \mu < 1$ and $1 < \mu < 2$ separately.

A.3.1. $\Delta^{\mu/2}$ on the Interval $0 < \mu < 1$

Partial integration of equations (A.14) and (A.15) with $n = [\mu] + 1 = 1$ yields

$$-_{-\infty}D_x^\mu f(x) = \frac{1}{\Gamma(-\mu)} \int_{-\infty}^x dy \frac{[f(y) - f(x)]}{(x-y)^{\mu+1}}, \quad (\text{A.18})$$

and

$${}_xD_\infty^\mu f(x) = -\frac{1}{\Gamma(-\mu)} \int_x^\infty dy \frac{[f(y) - f(x)]}{(y-x)^{\mu+1}}. \quad (\text{A.19})$$

Inserting (A.18) and (A.19) into the definition (A.17), taking into account that

$$-1/2\Gamma(-\mu) \cos(\pi\mu/2) = \Gamma(1 + \mu) \sin(\pi\mu/2)/\pi \quad (\text{A.20})$$

we obtain

$$\Delta_x^{\mu/2} f(x) = \frac{\Gamma(1 + \mu) \sin(\pi\mu/2)}{\pi} \int_0^\infty dy \frac{f(x+y) + f(x-y) - 2f(x)}{y^{1+\mu}} \quad (\text{A.21})$$

$$= \frac{\Gamma(1 + \mu) \sin(\pi\mu/2)}{\pi} \int_{-\infty}^\infty dy \frac{f(y) - f(x)}{|x-y|^{1+\mu}}. \quad (\text{A.22})$$

A.3.2. $\Delta^{\mu/2}$ on the Interval $1 < \mu < 2$

We proceed analogously to the previous case. With $n = 2$ two partial integrations of equations (A.14) and (A.15) give

$$-_{-\infty}D_x^\mu f(x) = \frac{1}{\Gamma(1-\mu)} \int_{-\infty}^x dy \frac{\mu(f(x) - f(y)) - f'(x)(x-y)}{(x-y)^{1+\mu}}, \quad (\text{A.23})$$

and

$${}_x D_{\infty}^{\mu} f(x) = -\frac{1}{\Gamma(1-\mu)} \int_x^{\infty} dy \frac{\mu(f(x) - f(y)) + f'(x)(y-x)}{(y-x)^{1+\mu}}. \quad (\text{A.24})$$

Luckily, when the expressions on the right are inserted into (A.17) the terms containing $f'(x)$ in the integrand cancel and we end up with an integral representation identical to (A.21) and (A.22).

A.3.3. The Boundary Cases $\mu = 1$ and $\mu = 2$

The boundary cases for the exponent μ require some care. Although the definition (A.17) does not give a useful result when $\mu \in \{1, 2\}$ is inserted, the limits $\mu \rightarrow 1$ and $\mu \rightarrow 2$ can be interpreted consistently. Since $\lim_{\mu \rightarrow 1} \Gamma(1+\mu) \sin(\pi\mu/2) = 1$ the operator $\Delta_x^{1/2}$ is well defined, i.e.

$$\Delta_x^{1/2} f(x) = \frac{1}{\pi} \int_{-\infty}^{\infty} dy \frac{[f(y) - f(x)]}{(x-y)^2}. \quad (\text{A.25})$$

Clearly, $\Delta^{1/2} \neq \nabla = d/dx$, since the ‘‘square-root’’ of the Laplacian is symmetric, whereas the first derivative is not². The limit $\mu \rightarrow 2$ is more involved, however one can show that in this limit the fractional Laplacian reduces to the ordinary second derivative [112].

In summary, for $\mu \in (0, 2]$ the integral representation of the fractional Laplacian $\Delta^{\mu/2}$ is given by

$$\Delta_x^{\mu/2} f(x) = \frac{\Gamma(1+\mu) \sin(\pi\mu/2)}{\pi} \int_{-\infty}^{\infty} dy \frac{[f(y) - f(x)]}{|x-y|^{1+\mu}}. \quad (\text{A.26})$$

The key characteristics of fractional differential operators are apparent in equation (A.26): They are non-local regularized singular integral operators. Whilst each integral on the rhs of (A.26) diverges by itself, their difference converges and can be interpreted consistently. However, care needs to be taken, when one applies common operations such as partial integration.

A.3.4. Simplicity in k -Space

The great technical benefit of fractional calculus is strikingly apparent when the problems at hand are reformulated in Fourier space. The Fourier representation

²In the literature the symbol ∇^{μ} is frequently used instead of $\Delta^{\mu/2}$ which can lead to some confusion if $\mu = 1$.



of $\Delta_x^{\mu/2}$ has a particularly simple form. If we define the Fourier transform of a function $f(x)$ by

$$\mathcal{F}[f](k) \equiv \tilde{f}(k) = \int dx e^{ikx} f(x), \quad (\text{A.27})$$

the transformed equations (A.14), (A.15) and (A.26) read

$$\mathcal{F}[-\infty D^\mu f](k) = (-ik)^\mu \tilde{f}(k), \quad (\text{A.28})$$

$$\mathcal{F}[D_\infty^\mu f](k) = (ik)^\mu \tilde{f}(k) \quad \text{and} \quad (\text{A.29})$$

$$\mathcal{F}[\Delta^{\mu/2} f](k) = -|k|^\mu \tilde{f}(k). \quad (\text{A.30})$$

Thus, in Fourier space fractional differentiation of order μ is equivalent to a multiplication by $|k|^\mu$. Because of this, the investigation of equations containing fractional differential operators is usually much easier when expressed in Fourier space.

The simplicity of equations (A.28), (A.29) and (A.30) is often a reason to chose the latter as definitions of fractional derivatives. On the other hand, the corresponding integral representations (A.14), (A.15) and (A.26) offer a more direct picture of the characteristic properties of the corresponding operator. For example, the propagator of the Cauchy process obeys

$$\partial_t \tilde{p}(k, t) = -|k| \tilde{p}(k, t) \quad (\text{A.31})$$

in Fourier space, a simple equation indeed. An inverse Fourier transform yields

$$\partial_t p(x, t) = (\Delta^{\mu/2} p)(x, t) \quad (\text{A.32})$$

$$= \int dy [w(x|y)p(y, t) - w(y|x)p(x, t)], \quad (\text{A.33})$$

where

$$w(x|y) = \frac{\pi^{-1}}{(x-y)^2}. \quad (\text{A.34})$$

In contrast to the Fourier representation the position representation shows that that the fractional operator $\Delta^{\mu/2}$ is non-local, involves singularities and appearing in the example given above describes a jump process with divergent rates, all facts not readily available in equation (A.31).

A.3.5. Examples

As opposed to the asymmetric fractional derivative of a constant which is non-vanishing (see (A.11)) the fractional Laplacian of a constant is zero, i.e.

$$\Delta^{\mu/2} 1 = 0. \quad (\text{A.35})$$

Another important example is the fractional Laplacian of a Gaussian (see for instance sections 4.4.3 and 4.4) which turns out to be

$$\Delta^{\mu/2} \exp\left[-\frac{x^2}{2}\right] = \sqrt{\frac{2}{\pi}} \int_0^{\infty} dk \cos(kx) k^{\mu} e^{-k^2/2} \quad (\text{A.36})$$

$$= \frac{2^{\mu/2}}{\sqrt{\pi}} {}_1F_1\left(\frac{1+\mu}{2}, \frac{1}{2}; -\frac{x^2}{2}\right), \quad (\text{A.37})$$

where ${}_1F_1(\alpha, \gamma; x)$ is a confluent hypergeometric function [50, pp. 1013].

The paradigmatic case of the fractional Laplacian in physics is the evolution equation for the propagator of the symmetric Lévy stable process of index μ , i.e.

$$\partial_t \tilde{p}(k, t) = -|k|^{\mu} \tilde{p}(k, t), \quad (\text{A.38})$$

which is solved by

$$\tilde{p}(k, t) = \exp(-|k|^{\mu} t). \quad (\text{A.39})$$

Employing the position representation of the fractional Laplacian, it is obvious that a process with a propagator of this type is a jump process governed by a master equation (A.33) with a rate

$$w(x|y) = \frac{\Gamma(1+\mu) \sin(\pi\mu/2)}{\pi} \frac{1}{(x-y)^{1+\mu}}. \quad (\text{A.40})$$

A.3.6. Higher Dimensions

To complete the picture, let us briefly mention that the form (A.30) of the fractional Laplacian can be generalized to arbitrary dimensions n . If we let $f(\mathbf{x})$ be a function on \mathbb{R}^n and denote by $\tilde{f}(\mathbf{k})$ the corresponding Fourier transform, then $\Delta^{\mu/2}$ defined by the n -dimensional variant of equation (A.30), i.e.

$$\mathcal{F}[\Delta^{\mu/2} f](\mathbf{k}) \equiv -|\mathbf{k}|^{\mu} \tilde{f}(\mathbf{k}) \quad (\text{A.41})$$

yields upon Fourier inversion a slightly more involved but structurally similar integral representation in position space,

$$\Delta_x^{\mu/2} f(\mathbf{x}) = -\frac{2^{\mu} \Gamma(\frac{\mu+n}{2})}{\pi^{n/2} \Gamma(-\frac{\mu}{2})} \int_{-\infty}^{\infty} d^n y \frac{[f(\mathbf{y}) - f(\mathbf{x})]}{|\mathbf{x} - \mathbf{y}|^{\mu+n}}. \quad (\text{A.42})$$





B. Langevin Dynamics and the Fokker-Planck Equation

A number of Markov processes can be described by Langevin dynamics, in which single realizations of the process are modeled by stochastic differential equations. Usually, the forces acting on the system segregate into a deterministic possibly non-linear drift and a stochastic force modeled by Gaussian white noise, i.e.

$$dX = -F(X, t) dt + \sqrt{D(X, t)} dW. \quad (\text{B.1})$$

The Gaussian white noise is represented by the differential of the Wiener process $W(t)$. In the following we assume that the value $X(t)$ of the process at time t and the increment $dW(t)$ are stochastically independent. Under these circumstances equation (B.1) is known as an Ito-stochastic differential equation [44].

The conditional pdf $p(x, t|x_0, t_0)$ of the process satisfies the Chapman-Kolmogorov equation (CKE) [44],

$$p(x, t|x_0, t_0) = \int dz p(x, t|z, t') p(z, t'|x_0, t_0), \quad t \geq t' \geq t_0, \quad (\text{B.2})$$

because $X(t)$ is a Markov process. Expanding $p(x, t|z, t')$ in powers of differential operators yields

$$\partial_t p(x, t|x_0, t_0) = \sum_{n=1} \frac{1}{n!} (-\partial_x)^n m_n(x, t) p(x, t|x_0, t_0). \quad (\text{B.3})$$

This is known as the Kramers-Moyal expansion [109]. The expansion coefficients $m_n(x, t)$ are the short time conditional moments of the process $X(t)$, i.e.

$$m_n(x, t) = \lim_{\Delta t \rightarrow 0} \frac{1}{\Delta t} \langle [X(t + \Delta t) - X(t)]^n | X(t) = x \rangle \quad (\text{B.4})$$

$$= \frac{1}{dt} \langle dX(t)^n | X(t) = x \rangle. \quad (\text{B.5})$$

The moments can be obtained from the stochastic differential equation (B.1) and the moments of the Wiener increments dW which are given by

$$\langle dW \rangle = 0 \quad \langle dW^2 \rangle = dt \quad (\text{B.6})$$

$$\langle dW^{2n+1} \rangle = 0 \quad \langle dW^{2n+2} \rangle = \frac{2^{1+n} \Gamma(3/2 + n)}{\sqrt{\pi}} dt^{1+n}, \quad n \in \mathbb{N}. \quad (\text{B.7})$$



Taking this into account, the infinitesimal moments of the displacement $dX(t)$ read

$$\langle dX(t) \rangle = \langle F(X(t), t) \rangle dt, \quad (\text{B.8})$$

and

$$\begin{aligned} \langle dX(t)^2 \rangle &= \langle D(X(t), t) dW^2 \rangle \\ &+ 2 \overbrace{\left\langle F(X(t), t) \sqrt{D(X(t), t)} dW \right\rangle}^0 dt + \mathcal{O}(dt^2). \end{aligned} \quad (\text{B.9})$$

The second term in (B.9) vanishes because the Wiener increment is independent of the process $X(t)$, the expectation value factorizes, and $\langle dW \rangle = 0$ and thus

$$\langle dX(t)^2 \rangle = \langle D(X(t), t) \rangle dt + \mathcal{O}(dt^2). \quad (\text{B.10})$$

All higher infinitesimal moments fulfill

$$\langle dX(t)^n \rangle = \mathcal{O}(dt^2), \quad n \geq 3. \quad (\text{B.11})$$

Inserted into the definition of the short time moments, we see that

$$m_n(x, t) = \frac{\langle dX(t)^n | X(t) = x \rangle}{dt} = \begin{cases} F(x, t) & n = 1 \\ D(x, t) & n = 2 \\ 0 & n \geq 3. \end{cases} \quad (\text{B.12})$$

Consequently, the Kramers-Moyal expansion terminates at $n = 2$, and the conditional pdf for ordinary Langevin dynamics is governed by the FPE, i.e.

$$\partial_t p(x, t | x_0, t_0) = \left\{ -\partial_x F(x, t) + \frac{1}{2} \partial_x^2 D(x, t) \right\} p(x, t | x_0, t_0). \quad (\text{B.13})$$



C. Homogeneous Detailed Balanced Stochastic Operators

In this Appendix some standard techniques are comprised which are helpful in the study of homogenous stochastic evolution equations such as

$$\partial_t p = \mathcal{L} p. \quad (\text{C.1})$$

Temporal homogeneity implies that the stochastic operator \mathcal{L} is independent of time. Furthermore, we require the condition of detailed balance. This condition is most transparent if equation (C.1) represents a master equation and the integral kernel of \mathcal{L} is given by

$$L(x|y) = w(x|y) - \left(\int dy w(y|x) \right) \delta(x - y). \quad (\text{C.2})$$

Generally, the rate $w(x|y)$ and thus $L(x|y)$ are not symmetric, i.e.

$$w(x|y) \neq w(y|x). \quad (\text{C.3})$$

However, detailed balance guarantees that the rates fulfill

$$w(x|y) p_s(y) = w(y|x) p_s(x) \quad \forall \quad x \neq y, \quad (\text{C.4})$$

where p_s is the solution to

$$\mathcal{L} p_s = 0. \quad (\text{C.5})$$

If p_s can be normalized properly and $w(x|y) \neq 0$ for all x and y , then $p_s(x)$ is the unique stationary solution to (C.1) and all initial conditions $p_0(x)$ will converge to it. For natural boundary conditions detailed balance is also fulfilled by FPEs with position dependent drift and diffusion coefficients, i.e.

$$\partial_t p(x, t|x_0, t_0) = \left(-\partial_x F(x) + \frac{1}{2} \partial_x^2 D(x) \right) p(x, t|x_0, t_0), \quad (\text{C.6})$$

although this is more difficult show [109]. The stationary solution, expressed in terms of $F(x)$ and $D(x)$ is given by

$$p_s(x) \propto \frac{1}{D(x)} \exp \left[2 \int_{-\infty}^x dx' \frac{F(x')}{D(x')} \right] \quad (\text{C.7})$$



The FFPE for topological superdiffusion

$$\partial_t p = e^{-\beta V/2} \Delta^{\mu/2} e^{\beta V/2} p - p e^{\beta V/2} \Delta^{\mu/2} e^{-\beta V/2} \quad (\text{C.8})$$

derived in chapter 3 fulfills detailed balance with Gibbs-Boltzmann equilibrium

$$p_s(x) = \exp[-\beta V(x)] \quad (\text{C.9})$$

as the stationary state.

The analysis of the evolution equation relies on a symmetrization of the operator \mathcal{L} and subsequent spectral decomposition. Adopting Dirac notation we can define a symmetric transformation $S^{1/2}$ which is a multiplication by the root of the solution $p_s(x)$ to (C.5), i.e.

$$S^{1/2} = \int \sqrt{p_s(x)} dP_x, \quad (\text{C.10})$$

where P_x is the spectral measure of the position operator X , that is $dP_x = |x\rangle\langle x| dx$. The integral kernel of $S^{1/2}$ is given by

$$\langle x | S^{1/2} | y \rangle = \sqrt{p_s(x)} \delta(x - y). \quad (\text{C.11})$$

Inserting

$$p = S^{1/2} |\psi\rangle \quad \text{and} \quad \mathcal{L} = -S^{1/2} H S^{-1/2}, \quad (\text{C.12})$$

into (3.48) we obtain a fractional Schrödinger equation

$$\partial_t |\psi\rangle = -H |\psi\rangle. \quad (\text{C.13})$$

for the wave function $|\psi\rangle$. The Hamilton operator H is symmetric. For example the integral kernel $H(x|y)$ for the master equation (C.2) is given by

$$\begin{aligned} H(x|y) &= -p_s^{-1/2}(x) L(x|y) p_s^{1/2}(x) \\ &= H(y|x), \end{aligned} \quad (\text{C.14})$$

because of the condition (C.4). The transformed FFPE for topological superdiffusion reads

$$\partial_t |\psi\rangle = -\left(\Delta^{\mu/2} - U(X)\right) |\psi\rangle \quad \text{with} \quad (\text{C.15})$$

$$U(x) = e^{\beta V(x)/2} \Delta_x^{\mu/2} e^{-\beta V(x)/2}. \quad (\text{C.16})$$

The operator defined by the rhs of (C.15) is clearly symmetric.

C.1. Properties of the Wave Function $|\psi_t\rangle$



Stochastic evolution according to (C.1) can now be interpreted in terms of quantum mechanical concepts. However, because the Schrödinger equation (C.13) is missing the imaginary prefactor the interpretation differ a little. Given an initial ($t = t_0$) condition for the wave function $\langle x|\psi_0\rangle = \psi(x, t_0)$ the Schrödinger equation (C.13) is formally solved by

$$|\psi_t\rangle = e^{-H(t-t_0)} |\psi_0\rangle, \quad (\text{C.17})$$

where $\langle x|\psi_t\rangle = \psi(x, t)$ is the wave function at time t . The pdf $p(x, t)$ can be obtained from it by the transformation (3.58). The wave function $\psi(x, t)$ has a number of properties which are related to the requirements the original pdf $p(x, t)$ must meet. The normalization condition $\int dx p(x, t) = 1$ requires that

$$\int dx e^{-\beta V(x)/2} \psi(x, t) = 1. \quad (\text{C.18})$$

Furthermore, $\psi(x, t)$ is nonnegative because $p(x, t)$ is. If we define the “bra” $\langle\psi_s|$ by $\langle\psi_s|x\rangle = e^{-\beta V(x)/2}$, equation (C.18) may be written more concisely as

$$\langle\psi_s|\psi_t\rangle = 1. \quad (\text{C.19})$$

Although the Hamiltonian H is self-adjoint in some appropriate Hilbert space \mathfrak{H} , for example $\mathcal{L}^2(\mathbb{C}, dx)$ neither $|\psi_s\rangle$ nor $|\psi_t\rangle$ need to be elements of \mathfrak{H} , because neither

$$\langle\psi_s|\psi_s\rangle = \int dx e^{-\beta V(x)} \quad \text{nor} \quad (\text{C.20})$$

$$\langle\psi_t|\psi_t\rangle = \int dx e^{\beta V(x)} p^2(x, t) \quad (\text{C.21})$$

need to exist. Nevertheless, for all practical purposes it is safe to assume that both functions are elements of \mathfrak{H} , because the bracket $\langle\psi_s|\psi_t\rangle$ is known to be unity and virtually all quantities of interest can be expressed in terms of the sandwich $\langle\psi_s| \cdot |\psi_t\rangle$. If $\exp[-\beta V]$ can be normalized then $|\psi_s\rangle \in \mathcal{L}^2(\mathbb{C}, dx)$ represents the stationary state of (C.13) and is an eigenstate of H and thus of e^{-Ht} with eigenvalues 0 and 1, respectively. In this case we have

$$\langle\psi_s|\psi_s\rangle = 1 \quad \text{and} \quad (\text{C.22})$$

$$P_0 = |\psi_s\rangle \langle\psi_s|. \quad (\text{C.23})$$

The operator P_0 projects onto the stationary state $|\psi_s\rangle$, i.e.

$$P_0 |\psi_s\rangle = P_0 |\psi_t\rangle = |\psi_s\rangle. \quad (\text{C.24})$$



Geometrically, the state vector $|\psi_t\rangle$ may be interpreted as evolving in the affine subspace \mathfrak{U} defined by

$$\mathfrak{U} = |\psi_s\rangle + (1 - P_0)\mathfrak{H}. \quad (\text{C.25})$$

Therefore, the length of $|\psi_t\rangle$ is always greater than or equal to unity, i.e.

$$\begin{aligned} \langle \psi_t | \psi_t \rangle &= \langle \psi_s | \psi_s \rangle + \langle \theta | \theta \rangle \quad \text{with} \quad |\theta\rangle \in \mathfrak{U} \\ &\geq 1. \end{aligned} \quad (\text{C.26})$$

Equality is attained only when $|\psi_t\rangle = |\psi_s\rangle$. Equation (C.26) only makes sense if for every a vector $|\phi\rangle$ in the domain of H the product $\langle \phi | \psi_t \rangle$ exists.

C.2. Spectral Decomposition

The symmetry of the Hamiltonian in (C.13) implies that H can be spectrally decomposed, i.e.

$$H = \int_{-\infty}^{\infty} \lambda dP_\lambda, \quad (\text{C.27})$$

where the self-adjoint projectors P_λ are parameterized by the real number λ and are referred to as the spectral family associated with H . The integral is a type of Lebesgue-Stieltjes integral, in which a spectral measure P_Δ is assigned to each Borel set $\Delta \subseteq \mathbb{R}$. The elements of the spectral family satisfy a number of conditions. Let \mathfrak{U}_μ and \mathfrak{U}_λ be the subspaces that P_μ and P_λ project on, respectively. If $\mu < \lambda$ then $\mathfrak{U}_\mu \subseteq \mathfrak{U}_\lambda$, i.e.

$$P_\mu \leq P_\lambda \quad \text{if} \quad \mu < \lambda. \quad (\text{C.28})$$

P_λ is monotonously increasing with λ . Furthermore, they fulfill

$$\lim_{\epsilon \rightarrow 0} P_{\lambda+\epsilon} = P_\lambda. \quad (\text{C.29})$$

In case P_λ is discontinuous at λ the value of P_λ at this point is given by the rhs limit. For general self-adjoint operators two more conditions hold, namely

$$P_{-\infty} = \emptyset, \quad \text{and} \quad P_\infty = 1, \quad (\text{C.30})$$

from which the resolution of unity,

$$1 = \int_{-\infty}^{\infty} dP_\lambda \quad (\text{C.31})$$

can be obtained. Since H is derived from a stochastic operator \mathcal{L} one can show that $P_\lambda = \emptyset$ for $\lambda < 0$ and we may set the lower boundary in (C.30) to zero, i.e.

$$P_{-\epsilon} = \emptyset \quad \forall \quad \epsilon > 0. \quad (\text{C.32})$$

This is a generalization of the statement that H does not possess negative eigenvalues. The spectral decomposition (C.27) yields a meaningful expression of the exponential $\exp[-Ht]$ or any other function of H in terms of the spectral family,

$$e^{-Ht} = \int_0^{\infty} e^{-\lambda t} dP_{\lambda}. \quad (C.33)$$

The spectrum $\sigma(H)$ may have both, continuous and discrete components, i.e.

$$\sigma(H) = \sigma_c(H) \cup \sigma_p(H) \subset \mathbb{R}. \quad (C.34)$$

If $\lambda \in \sigma(H)$ then P_{λ} changes in any neighborhood of λ and any neighborhood of λ has a nonzero Lebesgue measure. If $\lambda \in \sigma_p(H)$ then P_{λ} is discontinuous at λ , i.e. $P_{\lambda} \neq P_{\lambda-0}$ and λ is an eigenvalue of H .

C.2.1. Stationary Systems

If $P_0 \neq \emptyset$ then $\lambda = 0$ is an eigenvalue of H with eigenstate $|\psi_s\rangle$, because in this case P_{λ} is discontinuous at $\lambda = 0$ (i.e. $P_{-0} = \emptyset \neq P_0$). In this situation $|\psi_s\rangle$ can be normalized and $P_0 = |\psi_s\rangle \langle \psi_s|$. With this we may rewrite (C.33) as

$$\begin{aligned} e^{-Ht} &= \int_0^{\infty} e^{-\lambda t} dP_{\lambda} \\ &= P_0 + \int_{0+}^{\infty} e^{-\lambda t} dP_{\lambda} = |\psi_s\rangle \langle \psi_s| + \int_{0+}^{\infty} e^{-\lambda t} dP_{\lambda} \end{aligned} \quad (C.35)$$

Therefore, as $t \rightarrow \infty$ the evolution operator will eventually be a projection onto the stationary state, i.e.

$$\lim_{t \rightarrow \infty} e^{-Ht} = P_0. \quad (C.36)$$

C.2.2. Discrete Spectra

If $\sigma_c(H) = \emptyset$ the operator has a pure point spectrum of a countable set of eigenvalues λ_n . The projective measure is then given by

$$P_{\lambda} = \sum_n \Theta(\lambda_n - \lambda) P_n \quad (C.37)$$

for these type of systems. The function $\Theta(x)$ is the Heaviside step function and the P_n are the projectors onto the subspaces corresponding to λ_n . The differential dP_{λ} reads

$$dP_{\lambda} = \sum_n \delta(\lambda_n - \lambda) P_n d\lambda, \quad (C.38)$$



and from (C.27) we obtain the discrete spectral decomposition

$$e^{-Ht} = \sum_n e^{-\lambda_n t} P_n, \quad (\text{C.39})$$

and

$$\sum_n P_n = 1. \quad (\text{C.40})$$

Note however, that a discrete spectrum does not imply that a stationary solution exists. In other words, $P_0 = \emptyset$ may still hold or equivalently $\lambda_0 > 0$. An example for this type of spectrum is ordinary diffusion in the inverse harmonic potential. Furthermore, the existence of a stationary state (i.e. $P_0 \neq \emptyset$) does not imply a purely discrete spectrum, as for example diffusion in the potential $V(x) = |x|$. Both examples are discussed in [109].

C.2.3. Computing Expectation Values

The quantum mechanical formalism and spectral decomposition are both very useful for computing expectation values of the stochastic system. For example, the expectation value of some function of the process $\langle F(X(t)) \rangle$ may be expressed as

$$\begin{aligned} \langle F(X(t)) \rangle &= \int dx F(x) p(x, t) \\ &= \langle \psi_s | F e^{-H(t-t_0)} | \psi_0 \rangle \end{aligned} \quad (\text{C.41})$$

in which the operator

$$F = \int dx F(x) |x\rangle \langle x| \quad (\text{C.42})$$

represents a multiplication by $F(x)$. More complicated expectation values can be expressed along the same lines and acquire an unusually compressed form, for example

$$\left\langle \prod_{i=0}^n F_i(X(t_i)) \right\rangle = \left\langle \psi_s \left| \prod_{i=1}^n e^{+Ht_i} F_i e^{-Ht_i} \right| \psi_0 \right\rangle \quad (\text{C.43})$$

$$= \left\langle \psi_s \left| F_n \prod_{i=1}^{n-1} e^{-H(t_i-t_{i-1})} F_{i-1} \right| \psi_0 \right\rangle \quad (\text{C.44})$$

in which the sequence of times $t_n \geq t_{n-1} \geq \dots \geq t_1 \geq t_0 = 0$ is descending ordering of time and the operators F_i are defined analogously to (C.42). In (C.44) we see that multi time expectation values only depend on the time differences $t_i - t_{i-1}$ reflecting the temporal homogeneity of the process.

One can now utilize the spectral decomposition (C.33), insert it into expressions such as (C.43) and (C.44), and obtain complicated expectation values as functions of the spectrum and its measure.

C.2.3.1. Examples

One is frequently interested in the autocorrelation function of some function of a stationary process, i.e.

$$\begin{aligned} C_F(t) &= \langle (F(X(t)) - \langle F(X) \rangle_s) (F(X(0)) - \langle F(X) \rangle_s) \rangle_s \\ &= \langle F(X(t)) F(X(0)) \rangle_s - \langle F(X) \rangle_s^2, \end{aligned} \quad (\text{C.45})$$

where the subscript in the expectation value $\langle \cdot \rangle_s$ denotes the stationarity, i.e. $|\psi_0\rangle = |\psi_s\rangle$. The first term is of the form given in equation (C.44) and reads

$$\langle F(X(t)) F(X(0)) \rangle_s = \langle \psi_s | F e^{-Ht} F | \psi_s \rangle. \quad (\text{C.46})$$

Since the process is stationary, we may insert the spectral decomposition (C.35) and obtain

$$\langle \psi_s | F e^{-Ht} F | \psi_s \rangle = \langle \psi_s | F P_0 F | \psi_s \rangle + \int_{0+}^{\infty} e^{-\lambda t} d \langle \psi_s | F P_\lambda F | \psi_s \rangle. \quad (\text{C.47})$$

Recall that $P_0 = |\psi_s\rangle\langle\psi_s|$. Thus, the first term reduces to $\langle F(X) \rangle_s^2$. Defining the measure $\mu_F(\lambda) = \langle \psi_s | F P_\lambda F | \psi_s \rangle$ and inserting (C.47) into (C.46) we obtain

$$C_F(t) = \int_{0+}^{\infty} e^{-\lambda t} d\mu_F(\lambda). \quad (\text{C.48})$$

Therefore, the correlation of any observable F of any process which fulfilled the requirements stated initially vanishes as $t \rightarrow \infty$. The decay is a weighted sum of exponentials.

The conditional pdf $p(x, t | x_0, t_0)$ can be computed along the same lines. First define two observables

$$X = |x\rangle\langle x| \quad \text{and} \quad X_0 = |x_0\rangle\langle x_0|. \quad (\text{C.49})$$

The conditional pdf is defined by

$$p(x, t | x_0, t_0) = \frac{\langle \delta(X(t) - x) \delta(X(t_0) - x_0) \rangle}{\langle \delta(X(t_0) - x_0) \rangle}. \quad (\text{C.50})$$

Rewriting in Dirac notation yields

$$\begin{aligned} p(x, t | x_0, t_0) &= \frac{\langle \psi_s | X e^{-H(t-t_0)} X_0 | \psi_s \rangle}{\langle \psi_s | X_0 | \psi_s \rangle} \\ &= \frac{\langle x | \psi_s \rangle}{\langle x_0 | \psi_s \rangle} \langle x | e^{-H(t-t_0)} | x_0 \rangle \end{aligned} \quad (\text{C.51})$$





Assuming a spectral decomposition of the form (C.35) the terms on the rhs of (C.51) can be computed with ease and the conditional pdf is given by

$$p(x, t|x_0, t_0) = p_s(x) + \sqrt{\frac{p_s(x)}{p_s(x_0)}} \int_{0+}^{\infty} e^{-\lambda(t-t_0)} \mathbf{d} \langle x | \mathbf{P}_\lambda | x_0 \rangle. \quad (\text{C.52})$$

Thus, quite generally the probability of finding the process at the location x at a time t is not only the stationary probability but also independent of the initial condition as $t - t_0 \rightarrow \infty$.

D. The Fourier Transform

An indispensable tool for the study of fractional dynamics is the Fourier transform, since fractional differential operators are much easier to deal with in Fourier space. The Fourier transform exists in two forms, discrete and continuous. Both versions are related. Quite often one is annoyed if one wishes to determine the prefactors involved in either case, especially when dealing with convolutions, that is transforms of products of functions, and if one wishes to express the discrete transform as a special case of the continuous one. Here we collect a number of definitions and identities such that the reader will not be confused about the transform when it appears in the text and that equality symbols can be used instead of vague proportionality symbols.

What follows is applicable to one-dimensional systems, generalizations to n dimensions is straightforward. The Fourier transform is based on the identity

$$\delta(x) = \frac{1}{2\pi} \int dx e^{ikx}, \quad (\text{D.1})$$

in which $\delta(x)$ is the Dirac δ -function. In stochastics, we usually define the Fourier transform $\tilde{f}(k)$ of an appropriate function $f(x)$ as

$$\tilde{f}(k) \equiv \int dx e^{ikx} f(x). \quad (\text{D.2})$$

Note that there is not $1/\sqrt{2\pi}$ prefactor in this definition which is commonly used in quantum mechanics. In stochastics the prefactor is omitted because if f is a pdf then \tilde{f} is the characteristic function and is it often useful to rely on the fact that $\tilde{f}(0) = 1$ which follows from the fact that pdfs are normalized to unity. Combining (D.1) and (D.2) we see that the inverse Fourier transform is

$$f(x) = \frac{1}{2\pi} \int dk e^{-ikx} \tilde{f}(k). \quad (\text{D.3})$$

The Fourier transform of the product,

$$h(x) = f(x) g(x), \quad (\text{D.4})$$

is proportional to the convolution of the transforms of each factor if both functions



on the rhs of (D.4) vanish on the boundary,

$$\begin{aligned}\tilde{h}(k) &= \frac{1}{2\pi} \int dk' \tilde{f}(k-k') \tilde{g}(k') \\ &= \frac{1}{2\pi} \int dk' \tilde{g}(k-k') \tilde{f}(k') \\ &= \frac{1}{2\pi} (\tilde{f} \star \tilde{g})(k) = \frac{1}{2\pi} (\tilde{g} \star \tilde{f})(k).\end{aligned}\tag{D.5}$$

On the other hand the transform of the convolution

$$H(x) = \int dy f(x-y) g(y)\tag{D.6}$$

is just the product of the transforms,

$$\tilde{H}(k) = \tilde{f}(k) \tilde{g}(k).\tag{D.7}$$

Another simple but very useful transformation is that of a plane wave of wave number k_0 ,

$$\phi_{k_0}(x) = e^{-ik_0x},\tag{D.8}$$

which yields a δ -function at k_0 modified by a prefactor of 2π ,

$$\tilde{\phi}_{k_0}(k) = 2\pi \delta(k - k_0).\tag{D.9}$$

The discrete Fourier transform is used for functions which are periodic, in other words,

$$f(x) = f(x + nL) \quad n \in \mathbb{Z}.\tag{D.10}$$

Periodic functions can be expanded into a series of plane waves with wave numbers related to the periodicity of the function, i.e.

$$f(x) = \sum_n e^{-ik_n x} \hat{f}_n \quad \text{with} \quad k_n = \frac{2\pi n}{L}, \quad n \in \mathbb{Z}.\tag{D.11}$$

The discrete Fourier coefficients \hat{f}_n are determined by integrating the function over one period, i.e.

$$\hat{f}_n = \frac{1}{L} \int_{-L/2}^{L/2} dx e^{ik_n x} f(x)\tag{D.12}$$

Inserting equation (D.11) into the definition (D.2) we obtain the relation between the continuous transform $\tilde{f}(k)$ and the Fourier coefficients \hat{f}_n ,

$$\tilde{f}(k) = 2\pi \sum_n \delta(k - k_n) \hat{f}_n.\tag{D.13}$$

Again, if we let $\phi_m(x)$ be a plane wave satisfying condition (D.10),

$$\phi_m(x) = e^{ik_m x} \quad \text{with} \quad k_m = \frac{2\pi m}{L}, \quad m \in \mathbb{Z} \quad (\text{D.14})$$

we see that

$$\hat{\phi}_n = \delta_{n,m} \quad \text{and} \quad \tilde{\phi}_m(k) = 2\pi \delta(k - k_m). \quad (\text{D.15})$$

Moreover, if both functions in the product (D.4) are periodic we must admit that, after rearranging indices a little bit, $\tilde{h}(k)$ has the same form as (D.13), i.e.

$$\begin{aligned} \tilde{h}(k) &= 2\pi \int dk' \sum_{n,m} \hat{f}_n \hat{g}_m \delta(k - k_n - k') \delta(k' - k_m) \\ &= 2\pi \sum_{n,m} \hat{f}_n \hat{g}_m \delta(k - (k_n + k_m)) \\ &= 2\pi \sum_{n,m} \hat{f}_{n-m} \hat{g}_m \delta(k - k_n) \\ &= 2\pi \sum_n \hat{h}_n \delta(k - k_n), \end{aligned} \quad (\text{D.16})$$

with Fourier coefficients \hat{h}_n which are determined by a discrete convolution of the Fourier coefficient \hat{f}_n and \hat{g}_n ,

$$\hat{h}_n = \sum_m \hat{f}_{n-m} \hat{g}_m. \quad (\text{D.17})$$

Note the lack of prefactor 2π in this equation.



D. The Fourier Transform



E. Generating Random Numbers with Divergent Moments Numerically

In order to investigate superdiffusive phenomena by computer simulation quasi-random numbers with power law densities are required. Most programming languages provide methods for uniformly distributed random numbers $X \in [0, 1]$. Provided that such a method is available, it is straightforward to obtain random numbers Y with a pdf $\rho_Y(y)$ which is an inverse power law of y . The problem consists of finding a function f with an inverse f^{-1} such that the pdf of $Y = f(X)$ fulfills the posed requirements.

E.1. Transforming Random Variables

When a random variable X with a pdf $\rho_X(x)$ is transformed by a one-to-one function f with an inverse f^{-1} , the random variable $Z = f(X)$ has the density

$$\rho_Z(z) = \langle \delta(z - f(X)) \rangle \quad (\text{E.1})$$

$$= \int dx \delta(z - f(x)) \rho_X(x) \quad (\text{E.2})$$

$$= \rho_X(f^{-1}(z)) J(z). \quad (\text{E.3})$$

The function

$$J(z) = \left| \frac{df^{-1}(z)}{dz} \right| \quad (\text{E.4})$$

is the Jacobian of the inverse f^{-1} . Reversing the procedure, equation (E.3) can be employed to generate random numbers with a specified density $\rho_Z(z)$, in which case the function $f(x)$ must be determined. This is a simple task if we let X be uniformly distributed in the interval $[0, 1]$, i.e.

$$\rho_X(x) = \begin{cases} 1 & 0 \leq x \leq 1 \\ 0 & \text{otherwise.} \end{cases} \quad (\text{E.5})$$

This implies $f^{-1} > 0$ and from (E.4) we obtain

$$\rho_Z(z) = \frac{df^{-1}(z)}{dz}. \quad (\text{E.6})$$



Integration yields the probability $P_Z(z)$ of finding a value $Z \leq z$,

$$P_Z(z) = \int_{-\infty}^z dz' \rho_Z(z'), \quad (\text{E.7})$$

which is one-to-one and can be inverted. Combining equations (E.6) and (E.7) yields

$$f(x) = P_Z^{-1}(x). \quad (\text{E.8})$$

E.1.1. Example: Exponentially Distributed Random Variables

Let $Z \in [0, \infty)$ with a pdf

$$\rho_Z(z) = \mu e^{-\mu z} \quad \text{with} \quad \mu > 0. \quad (\text{E.9})$$

Inserting (E.9) into (E.7) yields $P_Z(z) = 1 - e^{-\mu z}$ and from (E.8) we obtain

$$Z = f(X) = -\frac{1}{\mu} \log(1 - X). \quad (\text{E.10})$$

If $X \in [0, 1)$ is uniformly distributed, the variable Z will have the desired exponential density (E.9).

E.2. Generating Random Numbers with a Power Law Density

Let $X \in [0, 1]$ be uniformly distributed as above. Furthermore, we define a new random variable S , which can take the two values ± 1 with equal probability,

$$\rho_S(s) = \frac{1}{2} [\delta(s + 1) + \delta(s - 1)]. \quad (\text{E.11})$$

Combining X and S according to

$$Y \equiv f_\mu(X, S) = \frac{y_0 S}{(1 - X)^{1/\mu}} \quad \text{with} \quad \mu > 0, \quad (\text{E.12})$$

produces a random variable Y with a symmetric inverse power law density

$$p_Y(y) = \frac{\mu y_0^\mu}{2} \begin{cases} |y|^{-(1+\mu)} & y_0 \leq |y| \leq \infty \\ 0 & \text{otherwise.} \end{cases} \quad (\text{E.13})$$

If $\mu \in (0, 2]$, the second moment $\langle Y^2 \rangle$ diverges. If $\mu \in (0, 1]$ the expectation value $\langle Y \rangle$ does, too.

E.2.1. Finite Intervals

A number of situations require random numbers within finite intervals, for example $[-y_1, -y_0] \cup [y_0, y_1]$ with $0 < y_0 < y_1$. If we wish to restrict the pdf (E.13) to a finite support, we must generalize the transformation (E.12) a little. More specifically, we must choose

$$Y = f_\mu(X, S) = \frac{y_0 y_1 S}{[y_0^\mu (1 - X) + y_1^\mu X]^{1/\mu}}. \quad (\text{E.14})$$

This type of transformation yields the appropriate density

$$\rho_Y(y) = \frac{\mu}{2(1/y_1^\mu - 1/y_0^\mu)} \begin{cases} |y|^{-(1+\mu)} & y_0 \leq |y| \leq y_1 \\ 0 & \text{otherwise,} \end{cases} \quad (\text{E.15})$$

which is identical to (E.13) in the limit $y_1 \rightarrow \infty$.

E.3. Random Numbers with Lévy Stable Densities

Although it is straightforward to generate random numbers with a density which follows an inverse power law, the matter is more subtle if $\rho_Y(y)$ is required to be a symmetric Lévy stable law

$$L_\mu(y) = \frac{1}{2\pi} \int dk e^{-iky - |k|^\mu}. \quad (\text{E.16})$$

Not only does $L_\mu(y)$ deviate from the density (E.13) for small values of y , the behavior

$$L_\mu(y) \sim \frac{1}{|y|^{1+\mu}} \quad (\text{E.17})$$

for large arguments ($|y| \gg 1$) is only asymptotically correct. In fact, a series expansion of (E.16) shows that $L_\mu(y)$ consists of an infinite number of algebraic tails [90],

$$L_\mu(y) = \frac{1}{\pi} \sum_{k=1}^{\infty} \frac{(-1)^{k+1}}{k!} y^{-(\mu k+1)} \Gamma(1 + k\mu) \sin(\pi\mu k/2). \quad (\text{E.18})$$

and only the leading term ($k = 1$) decreases as $|y|^{-(1+\mu)}$. Therefore, the difference between the leading term and the remainder of the sum decreases only as a power, and hence slowly, with distance. For some special choices of the Lévy exponent matters can be simplified. For example, when $\mu = 1$ equation (E.16) reduces to

$$L_1(y) = \frac{\pi^{-1}}{1 + y^2}. \quad (\text{E.19})$$



A random variable Y with this density can be obtained by dividing two normally distributed random variables X_1 and X_2 ,

$$Y = X_1/X_2. \tag{E.20}$$

However, no explicit form of $L_\mu(y)$ is known for general μ . Consequently, equation (E.7) cannot be integrated and no inverse of the result can be computed. Luckily, other means of generating random numbers with stable densities have been devised which extend the idea of dividing normally distributed random numbers [81].

Bibliography

- [1] Adamic, L. A., Lukose, R. M., Puniyani, A. R., and Huberman, B. A. Search in power-law networks. *Phys. Rev. E* **64**, 046135 (2001).
- [2] Albert, R. and Barabási, A.-L. Statistical mechanics of complex networks. *Rev. Mod. Phys.* **74**, 47 (2002).
- [3] Albert, R., Jeong, H., and Barabási, A. L. Diameter of the World Wide Web. *Nature* **410**, 130 (1999).
- [4] Amblard, F., Maggs, A. C., Yurke, B., Pargellis, A. N., and Leibler, S. Subdiffusion and anomalous local viscoelasticity in actin networks. *Phys. Rev. Lett.* **77**, 4470 (1996).
- [5] Anderson, P. W. Absence of diffusion in certain random lattices. *Phys. Rev.* **109**, 1492 (1958).
- [6] Aoyama, H., Souma, W., Nagahara, Y., Okozaki, M. P., Takayasu, H., and Takayasu, M. Pareto's law for income of individuals and debt of bankrupt companies. *Fractals* **8**, 293 (2000).
- [7] Ashcroft, N. W. and Mermin, N. D. *Solid State Physics*. Saunders College, Philadelphia (1976).
- [8] Bahill, A. T. and Stark, L. The trajectories of saccadic eye movements. *Scientific American* **240**, 108 (1979).
- [9] Barabási, A.-L. and Albert, R. Emergence of scaling in random networks. *Science* **286**, 509 (1999).
- [10] Barkai, E. Fractional Fokker-Planck equation, solution, and application. *Phys. Rev. E* **63**, 46118 (2001).
- [11] Barkai, E., Metzler, R., and Klafter, J. From continuous time random walks to the fractional Fokker-Planck equation. *Phys. Rev. E* **61**, 132 (2000).
- [12] Bartumeus, F., Catalan, J., Fulco, U. L., Lyra, M. L., and Viswanathan, G. M. Optimizing encounter rate in biological interactions: Lévy versus Brownian strategies. *Phys. Rev. Lett.* **88**, 097904 (2002).

- [13] Bauer, H.-U., Geisel, T., Pawelzik, K., and Wolf, F. Selbstorganisierende Neuronale Karten. *Spektrum der Wissenschaft* **4**, 38 (1996).
- [14] Beck, C. Dynamical foundations of nonextensive statistical mechanics. *Phys. Rev. Lett.* **87**, 180601 (2001).
- [15] Beck, C. and Schögl, F. *Thermodynamics of Chaotic Systems: An Introduction*, volume 4 of *Nonlinear Science Series*. Cambridge University Press, Cambridge (1993).
- [16] Berg, O. G., Winter, R., and von Hippel, P. Diffusion-driven mechanisms of protein translocation on nucleic acids – 1. models and theory. *Biochem.* **20**, 6929 (1981).
- [17] Berkolaiko, G. and Havlin, S. Number of distinct sites visited by Lévy flights injected into a d -dimensional lattice. *Phys. Rev. E* **57**, 2549 (1998).
- [18] Boguná, M. and Pastor-Satorras, R. Epidemic spreading in correlated complex networks. *Phys. Rev. E* **66**, 047104 (2002).
- [19] Bouchaud, J.-P. and Georges, A. Anomalous diffusion in disordered media: Statistical mechanisms, models and physical applications. *Phys. Rep.* **195**, 127 (1990).
- [20] Brockmann, D. and Geisel, T. Lévy flights in human visual search. (In preparation).
- [21] Brockmann, D. and Geisel, T. Lévy flights in thermal equilibrium. (In preparation).
- [22] Brockmann, D. and Geisel, T. Particle dispersion on rapidly folding random hetero-polymers. (Submitted), www.arXiv.org/cond-mat/0305056.
- [23] Brockmann, D. and Geisel, T. The ecology of gaze shifts. *Neurocomputing* **32-33**, 643 (2000).
- [24] Brockmann, D. and Geisel, T. Lévy flights in inhomogeneous media. *Phys. Rev. Lett.* **90**, 170601 (2003). www.arxiv.org/cond-mat/0211111.
- [25] Brockmann, D. and Sokolov, I. Lévy flights in external force fields: From models to equations. *Chem. Phys.* **284**, 409 (2002). www.arxiv.org/cond-mat/0210387.
- [26] Buiatti, M., Grigolini, P., and Montagnini, A. Dynamic approach to the thermodynamics of superdiffusion. *Phys. Rev. Lett.* **82**, 3383 (1999).

- [27] Buldyrev, S. V., Kazakov, A. Y., da Luz, M. G. E., Raposo, E. P., Stanley, H. E., and Viswanathan, G. M. Average time spent by Lévy flights and walks on an interval with absorbing boundaries. *Phys. Rev. E* **64**, 041108 (2001).
- [28] Cáceres, M. O. Lévy noise, Lévy flights, Lévy fluctuations. *J. Phys. A: Math. Gen.* **32**, 6009 (1999).
- [29] Caspi, A., Granek, R., and Elbaum, M. Enhanced diffusion in active intracellular transport. *Phys. Rev. Lett.* **85**, 5655 (2000).
- [30] Cole, B. J. Fractal time in animal behavior: The movement activity of drosophila. *Animal Behavior* **50**, 1317 (1995).
- [31] Compte, A. Stochastic foundation of fractional dynamics. *Phys. Rev. E* **53**, 4191 (1996).
- [32] de Gennes, P.-G. *Scaling Concepts in Polymer Physics*. Cornell University Press, Ithaca (1979).
- [33] Ditlevsen, P. D. Anomalous jumping in a double-well potential. *Phys. Rev. E* **60** (1999).
- [34] Ditlevsen, P. D. Observation of α -stable noise induced millennial climate changes from an ice-core record. *Geophys. Res. Lett.* **26**, 1441 (1999).
- [35] Doi, M. and Edwards, S. F. *The Theory of Polymer Dynamics*. Clarendon Press, Oxford (1995).
- [36] Drysdale, P. M. and Robinson, P. A. Lévy random walks in finite systems. *Phys. Rev. E* **58**, 5382 (1998).
- [37] Einstein, A. Über die von der molekularkinetischen Theorie der Wärme geforderte Bewegung der in ruhenden Flüssigkeiten suspendierten Teilchen. *Ann. d. Physik* **17**, 549 (1905).
- [38] Feller, W. *An Introduction to Probability Theory and Its Application*, volume II. Wiley, New York (1971).
- [39] Fogedby, H. C. Langevin equations for continuous time Lévy flights. *Phys. Rev. E* **50**, 1657 (1994).
- [40] Fogedby, H. C. Lévy flights in random environments. *Phys. Rev. Lett.* **73**, 2517 (1994).
- [41] Fogedby, H. C. Lévy flights in quenched random force fields. *Phys. Rev. E* **58**, 1690 (1998).

- [42] Fogedby, H. C., Bohr, T., and Jensen, H. J. Fluctuations in a Lévy flight gas. *J. Stat. Phys.* **66**, 583 (1992).
- [43] Ganlindo, A. and Pascual, P. *Quantum Mechanics*, volume I. Springer-Verlag, Berlin (1990).
- [44] Gardiner, C. W. *Handbook of Stochastic Methods*. Springer Verlag, Berlin (1985).
- [45] Geisel, T., Nierwetberg, J., and Zacherl, A. Accelerated diffusion in Josephson junctions and related chaotic systems. *Phys. Rev. Lett.* **54**, 616 (1985).
- [46] Geisel, T., Zacherl, A., and Radons, G. Generic $1/f$ -noise in chaotic Hamiltonian systems. *Phys. Rev. Lett.* **59**, 2503 (1987).
- [47] Geisel, T., Zacherl, A., and Radons, G. Chaotic diffusion and $1/f$ -noise of particles in two-dimensional solids. *Z. Phys. B* **71**, 117 (1988).
- [48] Gilchrist, I. D., Brown, V., and Findlay, J. M. Saccades without eye movements. *Nature* **390**, 130 (1997).
- [49] Gopikrishnan, P., Plerou, V., Amaral, L. A. N., Meyer, M., and Stanley, H. E. Scaling of the distribution of fluctuations of financial market indices. *Phys. Rev. E* **60**, 5305 (1999).
- [50] Gradshteyn, I. S. and Ryzhik, I. M. *Table of Integrals, Series, and Products*. Academic Press, New York, 6 edition (2000).
- [51] Haus, J. W. and Kehr, K. W. Diffusion in regular and disordered lattices. *Phys. Rep.* **150**, 263 (1998).
- [52] Heinrich, B. Recourse heterogeneity and patterns of movement in foraging bumblebees. *Oecologia* **40**, 235 (1979).
- [53] Helmstetter, A. and Sornette, D. Diffusion of epicenters of earthquake aftershocks, Omori's law, and generalized continuous-time random walk models. *Phys. Rev. E* **66**, 61104 (2002).
- [54] Hilfer, R. Classification theory for anequilibrium phase transitions. *Phys. Rev. E* **48**, 2466 (1993).
- [55] Hilfer, R. (editor). *Applications of Fractional Calculus in Physics*. World Scientific, Singapore (2000).
- [56] Honkonen, J. Asymptotic properties of Lévy flights in quenched random fields. *Phys. Rev. E* **62**, 7811 (2001).

- [57] Horowitz, T. and Wolfe, J. Visual search has no memory. *Nature* **394**, 575 (1998).
- [58] Jeong, H., Tombor, B., Albert, R., Oltvai, Z. N., and Barabási, A.-L. The large-scale organization of metabolic networks. *Nature* **407**, 651 (2000).
- [59] Jespersen, S. and Blumen, A. Small-world networks: Links with long-tailed distributions. *Phys. Rev. E* **62**, 6270 (2000).
- [60] Jespersen, S., Metzler, R., and Fogedby, H. C. Lévy flights in external force fields: Langevin and fractional Fokker-Planck equations and their solutions. *Phys. Rev. E* **59**, 2736 (1999).
- [61] Jespersen, S., Sokolov, I. M., and Blumen, A. Relaxation properties of small-world networks. *Phys. Rev. E* **62**, 4405 (2000).
- [62] Jespersen, S., Sokolov, I. M., and Blumen, A. Small-world networks as models of cross-linked polymers. *J. Chem. Phys.* **113**, 7652 (2000).
- [63] Khintchine, A. Y. and Lévy, P. Sur les lois stables. *C.R. Acad. Sci.* **202**, 374 (1936).
- [64] Klafter, J., Shlesinger, M. F., and Zumofen, G. Beyond Brownian motion. *Physics Today* **49**, 33 (1996).
- [65] Kleinberg, J. M. Navigation in a small world. *Nature* **406**, 845 (2000).
- [66] Larralde, H., Trunfio, P., Havlin, S., Stanley, H. E., and Weiss, G. H. Territory covered by n diffusing particles. *Nature* **355**, 423 (1992).
- [67] Laskin, N. Fractional quantum mechanics. *Phys. Rev. E* **62**, 3135 (2000).
- [68] Laskin, N. Fractional Schrödinger equation. *Phys. Rev. E* **66**, 056108 (2002).
- [69] Lathinen, J., Kertész, J., and Kaski, K. Scaling of random spreading in small world networks. *Phys. Rev. E* **64**, 057105 (2001).
- [70] Laughlin, R. B. and Pines, D. The theory of everything. *Proc. Natl. Acad. Sci. USA* **97**, 28 (2000).
- [71] Laughlin, R. B., Pines, D., Schmalian, J., Stojkovic, B. P., and Wolynes, P. The middle way. *Proc. Natl. Acad. Sci. USA* **97**, 32 (2000).
- [72] Levandowsky, M., Klafter, J., and White, B. S. Swimming behavior and chemosensory responses in the protistan microzooplankton as a function of the hydrodynamic regime. *Bull. Mar. Sci.* **43**, 758 (1988).

- [73] Levandowsky, M., White, B. S., and Schuster, F. L. Random movements of soil amoebas. *Acta Protozool.* **36**, 237 (1997).
- [74] Lévy, P. *Théorie de l'Addition des Variables Aléatoires*. Gauthier-Villars, Paris (1954).
- [75] Lillo, F. and Mantegna, R. N. Drift-controlled anomalous diffusion: A solvable Gaussian model. *Phys. Rev. E* **61**, R4675 (2000).
- [76] Lima, G. F., Martinez, A. S., and Kinouchi, O. Deterministic walks in random media. *Phys. Rev. Lett.* **87**, 010603 (2001).
- [77] Lipowsky, R., Klumpp, S., and Nieuwenhuizen, T. M. Random walks of cytoskeletal motors in open and closed compartments. *Phys. Rev. Lett.* **87**, 108101 (2001).
- [78] Lord Rayleigh. The problem of the random walk. *Nature* **72**, 318 (1905).
- [79] Lutz, E. Fractional Langevin equation. *Phys. Rev. E* **64**, 051106 (2001).
- [80] Lutz, E. Fractional transport equations for Lévy stable processes. *Phys. Rev. Lett.* **86**, 2208 (2001).
- [81] Mantegna, R. N. Fast, accurate algorithm for numerical simulation of Lévy stable stochastic processes. *Phys. Rev. E* **49**, 4677 (1994).
- [82] Mantegna, R. N. and Stanley, H. E. Stochastic process with ultraslow convergence to a Gaussian: The truncated Lévy flight. *Phys. Rev. Lett.* **73**, 2946 (1994).
- [83] Masoliver, J., Montero, M., and Weis, G. H. Continuous-time random-walk model for financial distributions. *Phys. Rev. E* **67**, 021112 (2003).
- [84] May, R. M. How many species are there on earth? *Science* **214**, 1441 (1988).
- [85] Medvinsky, A. B., Tikhonova, I. A., Aliev, R., Li, B.-L., Lin, Z.-S., and Malchow, H. Patchy environment as a factor of complex plankton dynamics. *Phys. Rev. E* **64**, 021915 (2001).
- [86] Metzler, R. Non-homogeneous random walks, generalised master equations, fractional Fokker-Planck equations, and the generalised Kramers-Moyal expansion. *Eur. Phys. J. B* **19**, 249 (2001).
- [87] Metzler, R. and Klafter, J. Boundary value problems for fractional diffusion equations. *Physica A* **278**, 107 (2000).

- [88] Metzler, R. and Klafter, J. The random walks guide to anomalous diffusion: A fractional dynamics approach. *Phys. Rep.* **339**, 1 (2000).
- [89] Metzler, R., Klafter, J., and Sokolov, I. M. Anomalous transport in external fields: Continuous time random walks and fractional diffusion equations extended. *Phys. Rev. E* **58**, 1621 (1998).
- [90] Montroll, E. W. and Bendler, J. T. On Lévy (or stable) distributions and the Williams-Watts model of dielectric-relaxation. *J. Stat. Phys.* **34**, 129 (1984).
- [91] Montroll, W. and Shlesinger, M. F. *On the Wonderful World of Random Walks*, volume 11 of *Studies in Statistical Mechanics*, chapter 1, pages 1–123. North Holland Physics Publishing, Amsterdam (1984).
- [92] Moukarzel, C. F. Spreading and shortest paths in systems with sparse long-range connections. *Phys. Rev. E* **60**, R6263 (1999).
- [93] Nossal, R. Stochastic aspects of biological locomotion. *Journal of Statistical Physics* **30**, 391 (1983).
- [94] Oldham, K. B. and Spanier, J. *The Fractional Calculus*. Academic Press, New York (1974).
- [95] O'Shaughnessy, B. and Procaccia, I. Analytical solutions for diffusion on fractal objects. *Phys. Rev. Lett.* **54**, 455 (1985).
- [96] Ott, A., Bouchaud, J. P., Langevin, D., and Urbach, W. Anomalous diffusion in "living polymers": A genuine Lévy flight? *Phys. Rev. Lett.* **65**, 2201 (1990).
- [97] Pandit, S. A. and Amritkar, R. E. Random spread on a family of small-world networks. *Phys. Rev. E* **63**, 041104 (2001).
- [98] Pareto, V. *Le Cours d'Économie Politique*. Macmillan, London (1897).
- [99] Pastor-Satorras, R. and Vespignani, A. Epidemic spreading in scale-free networks. *Phys. Rev. Lett.* **86**, 3200 (2001).
- [100] Pearson, K. The problem of the random walk. *Nature* **72**, 294 (1905).
- [101] Peseckis, F. E. Statistical dynamics of stable processes. *Phys. Rev. A* **36**, 892 (1987).
- [102] Plerou, V., Gopikrishnan, P., Amaral, L. A. N., Gabaix, X., and Stanley, H. E. Economic fluctuations and anomalous diffusion. *Phys. Rev. E* **62**, R2023 (2000).

- [103] Plerou, V., Gopikrishnan, P., Amaral, L. A. N., Meyer, M., and Stanley, H. E. Scaling of the distribution of price fluctuations of individual companies. *Phys. Rev. E* **60**, 6519 (1999).
- [104] Porta, A. L., Voth, G. A., Crawford, A. M., Alexander, J., and Bodenschatz, E. Fluid particle acceleration in fully developed turbulence. *Nature* **409**, 1017 (2001).
- [105] Prato, D. and Tsallis, C. Nonextensive foundation of Lévy distributions. *Phys. Rev. E* **60**, 2398 (1999).
- [106] Ramos-Fernandéz, G., Mateos, J. L., Miramontes, O., and Cocho, G. Lévy walk patterns in the foraging movements of spider monkeys (*ateles geofroyi*). www.arxiv.org/physics/0201019.
- [107] Reif, F. *Fundamentals of Statistical and Thermal Physics*. McGraw-Hill series in fundamentals of physics. McGraw-Hill, New York (1965).
- [108] Richardson, L. F. Atmospheric diffusion shown on a distance-neighbour graph. *Proc. Roy. Soc. A* **110**, 709 (1926).
- [109] Risken, H. *The Fokker-Planck Equation*. Springer Verlag, Berlin, 2nd edition (1996).
- [110] Robinson, D. A. Eye movement evoked by collicular stimulation in the alert monkey. *Vision Res.* **12**, 1975 (1972).
- [111] Sahimi, M. Non-linear and non-local transport processes in heterogeneous media: From long-range correlated percolation to fracture and materials breakdown. *Phys. Rep.* **306** (1998).
- [112] Saichev, A. I. and Zaslavsky, G. M. Fractional kinetic equations: Solutions and applications. *Chaos* **7**, 753 (1997).
- [113] Scher, H. and Montroll, E. W. Anomalous transit-time dispersion in amorphous solids. *Phys. Rev. B* **12**, 2455 (1975).
- [114] Schnitzler, M. A. Theory of continuum random walks and application to chemotaxis. *Phys. Rev. E* **48**, 2553 (1993).
- [115] Schoeder, M. *Fractals, Chaos, Power Laws. Minutes from an Infinite Paradise*. W. H. Freeman and Company, New York (1991).
- [116] Shlesinger, M. F., Zaslavsky, G., and Klafter, J. Strange kinetics. *Nature* **363**, 31 (1993).

- [117] Shlesinger, M. F., Zaslavsky, G. M., and Frisch, U. (editors). *Lévy Flights and Related Topics in Physics*, Lecture Notes in Physics. Springer Verlag, Berlin (1995).
- [118] Sinai, Y. G. The limiting behavior of a one-dimensional random walk in a random medium. *Theory of Probability and Its Applications* **27**, 257 (1982).
- [119] Sokolov, I. M. Lévy flights from a continuous-time process. *Phys. Rev. E* **63**, 011104 (2000).
- [120] Sokolov, I. M., Klafter, J., and Blumen, A. Do strange kinetics imply unusual thermodynamics? *Phys. Rev. E* **64**, 021107 (2001).
- [121] Sokolov, I. M., Klafter, J., and Blumen, A. Fractional kinetics - it isn't the calculus we knew. *Physics Today* **55**, 48 (2002).
- [122] Sokolov, I. M., Mai, J., and Blumen, A. Paradoxal diffusion in chemical space for nearest-neighbor walks over polymer chains. *Phys. Rev. Lett.* **79**, 857 (1997).
- [123] Tsallis, C., Levy, S. V. F., Souza, A. M. C., and Maynard, R. Statistical-mechanical foundation of the ubiquity of Lévy distributions in nature. *Phys. Rev. Lett.* **75**, 3589 (1995).
- [124] Uhlenbeck, G. E. and Ornstein, L. S. On the theory of the Brownian particle. *Phys. Rev.* **36**, 823 (1930).
- [125] Viecelli, J. A. On the possibility of singular low-frequency spectra and Lévy law persistence statistics in the planetary-scale turbulent circulation. *J. Atmos. Sci.* **55**, 677 (1998).
- [126] Viswanathan, G. M., Afanasyev, V., Buldyrev, S. V., Havlin, S., da Luz, M. G. E., Raposo, E. P., and Stanley, H. E. Lévy flights in random searches. *Physica A* **282**, 1 (2000).
- [127] Viswanathan, G. M., Afanasyev, V., Buldyrev, S. V., Murphy, E. J., Prince, P. A., and Stanley, H. E. Lévy flight search patterns of wandering albatrosses. *Nature* **381**, 413 (1996).
- [128] Viswanathan, G. M., Buldyrev, S. V., Havlin, S., da Luz, M. E. G., Raposo, E. P., and Stanley, H. E. Optimizing the success of random searches. *Nature* **401**, 911 (1999).
- [129] Volchenkov, D., Volchenkova, L., and Blanchard, P. Epidemic spreading in a variety of scale free networks. *Phys. Rev. E* **66**, 046137 (2002).

- [130] Watts, D. J. and Strogatz, S. H. Collective dynamics of 'small-world' networks. *Nature* **393**, 440 (1998).
- [131] West, B. J., Grigolini, P., Metzler, R., and Nonnenmacher, T. F. Fractional diffusion and Lévy stable processes. *Phys. Rev. E* **55**, 99 (1997).
- [132] Wiener, N. Differential space. *J. Math. Phys.* **2**, 131 (1923).
- [133] Wilcove, D. S., McLellan, C., and Dobson, A. P. Habitat fragmentation in the temperate zone. In Soule, M. E. (editor), *Conservation Biology: The Science of Scarcity and Diversity*, pages 237–256. Sinauer Assoc., Sunderland, MA (1986).
- [134] Wilke, C. O. and Matinetz, T. Adaptive walks on time-dependent fitness landscapes. *Phys. Rev. E* **60**, 2154 (1999).
- [135] Winter, R. B., Berg, O. G., and von Hippel, P. H. Diffusion-driven mechanisms of protein translocation on nucleic acids – 3. the *escherischia coli lac* repressor-operator interaction: Kinetic measurements and conclusions. *Biochem.* **20**, 6961 (1981).
- [136] Winter, R. B. and von Hippel, P. H. Diffusion-driven mechanisms of protein translocation on nucleic acids – 2. the *escherischia coli lac* repressor-operator interaction: Equilibrium measurements. *Biochem.* **20**, 6948 (1981).
- [137] Wurtz, R. H. and Munoz, D. P. Role of monkey superior colliculus in control of saccades and fixation. In Gazzaniga, M. S. (editor), *The Cognitive Neurosciences*, pages 533–548. MIT Press, Cambridge (1994).
- [138] Yarbus, A. L. *Eye Movements and Vision*. Plenum Press, New York (1967).
- [139] Zacherl, A., Geisel, T., Nierwetberg, J., and Radons, G. Power spectra for anomalous diffusion in the extended Sinai billiard. *Phys. Lett.* **114A**, 317 (1986).
- [140] Zanette, D. H. and Manrubia, S. C. Role of intermittency in urban development: A model of large-scale city formation. *Phys. Rev. Lett.* **79**, 523 (1997).
- [141] Zaslavsky, G. M. Chaos, fractional kinetics, and anomalous transport. *Phys. Rep.* **371**, 461 (2002).
- [142] Zipf, G. K. *Human Behavior and the Principle of Least Effort*. Addison-Wesley, Cambridge, MA (1949).
- [143] Zumofen, G. and Klafter, J. Scale-invariant motion in intermittent chaotic systems. *Phys. Rev. E* **47**, 851 (1993).
- [144] Zumofen, G. and Klafter, J. Absorbing boundary in one-dimensional anomalous transport. *Phys. Rev. E* **51**, 2805 (1995).

Acknowledgments

I shall now superdiffuse through the collection of individuals who supported me during the past seven years and thank them for it.

Theo Geisel is responsible for a work atmosphere which I have never seen anywhere else, and that is not because I travel so little. Theo let me do what I wanted, stressed the importance of creativity, and told me to concentrate on the essentials. He was patient and supported me all along and allowed me to establish the habit of four hour marathon talks. He didn't mind.

I thank Corinna for her support, management and her forgiveness concerning chocolate theft and my forgetfulness. When this is over, Corinna shall receive a kingsize pack of toblerone, assuming that I do not forget about it. I'll try.

I would like to thank Fred for changing my perspective on my own work and disentangling my thoughts every now and then. That has been very helpful.

I thank Quarky for his comments on matters and his will to start various interesting projects, despite my impatience. I hope that some day we are actually going to get started.

The Friesenkötta was my roommate for a number of years. He was the benchmark test for new flavors of humor that I was developing at various times. During the struggles of Eintracht Braunschweig in the Regionalliga he gave me support. He had an ear. Some day, Friesenkötta, we are going to go fishing.

When I started working at this institute, most of the people were still in Frankfurt. The first person here was Ragnar. He helped me on countless occasions, not only when computers were involved. I thank him for all his help and for going to the balcony with me.

I thank Gogge for the conversations we had at the Kabale and various other places. I am tempted to announce a specific greeting at this point, but I won't.

I thank Abigail for proof reading the entire manuscript.

I would also like to thank my two friends Niko and Aki. Their support was indirect but crucial. Where would I be without these two men?

I thank my family for the love and support they gave me. My parents Buchsen and Suse, my sister Rike. I thank Ines for dealing with my bad tempers and moods and the undisclosed strength she possessed in times of trouble. I apologize to my daughters Hannah and Lili for not spending enough time with them, especially during the past year. I thank them for not turning their backs on me. In a couple of years they are going to understand everything, I hope.

Kurt Broderix died in a motorcycle accident shortly after I consulted him on stochastic processes. If I can attach the term idol to anyone, it's him. I've always wanted to do physics like he did. It wouldn't make much sense to thank him for anything now that he's dead. Instead, I dedicate this thesis to him. You're on my mind, Kurt.

Lebenslauf

Name: Dirk Brockmann
geboren: 2.9.1969
Eltern: Susanna und Peter Brockmann
Geburtsort: Braunschweig
Staatsangehörigkeit: deutsch
Familienstand: verheiratet, zwei Töchter

Bildungsweg: 1976-1980: Grundschule Volkmarode, Braunschweig
1980-1982: Orientierungsstufe Volkmarode, Braunschweig
1982-1987: Neue Oberschule, Braunschweig
1987-1988: New Hanover High School, Wilmington N.C., USA
1988-1990: Undergraduate Studies of Physics , Duke University, Durham N.C., USA
1990-1995: Studium der Physik und Mathematik, Georg-August-Universität, Göttingen
1991: Vordiplom Physik
1994-1995: Diplomand am Institut für theoretische Physik, Georg-August-Universität Göttingen
1995: Diplom Physik
Thema der Diplomarbeit: *Rhythmogenese und Modulation der Atmung im ZNS*
1996-2003: Promotionsstudium, Institut für Nicht-lineare Dynamik, Georg-August-Universität, Göttingen
seit 1998: wissenschaftlicher Mitarbeiter am Max-Planck-Institut für Strömungsforschung, Göttingen